

Copyright
by
Joshua Brock Thomas
2006

The Dissertation Committee for Joshua Brock Thomas certifies that this is the approved version of the following dissertation:

Lightly Crosslinked Poly(ethylene glycol)-Tethered, pH-Responsive Biomaterials

Committee:

Nicholas A. Peppas, Supervisor

James W. McGinity, Co-Supervisor

Benny D. Freeman

Keith P. Johnston

Miguel Jose Yacaman

**Lightly Crosslinked Poly(ethylene glycol)-Tethered, pH-Responsive
Biomaterials**

by

Joshua Brock Thomas, B.S. Ch.E.

Dissertation

Presented to the Faculty of the Graduate School of

The University of Texas at Austin

in Partial Fulfillment

of the Requirements

for the Degree of

Doctor of Philosophy

The University of Texas at Austin

August 2006

Dedication

To my loving wife and ever-supportive parents.

Acknowledgements

Thanks so much to my wife, Christan, for her patience, love, and caring, all of which were the only things that made this entire Austin experience possible. My parents never spared their expression of how proud they were of me, and those simple words were always graciously received.

My path of educational experiences would not have been possible without a strong foundation built in high school by two exceptional educators, Mrs. Brenda Keller and Ms. Judy Rogers. Thanks are also given to those professors at the University of Tennessee, Professors Tom Broadhead and Paul Frymier, who furthered my educational experiences and provided great guidance.

Thanks to Professors Nicholas A. Peppas and James W. McGinity for their guidance, patience, encouragement, and advice throughout my graduate career. This work would not have been possible without the countless hours of time spent by Professor Peppas providing guidance and instruction for my research.

Life would not have been quite as enjoyable without my labmates to serve as an outlet for all the frustrations. This dissertation would not have been near error-free without the kind assistance of Daniel Carr. Special thanks goes to Don Owens for serving as my consultant and traveling partner on our travels to the far reaches of the world.

I would like to acknowledge financial support from the Department of Homeland Security and the University of Texas in the form of graduate research fellowships.

Lightly Crosslinked Poly(ethylene glycol)-Tethered, pH-Responsive Biomaterials

Publication No. _____

Joshua Brock Thomas, Ph.D.

The University of Texas at Austin, 2006

Supervisors: Nicholas A. Peppas and James W. McGinity

Significant effort has been spent on altering the pharmacokinetic profile of drugs and identifying ways to slow down the GI transit of the therapeutic, especially that of the small intestine, the location where the majority of absorption occurs. The two main areas of thrust for research pertaining to increasing the bioavailability of drugs possessing narrow absorption windows are retaining the dosage form in the stomach (gastroretentive) and slowing down transit time in the small intestine (mucoadhesive). Gastroretentive dosage forms maintain the drug delivery system above the absorption window and release the drug accordingly. Mucoadhesion affords the ability to slow upper GI transit by maintaining the dosage form at the site of absorption through some type of interaction with the intestinal mucosa. The motility of the gastrointestinal tract plays a major role in appropriately engineering a dosage form. The delivery system must be designed so that it works with the digestive system to accomplish the goal of targeting

the area where the narrow absorption window of the therapeutic exists and controlling the release to enhance the pharmacokinetic profile.

Smart biomaterials composed of pH responsive polymers, poly((meth)acrylic acid), were synthesized using a precipitation polymerization technique. The microparticles were grafted with linear polymer chains (PEG) that are capable of complexing with the hydroxyl groups of the polyacid and interpenetrating into the mucus gel layer upon entry into the small intestine. Upon introduction of an alkaline solution, these materials imbibe a significant amount of water and create a highly viscous solution. The gelled materials serve as both a controlled release membrane and resist the inertial forces associated with motility, thereby effectively slowing down the transit of the dosage form. The amount and length of the linear chain were varied to investigate their effects on the release behavior of a model compound.

Table of Contents

List of Tables	xii
List of Figures	xiv
Chapter 1: Introduction	1
References	5
Chapter 2: Background	8
Bioadhesion	8
Theoretical and Mechanistic Aspects of Bioadhesion	9
Drug Delivery	11
Gastrointestinal Motility	12
Mucous Gel Layer	14
Recent Developments	17
Tissue Engineering	20
Adhesion of Microbes and Pathogens	22
Future Directions and Conclusions	23
References	24
Chapter 3: Research Objectives	40
Chapter 4: Synthesis and Properties of Lightly Crosslinked Poly((meth)acrylic acid) Microparticles Prepared by Free Radical Precipitation Polymerization	42
Introduction	42
Materials and Methods	43
Materials	43
Synthesis	43
Characterization	44
Results and Discussion	46
Particle Size and Morphology	46
FT-IR Spectroscopy of Poly(carboxylic acid) Microparticles	46
Differential Scanning Calorimetry	47

Physicochemical Properties of Poly(carboxylic acid) Microparticles	48
Conclusions	50
References	51
Chapter 5: Dynamics of Poly(ethylene glycol)-Tethered, pH Responsive Biomaterials	63
Introduction	63
Materials and Methods	65
Materials	65
Synthesis	65
Characterization	66
Results and Discussion	68
Precipitation Polymerization for Synthesis of Tethered Microparticles	68
FT-IR Spectroscopy of Poly(ethylene glycol)-tethered Biomaterials	71
Differential Scanning Calorimetry	72
Swelling Behavior of PEG-tethered Hydrogel Networks	72
Gel/Gel Adhesion of Tethered Hydrogels	75
Conclusions	75
References	77
Chapter 6: Oral Minitablet Drug Delivery Matrices Containing Poly(ethylene glycol) Tethered, pH Responsive Excipients	101
Introduction	101
Materials and Methods	104
Materials	104
Synthesis	105
Preparation of Tablet Matrices	105
Dissolution of Tablet Matrices	106
Results and Discussion	106
Poly(acrylic acid)-containing Minitablets	108
Poly(methacrylic acid)-containing Minitablets	109
Minitablets composed of PEG-tethered PAA Microparticles	109

Minitablets Composed of PEG-tethered PMAA Microparticles	110
Conclusions.....	110
References.....	112
Chapter 7: Conclusions.....	145
Appendix A: Nanotechnology and Biomaterials.....	148
Introduction.....	149
Nanotechnology in Biomaterials Science	152
Current Research Efforts to Improve Biomedical Performance at the Nanoscale	156
Soft Biomaterials	157
Structural Characteristics	158
Surface Properties	159
Biomimetics	160
Nanoscale Biopolymer Carriers.....	161
Ceramic Nanomaterials.....	162
Increased Osteoclast Function	165
Decreased Competitive Cell Functions.....	166
Increased Osteoblast Functions on Nanofibrous Materials	167
Metal Nanomaterials.....	169
Polymeric Nanomaterials.....	170
Composite Nanomaterials.....	172
Areas of Application.....	173
Drug Delivery	173
Tissue Engineering.....	174
Biological Micro-Electro-Mechanical Systems (BioMEMS).....	176
Considerations and Future Directions.....	176
Acknowledgements.....	178
References.....	179
References.....	213
Vita	224

List of Tables

Table 2.1	Mucins found in the human body. Adapted from Ref. (30).....	29
Table 4.1	Composition of the P(M)AA microparticles prepared using a precipitation polymerization.	54
Table 5.1	Vibrational assignments for crosslinked PAA and the effect of PEG tether addition on the spectra of P(AA-g-PEG) microparticles.	79
Table 5.2	Equilibrium swelling ratio of crosslinked PAA microparticles.	80
Table 5.3	Equilibrium swelling ratio of crosslinked PMAA microparticles. ...	81
Table 5.4	Equilibrium swelling of crosslinked PEG-tethered PMAA microparticles (PEG-1000).	82
Table 6.1	Tablet formulations prepared by dry compression.	114
Table 6.2	Diffusional analysis of tablet matrices formulated according to Table 6.1 composed of poly(acrylic acid) and crosslinked poly(acrylic acid) microparticles synthesized with varying levels of crosslinking agent.	115
Table 6.3	Diffusional analysis of tablet matrices formulated according to Table 6.1 composed of poly(methacrylic acid) and crosslinked poly(methacrylic acid) microparticles synthesized with varying levels of crosslinking agent.	116
Table 6.4	Diffusional analysis of tablet matrices formulated according to Table 6.1 composed of crosslinked poly(acrylic acid) microparticles containing a poly(ethylene glycol) tether, with the tether concentration varied for each system below.	117

Table 6.5	Diffusional analysis of tablet matrices formulated according to Table 6.1 composed of crosslinked poly(methacrylic acid) microparticles containing a poly(ethylene glycol) tether, with the tether concentration varied for each system below.....	118
-----------	---	-----

List of Figures

- Figure 1.1 Physiological challenges encountered in both the development of modified or controlled release oral dosage forms for low molecular weight compounds and the effective delivery of macromolecules.....7
- Figure 2.1 Bioadhesion refers to the molecular contact (adherence) of two tissues through the application of a bioadhesive between these two surfaces. Adapted from Ref. (1).....30
- Figure 2.2 Examples of electrostatic forces occurring between amino acids. These forces are due to (a) the association of two ionic protein groups such as Lysine (Lys) and Glutamic acid (GLU) or (b) the dipole-dipole interactions such as the dipole-induced dipole interaction between Asparagine (Asn) and Threonine (Thr).....31
- Figure 2.3 Chemical structure of commonly employed poly(acrylic acid)-based materials in mucoadhesive drug delivery systems. 934P is crosslinked with allyl sucrose, 974P with allyl pentaerythritol, and AA-1 with divinyl glycol. A small amount of the acrylic acids are neutralized to potassium acrylate prior to polymerization.....32
- Figure 2.4 Polymer tethers grafted at a low surface coverage ($\sigma \rightarrow 0$) and in a pure solvent. The dashed circle has a diameter which is $2 \times R_F$ (Flory radius). The grafted chains are separated by a distance, D , that is directly proportional to the monomer size (a) and inversely proportional to the square root of the surface coverage (σ). Adapted from Ref. (51)....33

Figure 2.5	Tethered polymers in a good solvent take a strongly stretched conformation, and the thickness of this stretched polymer layer, L , is directly proportional to the degree of polymerization (N), the monomer size (a), and the surface coverage (σ) to the $1/3$ power. Adapted from Ref. (51).	34
Figure 2.6	Tethered polymers take on distinct conformations when exposed to a crosslinked network. Polymers take on a separate mushroom regime at low surface coverages.	35
Figure 2.7	At intermediate surface coverages, the tethered polymer layer interpenetrates into the crosslinked polymer with some of the polymers overlapping.	36
Figure 2.8	At high surface coverages, some polymers interpenetrate into the crosslinked network while others collapse onto the tethered surface resulting in partial interdigitation.	37
Figure 2.9	The theoretical framework developed in our laboratory by Huang et al. (48) includes the tethered polymers, the base gel to which these polymers are tethered, and the target gel representative of the tissue to be adhered. The position at $z = 0$ represents the base gel surface plane and d is the distance between the two hydrogel networks.	38
Figure 2.10	Structure of chitosan, which is derived by partially deacetylating chitin. The number of acetyl groups (m) and primary amine groups (n) is controlled through the extent of deacetylation.	39

Figure 4.1	Molecular structures of (a) the carboxylic acid monomer (R1 = H for AA or R1 = CH ₃ for MAA), (b) the tri-functional pentaerythritol (R2 = CH for APE or R2 = COH for PETA), and (c) the thermal initiator BCHPC.	55
Figure 4.2	Precipitation polymerization of (meth)acrylic acid in ethyl acetate.	56
Figure 4.3	Morphology of crosslinked PMAA as determined using SEM.	57
Figure 4.4	Morphology of crosslinked PAA microparticles as determined using SEM.	58
Figure 4.5	FT-IR spectrum of (a) crosslinked PMAA and (b) crosslinked PAA.	59
Figure 4.6	Glass transitions of crosslinked PMAA microparticles as a function of mol % crosslinking. Each bar represents the mean \pm SD (n=3).	60
Figure 4.7	Glass transitions of crosslinked PAA microparticles as a function of mol % crosslinking. Each bar represents the mean \pm SD (n=3).....	61
Figure 4.8	pH responsive equilibrium swelling behavior of crosslinked microparticles as a function of crosslinking ratio. Each point represents the mean \pm SD (n=4).....	62
Figure 5.1	Molecular structures of (a) the carboxylic acid-containing monomer (R1 = H for AA or R1 = CH ₃ for MAA), (b) a poly(ethylene glycol) tether (z ~ 5, 23, and 45), (c) the tri-functional pentaerythritol (R2 = CH for APE or R2 = COH for PETA), and (d) the thermal initiator di(4-tert-butylcyclohexyl) peroxydicarbonate (BCHPC).....	83
Figure 5.2	FT-IR spectrum of crosslinked PAA (0.75 mol % APE) showing the characteristic carbonyl stretching and fingerprint for the molecular structure of the polymer.	84

Figure 5.3	FT-IR spectrum of P(AA-g-PEG), PEG-1000, AA:EG 98:2, exhibiting the structural modifications introduced with the addition of the PEG tether.	85
Figure 5.4	FT-IR spectrum of P(AA-g-PEG), PEG-1000, AA:EG 90:10, exhibiting the structural modifications introduced with the addition of the PEG tether.	86
Figure 5.5	FT-IR spectrum of P(AA-g-PEG), PEG-1000, AA:EG 83:17, exhibiting the structural modifications introduced with the addition of the PEG tether.	87
Figure 5.6	FT-IR spectrum of P(AA-g-PEG), PEG-1000, AA:EG 60:40, exhibiting the structural modifications introduced with the addition of the PEG tether.	88
Figure 5.7	FT-IR spectrum of P(AA-g-PEG), PEG-1000, AA:EG 50:50, exhibiting the structural modifications introduced with the addition of the PEG tether.	89
Figure 5.8	FT-IR spectrum of (a) crosslinked PAA (0.75 mol % APE), (b) P(AA-g-PEG), PEG-1000, AA:EG 98:2, (c) 90:10, (d) 83:17, (e) 60:40, (f) 50:50.	90
Figure 5.9	DSC thermogram of crosslinked PAA (0.75 mol % APE) exhibiting a T_g at 131°C.	91
Figure 5.10	DSC thermogram P(AA-g-PEG), PEG-1000, AA:EG 98:2, exhibiting a T_g at 131°C.....	92
Figure 5.11	DSC thermogram of P(AA-g-PEG), PEG-1000, AA:EG 90:10, exhibiting a T_g at 130°C.....	93

Figure 5.12	DSC thermogram of P(AA-g-PEG), PEG-1000, AA:EG 83:17, exhibiting two T_g 's at 130°C and 94°C.	94
Figure 5.13	DSC thermogram of P(AA-g-PEG), PEG-1000, AA:EG 60:40, exhibiting a T_g at 68°C.....	95
Figure 5.14	DSC thermogram of P(AA-g-PEG), PEG-1000, AA:EG 50:50, exhibiting a T_g at 61°C.....	96
Figure 5.15	DSC thermogram of (a) crosslinked PAA (0.75 mol % APE), (b) PAA P(AA-g-PEG), PEG-1000, AA:EG 98:2, (c) 90:10, (d) 83:17, (e) 60:40, (f) 50:50.	97
Figure 5.16	Evaluation of the peak force obtained from neutralized hydrated gels containing (a) crosslinked PAA (0.75 mol % APE), (b) P(AA-g-PEG), PEG-1000, AA:EG 98:2, (c) 90:10, (d) 83:17, (e) 60:40, (f) 50:50.	98
Figure 5.17	Evaluation of the work of adhesion of neutralized hydrated gels containing (a) crosslinked PAA (0.75 mol % APE), (b) P(AA-g-PEG), PEG-1000, AA:EG 98:2, (c) 90:10, (d) 83:17, (e) 60:40, (f) 50:50.	99
Figure 5.18	Evaluation of the work of cohesion of neutralized hydrated gels containing (a) crosslinked PAA (0.75 mol % APE), (b) P(AA-g-PEG), PEG-1000, AA:EG 98:2, (c) 90:10, (d) 83:17, (e) 60:40, (f) 50:50.	100
Figure 6.1	The reversible complexation/decomplexation behavior of complexation hydrogels. The polymeric backbone consists of proton donating polyacids with proton accepting polymer tethers. At low pH's the polymers are participating in interpolymer complexation, effectively inhibiting diffusion out of the network. At pH's close and above the pKa of the polyacid, the interpolymer complexes dissociate, giving rise to an expansion of the polymer network.....	119

Figure 6.2	Theophylline release from minitabket matrices containing poly(acrylic acid) (PAA) microparticles in 0.1 N HCl.	120
Figure 6.4	Theophylline release from minitabket matrices containing poly(methacrylic acid) (PMAA) microparticles in 0.1 N HCl.	122
Figure 6.6	Theophylline release from minitabket matrices containing PEG-tethered PAA microparticles in 0.1 N HCl.	124
Figure 6.7	Theophylline release from minitabket matrices containing PEG-tethered PAA microparticles in pH 6.8 buffer.	125
Figure 6.8	Theophylline release from minitabket matrices containing PEG-tethered PMAA microparticles in 0.1 N HCl.	126
Figure 6.9	Theophylline release from minitabket matrices containing PEG-tethered PMAA microparticles in pH 6.8 buffer.	127
Figure 6.10	Diffusional analysis of the release of the model drug theophylline from minitabket matrices containing PAA microparticles in 0.1 N HCl and pH 6.8 buffer.	128
Figure 6.11	Diffusional analysis of the release of the model drug theophylline from minitabket matrices containing crosslinked PAA (0.2 mol % APE) microparticles in 0.1 N HCl and pH 6.8 buffer.	129
Figure 6.12	Diffusional analysis of the release of the model drug theophylline from minitabket matrices containing crosslinked PAA (0.43 mol % APE) microparticles in 0.1 N HCl and pH 6.8 buffer.	130
Figure 6.13	Diffusional analysis of the release of the model drug theophylline from minitabket matrices containing crosslinked PAA (0.75 mol % APE) microparticles in 0.1 N HCl and pH 6.8 buffer.	131

Figure 6.14	Diffusional analysis of the release of the model drug theophylline from minitab ^l et matrices containing crosslinked PAA (0.75 mol % APE) microparticles in 0.1 N HCl and pH 6.8 buffer.	132
Figure 6.15	Diffusional analysis of the release of the model drug theophylline from minitab ^l et matrices containing Carbopol 971P-NF microparticles in 0.1 N HCl and pH 6.8 buffer.....	133
Figure 6.16	Diffusional analysis of the release of the model drug theophylline from minitab ^l et matrices containing Carbopol 974P-NF microparticles in 0.1 N HCl and pH 6.8 buffer.....	134
Figure 6.17	Diffusional analysis of the release of the model drug theophylline from minitab ^l et matrices containing PMAA microparticles in 0.1 N HCl and pH 6.8 buffer.....	135
Figure 6.18	Diffusional analysis of the release of the model drug theophylline from minitab ^l et matrices containing crosslinked PMAA (0.43 mol % PETA) microparticles in 0.1 N HCl and pH 6.8 buffer.	136
Figure 6.19	Diffusional analysis of the release of the model drug theophylline from minitab ^l et matrices containing crosslinked PMAA (0.75 mol % PETA) microparticles in 0.1 N HCl and pH 6.8 buffer.	137
Figure 6.20	Diffusional analysis of the release of the model drug theophylline from minitab ^l et matrices containing P(AA-g-PEG), PEG-300, 90:10, microparticles in 0.1 N HCl and pH 6.8 buffer.	138
Figure 6.21	Diffusional analysis of the release of the model drug theophylline from minitab ^l et matrices containing P(AA-g-PEG), PEG-300, 70:30, microparticles in 0.1 N HCl and pH 6.8 buffer.	139

Figure 6.22	Diffusional analysis of the release of the model drug theophylline from minitab ^l et matrices containing P(AA-g-PEG), PEG-300, 50:50, microparticles in 0.1 N HCl and pH 6.8 buffer.	140
Figure 6.23	Diffusional analysis of the release of the model drug theophylline from minitab ^l et matrices containing P(AA-g-PEG), PEG-2000, 70:30, microparticles in 0.1 N HCl and pH 6.8 buffer.	141
Figure 6.24	Diffusional analysis of the release of the model drug theophylline from minitab ^l et matrices containing P(MAA-g-PEG), PEG-1000, 80:20, microparticles in 0.1 N HCl and pH 6.8 buffer.	142
Figure 6.24	Diffusional analysis of the release of the model drug theophylline from minitab ^l et matrices containing P(MAA-g-PEG), PEG-1000, 70:30, microparticles in 0.1 N HCl and pH 6.8 buffer.	143
Figure 6.24	Diffusional analysis of the release of the model drug theophylline from minitab ^l et matrices containing P(MAA-g-PEG), PEG-1000, 50:50, microparticles in 0.1 N HCl and pH 6.8 buffer.	144
Figure A.1:	Cell recognition of biomaterial surfaces controlled by initial protein interactions. Initial protein interactions can influence cell adhesion and, thus, degree of bone tissue formation on biomaterials. Changing material properties will alter protein interactions and influence subsequent cell function. (Adapted and redrawn from Schakenraad, J.M., in <i>Biomaterials Science: An Introduction to Materials in Medicine</i> , Ratner, B.D., Hoffman, A.S., Schoen, F.S., and Lemmons, J.E., Eds., Academic Press, New York, NY, 1996, pp. 133-140. With permission.).....	192

Figure A.2: Nanocomponents of bone provide a high degree of nanostructured surface roughness for bone cells. (Adapted and redrawn from Cowin, R., Handbook of Bioengineering, McGraw Hill, New York, NY, 1987. With permission.).....193

Figure A.3: Special surface properties of nanophase materials. (a) Higher number of atoms at the surface for nanophase compared to conventional materials. (b) Nanophase materials have higher surface areas, possess greater numbers of material defects at the surface, and altered electron delocalization. Such special properties will influence protein interactions for controlling cell functions. (Adapted and redrawn from Klabunde, K.J. et al., J. Phys. Chem., 100, 12141, 1996. With permission.) ..194

Figure A.4: Conventional grain size of currently used orthopedic implants. Bar = 10 and 1 micron for the left and right micrograph, respectively.195

Figure A.5: (a) Conventional and (b) nanophase titania. One of the first studies correlating increased osteoblast function with decreasing ceramic grain size was done on titania as pictured here. (From Webster, T.J., Siegel, R.W., and Bizios, R., Biomaterials, 20, 1221, 1999. With permission.)196

Figure A.6: Poly-lactic-glycolic acid (PLGA) molds of conventional and nanophase carbon fiber compacts. To highlight the importance of nanometer surface roughness regardless of substrate chemistry, studies have shown increased functions of osteoblasts on PLGA molds of nanophase compared to conventional carbon compacts. Studies have also shown increased functions of osteoblasts on compacts composed of nanometer compared to conventional carbon fibers. Bar = 1 micron. (From Elias, K.L., Price, R.L., and Webster, T.J., *Biomaterials*, 23, 3279-3287, 2002. With permission.).....197

Figure A.7: Increased *in vivo* bone regeneration on titanium coated with nanophase apatite. Scanning electron micrograph of nanometer dimensioned apatite (specifically, between 100 – 200 nm in size) is depicted in (a). Increased bone regeneration in titanium cages when coated with nano-apatite is depicted in (b). (From Li, P., *J. Biomed. Mat. Res* 66, 79-85, 2003. With permission.).....198

Figure A.8: Nanophase hydroxyapatite coated on titanium. Due to elevated temperatures, traditional coating techniques, like plasma spray deposition, cannot be used to coat metals with nanophase ceramics. This process developed by Spire Biomedical (Bedford, MA) uses high pressure at low temperatures so as to not allow for grain growth. Bar = 1 micron (upper left).199

Figure A.9: Transmission electron microscope image of alumina nanofibers. Compared to spherical conventional alumina, increased functions of osteoblasts have been reported on nanophase fibrous alumina. Scale bar = 10 nm. (From Price, R.L. et al., J. Biomed. Mat. Res, 67 (4), 1284, 2003. With permission.).....200

Figure A.10: Helical rosette nanotubes. Drawing of the cross-sectional (left) and longitudinal (right) view of self-assembled helical rosette nanotubes is depicted in (a) while helical rosette nanotubes coated on titanium is depicted in (b). Note the nanophase dimension of these organic tubes. Increased osteoblast function has been observed on helical rosette nanotubes coated on Ti. (From Chun, A. et al., Nanotechnology, 15, S234, 2004. With permission.)201

Figure A.11: Scanning electron micrographs of nanophase metals. Increased functions of osteoblasts have been observed on nanophase compared to conventional c.p. Ti, Ti6Al4V, and CoCrMo. Scale bar = 1 micron for nanophase Ti/Ti6Al4V and 10 microns for conventional Ti/Ti6Al4V. Scale bar = 10 microns for nanophase and conventional CoCrMo. (From Ejiiofor, J.U. and Webster, T.J., ASM Conference, Las Vegas, NV, in press, 2004. With permission.)202

Figure A.12: Scanning electron micrographs of adherent osteoblasts on nanophase c.p. Ti. Directed osteoblast adhesion on nanophase metal grain boundaries has been reported. Scale bar = 100 microns for top and 10 microns for bottom. Adhesion time = 30 minutes. (From Ejiiofor, J.U. and Webster, T.J., ASM Conference, Las Vegas, NV, in press, 2004. With permission.).....203

Figure A.13: Scanning electron micrographs of conventional and nanophase PLGA scaffolds. Increased osteoblast functions have been demonstrated on nanophase PLGA scaffolds. Scale bar = 10 microns. (From Park, G.E., Park, K., Webster, T.J., *Biomaterials*, in press, 2004. With permission.).....204

Figure A.14: Polymer nanoislands created by demixing polystyrene and polybromo-styrene. Altered cell functions have been observed on polymer nanoislands compared to conventional polymer topographies. (a) through (d) represents increased magnification. (From Li, W.-J. et al., *J. Biomed. Mat. Res*, 60, 613-621, 2002. With permission.)....205

Figure A.15: Scanning electron micrographs of poly-lactic-glycolic acid (PLGA): titania composites. Increased osteoblast function has been observed on polymer composites containing nanophase compared to conventional ceramics. Scale bar = 10 microns. (From Smith, T.A. and Webster, T.J., *J. Biomed. Mat. Res*, in press, 2004. With permission.).....206

Figure A.16: Scanning electron micrographs of poly-ether-urethane (PU): carbon nanofibers (wt.%) composites. Increased functions of osteoblasts have been observed on polymer composites containing carbon nanofibers. Scale bar = 1 micron. (From Price, R.L. et al., *Biomaterials*, 24(11), 1877, 2003. With permission.).....207

Figure A.17: TEM image of P(MAA-g-EG) nanospheres prepared from a MAA/EG molar feed ratio of 1:1. The P(MAA-g-EG) nanospheres were stained with uranyl acetate with a pH value of 4.0.208

Figure A.18: TEM image of P(MAA-g-EG) nanospheres prepared from a MAA/EG molar feed ratio of 1:1. The P(MAA-g-EG) nanospheres were stained with phosphotugstic acid with a pH value of 7.2.209

Figure A.19: Optical section of a Caco-2 cell monolayer grown on microporous Transwell® plates obtained with a confocal microscope. FITC-labeled insulin (green) was added to the apical chamber of the cell monolayer in the presence of poly(methacrylic acid-grafted-ethylene glycol) microparticles for 120 min and images were taken after fixing the cells with 3.7% formaldehyde.....210

Figure A.21: In (A) 3D projection a micropatterned square array of a biomimetic polymer network based on a crosslinked polyacrylamide obtained utilizing a confocal microscope. In (B) a slice of the square array is demonstrated.....212

Chapter 1: Introduction

The oral delivery of small molecular weight drugs, macromolecules, and vaccines remains the most favored route of administration. However, barriers exist in successfully administering drugs via the gastrointestinal tract and achieving a predictable and increased oral bioavailability. These barriers include but are not limited to a mucous gel layer lining the gastrointestinal epithelia, a degradative pH that varies from patient to patient, a relatively short transit time past the ideal absorption sites, and a system of degradative enzymes (Figure 1.1).

For small molecular weight drugs (500-700 Daltons), the narrow absorption window of the proximal intestine poses the greatest challenge in the development of a modified or controlled release product (1). Drugs that are transported across the small intestine through some form of facilitated transport or polar compounds are readily absorbed in the proximal gut; however the molecules exhibit very low absorption in the distal gut (or colon). The relatively short period of transit (3 h for the small intestine and as much as 20 h for the colon), and, in effect, absorption, can significantly affect the drug's oral bioavailability, necessitating a need for a prolonged residence time at the large absorptive surface area of the small intestine.

The successful oral delivery of macromolecules faces major challenges which are a result of their much larger size (> 500-700 Da), hydrophilicity, vulnerability to proteolytic degradation, and narrow window of effective absorption, all of which have limited their commercial and clinical development (2). Drug carriers have shown great promise in enabling the successful delivery of proteins and peptides by overcoming the aforementioned challenges without modifying the structure of the macromolecular therapeutic, damaging epithelial membranes, or creating new toxicities (3-7). However,

rapid transit of the drug carrier past the ideal site of absorption still poses a challenge in developing an effective and efficient oral macromolecular drug delivery system (8).

Two phenomena have been used to solve the problem of rapid transit of a therapeutic past the location of maximal absorption: gastroretention and bioadhesion. Both areas address the need for controlling the spatial location of an oral drug delivery system to achieve a maximal bioavailability. Gastroretentive dosage forms provide a system that maintains the drug above the compound's window of absorption, releasing the therapeutic slowly so that the time available for the body to effectively absorb the pharmaceutical ingredient is increased (9). Since the early 1980s, the phenomenon of bioadhesion has offered promise in enabling the development of drug delivery carriers and systems that are capable of an increased residence time in the narrow absorption window of the drug. Bioadhesion, or more specifically mucoadhesion, is defined as the attachment of a biological or synthetic moiety to a biological substrate such as the mucous gel layer lining the oral cavities of the body.

Mucoadhesive oral drug delivery systems allow for intimate contact to develop between the system and the ideal absorption site (most cases, the small intestine), which aids in maximizing the rate and extent to which a drug absorbs. Major adversities encountered in designing superior mucoadhesive systems include the motility of the digestive tract which is designed to move contents, the rate of mucus turnover and the amount of sloughed or free mucous gel that resides in the luminal environment.

A mucoadhesive is the synthetic or semi-natural material, most commonly a polymer, which is responsible for the interaction between the drug carrier and the mucous gel layer. Recent advances in mucoadhesives include polymer networks that contain thiolated moieties available for disulfide bond formation with mucin molecules (10), polymer tethers capable of interpenetrating the mucous gel layer to create a bridge

between the system and the mucous gel layer (11, 12), and mucin recognitive molecules (or their carbohydrate side-chains) such as lectins (13, 14), fimbrial proteins (15), and chitosan (16-18). These advances offer promise in that the technology is advancing and systems are evolving to become more effective. However, there is much knowledge to be gained in order for biomimetic systems to be developed that offer characteristics representative of biological mucoadhesive organisms, namely the bacteria comprising the intestinal microflora (19-21).

The surface of the polymeric drug delivery carrier remains the integral part in obtaining a mucoadhesive interaction with the mucous gel layer, as it is this surface that is at the interface with the mucosal lining. A surface layer of polymer has been shown to have the capacity to act as an adhesion promoter in developing intimate contact between the carrier and the mucosal lining (22).

The purpose of this work is to combine the theoretical framework developed for polymer tethers as adhesion promoters with a drug delivery system capable of achieving a controlled or modified release of a model compound. The objective is the design and evaluation of an oral mucoadhesive drug delivery that would be capable of spatially controlled release. Also, the molecular characteristics of the tethered polymers will be evaluated to determine their effects on mediating adhesion.

The research objectives and focus of this dissertation are presented in Chapter 3 in greater detail. Chapter 4 investigates the synthesis and characterization of lightly crosslinked microparticles composed of poly(acrylic acid) or poly(methacrylic acid) prepared using a free radical precipitation polymerization. Chapter 5 evaluates the dynamics of poly(acrylic acid) and poly(methacrylic acid) hydrogel microparticles containing poly(ethylene glycol) (PEG) tethers of varying molecular weights. Chapter 6 elucidates on the drug release behavior of polymer-containing matrices. The fundamental

properties of the polymer, such as amount of crosslinking agent incorporated, type of pH responsive monomer employed, pH of drug release media, amount of poly(ethylene glycol) (PEG) tether, and molecular weight of PEG tether, are controlled to analyze their affect on the release of a model compound.

REFERENCES

1. Davis SS, Formulation strategies for absorption windows, *Drug Discov. Today*, 10:249-257, 2005.
2. Goldberg M and Gomez-Orellana I, Challenges for the oral delivery of macromolecules, *Nat. Rev. Drug Discov.*, 2:289-295, 2003.
3. Baughman RA, Kapoor SC, Agarwal RK, Kisicki J, Catella-Lawson F, and FitzGerald GA, Oral delivery of anticoagulant doses of heparin - A randomized, double-blind, controlled study in humans, *Circulation*, 98:1610-1615, 1998.
4. Lowman AM, Morishita M, Kajita M, Nagai T, and Peppas NA, Oral delivery of insulin using pH-responsive complexation gels, *J. Pharm. Sci.*, 88:933-937, 1999.
5. Morishita M, Goto T, Nakamura K, Lowman AM, Takayama K, and Peppas NA, Novel oral insulin delivery systems based on complexation polymer hydrogels: Single and multiple administration studies in type 1 and 2 diabetic rats, *J. Control. Release*, 110:587-594, 2006.
6. Morishita M, Goto T, Peppas NA, Joseph JI, Torjman MC, Munsick C, Nakamura K, Yamagata T, Takayama K, and Lowman AM, Mucosal insulin delivery systems based on complexation polymer hydrogels: effect of particle size on insulin enteral absorption, *J. Control. Release*, 97:115-124, 2004.
7. Torres-Lugo M and Peppas NA, Molecular design and in vitro studies of novel pH-sensitive hydrogels for the oral delivery of calcitonin, *Macromolecules*, 32:6646-6651, 1999.
8. Lehr CM, Bioadhesion Technologies For The Delivery Of Peptide And Protein Drugs To The Gastrointestinal-Tract, *Crit. Rev. Ther. Drug Carr. Syst.*, 11:119-160, 1994.
9. Singh BN and Kim KH, Floating drug delivery systems: an approach to oral controlled drug delivery via gastric retention, *J. Control. Release*, 63:235-259, 2000.
10. Bernkop-Schnurch A, Thiomers: A new generation of mucoadhesive polymers, *Adv. Drug Deliv. Rev.*, 57:1569-1582, 2005.
11. Peppas NA and Huang YB, Nanoscale technology of mucoadhesive interactions, *Adv. Drug Deliv. Rev.*, 56:1675-1687, 2004.

12. Peppas NA and Sahlin JJ, Hydrogels as mucoadhesive and bioadhesive materials: A review, *Biomaterials*, 17:1553-1561, 1996.
13. Lee JW, Park JH, and Robinson JR, Bioadhesive-based dosage forms: The next generation, *J. Pharm. Sci.*, 89:850-866, 2000.
14. Lehr CM, Bouwstra JA, Kok W, Noach ABJ, Deboer AG, and Junginger HE, Bioadhesion By Means Of Specific Binding Of Tomato Lectin, *Pharm. Res.*, 9:547-553, 1992.
15. Caston A, Davis S, and Williams P, The potential of fimbrial proteins for delaying intestinal transit of oral drug delivery system, *Proceed. Intern. Symp. Controlled Release Bio. Mat.*, 17:313-314, 1990.
16. Felt O, Buri P, and Gurny R, Chitosan: A unique polysaccharide for drug delivery, *Drug Dev. Ind. Pharm.*, 24:979-993, 1998.
17. Harding SE, *Analysis of polysaccharides by ultracentrifugation. Size, conformation and interactions in solution*, in *Polysaccharides 1: Structure, Characterization And Use*. 2005. p. 211-254.
18. Hejazi R and Amiji M, Chitosan-based gastrointestinal delivery systems, *J. Control. Release*, 89:151-165, 2003.
19. Boekhorst J, Helmer Q, Kleerebezem M, and Siezen RJ, Comparative analysis of proteins with a mucus-binding domain found exclusively in lactic acid bacteria, *Microbiology-(UK)*, 152:273-280, 2006.
20. Eckburg PB, Bik EM, Bernstein CN, Purdom E, Dethlefsen L, Sargent M, Gill SR, Nelson KE, and Relman DA, Diversity of the human intestinal microbial flora, *Science*, 308:1635-1638, 2005.
21. Hooper LV and Gordon JI, Commensal host-bacterial relationships in the gut, *Science*, 292:1115-1118, 2001.
22. De Ascentiis A, Degrazia JL, Bowman CN, Colombo P, and Peppas NA, Mucoadhesion Of Poly(2-Hydroxyethyl Methacrylate) Is Improved When Linear Poly(Ethylene Oxide) Chains Are Added To The Polymer Network, *J. Control. Release*, 33:197-201, 1995.

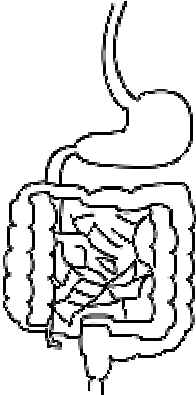
Small Molecules (<500-700 Da)		Macromolecules
<ul style="list-style-type: none"> • Compounds having low permeability (III) or solubility (II) or both (IV) can have a significant impact on the oral bioavailability • Molecules transported via facilitated transport are not absorbed in various regions of the GI • Drugs have a short transit time past ideal absorption site which is most commonly the small intestine 		<ul style="list-style-type: none"> • Proteins are hydrophilic and do not possess the lipophilicity needed for passive transport • The large molecular mass eliminates the paracellular route for transport • Proteolytic degradation by enzymes located in the stomach renders the drug inactive • Macromolecules have a short transit time past the ideal absorption site of the small intestine

Figure 1.1 Physiological challenges encountered in both the development of modified or controlled release oral dosage forms for low molecular weight compounds and the effective delivery of macromolecules.

Chapter 2: Background

BIOADHESION

Adhesion refers to the molecular contact (adherence) of two substances, which typically involves the application of an adhesive between these two entities (Figure 2.1). Historically, adhesives (1) and bioadhesives have been used as terms in two distinctly different areas of thought with very little overlap and continuity. The term adhesive, or biological adhesive, has been used to describe a particular biomaterial or system that is responsible for adherence. Bioadhesion has largely remained well entrained in the field of biology referring to cellular interactions (cytoadhesion) or to mucosal adhesion (mucoadhesion).

Whether it is cell-to-cell, soft or hard tissue, or mucosal adhesion, bioadhesion is the phenomenon of long term contact of a synthetic or biological macromolecule or hydrocolloid with a biological substrate (2-7). Therefore, bioadhesion can be extended to include any type of adhesion process in contact with or within the biological milieu. The term bioadhesive refers to the particular substance, natural or synthetic, responsible for this adhesion. Surfaces usually employed in bioadhesive applications involve synthetic, natural, or hybrid macromolecules, which can be found on biological components such as cells composing tissue and blood platelets. Mucoadhesion is often used to describe bioadhesion where mucus is the substrate, whereas cytoadhesion refers to cell-to-cell bioadhesion.

The substrate to which bioadhesion occurs is quite different in its physical properties than those employed in conventional adhesion. Soft tissue or a synthetic material is often used to adhere another soft tissue. Bioadhesives have found success in hard tissue applications such as orthopedics and dentistry due to the relatively more

favorable biological environment presented in these areas (8). Recently there has been significant interest in the development of more effective bioadhesives for tissue engineering (9-11) and carriers for drug delivery (2-7) applications, both areas in which clinical success has not been as successful. Also, the understanding of bacterial adhesion has received considerable attention to further the knowledge behind biofouling (biofilm formation) and the role bacterial bioadhesives play.

THEORETICAL AND MECHANISTIC ASPECTS OF BIOADHESION

The mechanisms that describe the phenomena of bioadhesion and the structural characteristics of bioadhesives were originally proposed by Peppas and Buri (5). The components of importance for obtaining adhesion are the surface containing the bioadhesive, the surface of the biological substrate, and the interface between these two. The bioadhesive must come into intimate contact with the substrate (either with an external applied force, through an attractive force, or by collision). For liquid bioadhesive formulations, the bioadhesive fills the inclusions provided by the surface roughness and develops a physical or mechanical bond, which is quite common in orthopedic or dental applications. Once contact has been achieved, the macromolecules responsible for the adhesive characteristics are then able to interact with specific moieties present on the substrate's surface. In some instances, due to the high mobility of the surface macromolecules, interdiffusion occurs and the interdigitated macromolecules are capable of interacting with other moieties present on the subsurface or entangling with other macromolecules composing the surface of the substrate to develop a bioadhesive bond. The molecule to molecule bioadhesion is attributed to bonding derived from either covalent or noncovalent interactions.

Primary chemical interactions occur through ionic bonding, disulfide bonds, or a chemical reaction between the functional groups of the adhesive and the substrate.

Secondary chemical interactions are attributed to electrostatic forces (ionic and dipole-dipole, Figure 2.2), hydrogen bonding, or hydrophobic forces. The theories that describe the chemical mechanisms include the electronic theory and the adsorption theory, and those that describe the physical mechanisms include the wetting theory, the interpenetration or diffusion theory, and the fracture theory (2, 4, 5).

The electronic theory describes adhesion in terms of the differences in the electronic structures of the materials involved. After the materials come into contact, a double layer of charge forms at the interface, and adhesion occurs due to these attractive forces (12). The adsorption theory describes materials that adhere to mucus due to secondary forces such as van der Waals, hydrogen bonding, or hydrophobic interactions (13, 14). Due to the presence of a large number of these types of forces, the net force is greater than that which is created by electrostatic forces. The wetting theory describes the ability of a mucoadhesive to spread over the mucus gel layer and develop an intimate contact (15-17). The parameters used to correlate a material's mucoadhesive capacity based upon this theory are the individual materials' spreading coefficients which aid in calculating the interfacial energy. The diffusion theory describes mucoadhesion as a process where the chains of the materials interpenetrate to a sufficient depth to create a semipermanent bond (18, 19).

Each individual theory fails to sufficiently describe the phenomenon of bioadhesion; therefore, combining various aspects of the theories enables a more appropriate description (20). As a bioadhesive approaches the biological substrate, it reaches equilibrium with the biological environment, which can include wetting and swelling. As the material comes into contact with the biological substrate, non-covalent secondary bonds are formed at the bioadhesive-substrate interface through either non-specific or specific interactions. As the bioadhesive continues to reside in contact with

the substrate, macromolecules of the respective materials interdiffuse into one another while forming more and more noncovalent bonds.

The field of bioadhesion is receiving a great deal of attention in a wide variety of fields related to biomedical engineering. These main areas of thrust are discussed along with the current research efforts.

DRUG DELIVERY

Drug delivery applications utilize bioadhesive macromolecules to localize treatment to a specific area of the body, thereby increasing the residence time of the therapeutic and improving the oral bioavailability (21-23). For intravascular applications, a targeting agent such as a ligand is incorporated into the drug delivery system, creating adhesion through the ligand-receptor interaction present at the endothelium surface. Bioadhesion in this instance is governed by (i) the shear stress caused by the hemodynamic force exerted over the cell/particle, the loading rate which is affected by the viscosity of the biological environment, and the ligand/receptor density ratio which can be controlled during the fabrication of the system (24). For oral drug delivery systems, mucoadhesion is the specific type of bioadhesion responsible for localizing the system at the mucous gel layer, which lines the absorptive regions of the alimentary canal.

Mucoadhesive polymer-based drug delivery systems were first utilized by Nagai and collaborators as carriers for local treatment to the buccal cavity (25, 26). Mucus is also present in the nasal and gastrointestinal cavity, the vagina, and other hollow organs, providing a diverse arena for the application of mucoadhesive drug delivery systems. Polymers that have typically been utilized in the development of mucoadhesive controlled release formulations include hydrophilic macromolecules containing numerous hydrogen bonding groups such as poly((meth)acrylic acid) which include the carbomer

and polycarbophil families (Figure 2.3), cellulose, and (semi)natural ones such as chitosan and alginate (27). Like so many other materials that were first utilized in biomedical applications (cellulose acetate dialysis tubing, Dacron® vascular grafts, and polyurethane heart molds), these materials were available off-the-shelf. Because their use was originally intended for other applications and was only transitioned into oral drug delivery systems, the drug delivery systems comprised of these materials have been classified as the first generation bioadhesive-based dosage forms (4).

Dosage forms have been engineered so that they take advantage of the abilities to molecularly design polymer networks to impart specific structural characteristics so that polymers comprising the dosage form are multifunctional. This new generation of bioadhesives has employed hybrid materials such as lectins, fimbrial proteins, or ligands which have specific interaction sites within the body. Biomimetic design of devices can take advantage of the natural processes of the body to be highly selective and effective, enabling the ability to localize and maintain treatment at a specific area within the body. However, to be both effective and selective, a thorough knowledge and understanding of the biological environment is a necessity.

Gastrointestinal Motility

The alimentary canal's physiology and motility play a key role in determining the fate of a drug delivery system. The specific state of the digestive system poses particular obstacles in allowing the therapeutic to be delivered as engineered. In developing site-specific delivery systems, one must take into consideration both the physiology and motility to better design the dosage form. After passing through the mouth and esophagus, the delivery system enters the stomach. The stomach is composed of three distinct muscular components, the fundus, the antrum, and the pylorus, and its primary

function is to mix and grind food up into small enough particles to pass through the pylorus (2).

The fundus is composed of three layers of muscle—inner circular layer, outer circular layer, and outermost oblique layer—which relax upon the entry of food and contract to force the food towards the antrum region. Through phases and contractile activity, the antrum functions both as a pump and a grinding mill. The pylorus possesses the ability to restrict the exit of liquids, prevent the passage of large particles, and close completely during the antral stroke. Once passing through the pylorus sphincter into the duodenum, the contents of the GI tract can be subjected to propagated bursts of contractions that often occur in association with propagated antropyloric pressure waves as the antroduodenal emptying stroke, isolated contractions, or retroperistaltic contractions that return the contents back into the stomach. The major motility function of the duodenum area is to further move the contents and the emptied gastric chyme downstream and is the site where the major digestive processes occur. The stomach and the duodenum work in a closely integrated fashion to control gastric emptying that is suitable for the person's physiological and emotional state.

Intestinal motility (small and large) is a broad generalization that refers to intraluminal flow, the motions of the wall that cause this flow, and the control systems that regulate these wall motions (28). The two muscle layers responsible for most of the motions associated with movement are the outer longitudinal and the inner circular muscle layers. The epithelium layers consist of the various types of cells lining the intestinal lumen including enterocytes and goblet cells, the cells responsible for absorption and mucus secretion, respectively. The small intestine moves its contents caudally with accompanying stirring and mixing. The two wall contractions responsible for the motility are ring contractions and sleeve contractions. Ring contractions are the

type of muscle movement most often associated with intestinal transit. The rings begin as circumferential indentations and then sweep across the small intestine. The point of inception and distance of movement is controlled by both the nervous system and hormones, reflecting the digestive needs of the luminal contents. These contractions are associated with a periodicity at a specific level of the small intestine with a drop in frequency caudally along the intestine. This particular type of contraction is what is often referred to as peristalsis.

Sleeve contractions are responsible for the mixing of the luminal contents by shifting fluid between the inside and outside of the lumen. Both types of major contractions work in a concerted effort to spread and mix the luminal contents across the mucosal surface to achieve maximum absorption. The viscosity of a suspension in the lumen has an effect on its GI transit due to its greater inertial ability to resist propulsive contractions (2). Therefore, a dosage form with a high viscosity has the capability of increasing the residence time of the therapeutic. To further enhance the intimate contact of the dosage form with the absorption site, the delivery system can be engineered with molecular characteristics capable of achieving greater bioadhesion, specifically mucoadhesion.

Mucous Gel Layer

The mucous gel layer, the target site for mucoadhesion, serves to protect and lubricate epithelial surfaces such as those of the gastrointestinal, respiratory, and urogenital tracts while still allowing specific interactions to occur by means of their complex structure (29). Mucins are filamentous glycoproteins that are the major component of the mucus that lines most hollow organs of the body and those organs that come into contact with exogenous environments. The family of mucin biopolymers is characterized by a protein backbone that consists of tandem repeat units of peptide

sequences, typically serine- and threonine-rich, which contain *O*-linked glycans (30). There are currently 17 different mucins (Table 2.1) all of which contain extended domains of the variable number of tandem repeats (VNTR), which are serine-, threonine-, and/or proline-rich (STP-rich regions). There are two structurally and functionally distinct classes of mucins which can either be classified as secreted gel-forming mucins or transmembrane mucins (31).

Secretory mucins such as MUC2, MUC5AC, MUC5B, MUC6, MUC7, and MUC8 are secreted by the goblet cells and receive extensive *O*-glycosylation in the *cis* to *trans* Golgi of the cell. These mucins have the capability to polymerize through disulfide bond linkages formed between the cysteine residues found in the von Willebrand factor (VWF)-like D domains (32). *O*-glycosylation begins in the *cis* Golgi and is completed after passing through the *trans* Golgi after which a significant increase occurs in the biopolymer's apparent molecular weight (30). The non-tandem repeating regions of MUC2 have over an 8% cysteine content which are positioned at the ends of the proteins and form dimers in the endoplasmic reticulum of the goblet cells. Along with glycosylation, polymerization occurs in the *cis* to *trans* compartments of the Golgi. Polymerization of the biopolymers begins with tail-to-tail dimerization at the C-terminal followed by head-to-head multimerization at the N-terminals (33).

The gel layer can be divided into one that is loosely adhered and one that is firmly adhered. The firmly adhered is composed of the membrane mucins and is approximately 20 μm in upper small intestine for rats. The loosely adhered mucus is composed of the secreted mucins such as MUC2 and MUC3. This gel layer is approximately 150 μm in the upper small intestine for rats (34). The mean turnover time of the mucous gel layer has been shown to vary between 47 and 270 min, which would indicate a significant factor in designing mucoadhesive drug delivery systems (35). The mucous gel layer

itself represents an unstirred water layer which impedes drug diffusion and adsorption across the epithelium.

MUC2 and MUC3 mucin mRNAs are prominently expressed in the small intestine, the most favorable site for orally delivered therapeutic absorption. The goblet cells are responsible for the MUC2 synthesis, whereas the enterocytes produce MUC3 (36). MUC2 is also the prominent mucin in the large intestine; therefore, its structure and functionality play a key role in the successful development of mucoadhesive drug delivery systems. The biopolymer MUC2 has a molecular weight of approximately 3,000 kDa (37) and is responsible for the formation of the viscoelastic gel (38) that covers the lumen of the small and large intestine. The protein backbone consists of over 4,500 residues which can be divided into three major structural domains: tandem repeat array, carboxyl-terminal domain, and amino-terminal domain.

Taking into consideration the steric constraints imposed by a relatively heavily *O*-glycosylated tandem repeat array domain, the mucin molecules are rigid and extended, taking on a filamentous structure (39). The other two domains are non-glycosylated and cysteine-rich which provide the groups necessary for disulfide bond formation and mucin polymerization. The mucus that is formed by multimers of MUC2 protects the underlying epithelial cells along the digestive tract from the acidic and proteolytic environment presented by the lumen, the shear forces naturally exerted during the digestive process, and the microorganisms and bacteria responsible for infections and disease. The gel-forming capabilities are directly affected by proteolytic degradation or mercaptoethanol reduction, signifying the importance of the presence of disulfide bonds and biopolymerization on the formation and stability of the gel layer (40). The mucous gel layer can be considered a loosely, physically entangled, biopolymeric network which is weakly viscoelastic in nature.

Recent Developments

Tethered Surfaces

The mucous gel network serves as a target for mucoadhesive biomaterials composed of polymer chains with the ability to interpenetrate and bridge the interface between the drug carrier and the mucus (19, 41). Polymer chains available at the surface of the biomaterial are often employed to serve as adhesion promoters (42-45). With the polymer chains at the periphery of the delivery system, they are able to develop an intimate contact with the mucous gel layer, diffuse across the interface, and form entanglements with the mucous gel layer. Once across the polymer/gel boundary, further non-covalent mechanisms can occur to strengthen the bond. The enhanced bridging is a result of further chain entanglement, secondary bonding, or electrostatic interactions. For further enhancement of the adhesive bond formed between a delivery system and the mucous gel layer, tethered polymers, both anionic and cationic, can be used to create a synergistic effect in developing a more effective mucoadhesive delivery system (46-49).

Polymer chains with one of their ends tethered onto a surface have found uses in a wide variety of applications such as surface energy enhancement (wetting), colloidal stability, biocompatibility, and adhesion (50-52). The pioneering work on the conformation of tethered polymers (Figure 2.4) was developed by de Gennes (51). The thickness of the polymer layer was shown to be dependent on the surface coverage, σ , of the chains, and either a mushroom or a stretched configuration is developed when in the low or high surface coverage regime, respectively. The thickness of the layer is directly proportional to the degree of polymerization and the width of the monomer (Figure 2.5).

Brochard-Wyart et al. (50) further elucidated on the role of grafted chains as adhesion promoters and provided evidence of maximum adhesion enhancement at an intermediate surface coverage (Figures 2.6-2.8). These results provided evidence that

polymers attached to a surface take on three distinct regimes: separate mushrooms, overlapping mushrooms, and partial interdigitation. The intermediate regime provides the greatest adhesion energy due to a higher percentage of chains participating in interdigitation.

The theory surrounding polymers attached to hydrogels was further developed in our laboratory by Huang et al. (48, 49) and included systems composed of two hydrogels such as those involved with the process of mucoadhesion. This theoretical framework provided evidence of the probability of finding both the chains and the free end segment outside the base gel available for interpenetration. Both were dependent on the surface coverage of the polymer tethers, with a large number of the chains and free ends present outside the base gel at low and intermediate coverage. However, at high coverages the chains penetrated back into the base gel due to the intermolecular interactions between neighboring chains. Adhesion enhancement associated with the base and target gel (mucus layer) was also shown to be maximized at an intermediate coverage. Therefore, in designing biomaterials for mucoadhesive applications, the surface coverage of grafted polymer chains can be controlled to achieve adhesion enhancement through polymer-gel interpenetration (53).

Thiomers

Thiolated polymers, or thiomers, have received considerable attention as potential mucoadhesive polymers (54). The list of thiol-bearing polymers includes chitosan-cysteine, chitosan-thiobutylamidine, chitosan-thioglycolic acid, poly(acrylic acid)-cysteine, poly(acrylic acid)-cysteamine, carboxy-methylcellulose-cysteine, and alginate cysteine. The nature of their action differs as compared to PEG adhesion promoters in that a covalent disulfide bond is formed between the cysteine residues on the mucin backbone and the free thiols along the mucoadhesive polymer backbone. This provides a

stronger bond as compared to the formation of weak non-covalent bonds such as hydrogen bonds, van der Waals forces, and electrostatic interactions. These thiomers have the ability to mimic what naturally occurs in the secretion of the mucous gel layer where oligomers of mucins are joined by disulfide bonds.

Cationic thiomers have largely been thiolated chitosan whereas anionic thiomers exhibit carboxylic groups as the anionic moieties. The reactions typically employ carbodiimide chemistry to form an amide bond between the primary amino group of the chitosan and the carboxylic acid group of the attached ligand, or the reverse for anionic polymers. Stability of the free thiol is maintained through an inert environment or a lowered pH. At a $\text{pH} < 5$, the number of thiolate anions is significantly reduced, thereby decreasing the oxidation of the thiol groups. Ellman's agent can be used to determine the amount of thiol groups present on the polymers backbone.

The interaction between the thiomers and mucin molecules can be attributed to the formation of a disulfide bond which occurs through either a thiol/disulfide exchange reaction or through the oxidation process of free thiols. Mucins covering the surfaces of the body typically all possess cysteine-rich subdomains along the mucin backbone which are free of *O*-glycosylation, allowing for interaction between other mucins and thiomers to occur. Disulfide bond formation is largely dependent on thiolate anion concentration. The anion concentration is further dependant on the pK_a of the thiol group, the pH of the thiomers (microclimate), and the pH of the surrounding medium.

Biopolymers

Biopolymers include polymers that are found in nature such as chitosan, alginates, and lectins, to name a few. Chitosan (Figure 2.10) has been used as a bioadhesive due to its ability to bind mucin through both i) electrostatic forces between the positively charged amine and the charged acidic groups of sialic acid and sulphonated residues and

ii) hydrophobic forces between the acetyl groups and fucose residues (55). Chitosan coated microparticles have been shown to adhere well to the intestine of animals when administered intraduodenally to rats, and the system maintained the plasma concentration for an extended period of time (56). Other polysaccharides can be found widely in the literature for their use as mucoadhesives, but their interactions are based on hydrogen bonding with their sedimentation ratios being close to unity. This sedimentation ratio indicates that there is little to no interaction on the molecular level between these other polysaccharides and mucin (55).

Lectins, plant proteins that bind specifically to carbohydrate groups found on mucins and cell membranes, have been introduced as a way to circumvent the problems associated with non-specific binding of the first generation bioadhesives to sloughed mucus or other components present in the gastrointestinal tract (57-59). Binding affinity relies heavily upon the conformation the lectin takes which can be significantly affected by the immobilization procedure and the application environment. Biomimetic mucoadhesive drug delivery systems have further evolved to employ fimbriae, long filamentous protein projections found on the surface of bacteria, as specific mucin binding moieties (60).

TISSUE ENGINEERING

Biomaterials (polymers, ceramics or metals) have made significant advances in the treatment of damaged tissue and organs and organ dysfunction. They have the capacity to restore biological function while maintaining compatibility with the surrounding biological environment (biocompatibility). The complexity and number of variables involved in achieving success with the usage of biomaterials has limited the understanding to a generalized scale without focusing on the fundamental mechanisms. An objective of recent biomaterial development has been to interact with the biological

environment more specifically as opposed to non-specific interactions based on the generalized properties such as cell's negative surface charge and common characteristics of the extracellular matrix.

The use of biomimetic materials, materials that mimic a biological environment to elicit a desired cellular response, provides a means to obtain specific interactions (61). One of the critical steps in achieving success with the application of a biomaterial is cytoadhesion. The critical processes involved with cell adhesion include cell attachment, cell spreading, organization of an actin cytoskeleton, and formation of focal adhesions. Cellular adhesion, more specifically cell attachment, can be made more effective through the deployment of ligands that interact specifically with integrins (receptors present at the surface of a cell) present in the environment where the biomaterial is applied (62-64). One of the more commonly used approaches is the attachment of an RGD (Arg-Gly-Asp, Arginine-Glycine-Aspartic acid) peptide to the biomaterial surface to enhance cell adhesion by targeting the integrin receptors on a cell's surface (64).

Biomaterial surface modifications are not limited to ligand-integrin receptor mediated adhesion. Heparin-binding peptides and lectins have also been used to increase cell attachment. Proteoglycans are the targets for the heparin-binding peptides whereas the carbohydrate-rich glycocalyx serves as the binding target for lectins. As the knowledge of the processes involved with cellular adhesion is increased, more effective biomaterials can be developed which provide the necessary surface characteristics to promote adhesion. More effective cellular adhesion will aid in a biomaterial's success which will result in better treatments for diseases and increased quality of life for these patients.

ADHESION OF MICROBES AND PATHOGENS

The fundamental understanding of how microorganisms are able to adhere to materials has a broad impact that ranges from having the ability to effectively clean contaminated soil, developing materials resistant to biofouling, and preventing inflammation and rejection due to biofilms formed on a biomedical implant's surface. Just as in the case of a bioadhesive polymer, the surface characteristics of the bacterium, the bacterium/material interface, and the surface characteristics play a pivotal role in determining whether or not a bacterium is capable of initial attachment.

Forces responsible for this initial attachment can be attributed to electrostatic forces, van der Waals, hydrophobic, water movement, or other specific interactions. Factors such as the residence time, loading force, pH, and ionic strength have been shown to be important in the adhesion of microbes to surfaces (65). Atomic force microscopy (AFM) has provided valuable information regarding molecular-level interactions between microbial and material surfaces through the use of novel biopolymer immobilization techniques such as biopolymer-coupled-carboxylated dextrans (66). Entire bacteria have been immobilized to glass to study the effect of pH on the surface polymer's conformation which drives the ability of the microbe to adhere to a surface (67).

Developing a fundamental understanding of the receptor/binding molecule interaction has implications in understanding how diseases are spread. Human-to-human virus transmission of certain strains of influenza, or the lack thereof, can be linked to the binding preference of the virus to certain carbohydrates present on epithelium surfaces. Human and avian influenza viruses bind specific sialic acids linked to galactose through an α -2,6 or an α -2,3 linkage, respectively (68). The reason why widespread transmission of this virus from infected avian populations to human ones has not occurred can be attributed to this subtle binding preference.

FUTURE DIRECTIONS AND CONCLUSIONS

The field of bioadhesion is one that is rapidly evolving to aid in the development of materials that are capable of more effective drug delivery, enhanced disease treatment, and the prevention and understanding of disease transmission. Biomimetic materials are quickly replacing those first-generation materials that relied heavily on the non-specific interactions they had with the natural tissue. Drug delivery systems are employing nature's method of covalent bond formation (thiomers) and specific interactions (lectins) through carefully designed surfaces (tethered surfaces). Tissue engineering matrices are incorporating macromolecules that the body is capable of recognizing and utilizing in the rehabilitation of organ dysfunction and failure. Some disease transmissions can be attributed to the ability of a microorganism or pathogen to adhere to an epithelial surface, and the fundamental understanding of this binding event could lead to more effective ways of prevention and treatment.

Successfully engineered materials for bioadhesive applications, or the prevention of bioadhesion in some instances, will continue to incorporate biologically relevant moieties to aid in their effective use by the biological host. Carbohydrates and their role in cell-cell and cell-matrix interactions are becoming increasingly important, and both the incorporation of carbohydrate structures and their binding molecules will be crucial for the success of biomedical devices (69).

REFERENCES

1. Zisman WA, *Influence of Constitution on Adhesion*, in *Handbook of Adhesives*, Skeist I, Editor. 1977, Van Nostrand Reinhold Company: New York, NY. p. 33-66.
2. Chickering DE and Mathiowitz E, *Definitions, Mechanisms, and Theories of Bioadhesion*, in *Bioadhesive Drug Delivery Systems: Fundamentals, Novel Approaches, and Development*, Mathiowitz E, Chickering DE, and Lehr CM, Editors. 1999, Marcel Dekker, Inc.: New York, NY. p. 1-10.
3. Junginger HE, Thanou M, and Verhoef JC, *Mucoadhesive Hydrogels in Drug Delivery*, in *Encyclopedia of Pharmaceutical Technology*, Swarbrick J and Boylan JC, Editors. 2002, Marcel Dekker, Inc.: New York, NY. p. 1848-1863.
4. Lee JW, Park JH, and Robinson JR, Bioadhesive-based dosage forms: The next generation, *J. Pharm. Sci.*, 89:850-866, 2000.
5. Peppas NA and Buri PA, Surface, Interfacial and Molecular Aspects of Polymer Bioadhesion on Soft Tissues, *J. Control. Release*, 2:257-275, 1985.
6. Peppas NA, Little MD, and Huang Y, *Bioadhesive Controlled Release Systems*, in *Handbook of Pharmaceutical Controlled Release Technology*, Wise DL, Editor. 2000, Marcel Dekker, Inc.: New York, NY. p. 255-269.
7. Smart JD, Recent developments in the use of bioadhesive systems for delivery of drugs to the oral cavity, *Crit. Rev. Ther. Drug Carr. Syst.*, 21:319-344, 2004.
8. Smith DC, *Adhesives and Sealants*, in *Biomaterials Science: An Introduction to Materials in Medicine*, Ratner BD, Hoffman AS, Schoen FJ, and Lemons JE, Editors. 2004, Academic Press: San Diego, CA. p. 572-583.
9. Hubbell JA, Biomaterials In Tissue Engineering, *Bio-Technology*, 13:565-576, 1995.
10. Kast CE, Frick W, Losert U, and Bernkop-Schnurch A, Chitosan-thioglycolic acid conjugate: a new scaffold material for tissue engineering? *Int. J. Pharm.*, 256:183-189, 2003.
11. Reyes CD and Garcia AJ, Engineering integrin-specific surfaces with a triple-helical collagen-mimetic peptide, *J. Biomed. Mater. Res. Part A*, 65A:511-523, 2003.
12. Derjaguin BV, Aleinikova IN, and Toporov YP, On The Role Of Electrostatic Forces In The Adhesion Of Polymer Particles To Solid-Surfaces, *Prog. Surf. Sci.*, 45:119-123, 1994.
13. Gu JM, Robinson JR, and Leung SHS, Binding Of Acrylic Polymers To Mucin Epithelial Surfaces - Structure-Property Relationships, *Crit. Rev. Ther. Drug Carr. Syst.*, 5:21-67, 1988.

14. Mikos AG and Peppas NA, Measurement Of The Surface-Tension Of Mucin Solutions, *Int. J. Pharm.*, 53:1-5, 1989.
15. Kaelble DH and Moacanin J, Surface-Energy Analysis Of Bioadhesion, *Polymer*, 18:475-482, 1977.
16. Lehr CM, Bodde HE, Bouwstra JA, and Junginger HE, A Surface-Energy Analysis Of Mucoadhesion.2. Prediction Of Mucoadhesive Performance By Spreading Coefficients, *Eur. J. Pharm. Sci.*, 1:19-30, 1993.
17. Lehr CM, Bouwstra JA, Bodde HE, and Junginger HE, A Surface-Energy Analysis Of Mucoadhesion - Contact-Angle Measurements On Polycarbophil And Pig Intestinal-Mucosa In Physiologically Relevant Fluids, *Pharm. Res.*, 9:70-75, 1992.
18. Peppas NA and Sahlin JJ, Hydrogels as mucoadhesive and bioadhesive materials: A review, *Biomaterials*, 17:1553-1561, 1996.
19. Ponchel G, Touchard F, Wouessidjewe D, Duchene D, and Peppas NA, Bioadhesive Analysis Of Controlled-Release Systems.3. Bioadhesive And Release Behavior Of Metronidazole-Containing Poly(Acrylic Acid)-Hydroxypropyl Methylcellulose Systems, *Int. J. Pharm.*, 38:65-70, 1987.
20. Dodou D, Breedveld P, and Wieringa PA, Mucoadhesives in the gastrointestinal tract: revisiting the literature for novel applications, *Eur. J. Pharm. Biopharm.*, 60:1-16, 2005.
21. Davis SS, Formulation strategies for absorption windows, *Drug Discov. Today*, 10:249-257, 2005.
22. Hou SYE, Cowles VE, and Berner B, Gastric retentive dosage forms: A review, *Crit. Rev. Ther. Drug Carr. Syst.*, 20:461-497, 2003.
23. Talukder R and Fassihi R, Gastroretentive delivery systems: A mini review, *Drug Dev. Ind. Pharm.*, 30:1019-1028, 2004.
24. Decuzzi P, Lee S, Decuzzi M, and Ferrari M, Adhesion of microfabricated particles on vascular endothelium: A parametric analysis, *Ann. Biomed. Eng.*, 32:793-802, 2004.
25. Ishida M, Machida Y, Nambu N, and Nagai T, Pharmaceutical Interactions In Dosage Forms And Processing.21. New Mucosal Dosage Form Of Insulin, *Chem. Pharm. Bull.*, 29:810-816, 1981.
26. Nagai T and Machida Y, Advances In Drug Delivery - Mucosal Adhesive Dosage Forms, *Pharm. Int.*, 6:196-200, 1985.
27. Smart JD, The basics and underlying mechanisms of mucoadhesion, *Adv. Drug Deliv. Rev.*, 57:1556-1568, 2005.
28. Christensen J, *Motility of the intestine*, in *Gastrointestinal Disease: Pathophysiology/Diagnosis/Management*, Sleisenger MH and Fordtran JS, Editors. 1993, W.B. Saunders Co.: Philadelphia, PA. p. 822-837.

29. Dekker J, Rossen JWA, Buller HA, and Einerhand AWC, The MUC family: an obituary, *Trends Biochem.Sci.*, 27:126-131, 2002.
30. Baldus SE, Engelmann K, and Hanisch FG, MUC1 and the MUCs: A family of human mucins with impact in cancer biology, *Crit. Rev. Clin. Lab. Sci.*, 41:189-231, 2004.
31. Williams SJ, Wreschner DH, Tran M, Eyre HJ, Sutherland GR, and McGuckin MA, MUC13, a novel human cell surface mucin expressed by epithelial and hemopoietic cells, *J. Biol. Chem.*, 276:18327-18336, 2001.
32. Moncada DM, Kammanadiminti SJ, and Chadee K, Mucin and Toll-like receptors in host defense against intestinal parasites, *Trends Parasitol.*, 19:305-311, 2003.
33. Gum JR, Human mucin glycoproteins: Varied structures predict diverse properties and specific functions, *Biochem. Soc. Trans.*, 23:795-799, 1995.
34. Atuma C, Strugala V, Allen A, and Holm L, The adherent gastrointestinal mucus gel layer: thickness and physical state in vivo, *Am. J. Physiol.-Gastroint. Liver Physiol.*, 280:G922-G929, 2001.
35. Lehr CM, Poelma FGJ, Junginger HE, and Tukker JJ, An Estimate Of Turnover Time Of Intestinal Mucus Gel Layer In The Rat Insitu Loop, *Int. J. Pharm.*, 70:235-240, 1991.
36. vanKlinken BJW, Dekker J, Buller HA, DeBolos C, and Einerhand AWC, Biosynthesis of mucins (MUC2-6) along the longitudinal axis of the human gastrointestinal tract, *Am. J. Physiol.-Gastroint. Liver Physiol.*, 36:G296-G302, 1997.
37. Vanklinken BJW, Dekker J, Buller HA, and Einerhand AWC, Mucin Gene Structure And Expression - Protection Vs Adhesion, *Am. J. Physiol.-Gastroint. Liver Physiol.*, 32:G613-G627, 1995.
38. Sellers LA, Allen A, Morris ER, and Rossmurphy SB, Mucus Glycoprotein Gels - Role Of Glycoprotein Polymeric Structure And Carbohydrate Side-Chains In Gel-Formation, *Carbohydr. Res.*, 178:93-110, 1988.
39. Gum JR, Hicks JW, Toribara NW, Rothe EM, Lagace RE, and Kim YS, The Human Muc2 Intestinal Mucin Has Cysteine-Rich Subdomains Located Both Upstream And Downstream Of Its Central Repetitive Region, *J. Biol. Chem.*, 267:21375-21383, 1992.
40. Allen A, Hutton DA, Pearson JP, and Sellers LA, Mucus Glycoprotein Structure, Gel Formation And Gastrointestinal Mucus Function, *Ciba Foundation Symp.*, 109:137-156, 1984.
41. Jabbari E, Wisniewski N, and Peppas NA, Evidence Of Mucoadhesion By Chain Interpenetration At A Poly(Acrylic Acid) Mucin Interface Using Atr-Ftir Spectroscopy, *J. Control. Release*, 26:99-108, 1993.

42. De Ascentiis A, Degrazia JL, Bowman CN, Colombo P, and Peppas NA, Mucoadhesion Of Poly(2-Hydroxyethyl Methacrylate) Is Improved When Linear Poly(Ethylene Oxide) Chains Are Added To The Polymer Network, *J. Control. Release*, 33:197-201, 1995.
43. Peppas NA, Molecular calculations of poly(ethyleneglycol) transport across a swollen poly(acrylic acid) mucin interface, *J. Biomater. Sci.-Polym. Ed.*, 9:535-542, 1998.
44. Peppas NA and Mongia NK, Ultrapure poly(vinyl alcohol) hydrogels with mucoadhesive drug delivery characteristics, *Eur. J. Pharm. Biopharm.*, 43:51-58, 1997.
45. Sahlin JJ and Peppas NA, Enhanced hydrogel adhesion by polymer interdiffusion: Use of linear poly(ethylene glycol) as an adhesion promoter, *J. Biomater. Sci.-Polym. Ed.*, 8:421-436, 1997.
46. Efremova NV, Huang Y, Peppas NA, and Leckband DE, Direct measurement of interactions between tethered poly(ethylene glycol) chains and adsorbed mucin layers, *Langmuir*, 18:836-845, 2002.
47. Huang YB, Leobandung W, Foss A, and Peppas NA, Molecular aspects of muco- and bioadhesion: Tethered structures and site-specific surfaces, *J. Control. Release*, 65:63-71, 2000.
48. Huang YB, Szleifer I, and Peppas NA, Gel-gel adhesion by tethered polymers, *J. Chem. Phys.*, 114:3809-3816, 2001.
49. Huang YB, Szleifer I, and Peppas NA, A molecular theory of polymer gels, *Macromolecules*, 35:1373-1380, 2002.
50. Brochardwyart F, Degennes PG, Leger L, Marciano Y, and Raphael E, Adhesion Promoters, *J. Phys. Chem.*, 98:9405-9410, 1994.
51. Degennes PG, Conformations Of Polymers Attached To An Interface, *Macromolecules*, 13:1069-1075, 1980.
52. Leger L, Raphael E, and Hervet H, *Surface-anchored polymer chains: Their role in adhesion and friction*, in *Polymers In Confined Environments*. 1999. p. 185-225.
53. Serra L, Doménech J, and Peppas NA, Design of poly(ethylene glycol)-tethered copolymers as novel mucoadhesive drug delivery systems, *Eur. J. Pharm. Biopharm*, 63:11-18, 2006.
54. Bernkop-Schnurch A, Thiomers: A new generation of mucoadhesive polymers, *Adv. Drug Deliv. Rev.*, 57:1569-1582, 2005.
55. Harding SE, *Analysis of polysaccharides by ultracentrifugation. Size, conformation and interactions in solution*, in *Polysaccharides 1: Structure, Characterization And Use*. 2005. p. 211-254.

56. Takishima J, Onishi H, and Machida Y, Prolonged intestinal absorption of cephadrine with chitosan-coated ethylcellulose microparticles in rats, *Biol. Pharmacol. Bull.*, 25:1498-1502, 2002.
57. Lehr CM, Lectin-mediated drug delivery: The second generation of bioadhesives, *J. Control. Release*, 65:19-29, 2000.
58. Lehr CM, Bouwstra JA, Kok W, Noach ABJ, Deboer AG, and Junginger HE, Bioadhesion By Means Of Specific Binding Of Tomato Lectin, *Pharm. Res.*, 9:547-553, 1992.
59. Bies C, Lehr CM, and Woodley JF, Lectin-mediated drug targeting: history and applications, *Adv. Drug Deliv. Rev.*, 56:425-435, 2004.
60. Caston A, Davis S, and Williams P, The potential of fimbrial proteins for delaying intestinal transit of oral drug delivery system, *Proceed. Intern. Symp. Controlled Release Bio. Mat.*, 17:313-314, 1990.
61. Drotleff S, Lungwitz U, Breunig M, Dennis A, Blunk T, Tessmar J, and Gopferich A, Biomimetic polymers in pharmaceutical and biomedical sciences, *Eur. J. Pharm. Biopharm.*, 58:385-407, 2004.
62. Mann BK, Schmedlen RH, and West JL, Tethered-TGF-beta increases extracellular matrix production of vascular smooth muscle cells, *Biomaterials*, 22:439-444, 2001.
63. Mann BK, Tsai AT, Scott-Burden T, and West JL, Modification of surfaces with cell adhesion peptides alters extracellular matrix deposition, *Biomaterials*, 20:2281-2286, 1999.
64. Ruoslahti E and Pierschbacher MD, New Perspectives In Cell-Adhesion - Rgd And Integrins, *Science*, 238:491-497, 1987.
65. Xu LC, Vadillo-Rodriguez V, and Logan BE, Residence time, loading force, pH, and ionic strength affect adhesion forces between colloids and biopolymer-coated surfaces, *Langmuir*, 21:7491-7500, 2005.
66. Stevens MM, Allen S, Davies MC, Roberts CJ, Schacht E, Tendler SJB, VanSteenkiste S, and Williams PM, The development, characterization, and demonstration of a versatile immobilization strategy for biomolecular force measurements, *Langmuir*, 18:6659-6665, 2002.
67. Camesano TA and Logan BE, Probing bacterial electrosteric interactions using atomic force microscopy, *Environ. Sci. Technol.*, 34:3354-3362, 2000.
68. Shinya K, Ebina M, Yamada S, Ono M, Kasai N, and Kawaoka Y, Influenza virus receptors in the human airway, *Nature*, 440:435-436, 2006.
69. Kelm S and Schauer R, *Sialic acids in molecular and cellular interactions*, in *International Review Of Cytology - A Survey Of Cell Biology, Vol 175*. 1997, Academic Press Inc: San Diego. p. 137-240.

Table 2.1 Mucins found in the human body. Adapted from Ref. (30).

Mucin species	Secretory/membraneous (S/M)	Chromosomal localization
MUC2	S	11p15.5
MUC5AC	S	11p15.5
MUC5B	S	11p15.5
MUC6	S	11p15.5
MUC7	S	4q13-21
MUC8	S	12q24.3
MUC1	M,S	1q21
MUC3	M,S	7q22
MUC4	M,S	3q29
MUC11	M	7q22
MUC12	M	7q22
MUC13	M	3q13.3
MUC15	M	11p14.3
MUC16	M	19p13.2
MUC17	M	7q22
MUC20	M	3q29
MUC9	?	1p13

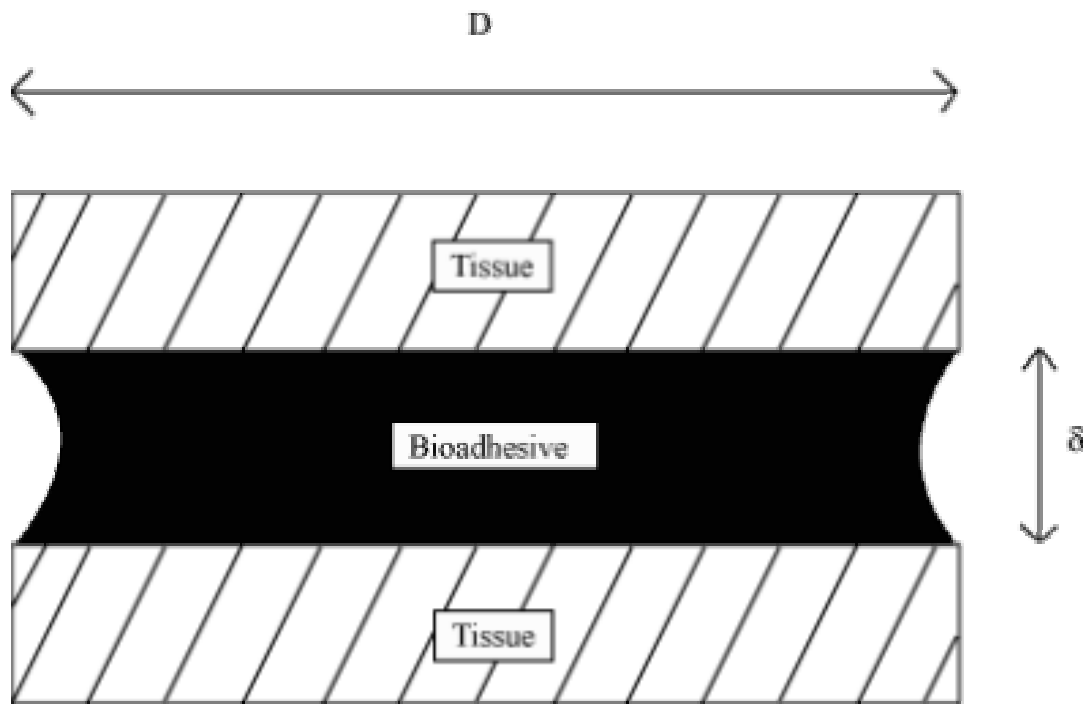


Figure 2.1 Bioadhesion refers to the molecular contact (adherence) of two tissues through the application of a bioadhesive between these two surfaces. Adapted from Ref. (1).

	Base Amino Acid Structure	$\begin{array}{c} \text{H} \\ \\ \text{H}_3\text{N}^+ - \text{C} - \text{C} \begin{array}{l} \text{=O} \\ \text{O}^- \end{array} \\ \\ \text{R1} \end{array}$	
Electrostatic Interactions	R1	$\begin{array}{c} \\ \text{H}_2\text{C} - \text{CH}_2 - \text{CH}_2 - \text{CH}_2 - \text{NH}_3^+ \\ \text{Lys} \end{array}$	$\begin{array}{c} \\ \text{CH}_2 \\ \\ \text{CH}_2 \\ \\ \text{C} \begin{array}{l} \text{=O} \\ \text{O}^- \end{array} \\ \text{Glu} \end{array}$
Dipole-Dipole Interactions		$\begin{array}{c} \delta^- \\ \text{O} \\ \delta^+ \text{C} \\ \\ \text{CH}_2 - \text{NH}_2 \\ \text{Asn} \end{array}$	$\begin{array}{c} \text{H} \delta^- \\ \\ \text{H}_3\text{C} - \text{C} \\ \\ \text{OH} \\ \delta^+ \end{array}$

Figure 2.2 Examples of electrostatic forces occurring between amino acids. These forces are due to (a) the association of two ionic protein groups such as Lysine (Lys) and Glutamic acid (GLU) or (b) the dipole-dipole interactions such as the dipole-induced dipole interaction between Asparagine (Asn) and Threonine (Thr).

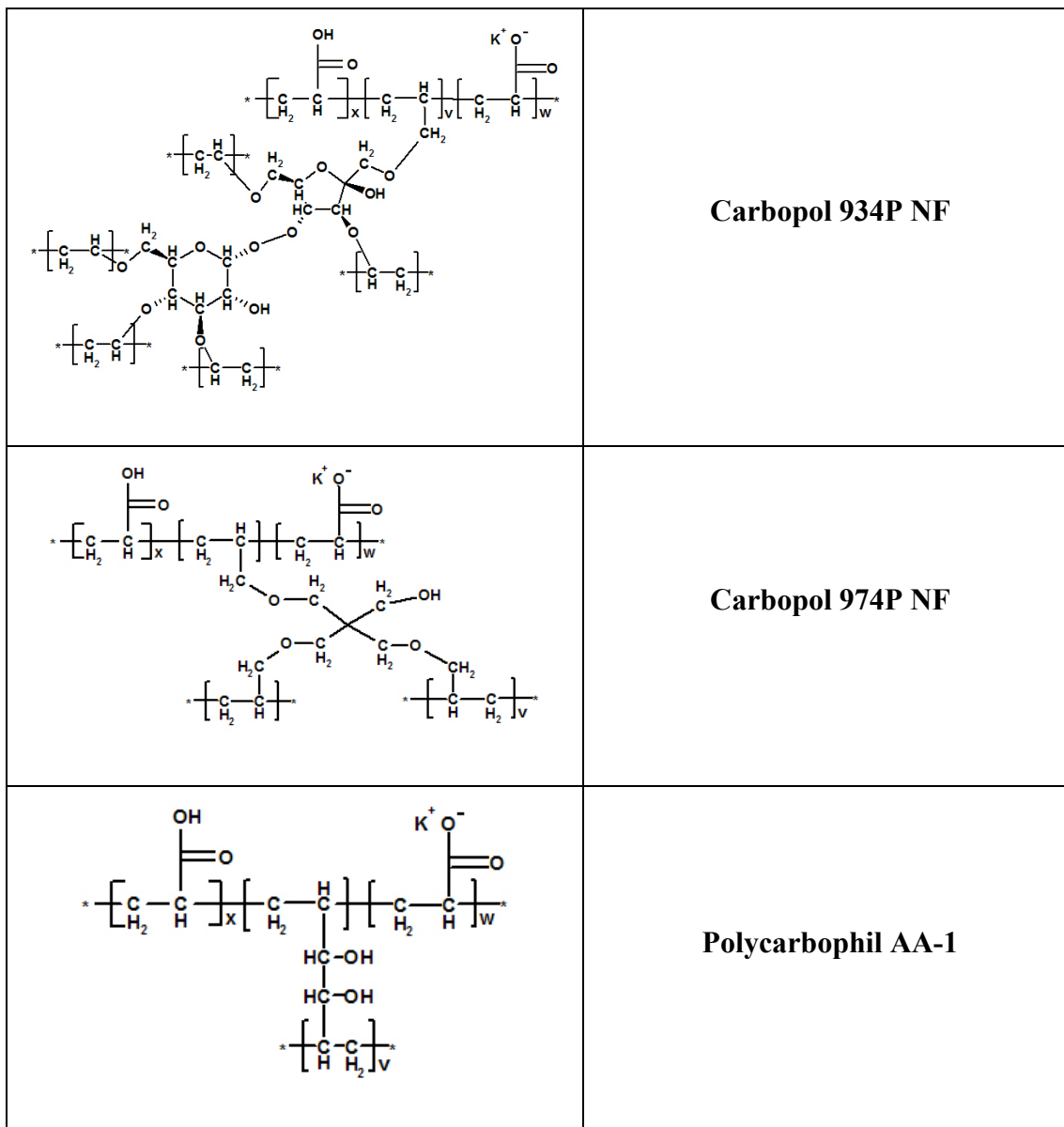


Figure 2.3 Chemical structure of commonly employed poly(acrylic acid)-based materials in mucoadhesive drug delivery systems. 934P is crosslinked with allyl sucrose, 974P with allyl pentaerythritol, and AA-1 with divinyl glycol. A small amount of the acrylic acids are neutralized to potassium acrylate prior to polymerization.

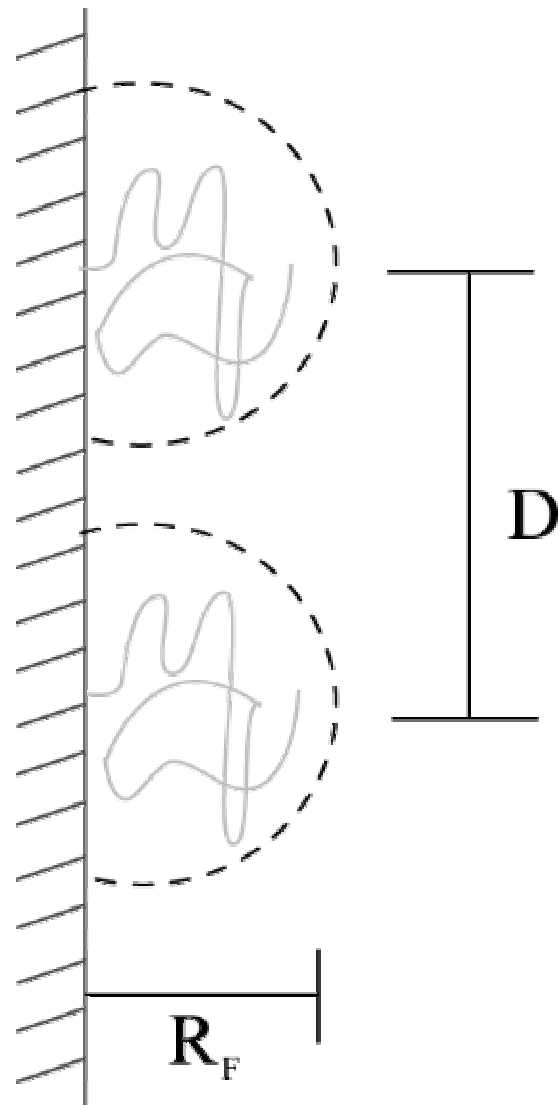


Figure 2.4 Polymer tethers grafted at a low surface coverage ($\sigma \rightarrow 0$) and in a pure solvent. The dashed circle has a diameter which is $2 \times R_F$ (Flory radius). The grafted chains are separated by a distance, D , that is directly proportional to the monomer size (a) and inversely proportional to the square root of the surface coverage (σ). Adapted from Ref. (51).

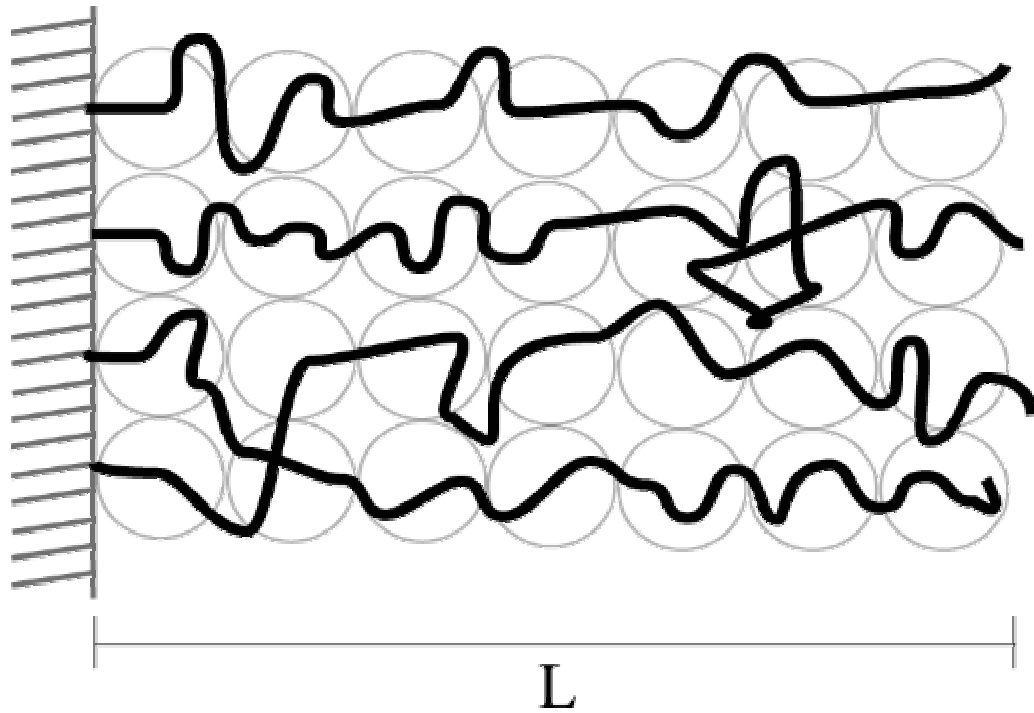


Figure 2.5 Tethered polymers in a good solvent take a strongly stretched conformation, and the thickness of this stretched polymer layer, L , is directly proportional to the degree of polymerization (N), the monomer size (a), and the surface coverage (σ) to the $1/3$ power. Adapted from Ref. (51).

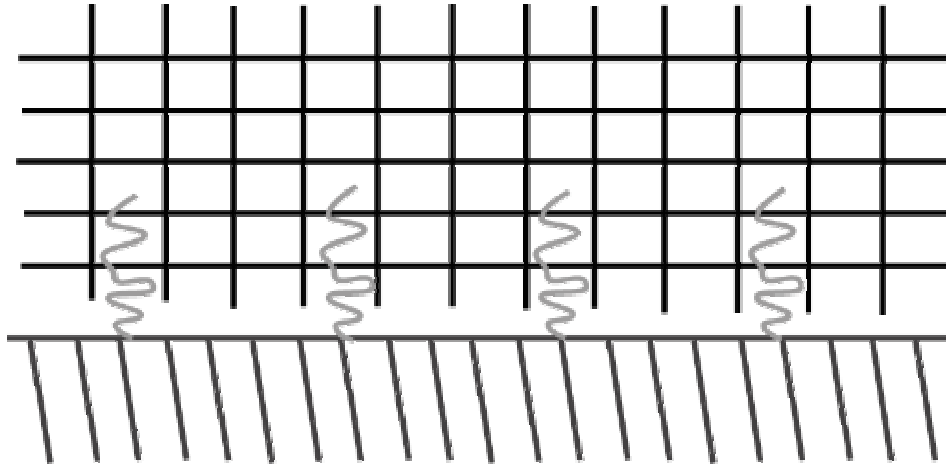


Figure 2.6 Tethered polymers take on distinct conformations when exposed to a crosslinked network. Polymers take on a separate mushroom regime at low surface coverages.

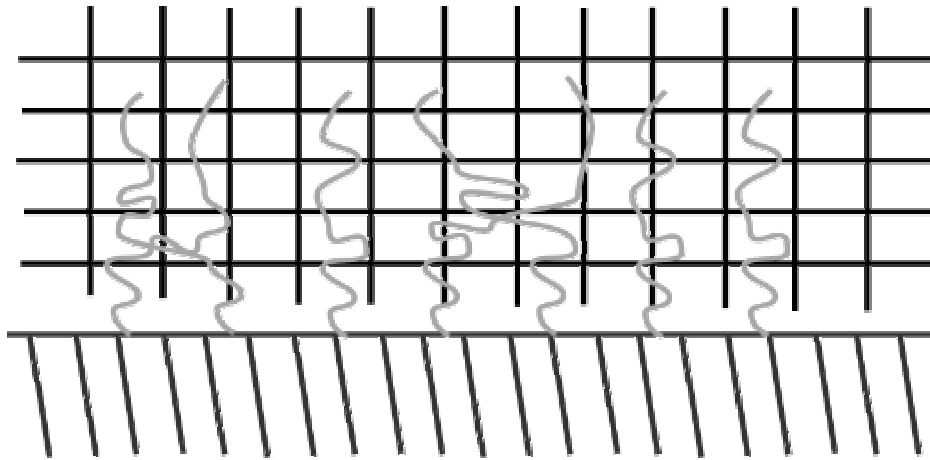


Figure 2.7 At intermediate surface coverages, the tethered polymer layer interpenetrates into the crosslinked polymer with some of the polymers overlapping.

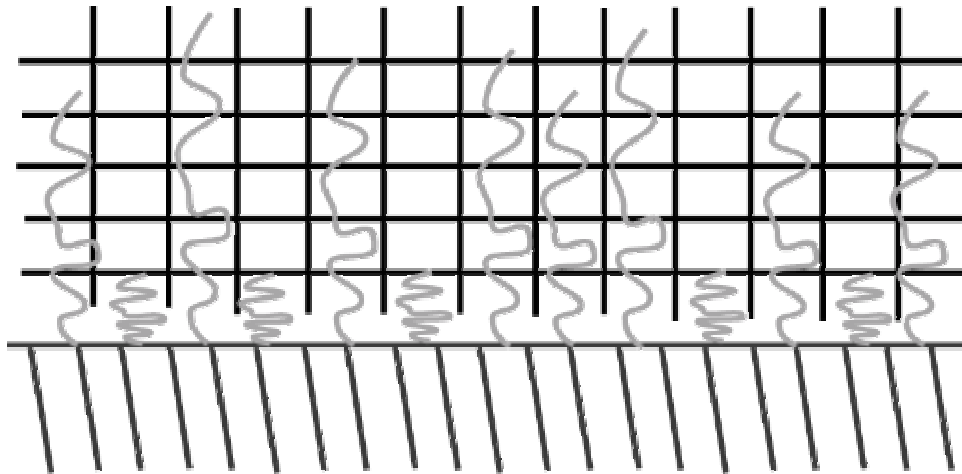


Figure 2.8 At high surface coverages, some polymers interpenetrate into the crosslinked network while others collapse onto the tethered surface resulting in partial interdigitation.

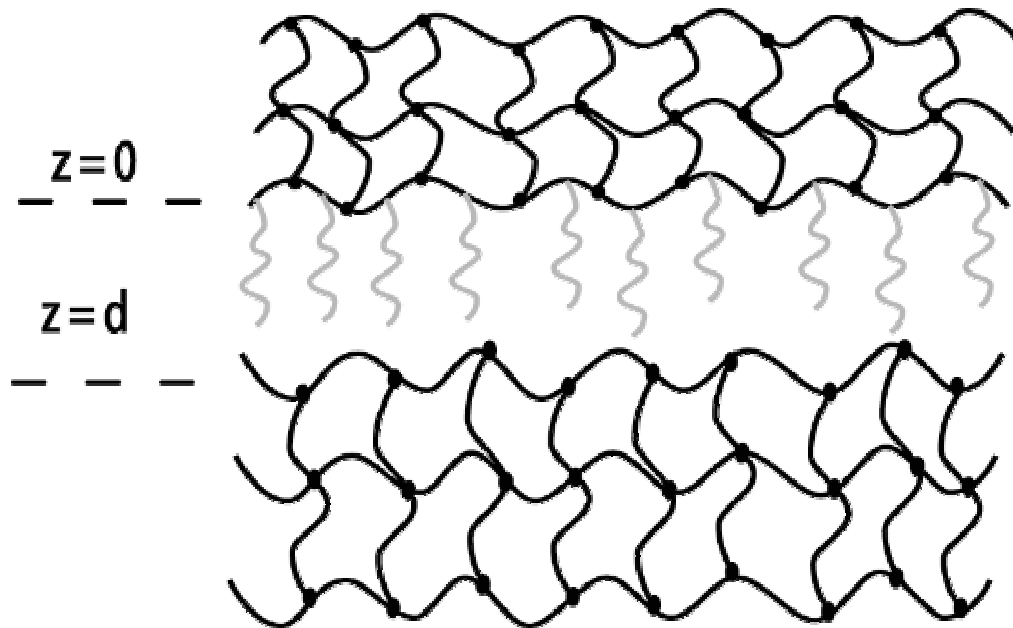


Figure 2.9 The theoretical framework developed in our laboratory by Huang et al. (48) includes the tethered polymers, the base gel to which these polymers are tethered, and the target gel representative of the tissue to be adhered. The position at $z = 0$ represents the base gel surface plane and d is the distance between the two hydrogel networks.

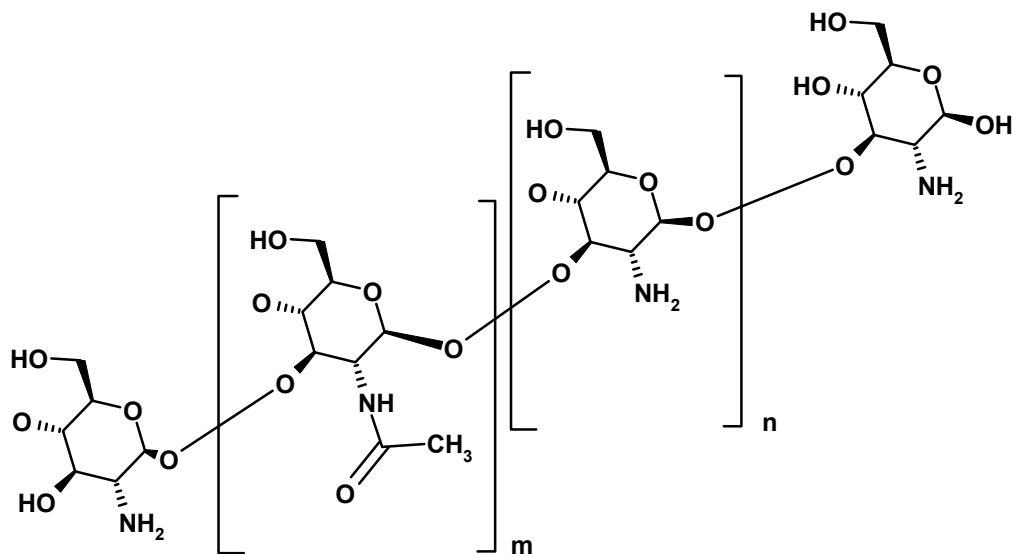


Figure 2.10 Structure of chitosan, which is derived by partially deacetylating chitin. The number of acetyl groups (m) and primary amine groups (n) is controlled through the extent of deacetylation.

Chapter 3: Research Objectives

The main goals of this research were to (a) synthesize polyacid pH responsive biomaterials in the form of microparticles, (b) characterize the physicochemical properties of these materials, (c) synthesize poly(ethylene glycol)-tethered polyacid complexation hydrogel microparticles, (d) characterize the physicochemical properties of these materials, (e) formulate these particles into multifunctional novel minitabket drug delivery systems capable of controlled release and adhesion, and (f) evaluate the gel/gel adhesive characteristics of these materials.

The aim of the study presented in Chapter 4 was to synthesize and characterize polyacid pH responsive biomaterials in the form of microparticles. The objective was to examine if microparticles possessing a stimuli response could be successfully synthesized to meet the requirements necessary for their successful incorporation into a drug delivery system. Methacrylic and acrylic acid were the two monomers that were investigated. The amount of tri-functional crosslinking agent was varied to investigate its effect on the structure and dynamics of the microparticles.

The aim of the study presented in Chapter 5 was to synthesize and characterize PEG-tethered polyacid complexation hydrogels in the form of microparticles. The objective was to examine the effect of the addition of the PEG tether on the synthesis and the dynamics of the materials synthesized. The gel/gel adhesive characteristics of gel suspensions of the hydrogels were elucidated.

The aim of the study presented in Chapter 6 was to formulate these polyacid pH responsive and complexation hydrogels into novel minitabket drug delivery systems. The effect of the monomer type, crosslinking agent, molecular mass of PEG tether, and amount of PEG tether on the release of a model compound were examined. The

parameters necessary for the development of a multifunctional drug delivery system were outlined.

Chapter 4: Synthesis and Properties of Lightly Crosslinked Poly((meth)acrylic acid) Microparticles Prepared by Free Radical Precipitation Polymerization

INTRODUCTION

Poly(carboxylic acid)-containing materials have been investigated for a diverse range of applications such as coatings (1, 2), superabsorbents (3-5), adhesives (6, 7), and drug delivery carriers (8-18). Through the combination of the later two concepts, drug delivery systems (DDS) employing poly(carboxylic acid)-containing hydrogels have the ability to contribute to the development of an adhesive bond between the drug carrier and the biological target of the therapeutic, acting as bioadhesive drug delivery systems (19-24). The prolonged residence time of a therapeutic at the site of administration, whether it is the gastrointestinal or respiratory tract, ocular cavity, or dermal layers, enhances the overall effectiveness of the drug leading to a higher bioavailability. Hydrogels possess the ability to swell upon contact with aqueous solutions due to the hydrophilic nature of the polymers and the presence of either physical or chemical crosslinks. Upon the introduction of ionizable carboxylic acids as pendant groups, the hydrogel network is capable of being triggered by an environmental stimulus such as pH (25-27).

By utilizing the pH shift that occurs as an oral DDS is transported from the acidic environment of the stomach to the near-neutral duodenum and small intestine, both drug release and adhesion can be triggered (28). Micro- and nano-sized devices and systems (29, 30) are desirable for their use in oral drug delivery due to their ability to be formulated into conventional dosage forms and the ease of administration of particle suspensions. For the development of conventional dosage forms such as tablets and capsules, the rate controlling polymer must possess a high degree of compressibility and

be in a particulate state that can be easily formulated with the active pharmaceutical ingredient (API). The synthesis of highly compressible microparticles is desirable to provide a polymeric material that is effectively utilized in these DDS. The integration of these biomaterials into a DDS that utilizes the polymer as a carrier is also facilitated by the synthesis of microparticles.

The aim of this work was to synthesize terpolymer microparticles prepared from pendant carboxylic acid monomers, pendant potassium carboxylate monomers, and a trifunctional pentaerythritol and characterize the polymer's physicochemical properties as a function of monomer and crosslinking agent composition.

MATERIALS AND METHODS

Materials

Methacrylic acid (MAA, inhibited with 250 ppm hydroquinone), anhydrous potassium carbonate (K_2CO_3), and ethyl acetate (EtAc) were obtained from Fisher Scientific and used as received. Acrylic acid (AA, inhibited with 200 ppm hydroquinone) was obtained from Sigma Aldrich (Milwaukee, WI) and was used as received. Allyl pentaerythritol (APE), pentaerythritol triacrylate (PETA), and di(4-tert-butylcyclohexyl) peroxydicarbonate (BCHPC) were kindly supplied by Perstorp Polyols (Toledo, OH), Sartomer (Exton, PA), and Degussa Initiators (Elyria, OH), respectively. All other chemicals were of reagent grade and used as received.

Synthesis

In a typical thermally-initiated free radical precipitation polymerization, (M)AA, K_2CO_3 , and deionized distilled water (ddH₂O) were combined and mixed to form a homogeneous mixture, allowing the escape of the neutralization by-product carbon dioxide. The crosslinking agent, APE or PETA, was dissolved in ethyl acetate. The

monomer mixture and crosslinking agent were added to a four-necked round bottom flask equipped with an overhead stirrer, nitrogen purge, and condenser containing the polymerization solvent EtAc. Following a 20 minute purge with nitrogen, the initiator BCHPC dissolved in the polymerization solvent was added to the vessel and further purged for an additional 10 minutes.

The molecular structures of the monomer, crosslinking agent, and thermal initiator are shown in Figure 4.1. The vessel was placed in a thermostatic bath at 50°C where precipitation was evident in a matter of minutes. The reaction was allowed to proceed for 16 hours to ensure a high percentage of monomer conversion. Following the polymerization, the particle slurry was centrifuged and washed with fresh ethyl acetate and dried using a rotary evaporator at elevated temperature and reduced pressure (90°C/40 mmHg). Table 1 lists the various polymer microparticles prepared.

Characterization

Particle suspensions of the microparticles were prepared using ethyl acetate, and the particle size distribution was determined with a laser light diffraction particle analyzer (Malvern Mastersizer-S, Malvern Instruments Ltd., Worcestershire, UK). The measurement was repeated three times. A scanning electron microscope (SEM, Hitachi Model S-4500, Hitachi Ltd., Tokyo, Japan) was used to obtain SEM photographs. The vacuum-dried polymer microparticles were mounted on an aluminum stage using double-sided carbon conductive tape and coated with gold for 45 seconds with a sputter-coater (Pelco Model 3, Pelco Int., Redding, CA) in an argon atmosphere.

Pellets containing 1 mg of sample and 150 mg of KBr were prepared on a Carver laboratory press using a 15,000 lb compression force. Infrared spectra of the microparticles were obtained in the wavenumber range of 400-4000 cm^{-1} on a Fourier transform infrared spectrophotometer (FT-IR, Thermo Mattson Infinity, Thermo Electron

Corp., Waltham, MA) in transmission mode equipped with a KBr beamsplitter and DTGS detector. Each spectrum is an average of 64 scans at a resolution of 1 cm^{-1} .

The thermal properties of the microparticles were characterized using a differential scanning calorimeter (DSC, MDSC 2920, TA Instruments, New Castle, DE). Approximately 10-15 mg samples were analyzed at a sample rate of $10^{\circ}\text{C}/\text{min}$ over the range of 80°C to 160°C for poly(acrylic acid) and 80°C to 300°C for poly(methacrylic acid) using a heat/cool/heat method to erase the thermal history.

The equilibrium weight swelling ratio of the polymeric hydrogel microparticles was determined by carefully weighing 50 mg of dried particles and combining them with 35 mL of NaHCO_3 solution (1.5 g / 100 mL). The suspension was agitated for 60 min and then centrifuged for 60 min at 2000 rpm, carefully discarding the supernatant. The pellet was resuspended in an additional 35 mL of NaHCO_3 solution and agitated for 60 min. The suspension was centrifuged at 2000 rpm for 60 min, carefully removing the supernatant, and the weight of the gelled mass was determined. This procedure was also carried out in a 0.1 N HCl solution.

Potentiometric titrations were carried out on aqueous solutions of the microparticles. Approximately 400 mg of polymer were slowly added to 400 mL of deionized distilled water. During the polymer addition, the solution was agitated using a three-blade marine style propeller at 1000 rpm. The particles were allowed to agitate and hydrate for 15 minutes before recording the initial pH of the suspension. After a reduction in the agitation speed, titration was performed using a 1 N NaOH solution. The pH was allowed to equilibrate before any further addition was made.

RESULTS AND DISCUSSION

Particle Size and Morphology

All monomers, crosslinking agent, and initiator are soluble in the ethyl acetate polymerization solvent. Upon heating the reaction mixture to the polymerization temperature, oligomers begin to form as outlined in Figure 4.2. As these oligomers grow into polymers, the polymers become insoluble in the solvent. At this point, precipitation is evident and particle formation occurs. Microparticle formation occurs through the continuation of agglomeration of these primary particles. Polymerization of copolymers of PMAA and PAA and the crosslinked terpolymers result in no significant differences in their particle size.

As determined using laser light diffraction, the particle size of both copolymers and terpolymers as suspensions in EtAc results in a $D(v, 0.5)$ of approximately 15 μm and $D(v, 0.9)$ of approximately 30 μm . Particles composed of MAA show significantly different primary particle morphology as can be seen in Figures 4.3 and 4.4. This is due to the additional polymer growth that occurs at the primary particle's surface as opposed to negligible growth upon the PAA surface. Through polymer bridging and crosslinking that occurs within the primary particles of both monomers, the resulting microparticles are physically and chemically inseparable. However, for the copolymers, polymer dissolution is achieved upon polymer neutralization indicating the absence of crosslinking.

FT-IR Spectroscopy of Poly(carboxylic acid) Microparticles

Figure 4.5 shows the IR spectra for both crosslinked PMAA and crosslinked PAA microparticles recorded at ambient temperature in the dried state. Both structures exhibit the characteristic C=O stretching, with the acrylic acid carbonyl stretching occurring at

1710 cm^{-1} and methacrylic acid at about 1715 cm^{-1} . The potassium carboxylate in both materials is represented by the shift in the carbonyl stretching to approximately 1560 cm^{-1} . The stretching of C=O coupled with the bending of O-H is responsible for the peaks occurring in the region between 1180 and 1270 for both crosslinked PMAA and crosslinked PAA (31, 32). The symmetric bending of the CH_3 planar deformation occurs at 1391 cm^{-1} for crosslinked PMAA. The CH_2 deformation bending gives a band about 1456 cm^{-1} for both structures with CH_3 deformation asymmetric bending at about 1488 cm^{-1} . O-H bonded groups give rise to vibration bands at about 2620 cm^{-1} for both materials. CH_2 stretching exhibits bands at about 2948 cm^{-1} , while the spectrum of crosslinked PMAA exhibits the asymmetric vibration of the CH_3 group at 2997 cm^{-1} . The broad region from 3100 to 3500 shows the O-H stretching (3100 cm^{-1}) for both structures along with the free O-H groups at approximately 3440 cm^{-1} for crosslinked PMAA.

Differential Scanning Calorimetry

The glass transition temperature, T_g , of potassium acrylate is approximately 194°C, and due to its presence in the uncrosslinked PAA copolymer, the T_g is expected to be higher than the reported value of 105°C for PAA (33). As the pentaerythritol crosslinking agent was incorporated into the networks, the T_g passed through a transition regime indicating heterogeneous crosslinking or branching that occurred, thus limiting the mobility of the polymer network as shown in Figure 4.7. As the crosslinking agent was increased to 0.43 mol %, a significant increase in the glass transition indicated homogenous crosslinking, which was verified by the polymer microparticles' insolubility in aqueous solutions as compared to the 0.2 mol % crosslinked PAA and the linear copolymer. As the level of crosslinking was increased, the mobility of the polymer chains was decreased, which is evident by the higher glass transitions.

Upon heating of the PMAA copolymer and terpolymers to 300°C, a large endotherm is observed indicating dehydration and anhydride formation (31). The glass transition observed after this initial heating and cooling step is shown in Figure 4.6. The PMAA copolymer exhibits a higher T_g than the PAA due to both the mobility inhibition of the methyl group and the anhydride formation. As the mobility is hindered by the presence of crosslinks, the T_g increases with more significance than the crosslinking effects of PAA. This is due to the synergistic effects of both crosslinking and anhydride formation and their effects on the mobility of the chains in the network.

Physicochemical Properties of Poly(carboxylic acid) Microparticles

The equilibrium weight swelling ratio, q , was calculated using equation (4.1), where W_s and W_d are the weights of swollen and dry polymer, respectively.

$$q = W_s / W_d \quad (4.1)$$

The crosslinked PAA samples show a significantly higher equilibrium swelling ratio in the carbonate buffer than polymers containing MAA at similar crosslinking ratios as can be seen in Figure 4.8.

This is due to the more hydrophilic acrylic acid. The presence of the methyl group in methacrylic acid imparted more hydrophobicity to the hydrogel structure, limiting the amount of solution uptake. The swelling of the carboxylic acid microparticles was heavily dependent on the crosslinking ratio, with the heavier crosslinked particles exhibiting a significantly lower swelling ratio. The pH dependent swelling of these polymers was evident by the effects of the acidic medium on the equilibrium swelling ratio. Both crosslinked PAA and crosslinked PMAA exhibit a significantly lower swelling ratio in 0.1 N HCl than in the carbonate buffer due to protonation of the carboxylic acid groups and the lack of ionization. Due to the ability of

crosslinked PMAA to form stronger inter- and intra- polymer complexation at a pH below its pKa, the swelling ratio of these polymers was lower than crosslinked PAA. Ionization of the acidic groups caused the polymer chains to repel one another, expanding the hydrogel network.

The number of carboxyl groups, n_{COOH} , present in the microparticles was calculated according to equation 2, where V is the volume of NaOH consumed at the endpoint of the titration, N is the normality of the NaOH solution, and $m_{particles}$ is the weight in mg of microparticles.

$$n_{COOH} = (45.02 \cdot V_{NaOH} \cdot N_{NaOH}) / m_{particles} \quad (4.2)$$

The degree of neutralization, α_n , was calculated according to equation (4.3) where C_{Base} , C_{H^+} , C_{OH^-} , and C_{COOH} are the molarities of base, hydrogen ions, hydroxide ions, and microparticle contributed carboxylic acid in the titration solution (33).

$$\alpha_n = (C_{Base} + C_{H^+} - C_{OH^-}) / C_{COOH} \quad (4.3)$$

The molarity of microparticle contributed carboxylic acid was determined from n_{COOH} according to equation 4.

$$C_{COOH} = (n_{COOH} \cdot m_{particles}) / (45.02 \cdot V_{total\ solution}) \quad (4.4)$$

The apparent dissociation constant, pK_{app} , was obtained from the degree of dissociation and pH according to equation (4.5). The value of the pK_a , which corresponds to $\alpha_d = 1/2$, was determined from the titration curve.

$$pK_{app} = pH + \log[(1 - \alpha_n) / \alpha_n] \quad (4.5)$$

Crosslinked PAA microparticles exhibit a pK_a of 6.9 with the particles containing approximately 0.55 carboxyl groups. Crosslinked PMAA microparticles exhibit a pK_a of 7.4 and contain approximately 0.44 COOH groups. The difference in pK_a is derived from the slight difference in the pK_a of the acidic monomers. The lower number of carboxyl groups as compared to the theoretical maximum is due to the presence of the potassium

carboxylates. Also, due to the methyl group, the crosslinked MAA particles possess a lower amount of carboxyl groups.

CONCLUSIONS

Microparticles composed of (meth)acrylic acid were successfully prepared using a thermally-initiated free-radical precipitation polymerization in ethyl acetate. Particle size was shown to be dependent on crosslinking and monomer. Slight morphological differences were observed due to differing polymer growth at the surface of the primary particle. Structural differences were observed and interpreted using FT-IR with only slight differences being observed due to the presence of the methyl group. The glass transition behavior of the materials was significantly different with MAA-based materials exhibiting a much higher T_g . The T_g was also heavily dependent on the amount of crosslinking present in the network. Crosslinked PAA possesses a higher swelling ratio than crosslinked PMAA with both polymers exhibiting pH dependent swelling.

REFERENCES

1. Ditsch A, Laibinis PE, Wang DIC, and Hatton TA, Controlled clustering and enhanced stability of polymer-coated magnetic nanoparticles, *Langmuir*, 21:6006-6018, 2005.
2. Hilt JZ, Gupta AK, Bashir R, and Peppas NA, Ultrasensitive biomems sensors based on microcantilevers patterned with environmentally responsive hydrogels, *Biomed. Microdevices*, 5:177-184, 2003.
3. Askari F, Nafisi S, Omidian H, and Hashemi SA, Synthesis And Characterization Of Acrylic-Based Superabsorbents, *J. Appl. Polym. Sci.*, 50:1851-1855, 1993.
4. Li A and Wang AQ, Synthesis and properties of clay-based superabsorbent composite, *Eur. Polym. J.*, 41:1630-1637, 2005.
5. Argade AB and Peppas NA, Poly(acrylic acid) poly(vinyl alcohol) copolymers with superabsorbent properties, *J. Appl. Polym. Sci.*, 70:817-829, 1998.
6. Soeno K, Suzuki S, Taira Y, Sawase T, and Atsuta M, Influence of mechanical properties of two resin cements on durability of bond strength to dentin after cyclic loading, *Dent. Mater. J.*, 24:351-355, 2005.
7. Sosson F, Chateauinois A, and Creton C, Investigation of shear failure mechanisms of pressure-sensitive adhesives, *J. Polym. Sci. Pt. B-Polym. Phys.*, 43:3316-3330, 2005.
8. Bell CL and Peppas NA, Modulation of drug permeation through interpolymer complexed hydrogels for drug delivery applications, *J. Control. Release*, 39:201-207, 1996.
9. Bures P and Peppas NA, Structural and Morphological Characteristics of Carriers Based on Poly(acrylic acid), *Polym. Prepr.*, 40:345-346, 1999.
10. Ficek B and Peppas N. *Biomaterials for Drug and Cell Delivery*. in *Materials Research Society*. 1994. Pittsburgh, PA.
11. Lopez JE and Peppas NA, Effect of poly (ethylene glycol) molecular weight and microparticle size on oral insulin delivery from P(MAA-g-EG) microparticles, *Drug Dev. Ind. Pharm.*, 30:497-504, 2004.
12. Mikos AG, Mathiowitz E, Langer R, and Peppas NA, Interaction Of Polymer Microspheres With Mucin Gels As A Means Of Characterizing Polymer Retention On Mucus, *J. Colloid Interface Sci.*, 143:366-373, 1991.

13. Peppas NA, Devices based on intelligent biopolymers for oral protein delivery, *Int. J. Pharm.*, 277:11-17, 2004.
14. Podual K, Doyle FJ, and Peppas NA, Dynamic behavior of glucose oxidase-containing microparticles of poly(ethylene glycol)-grafted cationic hydrogels in an environment of changing pH, *Biomaterials*, 21:1439-1450, 2000.
15. Yan XL and Gemeinhart RA, Cisplatin delivery from poly(acrylic acid-co-methyl methacrylate) microparticles, *J. Control. Release*, 106:198-208, 2005.
16. Zhang J and Peppas NA, Structure and Solute Size Exclusion of Poly(N-isopropylamide)/Poly(methacrylic acid) Interpenetrating Polymeric Networks, *Polym. Prepr.*, 39:228-229, 1998.
17. Zhang J and Peppas NA, Molecular interactions in poly(methacrylic acid)/Poly(N-isopropyl acrylamide) interpenetrating polymer networks, *J. Appl. Polym. Sci.*, 82:1077-1082, 2001.
18. Zhang J and Peppas NA, Morphology of poly(methacrylic acid)/poly(N-isopropyl acrylamide) interpenetrating polymeric networks, *J. Biomater. Sci.-Polym. Ed.*, 13:511-525, 2002.
19. Hubbell JA, Biomaterials In Tissue Engineering, *Bio-Technology*, 13:565-576, 1995.
20. Lee JW, Park JH, and Robinson JR, Bioadhesive-based dosage forms: The next generation, *J. Pharm. Sci.*, 89:850-866, 2000.
21. Mathiowitz E, Chickering DE, and Lehr CM, *Bioadhesive Drug Delivery Systems: Fundamentals, Novel Approaches, and Development*. 1999, New York, NY: Marcel Dekker, Inc.
22. Peppas NA and Buri PA, Surface, Interfacial and Molecular Aspects of Polymer Bioadhesion on Soft Tissues, *J. Control. Release*, 2:257-275, 1985.
23. Peppas NA and Sahlin JJ, Hydrogels as mucoadhesive and bioadhesive materials: A review, *Biomaterials*, 17:1553-1561, 1996.
24. Smart JD, The basics and underlying mechanisms of mucoadhesion, *Adv. Drug Deliv. Rev.*, 57:1556-1568, 2005.
25. Achar L and Peppas NA, Preparation, Characterization And Mucoadhesive Interactions Of Poly(Methacrylic Acid) Copolymers With Rat Mucosa, *J. Control. Release*, 31:271-276, 1994.

26. Ende MTA and Peppas NA, Transport of ionizable drugs and proteins in crosslinked poly(acrylic acid) and poly(acrylic acid-co-2-hydroxyethyl methacrylate) hydrogels.2. Diffusion and release studies, *J. Control. Release*, 48:47-56, 1997.
27. Kim B, La Flamme K, and Peppas NA, Dynamic swelling Behavior of pH-sensitive anionic hydrogels used for protein delivery, *J. Appl. Polym. Sci.*, 89:1606-1613, 2003.
28. Peppas NA and Tennenhouse D, Semicrystalline poly(vinyl alcohol) films and their blends with poly(acrylic acid) and poly(ethylene glycol) for drug delivery applications, *J. Drug Deliv. Sci. Technol.*, 14:291-297, 2004.
29. Robinson DN and Peppas NA, Preparation and characterization of pH-responsive poly(methacrylic acid-g-ethylene glycol) nanospheres, *Macromolecules*, 35:3668-3674, 2002.
30. Torres-Lugo M and Peppas NA, Transmucosal delivery systems for calcitonin: a review, *Biomaterials*, 21:1191-1196, 2000.
31. Dong J, Ozaki Y, and Nakashima K, Infrared, Raman, and near-infrared spectroscopic evidence for the coexistence of various hydrogen-bond forms in poly(acrylic acid), *Macromolecules*, 30:1111-1117, 1997.
32. Lazzari M, Kitayama T, Hatada K, and Chiantore O, Effect of stereoregularity on the thermal behavior of poly(methacrylic acid)s. 2. Decomposition at low temperatures, *Macromolecules*, 31:8075-8082, 1998.
33. Wang C, Tam KC, and Jenkins RD, Dissolution behavior of HASE polymers in the presence of salt: Potentiometric titration, isothermal titration calorimetry, and light scattering studies, *J. Phys. Chem. B*, 106:1195-1204, 2002.

Table 4.1 Composition of the P(M)AA microparticles prepared using a precipitation polymerization.

monomer/crosslinking agent	AA/APE	MAA/PETA
wt % initiator	0.5	0.5
wt % monomer	10.0	10.0
mol % crosslinking agent	0, 0.2, 0.43, 0.75, 1.46, 3.00	0, 0.43, 0.75, 1.46, 3.00
mol % neutralized	3.1	3.1
vol % H ₂ O in EtAc	0.27	0.27

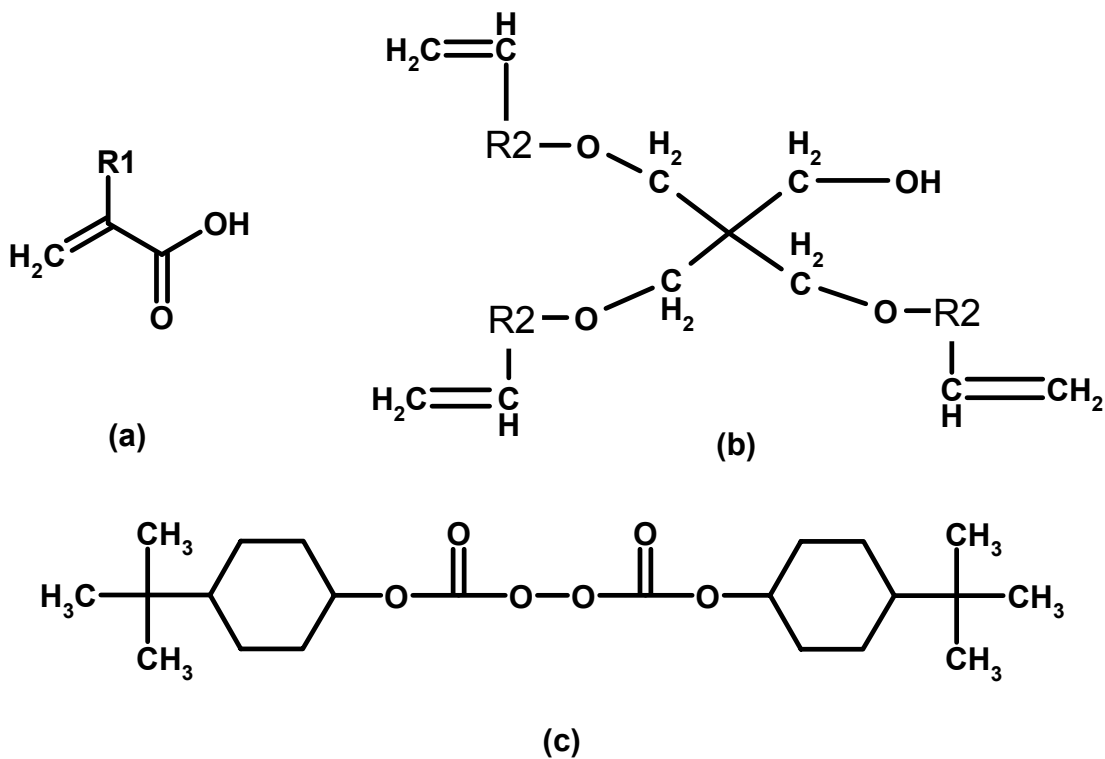


Figure 4.1 Molecular structures of (a) the carboxylic acid monomer (R1 = H for AA or R1 = CH3 for MAA), (b) the tri-functional pentaerythritol (R2 = CH for APE or R2 = COH for PETA), and (c) the thermal initiator BCHPC.

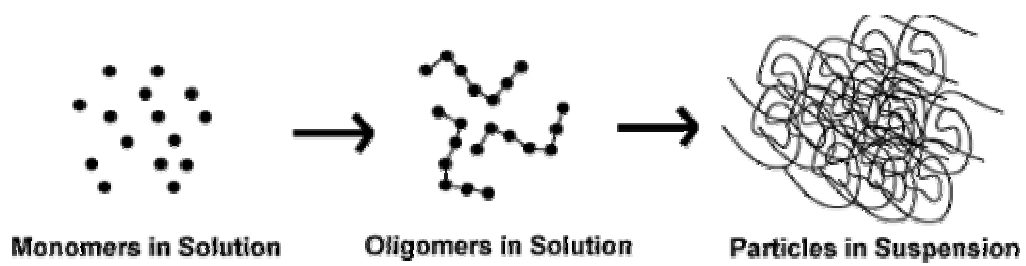


Figure 4.2 Precipitation polymerization of (meth)acrylic acid in ethyl acetate.

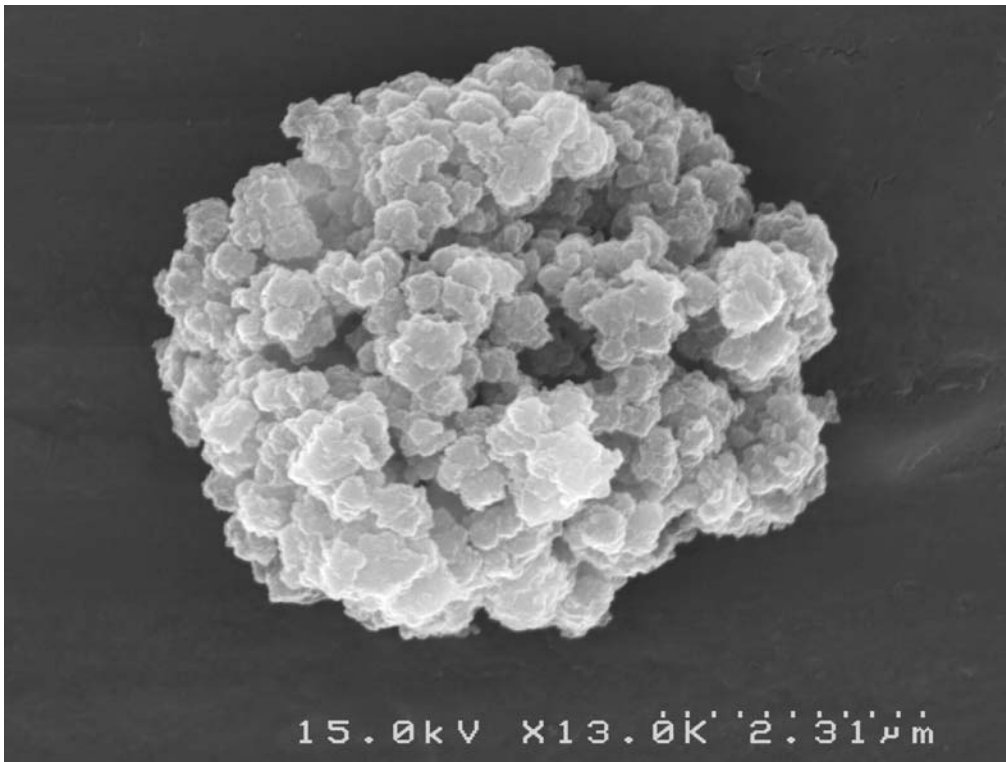


Figure 4.3 Morphology of crosslinked PMAA as determined using SEM.

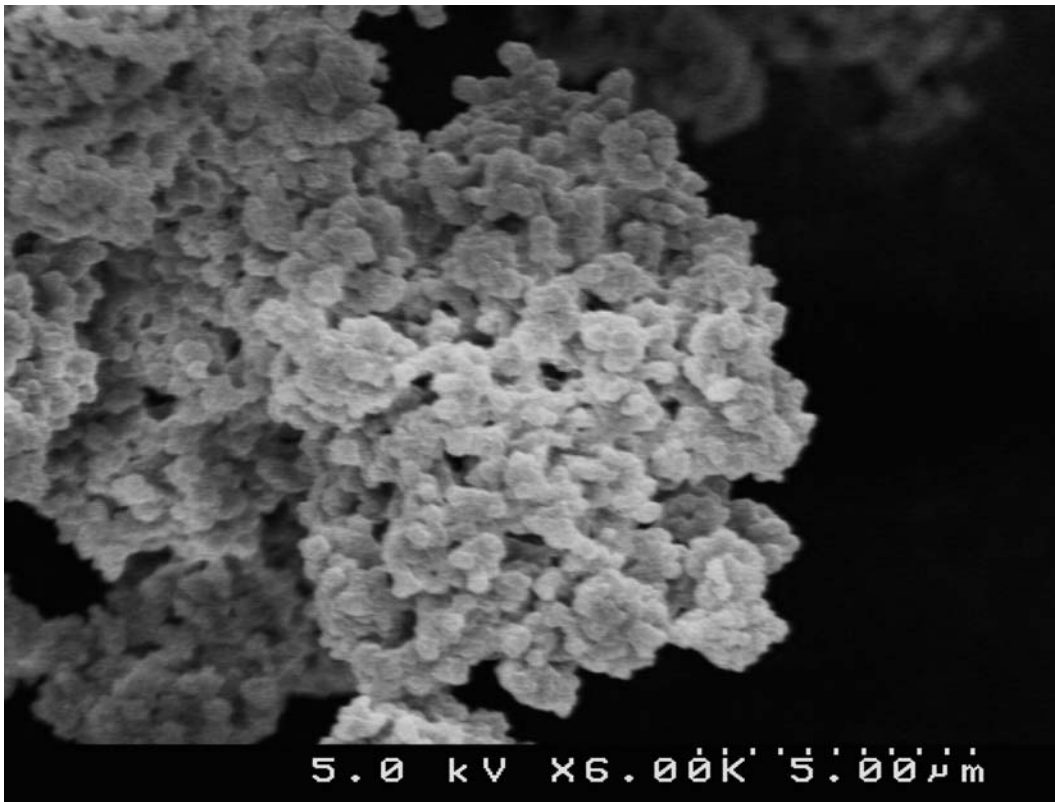


Figure 4.4 Morphology of crosslinked PAA microparticles as determined using SEM.

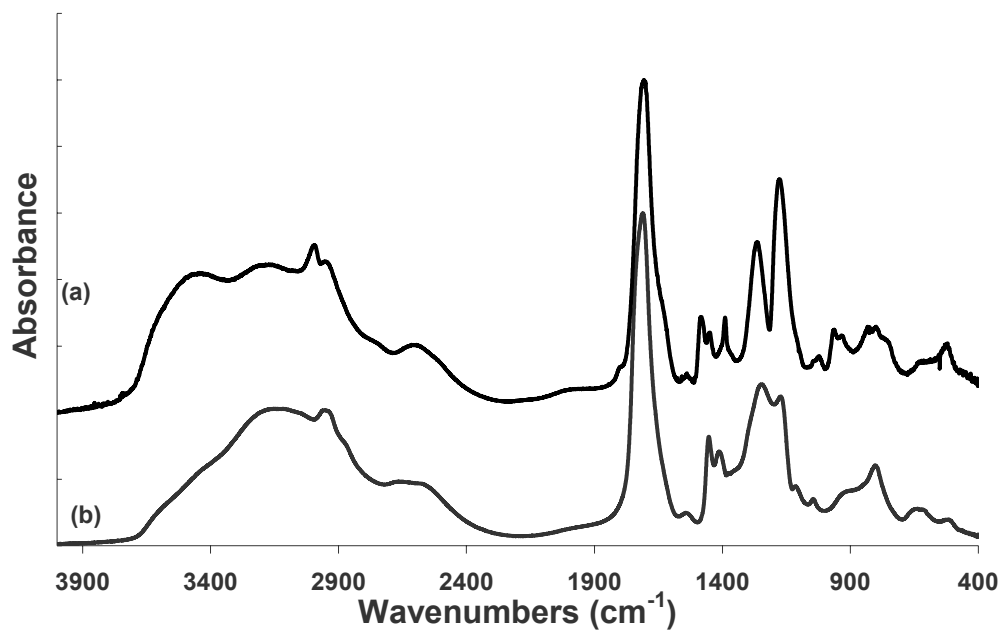


Figure 4.5 FT-IR spectrum of (a) crosslinked PMAA and (b) crosslinked PAA.

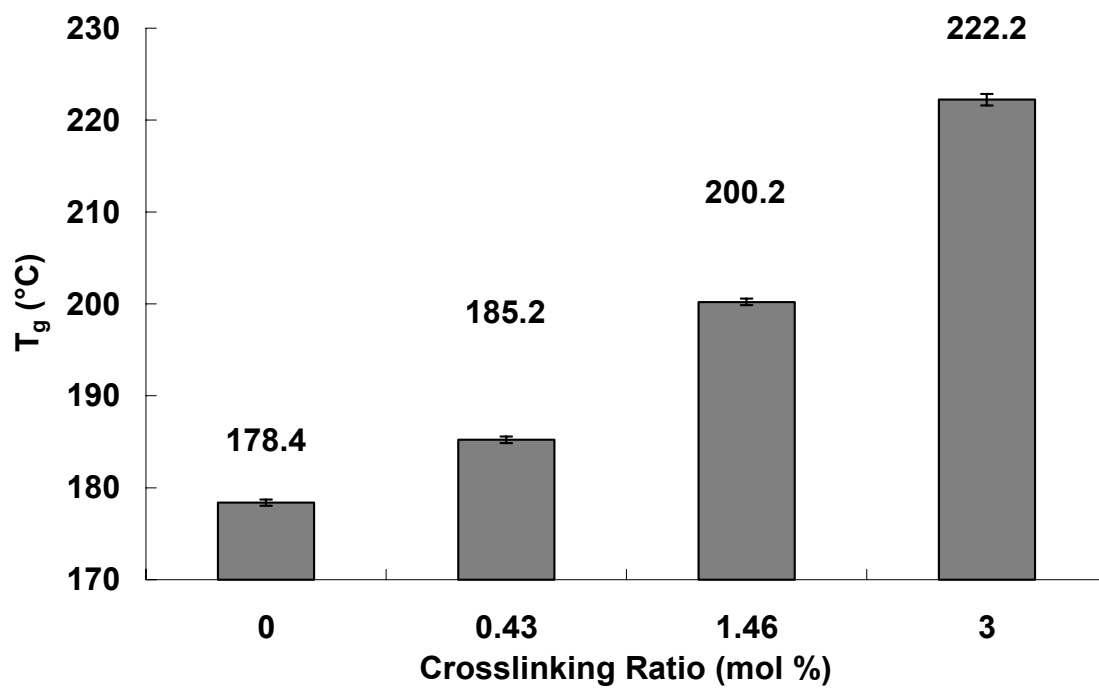


Figure 4.6 Glass transitions of crosslinked PMAA microparticles as a function of mol % crosslinking. Each bar represents the mean \pm SD (n=3).

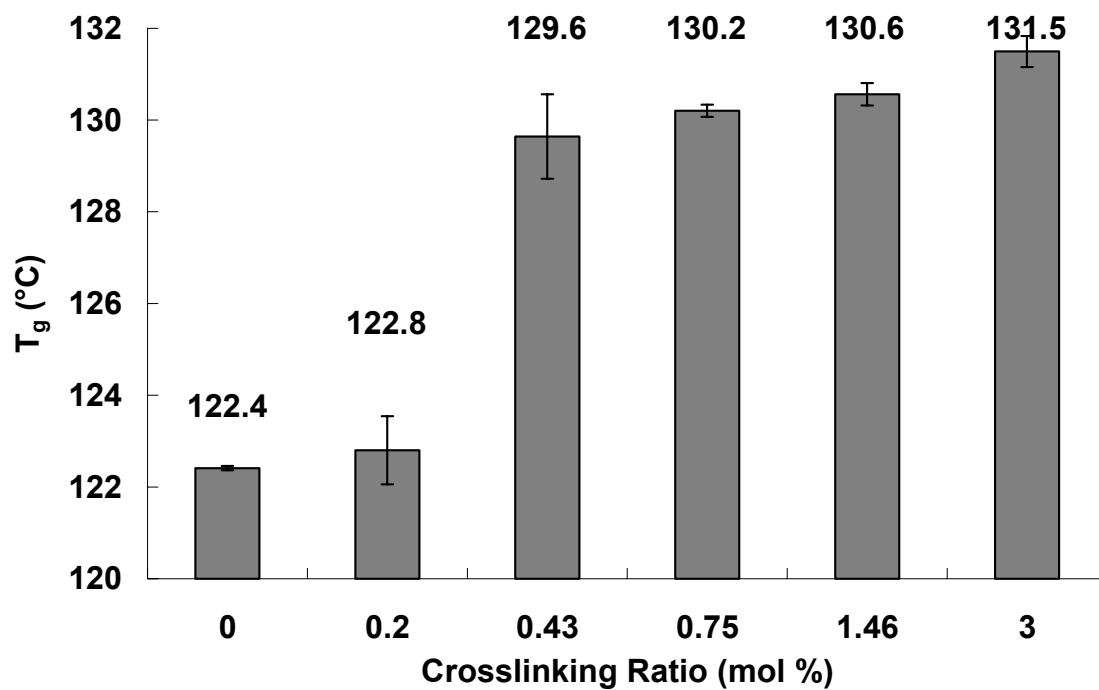


Figure 4.7 Glass transitions of crosslinked PAA microparticles as a function of mol % crosslinking. Each bar represents the mean \pm SD (n=3).

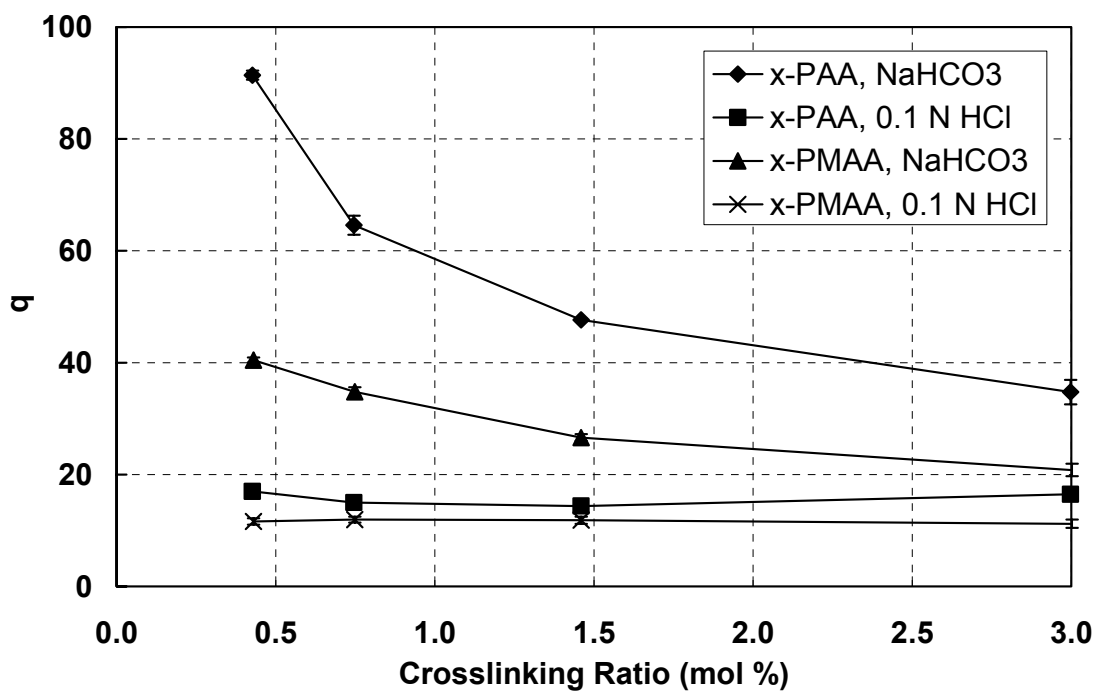


Figure 4.8 pH responsive equilibrium swelling behavior of crosslinked microparticles as a function of crosslinking ratio. Each point represents the mean \pm SD (n=4).

Chapter 5: Dynamics of Poly(ethylene glycol)-Tethered, pH Responsive Biomaterials

INTRODUCTION

Tethered polymer networks have received considerable attention for their use in modifying surface adhesion and friction (1-3), drug delivery systems (4-8), and bioadhesives (2, 3, 9, 10). Biomimetic systems, biomaterials that mimic a biological environment to elicit a desired cellular response (11), have also utilized tethered macromolecules to effectively enhance cellular adhesion (12-14) or prevent protein adsorption (15). Certain tethered polymer surfaces have been theorized to act as adhesion promoters by interpenetrating into the mucous gel layer, bridging the interface between the hydrogel-based drug delivery system and the absorption site (16).

Hydrogels have been frequently used in biomedical applications because of the many shared characteristics with natural tissue. The gel/gel adhesion between the hydrogel and the natural tissue can be controlled with the use of tethered polymers at the surface of the biomaterial. Since hydrogels are porous penetrable materials much like natural tissue, the tethered layer along with the bulk structure of the polymer requires a fundamental understanding to evaluate the structure-property relationships and dynamics.

Synthesis of polymer microparticles as the geometry for the hydrogel material is preferred due to their ease of incorporation into traditional dosage forms such as tablets and capsule formulations. Drug-loaded microparticles can be used on their own as drug delivery systems due to their relatively high loading capacity and ease of administration. Thermally initiated free-radical precipitation polymerizations are typically utilized as the preparation technique for obtaining microparticles possessing the necessary compressibility characteristics needed for successful tablet compression (17).

The incorporation of an (meth)acrylic acid monomer possessing a carboxylic acid moiety imparts pH responsive behavior into the hydrogel network. The anionic behavior of the polymer allows for ionic repulsion to occur along the polymer backbone, causing the hydrogel networks to expand and collapse depending on whether the pH of the environment is above or below the pK_a of the polymer. The addition of a polymer tether capable of participating in interpolymer complexation may affect the swelling behavior, mechanical properties, and solute transport characteristics dependent upon the state of the network, complexed or uncomplexed.

Interpolymer complexation forms between electron deficient moieties, such as the carboxylic acid groups found along the backbone of polyacids, and moieties containing regions of high electron density, such as the ether groups comprising poly(ethylene glycol) (PEG). The complexation behavior is a result of the non-covalent association between the polyacid and the tether as a result of hydrogen-bonding between the carboxyl group and the ether oxygen. This interpolymer complexation is a thermodynamically favorable event and is reversible in nature. The stability of the complex formed is strongly dependent on the structure of the polymers and their relative amounts incorporated into the network.

For complexation to occur, the pH of the environment must be substantially lower than the pK_a of the polyacid network to allow for sufficient protonation of the carboxylic acid group. Upon approach to the pK_a, deprotonation occurs, causing the network to decomplex. Upon decomplexation, the dynamics of the network are significantly altered, allowing for increased swelling, a decrease in the mechanical integrity of the network, and increased solute diffusion. Due to these interesting characteristics, these polymer networks can be utilized in biosensing applications, molecular recognition, and drug delivery systems.

In our research, we focus on the synthesis and characterization of microparticles composed of polymers possessing the ability to form interpolymer complexes stabilized by hydrogen bonding. These tethers are also present to act as adhesion promoters between the hydrogel and other gel networks such as the mucous gel layer covering the epithelium of the gastrointestinal tract. The conditions necessary for a successful polymerization are elucidated. The effects of the concentration and size of the polymer tether on the dynamics of the polymer networks are evaluated. Also, the behavior of two different polyacids in conjunction with the polymer tether is studied.

MATERIALS AND METHODS

Materials

Methacrylic acid (MAA, inhibited with 250 ppm hydroquinone), anhydrous potassium carbonate (K_2CO_3), and ethyl acetate (EtAc) were obtained from Fisher Scientific and used as received. Acrylic acid (AA, inhibited with 200 ppm hydroquinone), poly(ethylene glycol) monomethyl ether monomethacrylate (PEGMMA, $M_n \sim 300, 1100$) and PEGMMA solution ($M_n \sim 2080$, 50 wt % in H_2O) was obtained from Sigma Aldrich (Milwaukee, WI). The PEGMMA 50 wt % in H_2O solution was freeze dried to obtain anhydrous PEGMMA $M_n \sim 2080$. Allyl pentaerythritol (APE), pentaerythritol triacrylate (PETA), and di(4-tert-butylcyclohexyl) peroxydicarbonate (BCHPC) were kindly supplied by Perstorp Polyols (Toledo, OH), Sartomer (Exton, PA), and Degussa Initiators (Elyria, OH), respectively. All other chemicals were of reagent grade and used as received.

Synthesis

In a typical thermally-initiated free radical precipitation polymerization, MAA, K_2CO_3 , PEGMMA, and deionized distilled water (ddH_2O) were combined and mixed to

form a homogeneous mixture, allowing the escape of the neutralization by-product carbon dioxide (17). The crosslinking agent, APE or PETA, was dissolved in ethyl acetate. The monomer mixture and crosslinking agent were added to a four-necked round bottom flask equipped with an overhead stirrer, nitrogen purge, and condenser containing the polymerization solvent EtAc. Following a 20 minute purge with nitrogen, the initiator BCHPC dissolved in the polymerization solvent was added to the vessel and further purged for an additional 10 minutes.

The molecular structures of the monomer, crosslinking agent, and thermal initiator are shown in Figure 5.1. The vessel was placed in a thermostatic bath at $50^{\circ}\text{C} \pm 0.5^{\circ}\text{C}$ where precipitation was evident in a matter of minutes. The reaction was allowed to proceed for 16 hours to ensure a high percentage of monomer conversion. Following the polymerization, the particle slurry was centrifuged and washed with fresh ethyl acetate and dried using a rotary evaporator at elevated temperature and reduced pressure ($90^{\circ}\text{C}/40\text{ mmHg}$).

Characterization

Discs containing 1 mg of sample and 150 mg of KBr were prepared on a Carver laboratory press using a 15,000 lb compression force. Infrared spectra of the microparticles were obtained in the wavenumber range of 400-4000 cm^{-1} on a Fourier transform infrared spectrophotometer (FT-IR, Thermo Mattson Infinity, Thermo Electron Corp., Waltham, MA) in transmission mode equipped with a KBr beamsplitter and DTGS detector. Each spectrum is an average of 64 scans at a resolution of 1 cm^{-1} .

The thermal properties of the microparticles were characterized using a differential scanning calorimeter (DSC, MDSC 2920, TA Instruments, New Castle, DE). Approximately 10-15 mg samples were analyzed at a sample rate of $10^{\circ}\text{C}/\text{min}$ over the

range of 80°C to 160°C for poly(acrylic acid) and 80°C to 300°C for poly(methacrylic acid) using a heat/cool/heat method to erase the thermal history.

The equilibrium weight swelling ratio of the polymeric hydrogel microparticles was determined by carefully weighing 50 mg of dried particles and combining them with 35 mL of NaHCO₃ solution (1.5 g / 100 mL). The suspension was agitated for 60 min and then centrifuged for 60 min at 2000 rpm, carefully discarding the supernatant. The pellet was resuspended in an additional 35 mL of NaHCO₃ solution and agitated for 60 min. The suspension was centrifuged at 2000 rpm for 60 min, carefully removing the supernatant, and the weight of the gelled mass was determined. This procedure was also carried out in a 0.1 N HCl solution.

Approximately 4.0 g of the prepared polymer microparticles previously dried at 30°C and 28 inHg were added to 350 mL of an agitated aqueous solution containing the appropriate amount of NaCl to achieve the specified ionic strength. After a 15 minute hydration period, the pH of the microparticle slurry was adjusted accordingly using 1 N NaOH, and a sufficient volume of ddH₂O was added to make the final volume of liquid 400 mL.

One mL of the polymer gel was placed on the lower of the two cylindrical (D = 19 mm) agarose sample mounts (0.5 g agarose in 50 mL of ddH₂O) in a tensile tester (Instron 4301, 10 N load cell, Canton, MA) at 22°C. The upper sample mount was brought into contact with a 42 mN impingement force achieved through resting the upper sample mount on the gel sample and lower sample mount, and the gel was allowed to relax for five minutes. The upper sample mount was raised at 6 mm/min until failure of the gel bond occurred, and the detachment force was measured as a function of displacement. The area under the curve of force versus length up until the peak force is

defined as the work of adhesion, and the area post peak force is defined as the work of cohesion.

RESULTS AND DISCUSSION

Precipitation Polymerization for Synthesis of Tethered Microparticles

The main requirements for a precipitation polymerization are the presence of an inert diluent which dissolves the monomer but precipitates the polymer as it is formed. In the formation of the tethered microparticles, the monomer, crosslinking agent, tether, and initiator are dissolved in ethyl acetate which is a non-solvent for the formed polymer (18). Polymer precipitates out and forms agglomerated microparticles as it is formed. These types of polymerizations are different than those of dispersion polymerizations in that there is no polymeric dispersant present to stabilize the polymer particles as they are formed. This stabilizer forms a dissolved protective layer around the polymer particles as they grow, and its absence presents an unstable dispersion which results in flocculation of the growing polymeric particles. The resultant microparticle is composed of primary polymeric particles which have agglomerated together.

The processes involved with precipitation polymerizations depend on the solubility characteristics of the polymer, especially those processes related to the formation and growth of polymer particles. The free energy change ΔG_m must be negative for the monomers and the diluent to mix. More specifically the heat of mixing ΔH_m must be smaller than the entropy factor $T\Delta S_m$ since the entropy of mixing will always be positive as can be seen in equation (5.1).

$$\Delta G_m = \Delta H_m - T\Delta S_m \quad (5.1)$$

The total cohesion energy, the total energy needed to separate the molecules of each liquid to a distance infinitely far from one another, is given by equation (5.2).

$$E = (\Delta H_v - RT) / V_m \quad (5.2)$$

The solubility parameter δ is defined as the square root of the cohesive energy density since the interaction between the unlike molecules can be taken as the geometric mean of the cohesive energy densities of the two components.

$$E_1 = \delta_1^2; \quad E_2 = \delta_2^2; \quad E_{12} = \delta_1 \delta_2 \quad (5.3)$$

The heat of mixing can be obtained by subtracting the contributions of a mixture from the cohesive energies of the separate unmixed components as shown in equation (5.4) where V_m is the average molar volume of the mixture. Because the interactions between like molecules are counted twice, a factor of 2 is added.

$$\Delta H_m / V_m = (E_1 \phi_1 + E_2 \phi_2) - (E_1 \phi_1^2 + E_2 \phi_2^2 + 2E_{12} \phi_1 \phi_2) \quad (5.4)$$

From these equations, the heat of mixing can be expressed in the following form and is minimized when the difference between the solubility parameters of the liquids are as small as possible.

$$\Delta H_m = V_m \phi_1 \phi_2 (\delta_1 - \delta_2)^2 \quad (5.5)$$

Flory-Huggins solution theory shows that the free energy of mixing (5.6) is highly dependent on the molecular weight of the polymer.

$$(\Delta G_m)_v = (RT/V) (\phi_1 \ln \phi_1 + (\phi_2 / m) \ln \phi_2 + \chi \phi_1 \phi_2) \quad (5.6)$$

χ is the Flory polymer-solvent interaction parameter which is related to the solubility parameters of the components by equation, where β is a correction to the Flory combinatorial entropy with a value between 0.2-0.4.

$$\chi = \beta + (\delta_1 - \delta_2)^2 V_1 / RT \quad (5.7)$$

Further evaluation of precipitation and phase separation can be described as an equilibrium process by the Flory-Huggins theory and one can derive the chemical potential for each component of the precipitation polymerization. These derivations yield that the solubility of a polymer in a liquid diluent falls off very rapidly as the

molecular weight is increased and as the difference in solubility parameters for each component increases (18).

The precipitation polymerization of tethered microparticles synthesized in this work occurs through the following stages: (a) the polymer formed is insoluble in the diluent and polymer particles precipitate from the initially homogeneous reaction solution; (b) opalescence is detected almost immediately after initiation of polymerization due to the formation of polymer particles at very low conversions; (c) high molecular weight polymers are obtained due to restricted radical termination in the formed glassy particle (19).

Due to the application of the particles in drug delivery systems, the absence of a dispersant was desired to eliminate the need for removal. The resulting size distribution is rather polydisperse with 95% of the particles being smaller than 30 μm (data not shown). The addition of the low molecular weight PEG used in these studies did not act as a polymerizable stabilizer as can be noted from the presence of the agglomeration and the absence of individual primary particles.

For AA precipitation polymerizations, it is necessary to preneutralize a small portion of the acrylic acid monomers to form potassium acrylate. Potassium acrylate imparts the proper solubility characteristics onto the formed polymer to precipitate out of solution. Without the addition of potassium acrylate to the monomer solution, polymerization and marginal precipitation occurs, but the large agglomerates formed are undesirable. The polymerization proceeds as a solution polymerization without production of any microparticles. For PMAA, the preneutralization is not necessary due to the solubility characteristics of the formed polymer, but can be utilized to increase the microclimate pH of the particles formed. However, a large concentration of potassium

acrylates and methacrylates is insoluble in ethyl acetate, resulting in a heterogeneous monomer/diluent mixture.

For the P(AA-g-PEG) polymerizations, the PEG does affect the solubility of the formed microparticles. With PEG being soluble in ethyl acetate, its incorporation results in a higher propensity for salvation of the growing polymer chains. This effect can be kinetically controlled by decreasing the reaction temperature after initiation to decrease the extent of agglomeration that occurs. For P(MAA-g-PEG) polymerizations, this effect is negligible due to large extent of the insolubility of PMAA in ethyl acetate.

The choice of initiator relies on the fact that a lower reaction temperature is needed for increasing concentrations of PEG. The peroxydicarbonate provides this element, however, lauroyl peroxide can also be utilized as the initiator for systems composed of a high AA:EG ratio or for all MAA systems. The choice of crosslinking agent is also dependent on the monomer employed. Due to the reactivity ratios of acrylic and methacrylic acid, an allyl or acrylate functionalized crosslinking agent, respectively, must be used to achieve a crosslinked network.

FT-IR Spectroscopy of Poly(ethylene glycol)-tethered Biomaterials

Figures 5.2 through 5.8 show the IR spectra for crosslinked poly(acrylic acid) (PAA) microparticles containing the PEGMMA tether at various concentrations and potassium acrylate (P(AA-g-PEG)) and Table 5.1 lists the vibrational assignments for the various peaks present in the spectra. All spectra exhibit the characteristic C=O stretching, with crosslinked PAA stretching occurring at 1710 cm^{-1} and moving to a slightly higher wavenumber with increasing PEG tether concentration (1740 cm^{-1} for AA:EG 50:50). This indicates a higher prevalence of obtaining cyclic hydrogen-bonded COOH groups in dimeric form with a decreasing concentration of the PEG tether (20). As the concentration of PEG increases in the network, free (non-hydrogen-bonded)

COOH groups increases due to the disruption or prevention of dimeric formation with the addition of the PEG macromolecule into the structure. The asymmetric vibration of the methyl group present at the end of the PEG tether is exhibited on the FT-IR spectrum at approximately 2890 cm^{-1} . The characteristic C-O-C stretching of the PEG tether is clearly evident at approximately 1110 cm^{-1} .

Differential Scanning Calorimetry

The glass transition temperature, T_g , of the dry crosslinked PAA is approximately 131°C , which is significantly higher than that reported for linear PAA. As reported previously (17), this can be attributed to the presence of the pentaerythritol crosslinking agent and potassium acrylate. Upon incorporation of small amounts of the PEG tether (AA:EG 98:2 and 90:10), the ΔC_p is decreased with no change or appearance of a second T_g observed. It is not until the ratio of AA:EG is increased to 83:17 that a second T_g is observed. This is due to a heterogeneous network consisting of crosslinked PAA rich domains and domains containing both crosslinked PAA and the PEG tether. Upon further increase of the PEG concentration, a single lower T_g is observed, indicating the return to a more homogenous network.

Swelling Behavior of PEG-tethered Hydrogel Networks

To evaluate the swelling properties of the PEG-tethered hydrogel networks, the amount of water uptake of the microparticles, q , was calculated according to equation (5.8), where W_s and W_d are the weight of the swollen polymer and the dry polymer, respectively.

$$q = \frac{W_s}{W_d} \quad (5.8)$$

The polymer volume fraction after equilibrium swelling, $v_{2,s}$, was calculated according to equation (5.9), where ρ_d and ρ_{water} are the density of the polymer (1.41 g/cm³) and water (0.995 g/cm³), respectively .

$$v_{2,s} = \frac{\frac{W_d}{\rho_d}}{\frac{W_d}{\rho_d} + \frac{W_s}{\rho_{\text{water}}}} \quad (5.9)$$

The average molecular weight between crosslinks, \overline{M}_c , was calculated according to the Flory-Rehner equation, (5.10), where \overline{M}_n is the number average molecular weight of the uncrosslinked polymer (20,000 for PMAA, 50,000 for PAA), \overline{v} is the specific volume of the polymer (0.71 cm³/g), V_1 is the molar volume of the swelling medium (18.1 cm³/mol), and χ is the Flory polymer-solvent interaction parameter in water which is calculated as a weighted average for the values PMAA, $\chi = 0.5987$, PAA, $\chi = 0.495$, and PEG, $\chi = 0.55$.

$$\frac{1}{\overline{M}_c} = \frac{2}{\overline{M}_n} - \frac{\frac{\overline{v}}{V_1} [\ln(1-v_{2,s}) + v_{2,s} + \chi v_{2,s}^2]}{\left(v_{2,s}^{\frac{1}{3}} - \frac{v_{2,s}}{2} \right)} \quad (5.10)$$

After determining \overline{M}_c , the number of links between two crosslinks, n , was calculated according to equation (5.11), where M_r is the average molecular weight of the repeat unit (MAA, 86.09; AA, 72.06; EG, 44).

$$n = \frac{2\overline{M}_c}{M_r} \quad (5.11)$$

The value of the root mean squared end-to-end distance of the polymer chain in the freely jointed state was calculated using equation (5.12), where ℓ is the carbon-carbon bond length (1.54 Å).

$$\left(\overline{r^2} \right)^{1/2} = \ell \sqrt{n} \quad (5.12)$$

The root mean squared end-to-end distance of the polymer chain in the unperturbed state was calculated according to equation (5.6) where C_n is the Flory characteristic ratio or rigidity factor of the polymer (PMAA, $C_n = 14.6$, PAA, $C_n = 14.6$, and PEG, $C_n = 3.8$).

$$\left(\overline{r_o^2}\right)^{1/2} = \sqrt{C_n} \left(\overline{r^2}\right)^{1/2} \quad (5.13)$$

Lastly, the mesh size of the hydrogel network, ξ , was determined according to equation (5.14).

$$\xi = \nu_{2,s}^{-1/3} \left(\overline{r_o^2}\right)^{1/2} \quad (5.14)$$

The results for the swelling dynamics of PAA microparticles can be found in Table 5.2. Loosely crosslinked PAA (0.43 mol % APE) imbibes a significant amount of water in the sodium carbonate buffer (pH~9) as compared to 0.1 N HCl. As the amount of crosslinking agent increases, the degree of swelling in the carbonate buffer decreases. The results for the swelling dynamics of PMAA microparticles (Table 5.3) show a similar trend. At similar crosslinking levels, PMAA microparticles imbibe a significantly lower amount of water due to the presence of the methyl group along the backbone of the polyacid. Swelling for both networks occurs due to deprotonation of the carboxyl group resulting in ionic repulsion of the neighboring chains. This causes the network to expand and imbibe more water. In the 0.1 N HCl buffer, the carboxylic acid groups remain protonated and water uptake is minimal. This expansion is also evident through the significant increase in the mesh size for the polymers in the carbonate buffer as compared to the 0.1 N HCl solution. As crosslinking is increased, the mesh size decreases which corresponds to the lower solution uptake.

Upon incorporation of PEG, the swelling dynamics of the PMAA microparticles changes significantly (Table 5.4). The swelling capacity of the tethered hydrogels is significantly lower as compared to crosslinked PMAA microparticles containing no

tether. The degree of swelling is similar with a slightly smaller mesh size. The ratio of the mesh size in carbonate buffer versus 0.1 N HCl is significantly greater for tethered hydrogels. This allows for a dramatic increase in the amount of water uptake in higher pH solutions compared with lower pH.

Gel/Gel Adhesion of Tethered Hydrogels

Crosslinked PAA hydrogel microparticles, upon neutralization, produce a highly viscous suspension at low concentrations (1 wt % polymer). This viscous gel suspension possesses tack which is capable of adhering to other hydrogel materials. This characteristic is exhibited in Figure 5.16 for crosslinked PAA microparticles containing a PEG tether. The gel adhesion remains relatively unchanged upon incorporation of low amounts of the PEG tether (AA:EG 83:17). However, as the concentration is increased to a ratio of AA:EG 60:40, a significant decrease in the adhesive characteristics is obtained. The viscosity of the neutralized hydrated gel is the key factor that contributes to the ability of the gel to act as a bioadhesive. With higher concentrations of PEG, the amount of ionizable groups present in the network are decreased which leads to a significant reduction in the viscosity of the gel. The lowered viscosity in turn causes the adhesive characteristics to be lower than hydrogels containing lowered amounts of PEG.

CONCLUSIONS

The fundamental understanding of the behavior of tethered gel networks has implications in tissue engineering, adhesion, and drug delivery. In this research, ionizable hydrogel networks containing a PEG tether were successfully synthesized using a thermally initiated free radical precipitation polymerization. The effects of the PEG tether on the structure of the microparticles were evaluated. The addition of the PEG was shown to cause disruption of the dimer formation of PAA. Differential scanning

calorimetry exhibited a concentration dependent decrease in the T_g of xerogels. At low concentrations, the network exhibits a heterogeneous behavior which is evident through a lowered ΔC_p and the presence of two distinct T_g 's.

The gel adhesion of a neutralized gel was shown to be dependent on the amount of PEG incorporated into the network, which in turn affected the viscosity of the gel. These materials possess interesting swelling properties which can be beneficial in the development of pH responsive drug delivery systems.

REFERENCES

1. Leger L, Raphael E, and Hervet H, *Surface-anchored polymer chains: Their role in adhesion and friction*, in *Polymers In Confined Environments*. 1999, Springer-Verlag Berlin: Berlin. p. 185-225.
2. Huang YB, Szleifer I, and Peppas NA, Gel-gel adhesion by tethered polymers, *J. Chem. Phys.*, 114:3809-3816, 2001.
3. Huang YB, Szleifer I, and Peppas NA, A molecular theory of polymer gels, *Macromolecules*, 35:1373-1380, 2002.
4. Lowman AM, Cowans BA, and Peppas NA, Investigation of interpolymer complexation in swollen polyelectrolyte networks using solid-state NMR spectroscopy, *J. Polym. Sci. Pt. B-Polym. Phys.*, 38:2823-2831, 2000.
5. Lowman AM, Morishita M, Kajita M, Nagai T, and Peppas NA, Oral delivery of insulin using pH-responsive complexation gels, *J. Pharm. Sci.*, 88:933-937, 1999.
6. Lowman AM and Peppas NA, Analysis of the complexation/decomplexation phenomena in graft copolymer networks, *Macromolecules*, 30:4959-4965, 1997.
7. Lowman AM and Peppas NA, Solute transport analysis in pH-responsive, complexing hydrogels of poly(methacrylic acid-g-ethylene glycol), *J. Biomater. Sci.-Polym. Ed.*, 10:999-1009, 1999.
8. Lowman AM and Peppas NA, Molecular analysis of interpolymer complexation in graft copolymer networks, *Polymer*, 41:73-80, 2000.
9. Bromberg L, Temchenko M, Alakhov V, and Hatton TA, Bioadhesive properties and rheology of polyether-modified poly(acrylic acid) hydrogels, *Int. J. Pharm.*, 282:45-60, 2004.
10. Cleary J, Bromberg L, and Magner E, Adhesion of polyether-modified poly(acrylic acid) to mucin, *Langmuir*, 20:9755-9762, 2004.
11. Drotleff S, Lungwitz U, Breunig M, Dennis A, Blunk T, Tessmar J, and Gopferich A, Biomimetic polymers in pharmaceutical and biomedical sciences, *Eur. J. Pharm. Biopharm.*, 58:385-407, 2004.
12. Mann BK, Schmedlen RH, and West JL, Tethered-TGF-beta increases extracellular matrix production of vascular smooth muscle cells, *Biomaterials*, 22:439-444, 2001.
13. Mann BK, Tsai AT, Scott-Burden T, and West JL, Modification of surfaces with cell adhesion peptides alters extracellular matrix deposition, *Biomaterials*, 20:2281-2286, 1999.
14. Ruoslahti E and Pierschbacher MD, New Perspectives In Cell-Adhesion - Rgd And Integrins, *Science*, 238:491-497, 1987.

15. Jeon SI, Lee JH, Andrade JD, and Degennes PG, Protein Surface Interactions In The Presence Of Polyethylene Oxide.1. Simplified Theory, *J. Colloid Interface Sci.*, 142:149-158, 1991.
16. Peppas NA and Huang YB, Nanoscale technology of mucoadhesive interactions, *Adv. Drug Deliv. Rev.*, 56:1675-1687, 2004.
17. Thomas JB, Creecy CM, McGinity JW, and Peppas NA, Synthesis and properties of lightly crosslinked poly((meth)acrylic acid) microparticles prepared by free radical precipitation polymerization, *Polym. Bull.*, 57:11-20, 2006.
18. Barrett KEJ and Thomas HR, *Kinetics and Mechanism of Dispersion Polymerization*, in *Dispersion Polymerization in Organic Media*, Barrett KEJ, Editor. 1975, John Wiley & Sons: New York, NY. p. 115-200.
19. Barrett KEJ and Thomas HR, Kinetics of Dispersions Polymerization of Soluble Monomers. I. Methyl Methacrylate, *J. Polym. Sci.*, 7:2621-2650, 1969.
20. Dong J, Ozaki Y, and Nakashima K, Infrared, Raman, and near-infrared spectroscopic evidence for the coexistence of various hydrogen-bond forms in poly(acrylic acid), *Macromolecules*, 30:1111-1117, 1997.

Table 5.1 Vibrational assignments for crosslinked PAA and the effect of PEG tether addition on the spectra of P(AA-g-PEG) microparticles.

Wavenumber (cm ⁻¹)		Intensity ¹	Assignment ²
x-PAA	P(AA-g-PEG)		
3440		v	ν (O-H) free groups
~3200		m	ν (O-H) associated w/ water
2970		w	ν _a (C-H) CH ₂
	2890	m-s	ν _a (CH ₃)
~2620		w	ν (O-H) bonded groups
1710	shifts to slightly higher	s	ν (C=O)
1560		s	ν carboxylate ion
1460	1460	w	δ (CH ₂) out of plane
1260		s	ν (C=O) or δ (O-H)
1190		s	related to 1260
	1110	s	ν (C-O-C)
820		w	γ (CH ₂)

¹Intensity: v, variable; w, weak; m, medium; s, strong. ²Vibrations: ν, stretching; a, asymmetric; δ, bending; γ, rocking.

Table 5.2 Equilibrium swelling ratio of crosslinked PAA microparticles.

Theoretical Crosslinking Ratio (X_{theo})	0.1 N HCl		NaHCO ₃ Buffer	
	Weight swelling ratio (q)	Mesh Size (ξ , Å)	Weight swelling ratio (q)	Mesh Size (ξ , Å)
0.0043	17.0 ± 0.3	420	91.4 ± 0.8	780
0.0075	15.0 ± 0.2	400	64.6 ± 1.7	700
0.0148	14.4 ± 0.2	390	47.6 ± 0.2	630
0.0309	16.5 ± 0.7	420	34.7 ± 2.2	561

Table 5.3 Equilibrium swelling ratio of crosslinked PMAA microparticles.

Theoretical Crosslinking Ratio (X_{theo})	0.1 N HCl		NaHCO ₃ Buffer	
	Weight swelling ratio (q)	Mesh Size (ξ , Å)	Weight swelling ratio (q)	Mesh Size (ξ , Å)
0.0043	11.6 ± 0.6	270	40.5 ± 0.4	350
0.0079	11.9 ± 0.5	270	34.8 ± 0.8	340
0.0148	11.8 ± 0.6	270	26.6 ± 0.6	310
0.0309	11.2 ± 0.7	260	20.8 ± 1.1	290

Table 5.4 Equilibrium swelling of crosslinked PEG-tethered PMAA microparticles (PEG-1000).

MAA:EG	0.1 N HCl		NaHCO ₃ Buffer	
	Weight swelling ratio (q)	Mesh Size (ξ , Å)	Weight swelling ratio (q)	Mesh Size (ξ , Å)
83:17	6.1 ± 0.2	61	41.6 ± 0.9	300
69:31	5.8 ± 0.3	54	42.0 ± 0.5	290
50:50	5.3 ± 0.4	45	43.4 ± 1.2	270

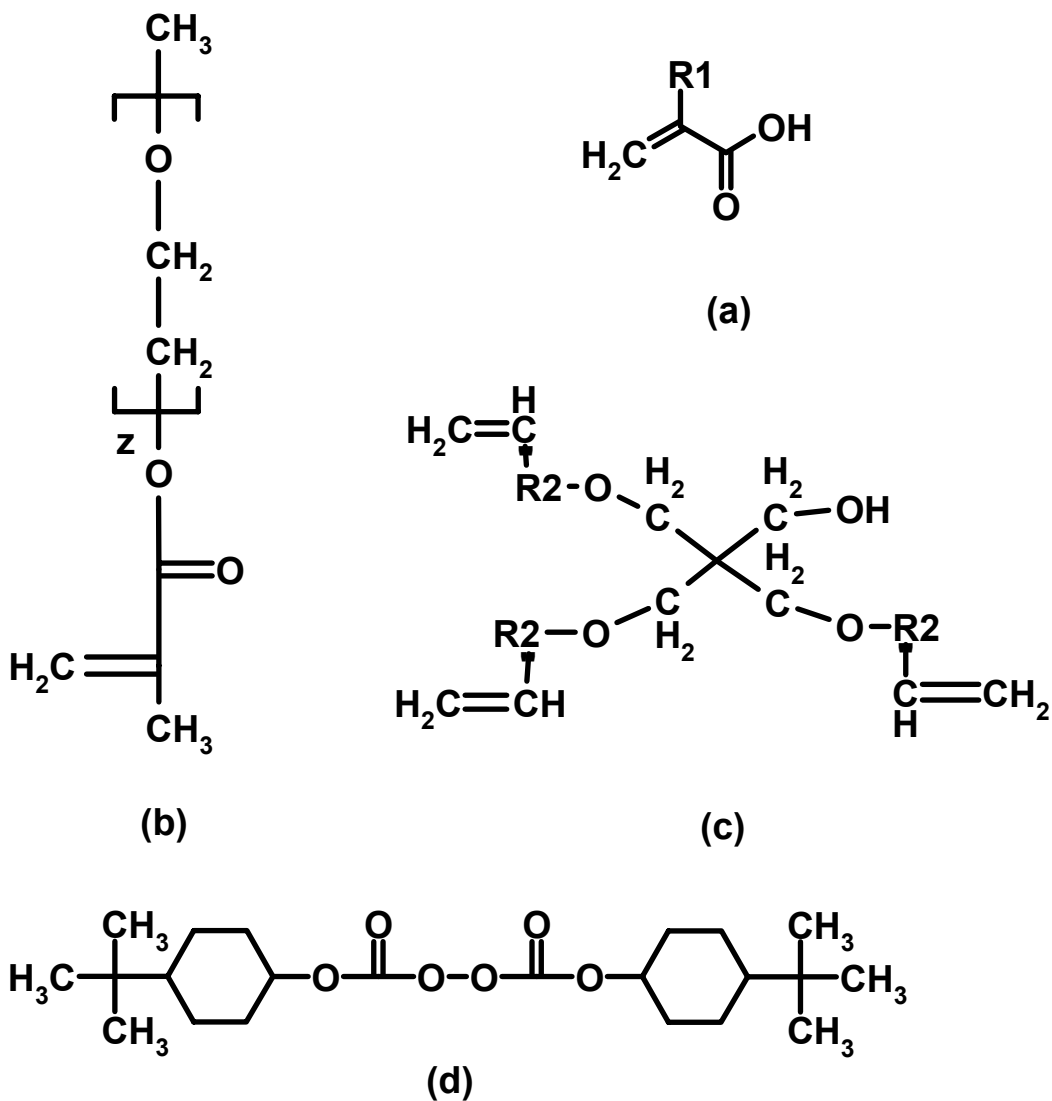


Figure 5.1 Molecular structures of (a) the carboxylic acid-containing monomer ($\text{R1} = \text{H}$ for AA or $\text{R1} = \text{CH}_3$ for MAA), (b) a poly(ethylene glycol) tether ($z \sim 5, 23,$ and 45), (c) the tri-functional pentaerythritol ($\text{R2} = \text{CH}$ for APE or $\text{R2} = \text{COH}$ for PETA), and (d) the thermal initiator di(4-tert-butylcyclohexyl) peroxydicarbonate (BCHPC).

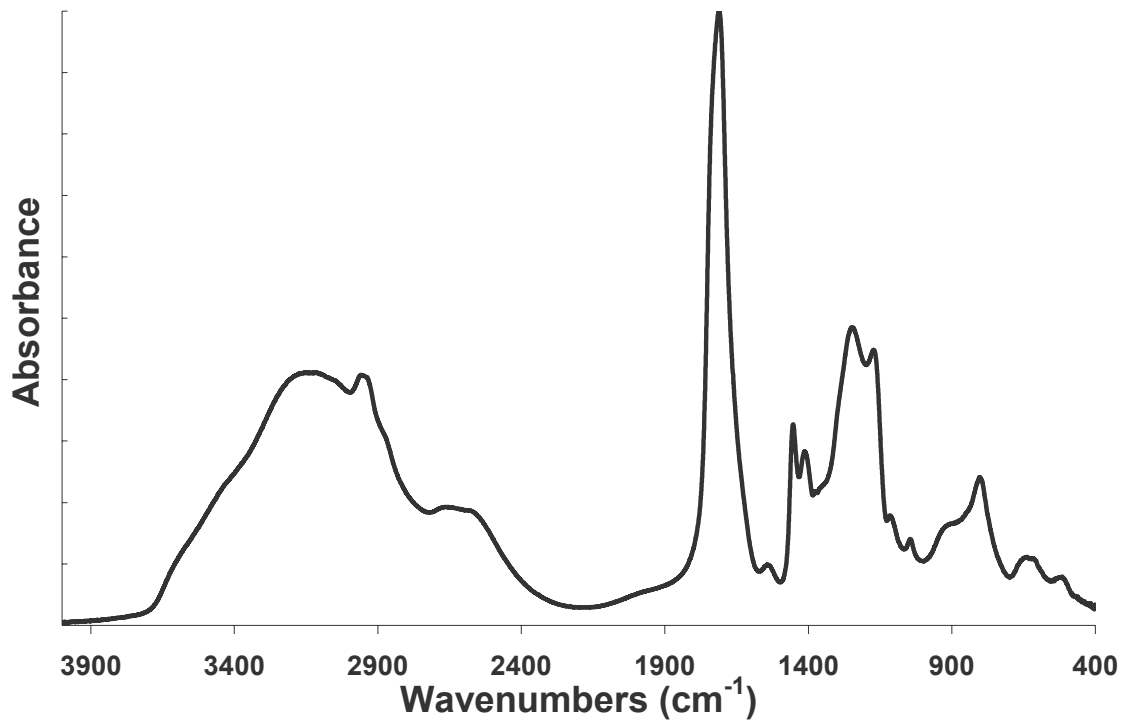


Figure 5.2 FT-IR spectrum of crosslinked PAA (0.75 mol % APE) showing the characteristic carbonyl stretching and fingerprint for the molecular structure of the polymer.

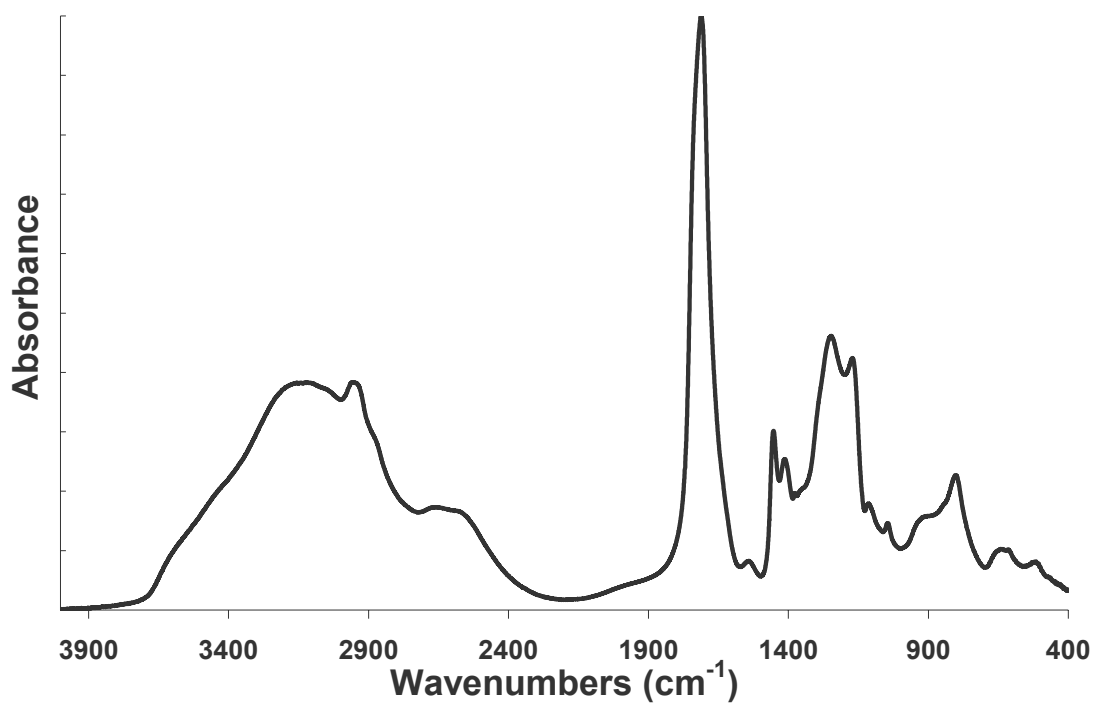


Figure 5.3 FT-IR spectrum of P(AA-g-PEG), PEG-1000, AA:EG 98:2, exhibiting the structural modifications introduced with the addition of the PEG tether.

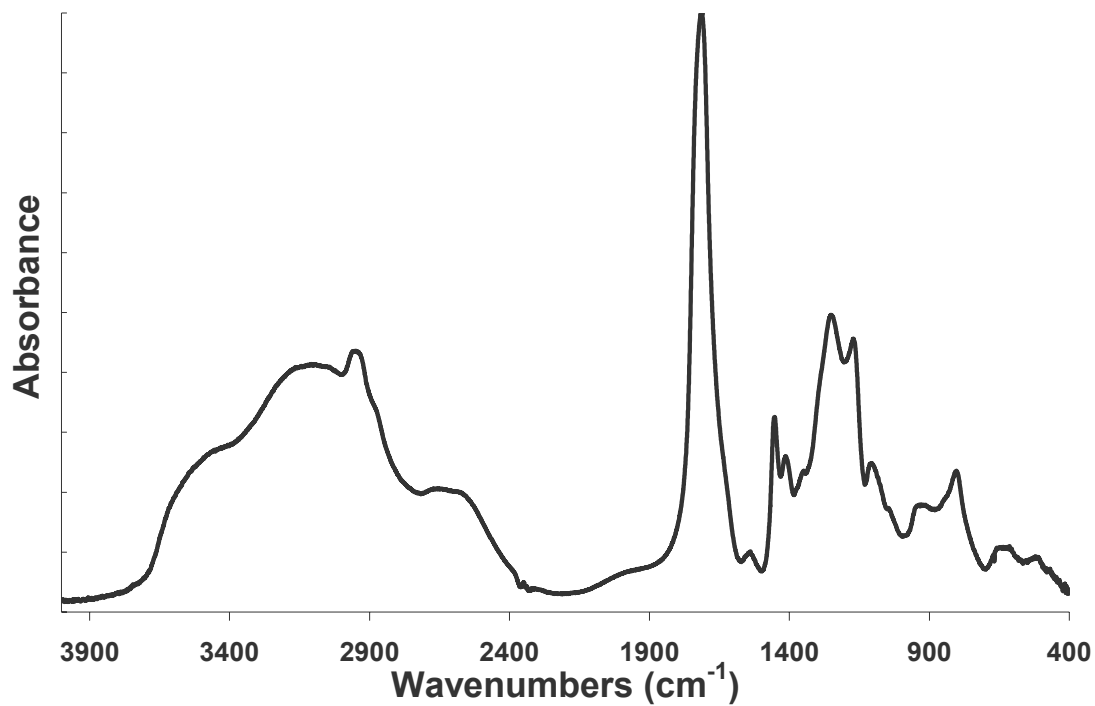


Figure 5.4 FT-IR spectrum of P(AA-g-PEG), PEG-1000, AA:EG 90:10, exhibiting the structural modifications introduced with the addition of the PEG tether.

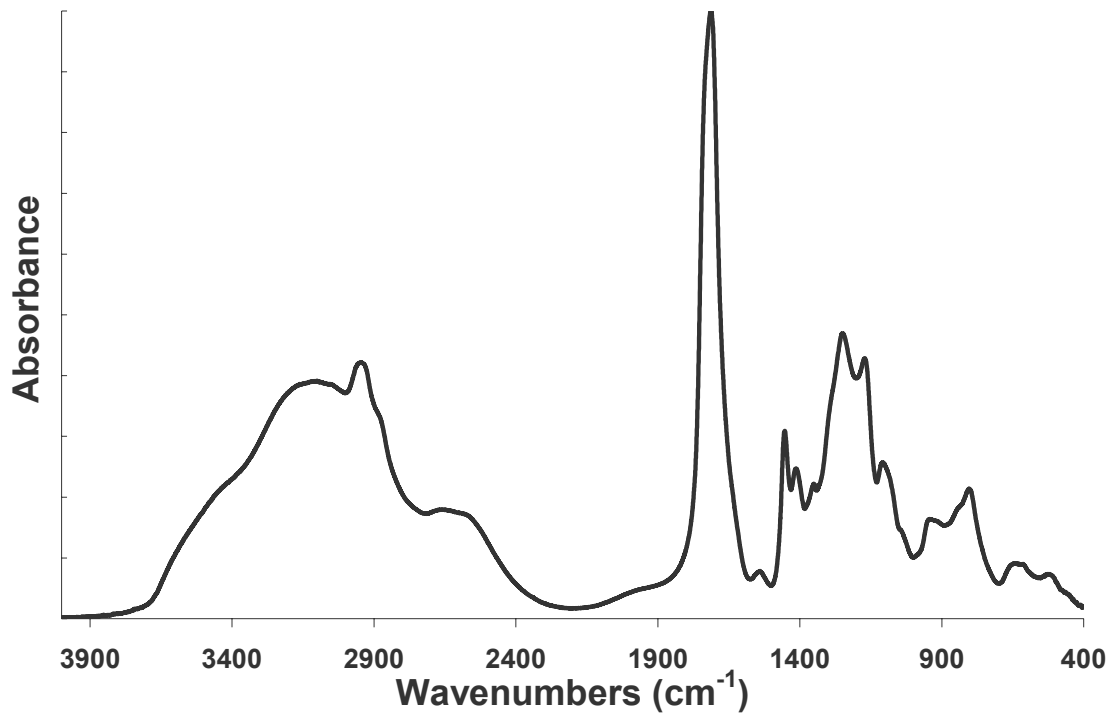


Figure 5.5 FT-IR spectrum of P(AA-g-PEG), PEG-1000, AA:EG 83:17, exhibiting the structural modifications introduced with the addition of the PEG tether.

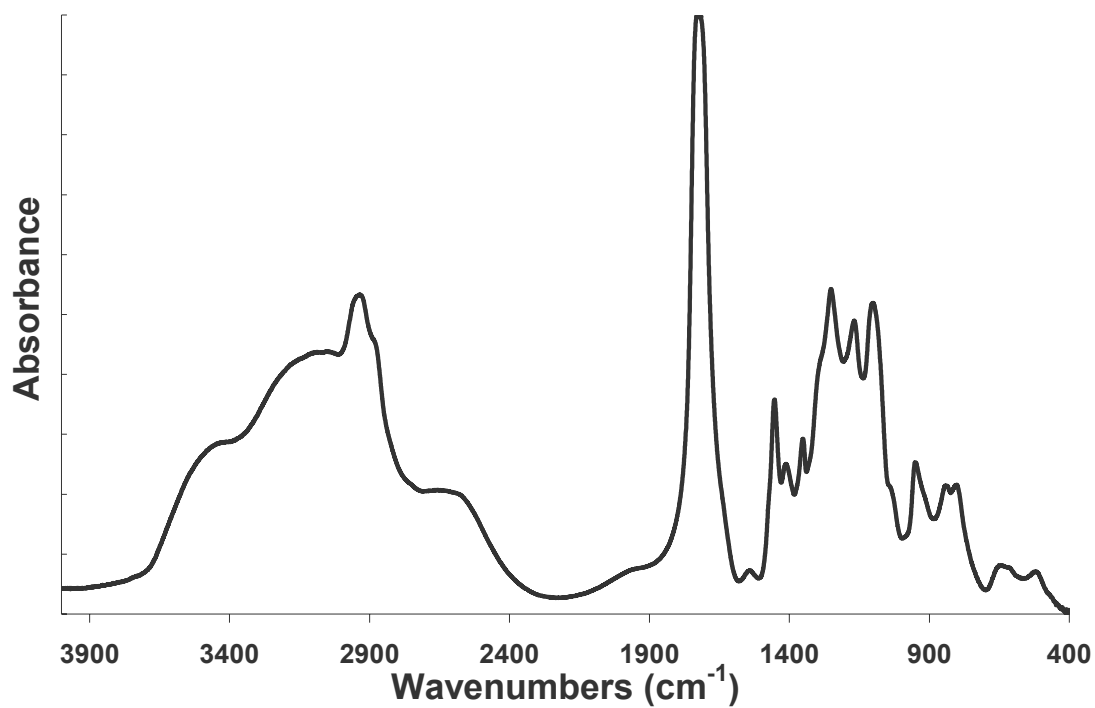


Figure 5.6 FT-IR spectrum of P(AA-g-PEG), PEG-1000, AA:EG 60:40, exhibiting the structural modifications introduced with the addition of the PEG tether.

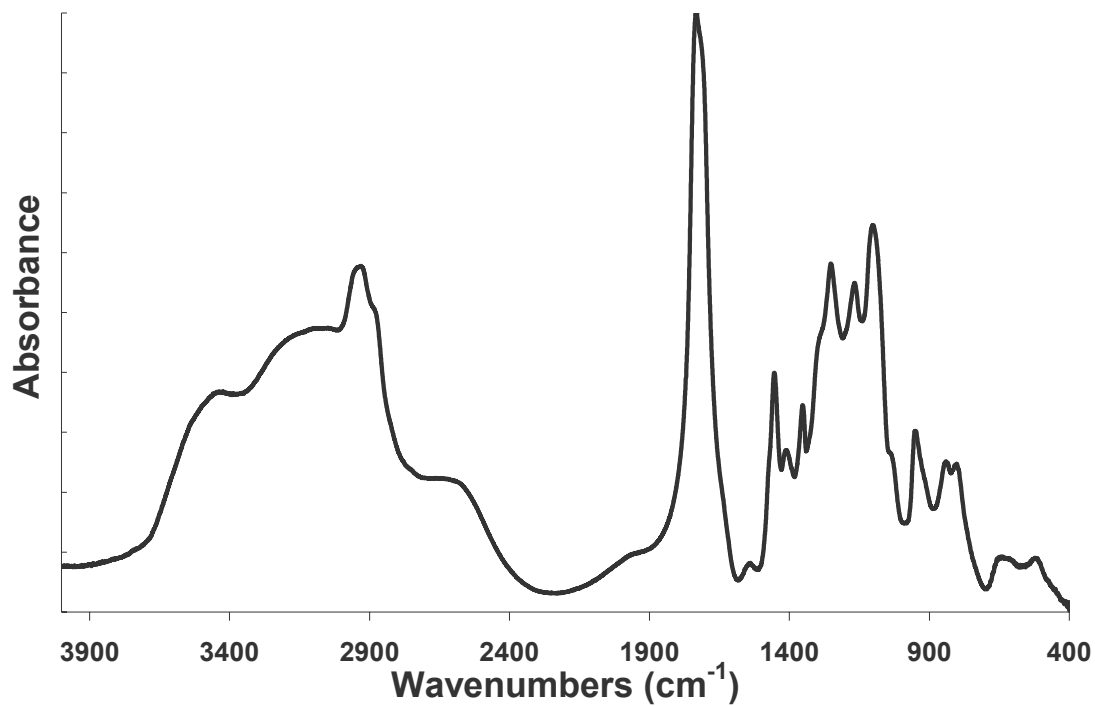


Figure 5.7 FT-IR spectrum of P(AA-g-PEG), PEG-1000, AA:EG 50:50, exhibiting the structural modifications introduced with the addition of the PEG tether.

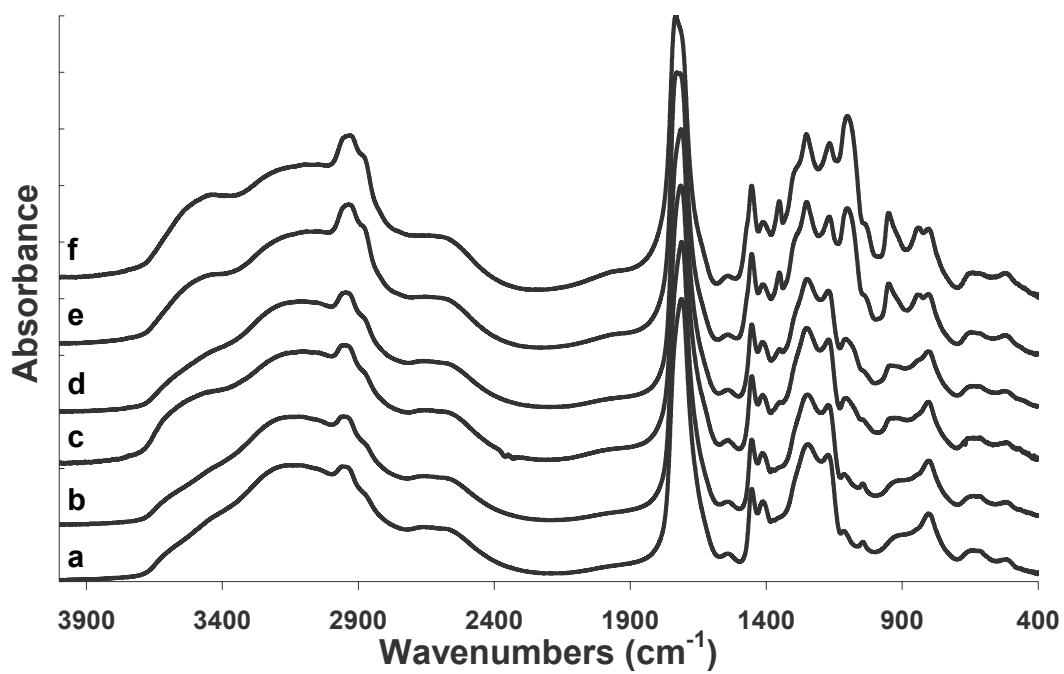


Figure 5.8 FT-IR spectrum of (a) crosslinked PAA (0.75 mol % APE), (b) P(AA-g-PEG), PEG-1000, AA:EG 98:2, (c) 90:10, (d) 83:17, (e) 60:40, (f) 50:50.

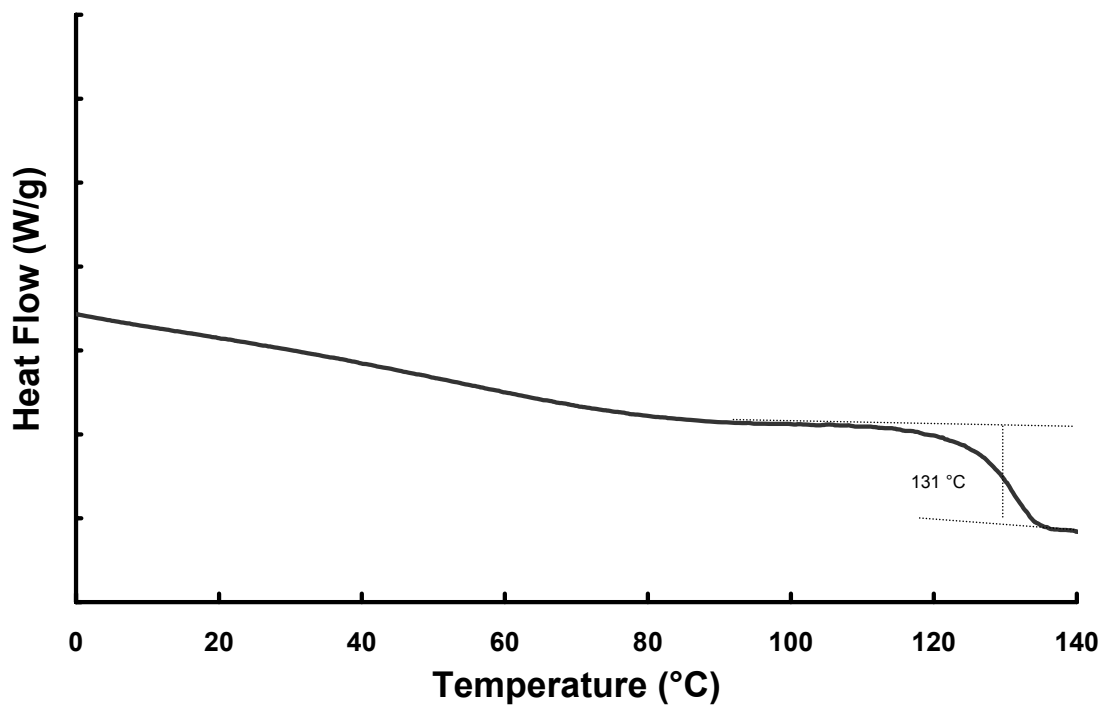


Figure 5.9 DSC thermogram of crosslinked PAA (0.75 mol % APE) exhibiting a T_g at 131°C.

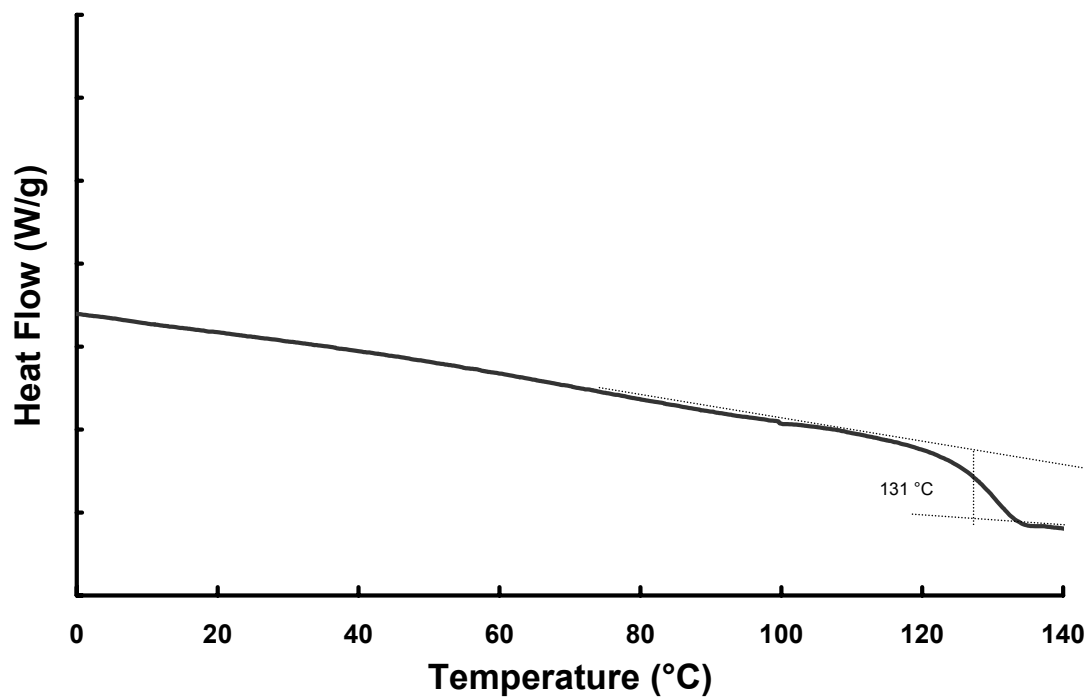


Figure 5.10 DSC thermogram P(AA-g-PEG), PEG-1000, AA:EG 98:2, exhibiting a T_g at 131°C.

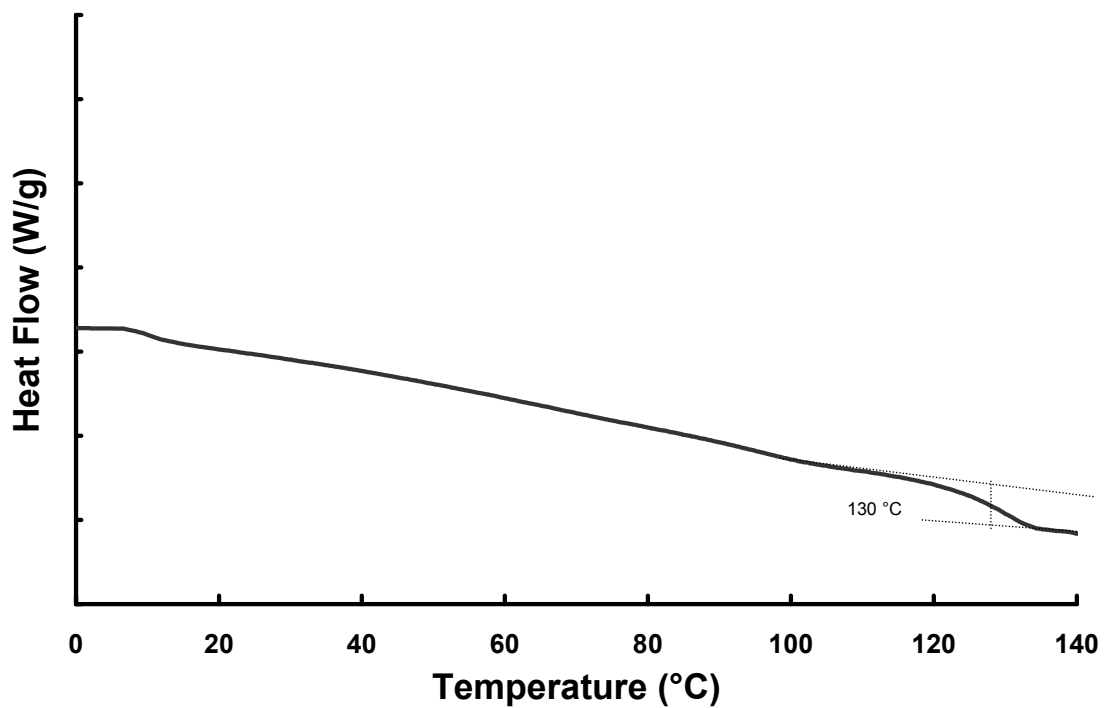


Figure 5.11 DSC thermogram of P(AA-g-PEG), PEG-1000, AA:EG 90:10, exhibiting a T_g at 130°C.

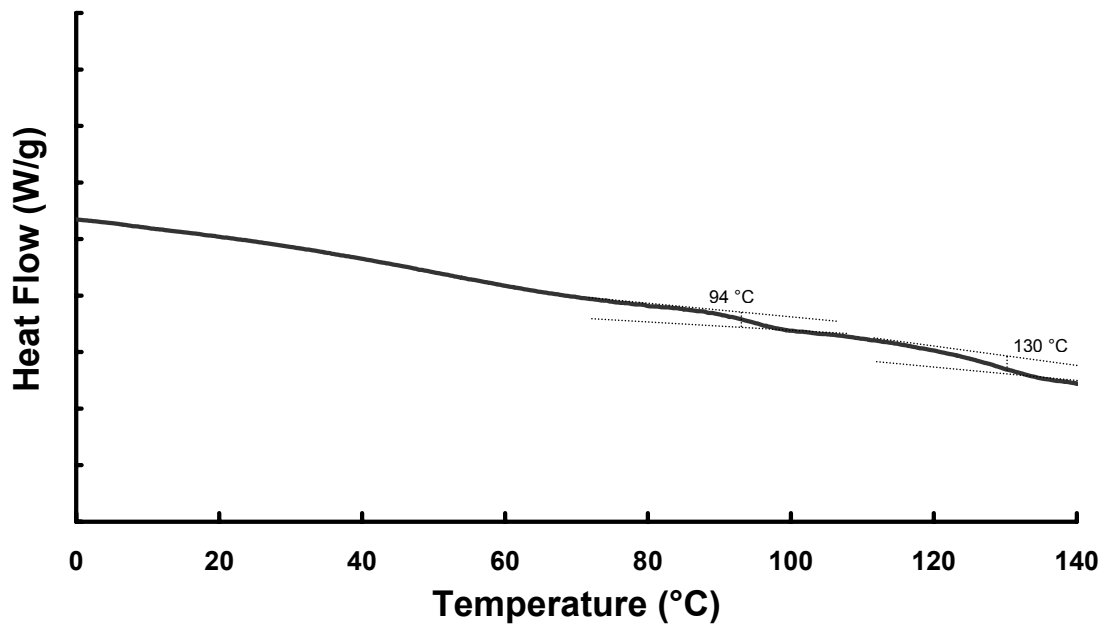


Figure 5.12 DSC thermogram of P(AA-g-PEG), PEG-1000, AA:EG 83:17, exhibiting two T_g's at 130°C and 94°C.

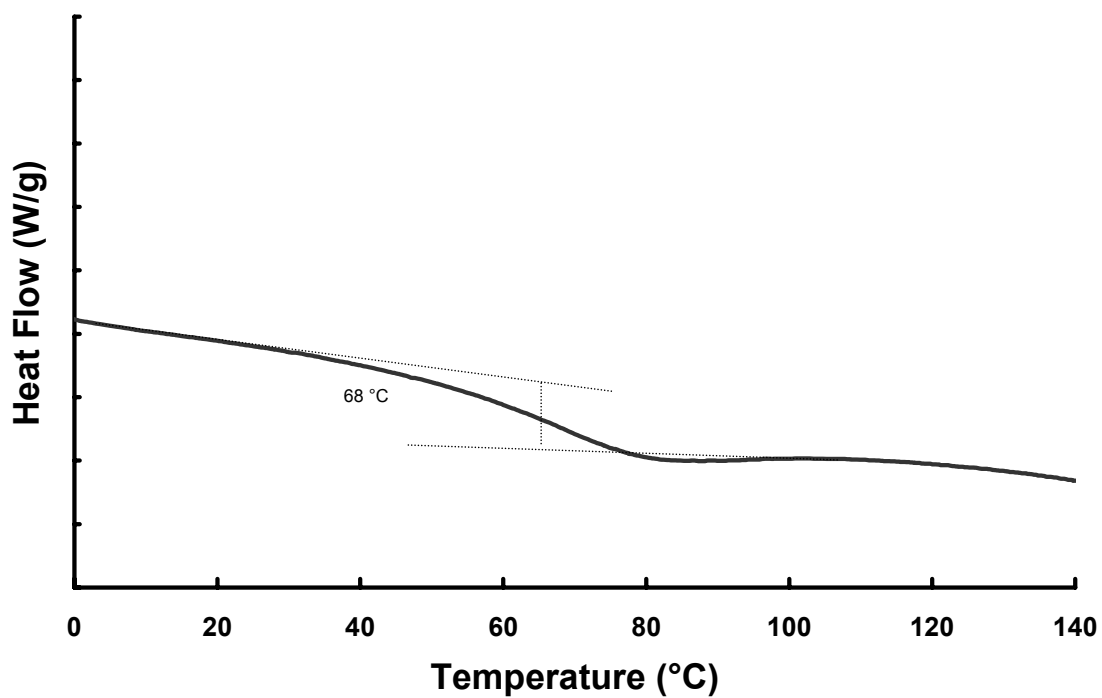


Figure 5.13 DSC thermogram of P(AA-g-PEG), PEG-1000, AA:EG 60:40, exhibiting a T_g at 68°C.

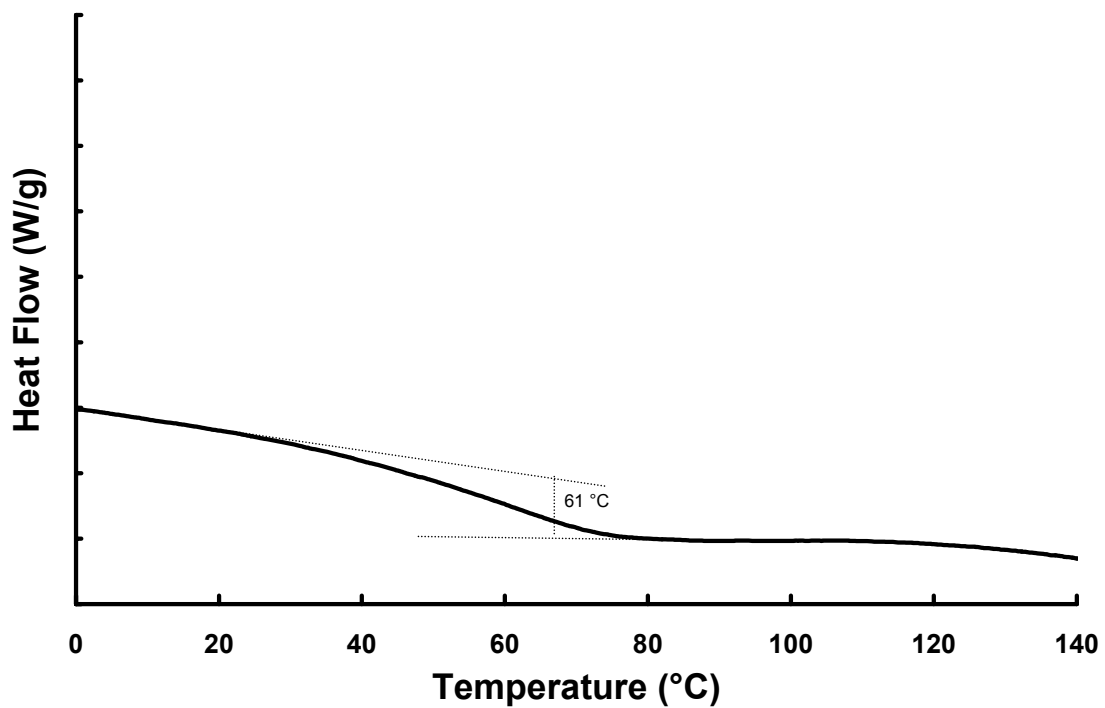


Figure 5.14 DSC thermogram of P(AA-g-PEG), PEG-1000, AA:EG 50:50, exhibiting a T_g at 61°C.

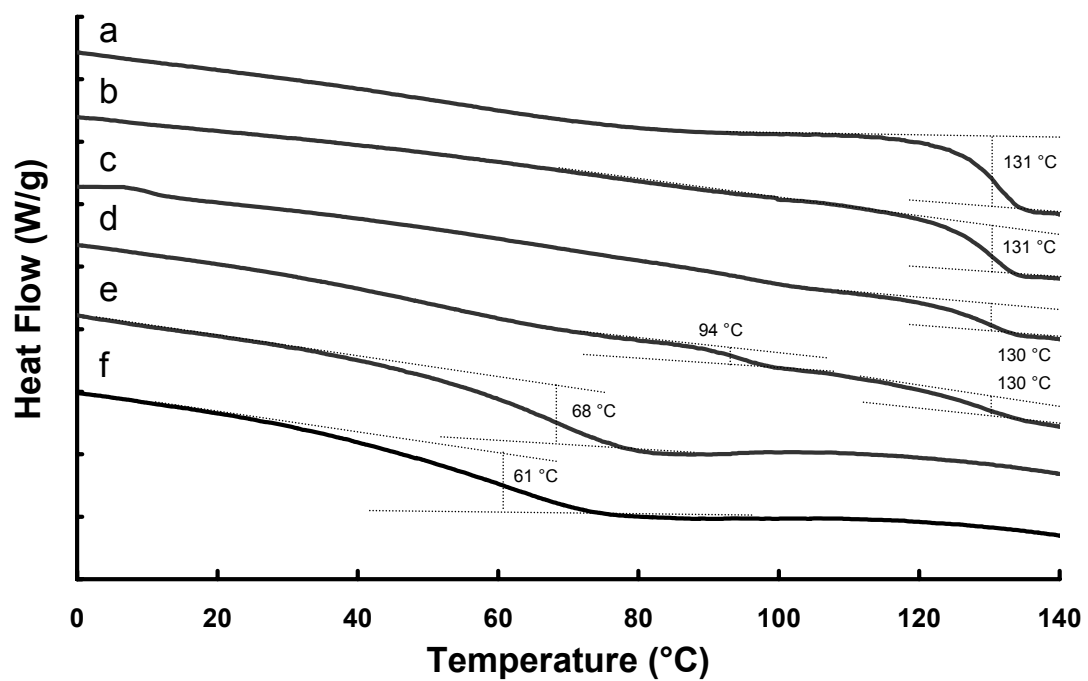


Figure 5.15 DSC thermogram of (a) crosslinked PAA (0.75 mol % APE), (b) PAA P(AA-g-PEG), PEG-1000, AA:EG 98:2, (c) 90:10, (d) 83:17, (e) 60:40, (f) 50:50.

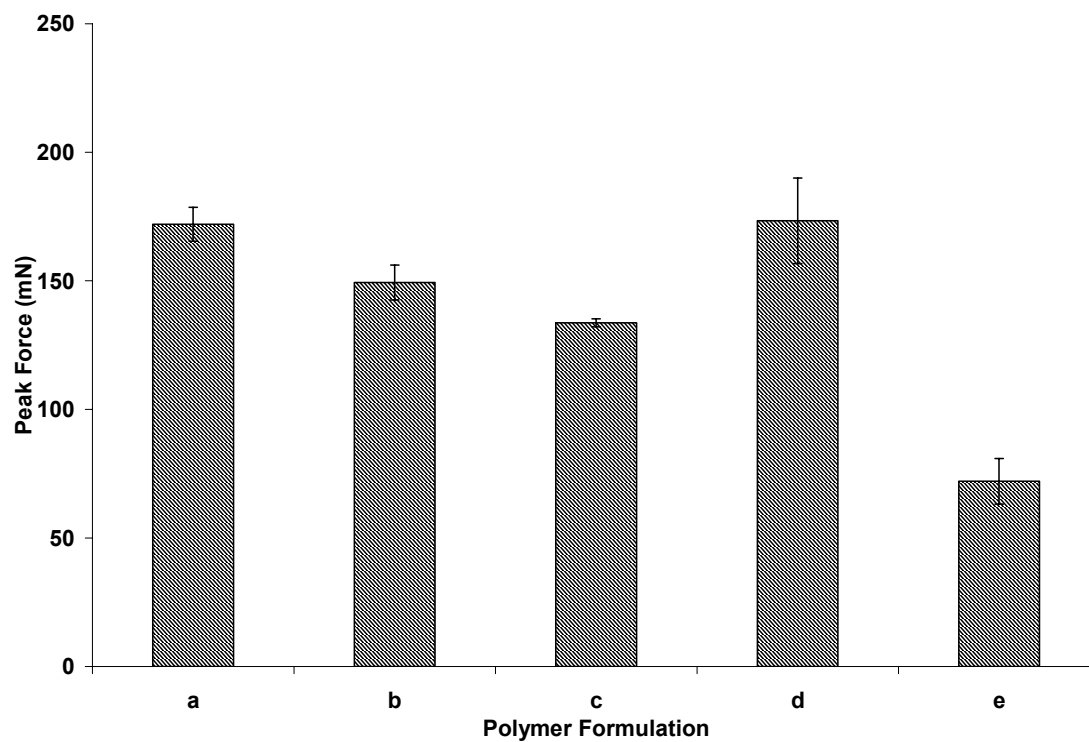


Figure 5.16 Evaluation of the peak force obtained from neutralized hydrated gels containing (a) crosslinked PAA (0.75 mol % APE), (b) P(AA-g-PEG), PEG-1000, AA:EG 98:2, (c) 90:10, (d) 83:17, (e) 60:40, (f) 50:50.

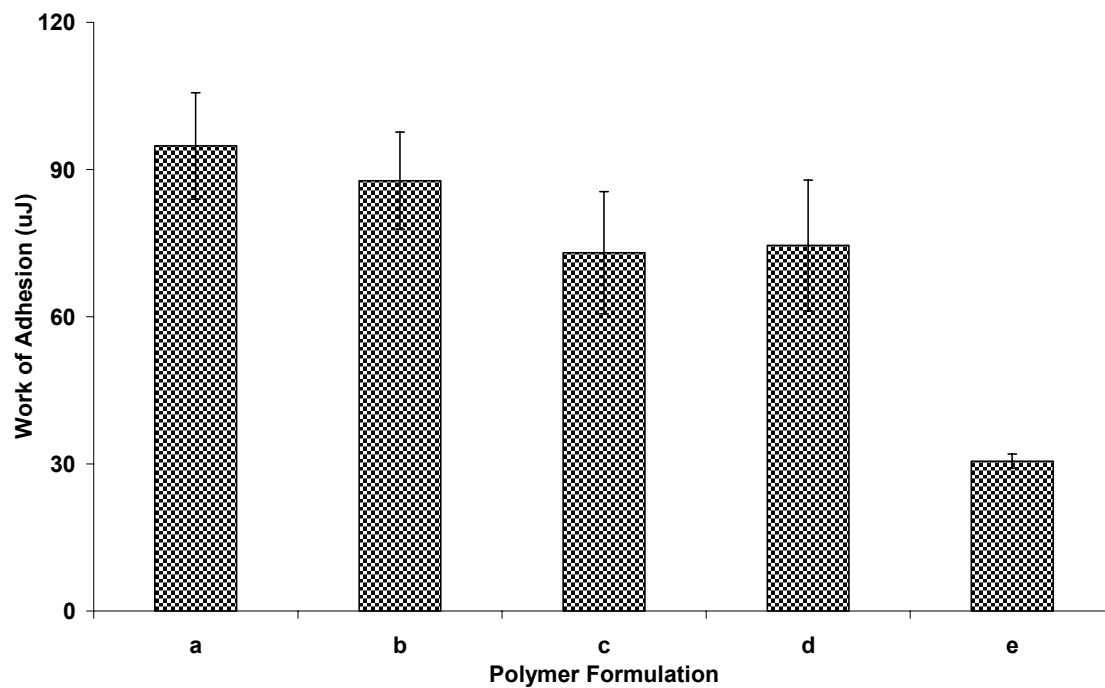


Figure 5.17 Evaluation of the work of adhesion of neutralized hydrated gels containing (a) crosslinked PAA (0.75 mol % APE), (b) P(AA-g-PEG), PEG-1000, AA:EG 98:2, (c) 90:10, (d) 83:17, (e) 60:40, (f) 50:50.

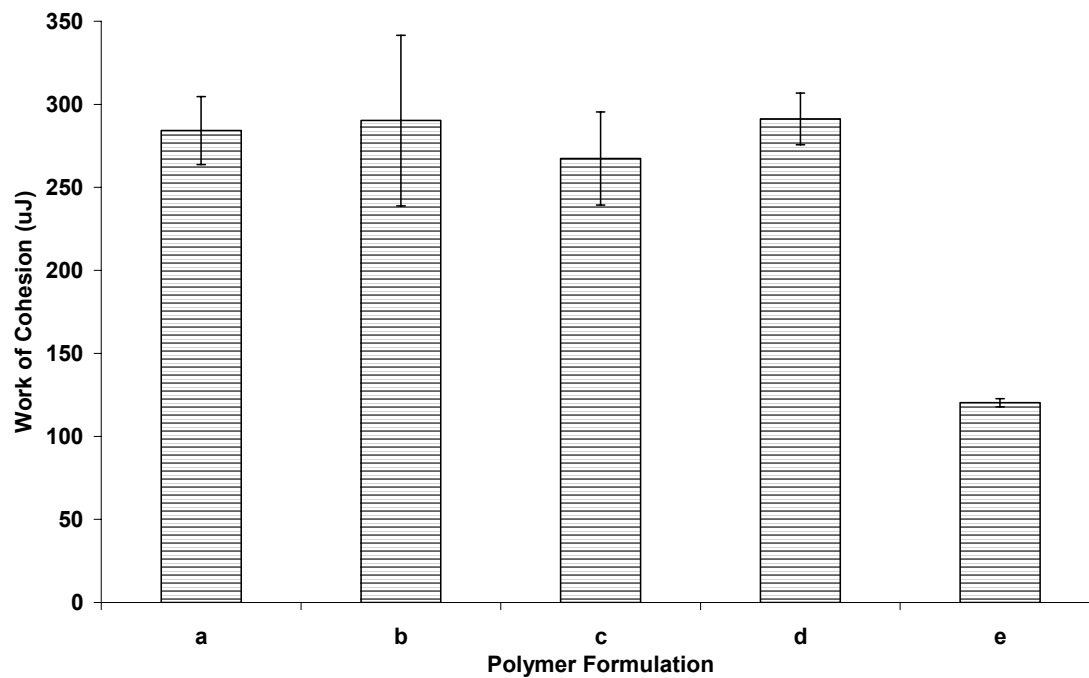


Figure 5.18 Evaluation of the work of cohesion of neutralized hydrated gels containing (a) crosslinked PAA (0.75 mol % APE), (b) P(AA-g-PEG), PEG-1000, AA:EG 98:2, (c) 90:10, (d) 83:17, (e) 60:40, (f) 50:50.

Chapter 6: Oral Minitablet Drug Delivery Matrices Containing Poly(ethylene glycol) Tethered, pH Responsive Excipients

INTRODUCTION

Mucoadhesive controlled drug delivery systems have the ability to maintain a controlled rate of release of the drug while localizing the drug at a specific absorption site. Both controlling release and localizing the drug concentration results in a prolonged duration of action and increased bioavailability. A mucous gel layer covers the hollow cavities of the body which include the buccal, nasal, gastrointestinal, and the urogenital paths. The gastrointestinal or oral delivery of therapeutics is the most preferred route of administration due to the higher patient compliance and ease of administration. Therefore, the development of controlled release drug delivery systems that are mucoadhesive has the potential to be effective at increasing the bioavailability of formulations in which efficacy has been difficult to achieve.

Challenges for the oral delivery of small and large molecular mass drugs include the harsh acidic environment of the stomach, the presence of degradative enzymes, and the narrow absorption window (low residence time) for certain compounds. To combat these effects, a drug delivery system that prevents denaturation or degradation and increases the residence time can increase the bioavailability of these problem ridden compounds. Carriers based on polyacid poly(ethylene glycol)-tethered complexation hydrogels have the capacity to overcome these formulation issues.

Mucoadhesive polymer-based drug delivery systems were first utilized by Nagai and collaborators as carriers for local treatment to the buccal cavity (1, 2). Mucus is also present in the nasal and gastrointestinal cavity, the vagina, and other hollow organs, providing a diverse arena for the application of mucoadhesive drug delivery systems.

Polymers that have typically been utilized in the development of mucoadhesive controlled release formulations include hydrophilic macromolecules containing numerous hydrogen bonding groups such as poly((meth)acrylic acid) which include the carbomer and polycarbophil families (Figure 2.3), cellulosics, and (semi)natural ones such as chitosan and alginate (3). Like so many other materials that were first utilized in biomedical applications (cellulose acetate dialysis tubing, Dacron® vascular grafts, and polyurethane heart molds), these materials were available off-the-shelf. Because their use was originally intended for other applications and was only transitioned into oral drug delivery systems, the drug delivery systems comprised of these materials have been classified as the first generation bioadhesive-based dosage forms (4).

Poly(acrylic acids) have been widely utilized for mucoadhesive applications due to their ability to form strong bonds with tissues and maintain a therapeutic at the desired site of administration for extended periods of time. Their polyelectrolytic behavior imparts a pH responsive behavior into the hydrogel network due to the ionization of the acrylic acid units and repulsion of the neighboring polymeric chains. This pH responsive behavior inhibits drug diffusion out of the matrix at a low pH (such as in the stomach) and allows drug release at a higher pH (such as in the small intestine). This delayed release prevents drug degradation and denaturation that would occur otherwise. Poly(acrylic acids) have also been shown to bind calcium which renders degradative enzymes such as trypsin ineffective. This effect further prevents the rapid degradation of therapeutic proteins and peptides.

The incorporation of poly(ethylene glycol) (PEG) tethers into the polymer network provides interpolymer complexes due to the association between the etheric oxygen on the PEG backbone and the carboxyl group of the polyacid. This complexation provides a more effective drug diffusion barrier at low pH's (stomach), allowing for more

protection of the labile drug and enhanced pH responsive delivery. The addition of PEG has been shown to act as an adhesion promoter, increasing the adhesion capacity of polymer networks containing the PEG tether (4).

The mucous gel network serves as a target for mucoadhesive biomaterials composed of polymer chains with the ability to interpenetrate and bridge the interface between the drug carrier and the mucus (5, 6). Polymer chains available at the surface of the biomaterial are often employed to serve as adhesion promoters (7-10). With the polymer chains at the periphery of the delivery system, these polymer chains are able to develop an intimate contact with the mucous gel layer, diffuse across the interface, and form entanglements with the mucous gel layer. Once the chains are across the polymer/gel boundary, further non-covalent mechanisms can occur to strengthen the bond. The enhanced bridging is a result of further chain entanglement, secondary bonding, or electrostatic interactions. For further enhancement of the adhesive bond formed between a delivery system and the mucous gel layer, tethered polymers, both anionic and cationic, can be used to create a synergistic effect in developing a more effective mucoadhesive delivery system (11-14).

The theory surrounding polymers attached to hydrogels was further developed in our laboratory by Huang et al. (13, 14) who studied systems composed of two hydrogels involved with the process of mucoadhesion. This theoretical framework provided evidence of the probability of finding both the chains and the free end segment outside the base gel available for interpenetration. Both were dependent on the surface coverage of the polymer tethers, with a large number of the chains and free ends present outside the base gel at low and intermediate coverage. However, at high coverages the chains penetrated back into the base gel due to the intermolecular interactions between neighboring chains. Adhesion enhancement associated with the base and target gel

(mucus layer) was also shown to be maximized at an intermediate coverage. Therefore, in designing biomaterials for mucoadhesive applications, the surface coverage of grafted polymer chains can be controlled to achieve adhesion enhancement through polymer-gel interpenetration (4).

The objectives of this research were to synthesize PEG-tethered pH responsive biomaterials composed of polyacids, formulate these polymers into minitabiet oral drug delivery matrices, and evaluate the ability of the polymer to act as a pH responsive controlled release excipients.

MATERIALS AND METHODS

Materials

Methacrylic acid (MAA, inhibited with 250 ppm hydroquinone), anhydrous potassium carbonate (K_2CO_3), and ethyl acetate (EtAc) were obtained from Fisher Scientific and used as received. Acrylic acid (AA, inhibited with 200 ppm hydroquinone) was obtained from Sigma Aldrich (Milwaukee, WI) and was used as received. Allyl pentaerythritol (APE), pentaerythritol triacrylate (PETA), and di(4-tert-butylcyclohexyl) peroxydicarbonate (BCHPC) were kindly supplied by Perstorp Polyols (Toledo, OH), Sartomer (Exton, PA), and Degussa Initiators (Elyria, OH), respectively. Poly(ethylene glycol) monomethyl ether monomethacrylate with a molecular weight of 300, 1100, 2100 (PEGMMA-300, 1100, 2100) were obtained from Sigma Aldrich (Milwaukee, WI). The 300 and 1100 molecular weights were used as received. PEGMMA-2100 was freeze dried to remove the water (commercially available as a 50 % w/w solution in water). Anhydrous lactose, magnesium stearate, and theophylline were purchased from Spectrum Chemical (Pasadena, CA). Carbopol 971P NF and Carbopol

974P NF were donated by Noveon (Cleveland, OH). All other chemicals were of reagent grade and used as received.

Synthesis

The synthesis of the microparticles utilized in the dosage forms has been described previously (15, 16). Briefly, in a typical thermally-initiated free radical precipitation polymerization, (M)AA, K_2CO_3 , PEGMMA, and deionized distilled water (ddH₂O) were combined and mixed to form a homogeneous mixture, allowing the escape of the neutralization by-product carbon dioxide. The crosslinking agent, APE or PETA, was dissolved in ethyl acetate. The monomer mixture and crosslinking agent were added to a four-necked round bottom flask equipped with an overhead stirrer, nitrogen purge, and condenser containing the polymerization solvent EtAc. Following a 20 minute purge with nitrogen, the initiator BCHPC dissolved in the polymerization solvent was added to the vessel and further purged for an additional 10 minutes.

The vessel was placed in a thermostatic bath at 50°C where precipitation was evident in a matter of minutes. The reaction was allowed to proceed for 16 hours to ensure a high percentage of monomer conversion. Following the polymerization, the particle slurry was centrifuged and washed with fresh ethyl acetate and dried using a rotary evaporator at elevated temperature and reduced pressure (90°C/40 mmHg). Table 1 lists the various polymer microparticles prepared.

Preparation of Tablet Matrices

The tablets were prepared according to the formulation listed in Table 6.1. All components were sieved prior to preparation. The multifunctional polymer, theophylline, and anhydrous lactose were mixed in a mortar and pestle. The magnesium stearate and Cab-O-Sil were combined with this mixture and further mixed until a homogeneous

mixture was obtained. An 80 mg portion of the sample mixture was compressed using a hydraulic compactor (Fred S. Carver Inc., Menomonee Falls, WI) at a pressure of 2000 kg.

Dissolution of Tablet Matrices

The drug-release properties of the matrix tablets were evaluated according to United States Pharmacopeia (USP) 27 apparatus 2 at 50 rpm and 37°C, using a dissolution system (Distek Dissolution System 2100B, North Brunswick, NJ). For diffusional analysis, tablets were placed in either 750 mL of 0.1 N HCl or 750 mL of 0.1 N HCl and 250 mL 0.2 M Na₃PO₄ (pH of the respective buffers being ~ 1 and 6.8), and 5 mL samples were removed. A final sample was withdrawn at 24 hours to represent the amount released at time infinity. To evaluate the pH responsive behavior of the matrices, a modified USP enteric test was performed. Briefly, the tablets were first placed in 750 mL of 0.1 N HCl for one hour and 5 mL samples were withdrawn. At the end of the hour time period, 0.1 N HCl buffer was added to replace the withdrawn volume, and 250 mL of 0.2 M Na₃PO₄ buffer was added to the vessel to increase the pH to 6.8. Samples were withdrawn, with the time infinity sample withdrawn at 24 hours.

Dissolution samples were analyzed using a Bio-Tek® Synergy HT 96-well plate ultraviolet/visible (UV/Vis) spectrophotometer at a wavelength of 272 nm, corresponding to the peak absorbance for theophylline.

RESULTS AND DISCUSSION

Most drug delivery systems composed of a release rate controlling polymer can be described by the following two forms of Fick's law of diffusion, where c_i and j_i are the concentration and mass flux of drug i , respectively; x and t are position and time of release; and D_{ip} is the drug diffusion coefficient through the polymer.

$$j_i = D_{ip} \frac{dc_i}{dx} \quad (6.1)$$

$$\frac{\partial c_i}{\partial t} = D_{ip} \frac{\partial^2 c_i}{\partial x^2} \quad (6.2)$$

The solution to equation (6.2) provides the time-dependent release of the matrix containing the rate controlling polymer. In matrix systems, the drug is incorporated in the polymer by physically mixing the compound with the polymer and other excipients. The solubility of the drug becomes a controlling factor in the modeling of the release depending on whether or not the initial drug loading is above or below the solubility limit. For the cases represented in this study, the initial loading was below the solubility limit, allowing for simple molecular diffusion of the drug through the polymer.

The systems investigated in this research were matrix tablets that were uniformly loaded at an initial concentration, $c_{i,0}$. When the surface concentration of the drug in the dissolution medium is kept constant, i.e. sink conditions, and for small release times ($M_t/M_\infty < 0.6$), the following solution can be derived:

$$\frac{M_t}{M_\infty} = 4 \left[\frac{D_{ip} t}{\delta^2} \right]^{1/2} \left[\frac{1}{\sqrt{\pi}} + 2 \sum_{n=1}^{\infty} (-1)^n \operatorname{ierfc} \frac{n\delta}{\sqrt{D_{ip} t}} \right] \quad (6.3)$$

Equation (6.3) can be further simplified to the form used in this work to describe the diffusional release to give

$$\frac{M_t}{M_\infty} = 4 \left[\frac{D_{ip} t}{\pi \delta^2} \right]^{1/2} \quad (6.4)$$

The fractional release of a compound in a slab drug delivery system is clearly proportional to the $t^{1/2}$ for early times. For systems possessing a lag time before release

occurs, an additional term, θ , is amended to equation (6.4) to account for this time where negligible release occurs.

$$\frac{M_t}{M_\infty} = 4 \left[\frac{D_{ip}(t - \theta)}{\pi \delta^2} \right]^{1/2} \quad (6.5)$$

Poly(acrylic acid)-containing Minitablets

Figure 6.2 and 6.3 show the release profile for dissolution studies of PAA tablets in 0.1 N HCl and pH 6.8 buffer, respectively. As PAA is soluble in both the acidic and near-neutral solutions, the polymer dissolves at the surface of the tablet. Dissolution is not as rapid in the acidic environment, and the matrix slightly swells under these conditions due to the hydrophilic nature of the polymer. In the pH 6.8 buffer, ionization of the PAA polymer occurs and polymer dissolution is more rapid, which results in a slightly higher effective diffusion coefficient, D_{eff} , for the model compound.

Table 6.2 displays the results of the diffusional analysis of novel mintablet matrices composed of poly(acrylic acid) (PAA) microparticles. Upon incorporation of a small amount of crosslinking agent (0.2, 0.43, and 0.75 mol % APE), the calculated value, D_{eff} was significantly decreased in both dissolution media. In the low pH environment, the matrices swell due to the hydrophilic nature of the polymer carrier which increases the porosity of the tablet allowing for a slightly higher D_{eff} than in the pH 6.8 buffer. Due to the pH responsive nature of the polymers in the tablets causing ionization and swelling, a gel layer is formed at the surface of the tablet for the loosely crosslinked polymers (0.2 and 0.43 mol % APE and Carbopols) which acts as a diffusion inhibiting layer. For the more densely crosslinked particles, the release behavior in the acidic buffer dissolution media is similar to that of linear PAA. In the pH 6.8 buffer, the

individual particles at the periphery of the tablet swell and are released, resulting in significantly higher D_{eff} for the model compound.

Poly(methacrylic acid)-containing Minitablets

Figures 6.4 and 6.5 show the release profile of theophylline from these tablets. Table 6.3 displays the results for the diffusional analysis of poly(methacrylic acid)-containing (PMAA) tablets. PMAA is more hydrophobic than PAA due to the presence of the methyl group. In the low pH environment, the PMAA tablets only slightly swell and polymer dissolution is negligible during the time scale of these experiments. However, in the higher pH environment, ionization occurs and a dissolving gel layer of polymer is formed.

The trend is similar for tablets containing crosslinked PMAA. The slight polymer swelling induces an increase in the porosity of the tablets resulting in an affected D_{eff} . At the higher pH, loosely crosslinked polymers behave similarly to linear PMAA. With increased crosslinking, swollen particle release from the surface of the tablet is more prevalent.

Minitablets composed of PEG-tethered PAA Microparticles

The release profile of theophylline from these systems can be observed in Figure 6.6 and 6.7. The release behavior for tablets containing a low concentration of PEG is similar to that obtained for PAA systems. The effect of the PEG tether is not significantly evident until a 50:50 AA:EG ratio for PEG-300 and 70:30 AA:EG for PEG-2000. Release is inhibited in the 0.1 N HCl media due to the complexation of the etheric oxygens and the carboxyl groups present on the PAA backbone. In the pH 6.8 buffer, interpolymer decomplexation occurs, resulting in an increase in the porosity of the tablet and, subsequently, the release of the theophylline. Table 6.4 displays the results for the

diffusional analysis for the release of theophylline from minitables composed of poly(ethylene glycol)-tethered (PEG) PAA.

Minitables Composed of PEG-tethered PMAA Microparticles

The release profile for these systems in either 0.1 N HCl or pH 6.8 buffer can be observed in Figures 6.8 and 6.9, respectively. The result of the diffusional analysis for minitables containing PEG-tethered PMAA microparticles is exhibited in Table 6.5. Due to interpolymer complexation, which causes a lower degree of swelling and expansion of the minitablet, the D_{eff} for these tablets is significantly lower in the low pH environment. Upon introduction to a higher pH environment, decomplexation occurs allowing for the matrix to open up and release the drug. However, for relatively large amounts of PEG (MAA:EG 50:50), release is significantly inhibited at both pH's. The reason for inhibition at higher pH's is due to the slower dynamics of the decomplexation which can be attributed to decreased penetrant diffusion. Less water is uptaken by the minitablet, which results in slower decomplexation dynamics and a lowered D_{eff} for theophylline.

CONCLUSIONS

Novel oral minitablet drug delivery matrices were successfully formulated using pH responsive hydrogel microparticles. The release of a model drug was shown to be dependent on the amount of crosslinking agent incorporated during microparticle synthesis with lower degrees of crosslinking being preferred for effective release characteristics. The amount of PEG was shown to significantly alter the release behavior due to interpolymer complexation between the ether oxygens and the carboxylic acid groups. The release behavior was modeled according to a simplified model for monolithic matrices taking into account a lag time. The effective diffusion coefficient

was calculated and shown to be affected by the monomer type, degree of crosslinking, and presence of PEG tether.

REFERENCES

1. Ishida M, Machida Y, Nambu N, and Nagai T, Pharmaceutical Interactions In Dosage Forms And Processing.21. New Mucosal Dosage Form Of Insulin, *Chem. Pharm. Bull.*, 29:810-816, 1981.
2. Nagai T and Machida Y, Advances In Drug Delivery - Mucosal Adhesive Dosage Forms, *Pharm. Int.*, 6:196-200, 1985.
3. Smart JD, The basics and underlying mechanisms of mucoadhesion, *Adv. Drug Deliv. Rev.*, 57:1556-1568, 2005.
4. Serra L, Domenech J, and Peppas NA, Design of poly(ethylene glycol)-tethered copolymers as novel mucoadhesive drug delivery systems, *Eur. J. Pharm. Biopharm.*, 63:11-18, 2006.
5. Jabbari E, Wisniewski N, and Peppas NA, Evidence Of Mucoadhesion By Chain Interpenetration At A Poly(Acrylic Acid) Mucin Interface Using Atr-Ftir Spectroscopy, *J. Control. Release*, 26:99-108, 1993.
6. Ponchel G, Touchard F, Wouessidjewe D, Duchene D, and Peppas NA, Bioadhesive Analysis Of Controlled-Release Systems.3. Bioadhesive And Release Behavior Of Metronidazole-Containing Poly(Acrylic Acid)-Hydroxypropyl Methylcellulose Systems, *Int. J. Pharm.*, 38:65-70, 1987.
7. De Ascentiis A, Degrazia JL, Bowman CN, Colombo P, and Peppas NA, Mucoadhesion Of Poly(2-Hydroxyethyl Methacrylate) Is Improved When Linear Poly(Ethylene Oxide) Chains Are Added To The Polymer Network, *J. Control. Release*, 33:197-201, 1995.
8. Peppas NA, Molecular calculations of poly(ethyleneglycol) transport across a swollen poly(acrylic acid) mucin interface, *J. Biomater. Sci.-Polym. Ed.*, 9:535-542, 1998.
9. Peppas NA and Mongia NK, Ultrapure poly(vinyl alcohol) hydrogels with mucoadhesive drug delivery characteristics, *Eur. J. Pharm. Biopharm.*, 43:51-58, 1997.
10. Sahlin JJ and Peppas NA, Enhanced hydrogel adhesion by polymer interdiffusion: Use of linear poly(ethylene glycol) as an adhesion promoter, *J. Biomater. Sci.-Polym. Ed.*, 8:421-436, 1997.
11. Efremova NV, Huang Y, Peppas NA, and Leckband DE, Direct measurement of interactions between tethered poly(ethylene glycol) chains and adsorbed mucin layers, *Langmuir*, 18:836-845, 2002.

12. Huang YB, Leobandung W, Foss A, and Peppas NA, Molecular aspects of muco- and bioadhesion: Tethered structures and site-specific surfaces, *J. Control. Release*, 65:63-71, 2000.
13. Huang YB, Szleifer I, and Peppas NA, Gel-gel adhesion by tethered polymers, *J. Chem. Phys.*, 114:3809-3816, 2001.
14. Huang YB, Szleifer I, and Peppas NA, A molecular theory of polymer gels, *Macromolecules*, 35:1373-1380, 2002.
15. Thomas JB, Tingsanchali J, Creecy CM, Rosales AM, McGinity JW, and Peppas NA, Dynamics of Poly(ethylene glycol) Tethered pH Responsive Biomaterials, (*in preparation*), 2006.
16. Thomas JB, Creecy CM, McGinity JW, and Peppas NA, Synthesis and properties of lightly crosslinked poly((meth)acrylic acid) microparticles prepared by free radical precipitation polymerization, *Polym. Bull.*, 57:11-20, 2006.

Table 6.1 Tablet formulations prepared by dry compression.

Component	wt %
Multifunctional Polymer	50%
Anhydrous Lactose	38%
Theophylline	10%
Cab-O-Sil	1.25%
Magnesium Stearate	0.75%
Total	100%

Table 6.2 Diffusional analysis of tablet matrices formulated according to Table 6.1 composed of poly(acrylic acid) and crosslinked poly(acrylic acid) microparticles synthesized with varying levels of crosslinking agent.

	$D_{\text{eff}} (\times 10^6 \text{ cm}^2/\text{s})$	
	pH = 1.2	pH = 6.8
PAA	3.6 ± 0.21	4.2 ± 1.8
x-PAA (0.20 mol % APE)	1.1 ± 0.04	0.74 ± 0.03
x-PAA (0.43 mol % APE)	0.96 ± 0.76	0.81 ± 0.04
x-PAA (0.75 mol % APE)	2.9 ± 0.47	3.9 ± 0.19
Carbopol 971P-NF	1.20 ± 0.01	0.85 ± 0.01
Carbopol 974P-NF	1.50 ± 0.15	1.60 ± 0.01

Table 6.3 Diffusional analysis of tablet matrices formulated according to Table 6.1 composed of poly(methacrylic acid) and crosslinked poly(methacrylic acid) microparticles synthesized with varying levels of crosslinking agent.

	$D_{\text{eff}} (\times 10^6 \text{ cm}^2/\text{s})$	
	pH = 1.2	pH = 6.8
PMAA	0.62 ± 0.24	2.23 ± 0.02
x-PMAA (0.43 mol % PETA)	1.24 ± 0.04	2.41 ± 0.02
x-PMAA (0.75 mol % PETA)	1.72 ± 0.03	4.54 ± 0.08

Table 6.4 Diffusional analysis of tablet matrices formulated according to Table 6.1 composed of crosslinked poly(acrylic acid) microparticles containing a poly(ethylene glycol) tether, with the tether concentration varied for each system below.

	$D_{\text{eff}} (\times 10^6 \text{ cm}^2/\text{s})$	
	pH = 1.2	pH = 6.8
P(AA-g-PEG), PEG-300, 90:10	1.35 ± 0.09	1.50 ± 0.05
P(AA-g-PEG), PEG-300, 70:30	0.86 ± 0.02	1.01 ± 0.02
P(AA-g-PEG), PEG-300, 50:50	1.02 ± 0.05	3.90 ± 0.56
P(AA-g-PEG), PEG-2000, 70:30	1.18 ± 0.08	4.28 ± 0.20

Table 6.5 Diffusional analysis of tablet matrices formulated according to Table 6.1 composed of crosslinked poly(methacrylic acid) microparticles containing a poly(ethylene glycol) tether, with the tether concentration varied for each system below.

	$D_{\text{eff}} (\times 10^6 \text{ cm}^2/\text{s})$	
	pH = 1.2	pH = 6.8
PMAA-g-PEG, PEG-1000, 80:20	0.69 ± 0.06	3.85 ± 0.20
PMAA-g-PEG, PEG-1000, 70:30	0.69 ± 0.01	3.93 ± 0.14
PMAA-g-PEG, PEG-1000, 50:50	0.18 ± 0.02	0.36 ± 0.04

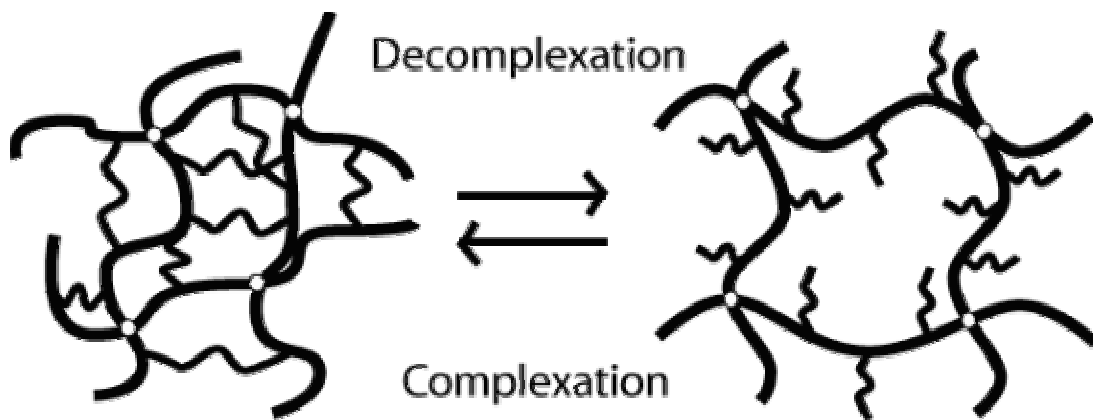


Figure 6.1 The reversible complexation/decomplexation behavior of complexation hydrogels. The polymeric backbone consists of proton donating polyacids with proton accepting polymer tethers. At low pH's the polymers are participating in interpolymer complexation, effectively inhibiting diffusion out of the network. At pH's close and above the pKa of the polyacid, the interpolymer complexes dissociate, giving rise to an expansion of the polymer network.

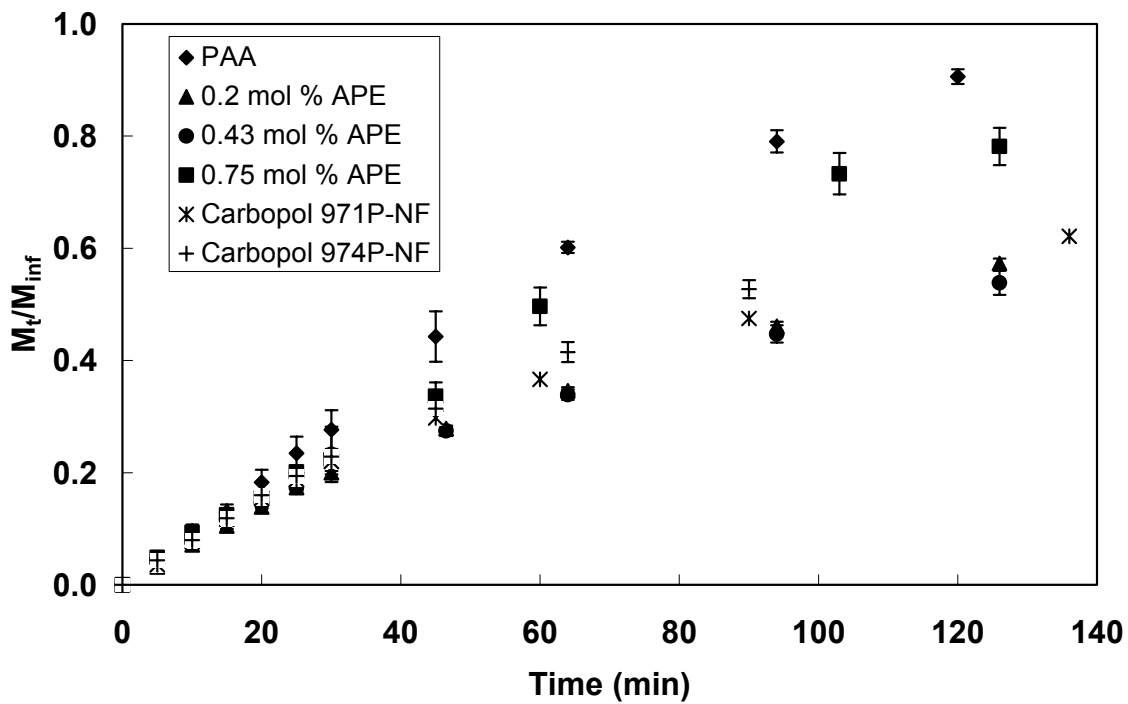


Figure 6.2 Theophylline release from minitablet matrices containing poly(acrylic acid) (PAA) microparticles in 0.1 N HCl.

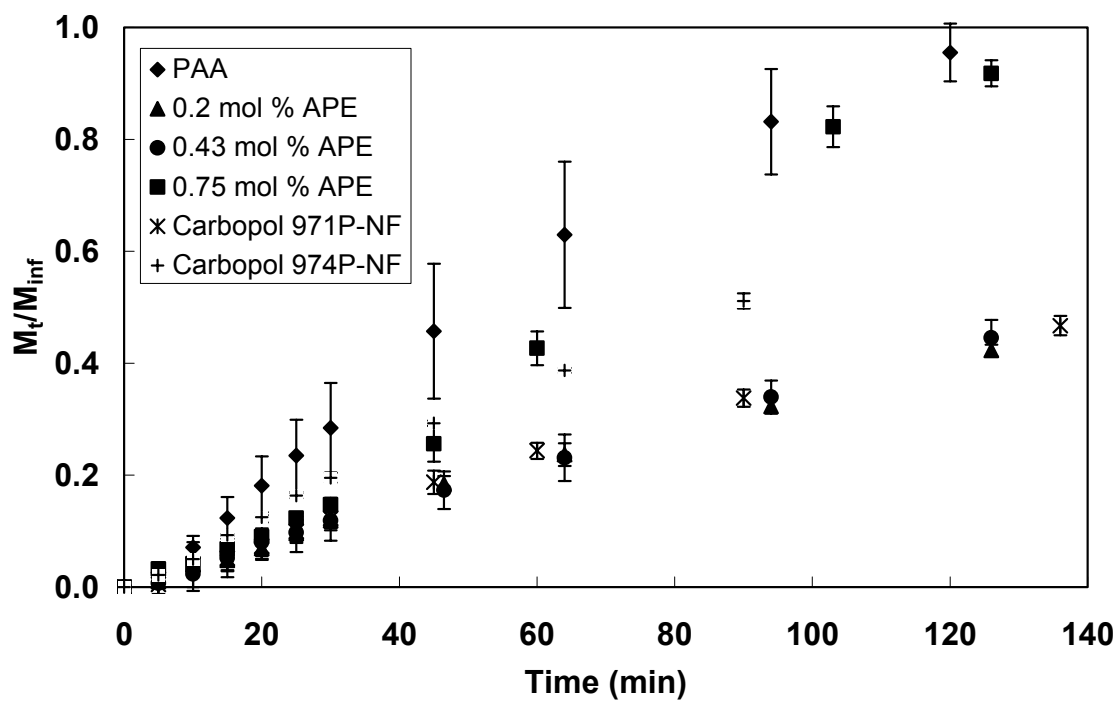


Figure 6.3 Theophylline release from minitablet matrices containing poly(acrylic acid) (PAA) microparticles in pH 6.8 buffer.

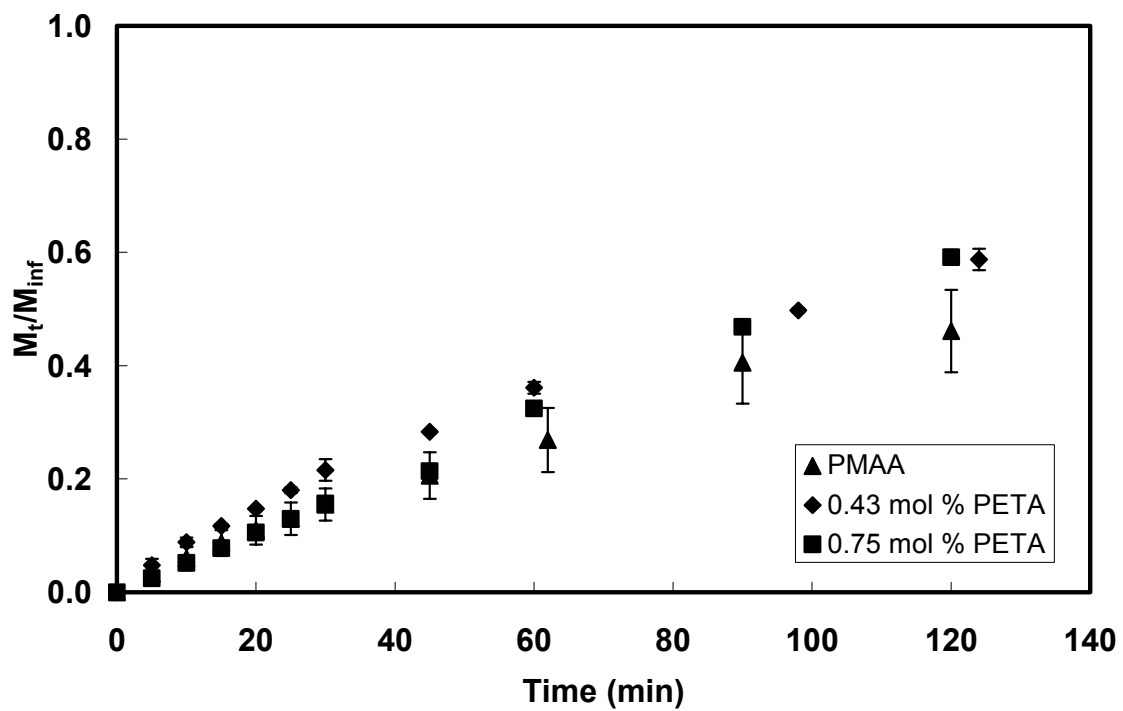


Figure 6.4 Theophylline release from minitablet matrices containing poly(methacrylic acid) (PMAA) microparticles in 0.1 N HCl.

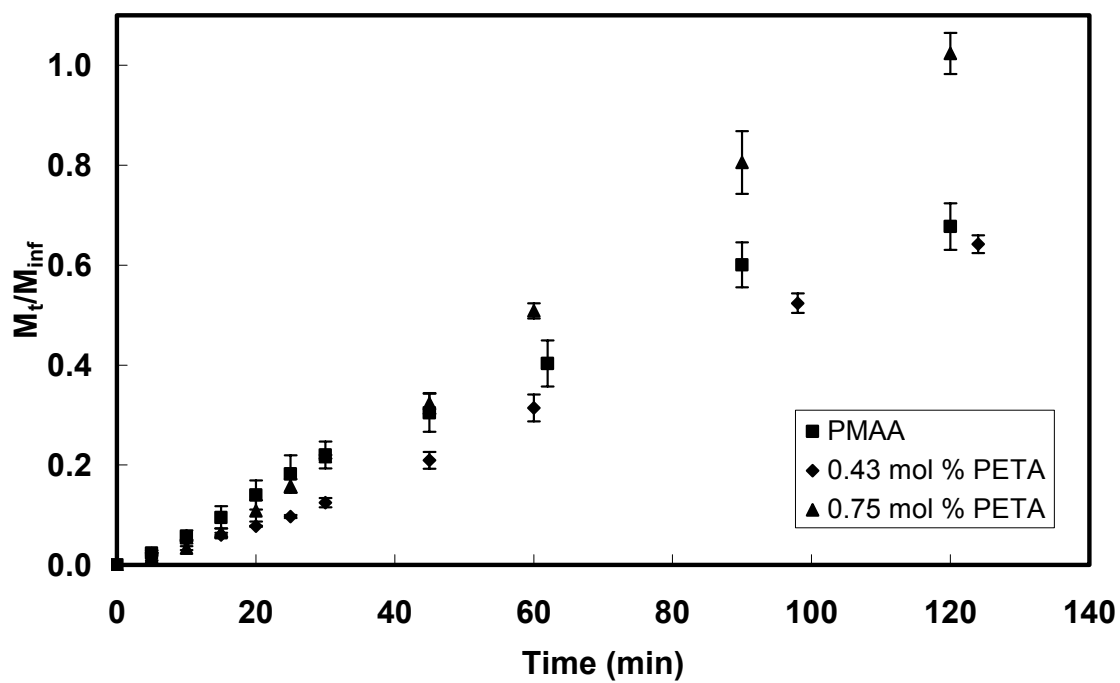


Figure 6.5 Theophylline release from minitab matrices containing poly(methacrylic acid) (PMAA) microparticles in pH 6.8 buffer.

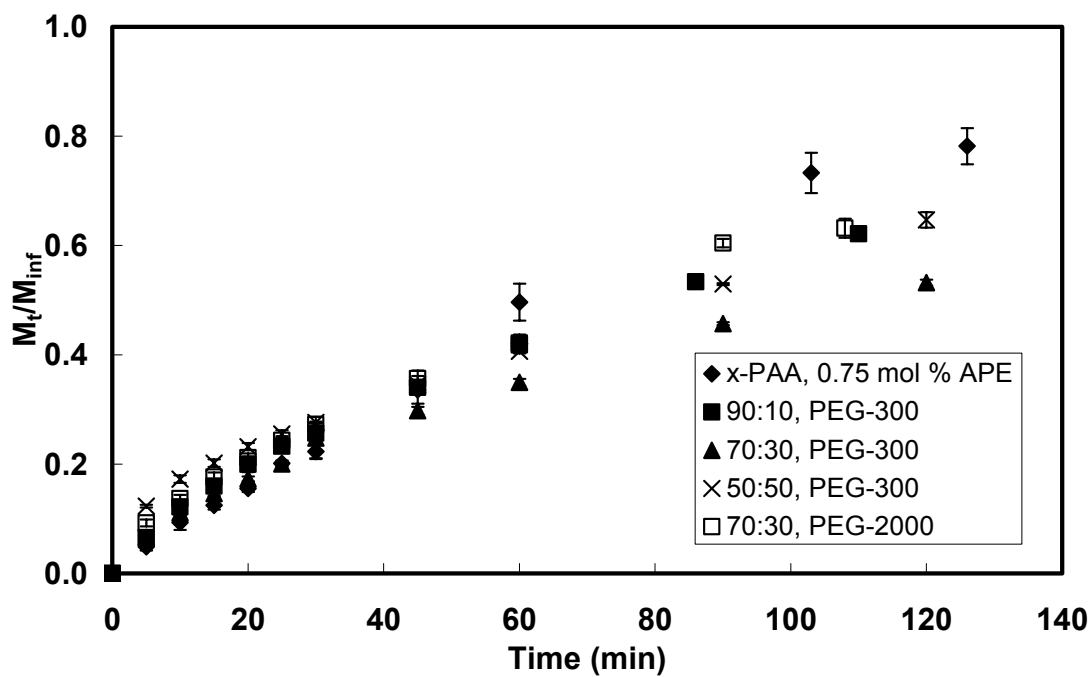


Figure 6.6 Theophylline release from minitab matrix containing PEG-tethered PAA microparticles in 0.1 N HCl.

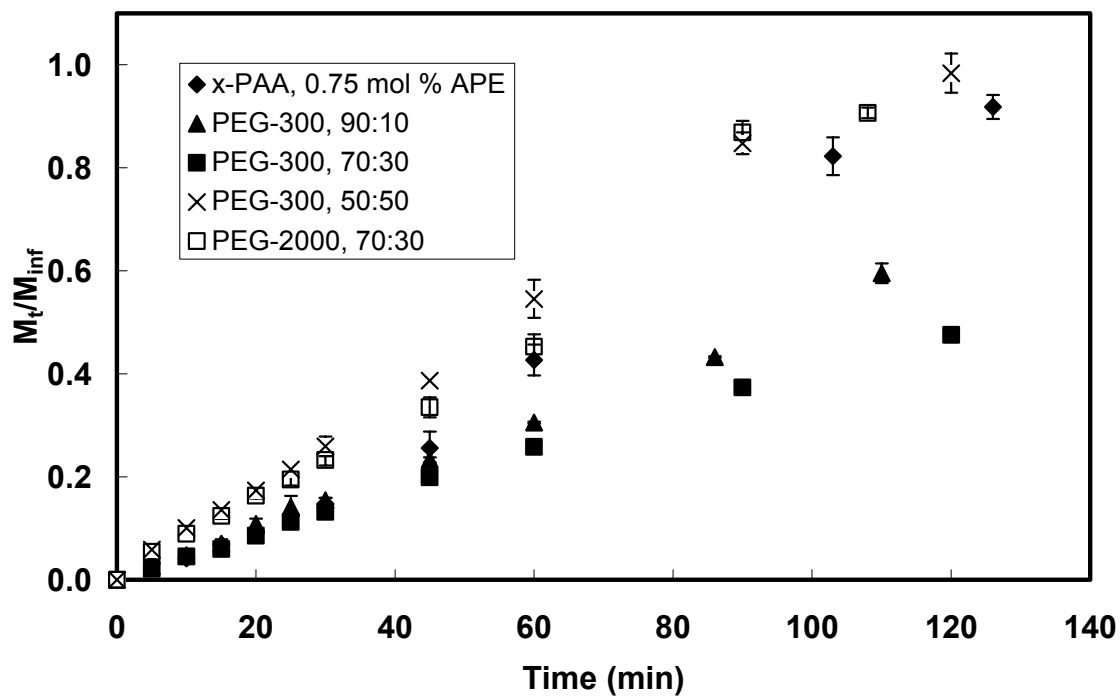


Figure 6.7 Theophylline release from minitab matrices containing PEG-tethered PAA microparticles in pH 6.8 buffer.

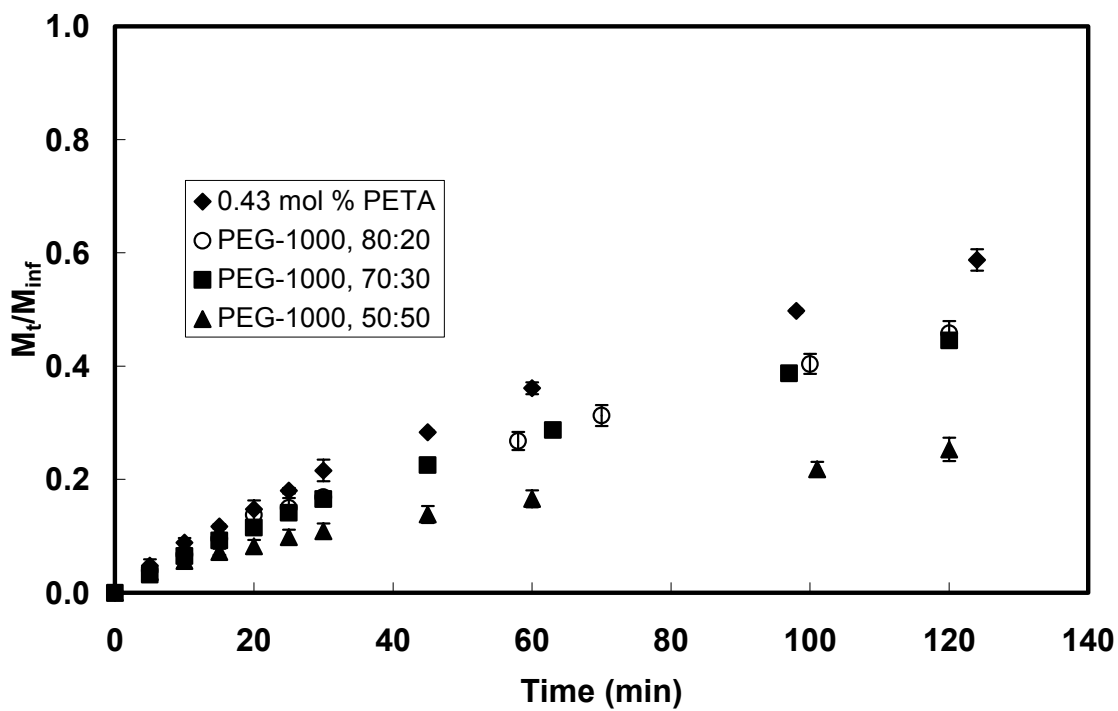


Figure 6.8 Theophylline release from minitab matrix containing PEG-tethered PMAA microparticles in 0.1 N HCl.

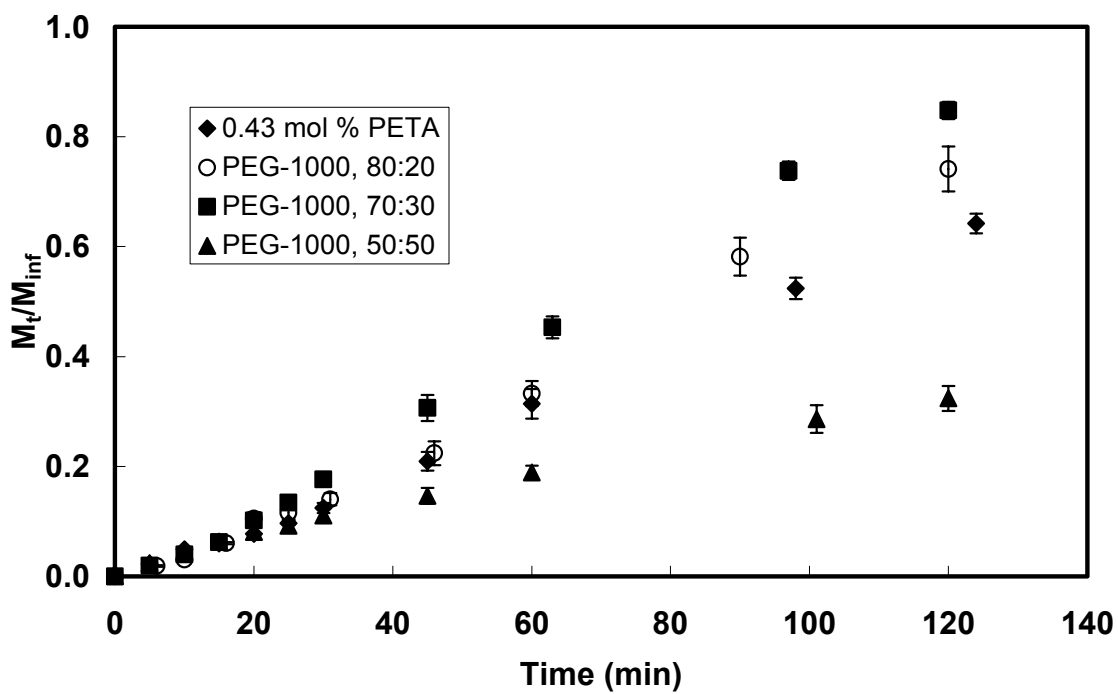


Figure 6.9 Theophylline release from minitab matrixes containing PEG-tethered PMAA microparticles in pH 6.8 buffer.

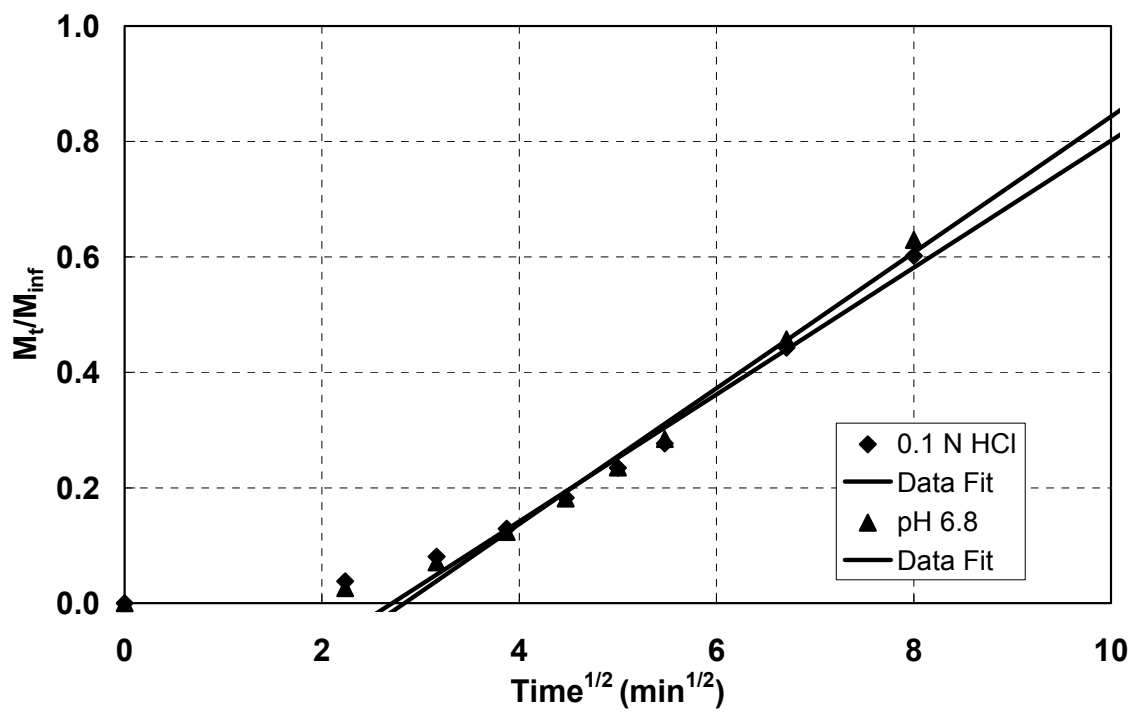


Figure 6.10 Diffusional analysis of the release of the model drug theophylline from minitabiet matrices containing PAA microparticles in 0.1 N HCl and pH 6.8 buffer.

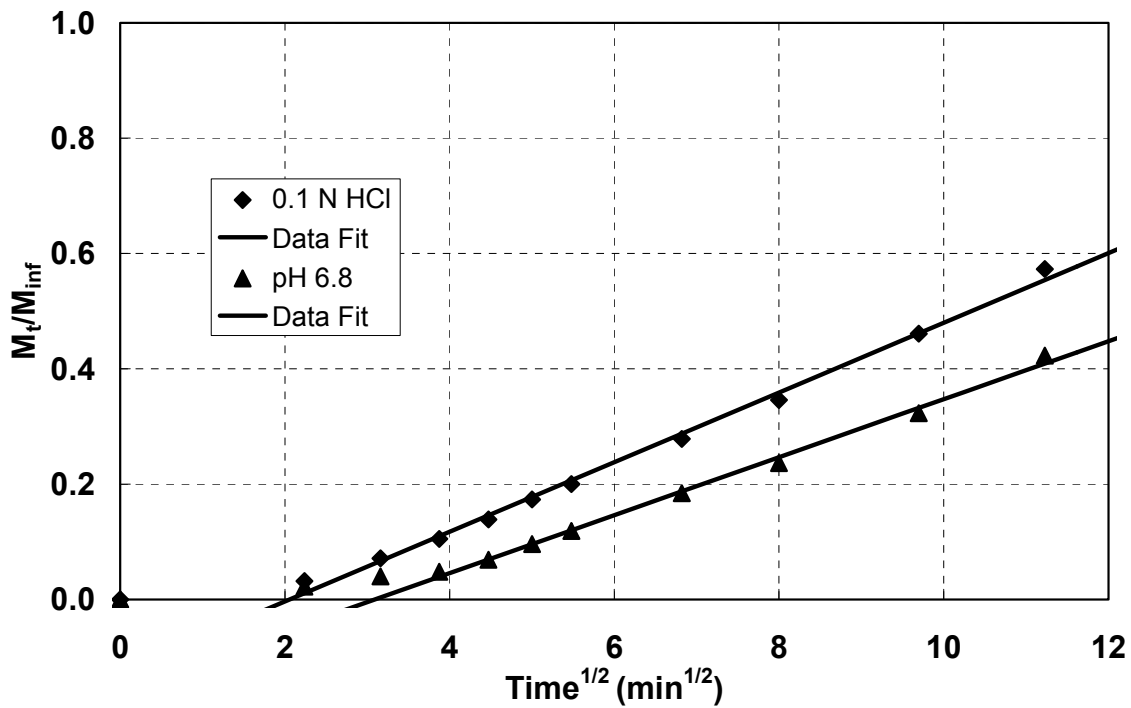


Figure 6.11 Diffusional analysis of the release of the model drug theophylline from minitabiet matrices containing crosslinked PAA (0.2 mol % APE) microparticles in 0.1 N HCl and pH 6.8 buffer.

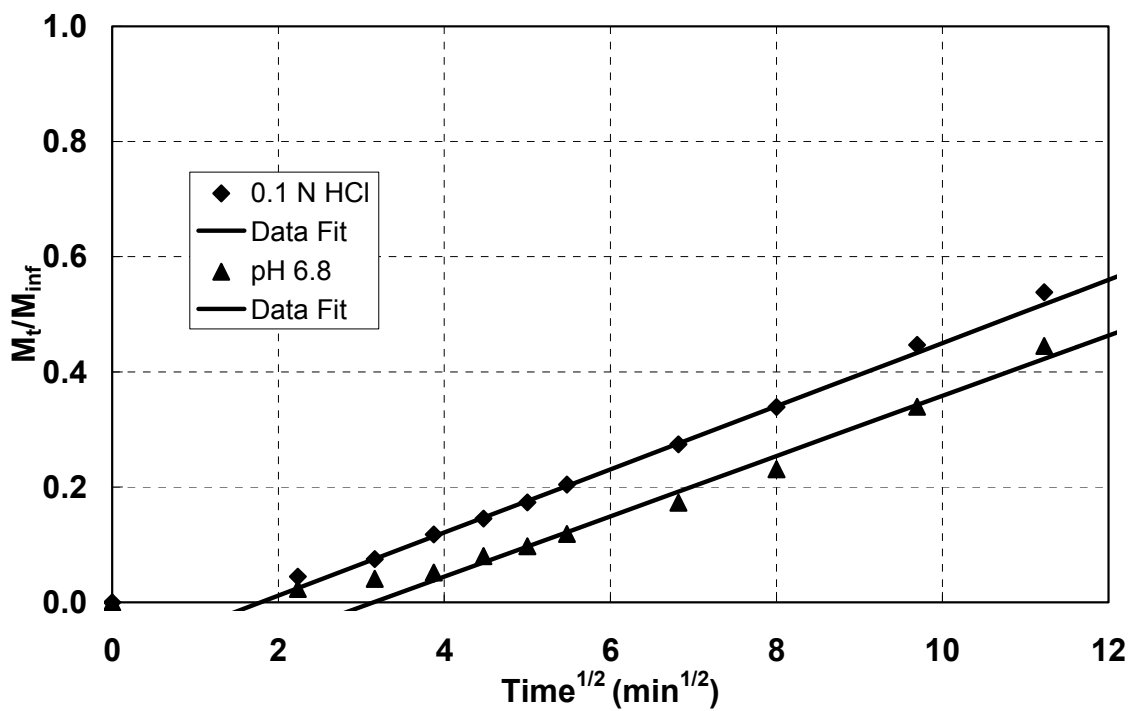


Figure 6.12 Diffusional analysis of the release of the model drug theophylline from minitabiet matrices containing crosslinked PAA (0.43 mol % APE) microparticles in 0.1 N HCl and pH 6.8 buffer.

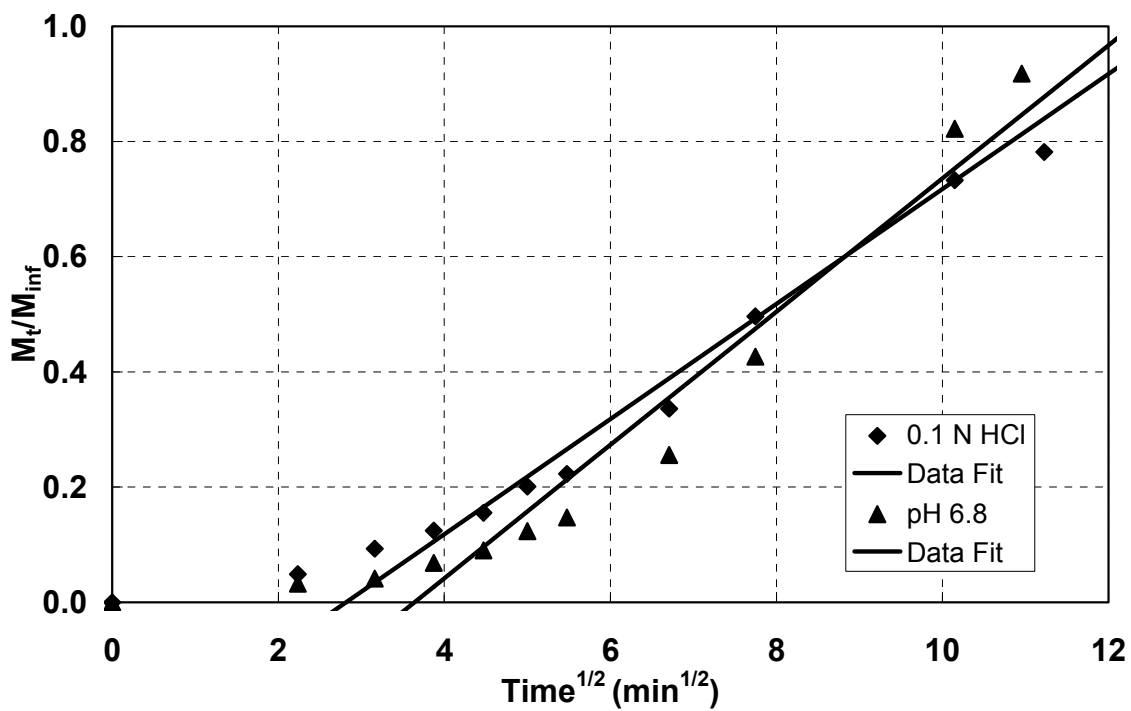


Figure 6.13 Diffusional analysis of the release of the model drug theophylline from minitabiet matrices containing crosslinked PAA (0.75 mol % APE) microparticles in 0.1 N HCl and pH 6.8 buffer.

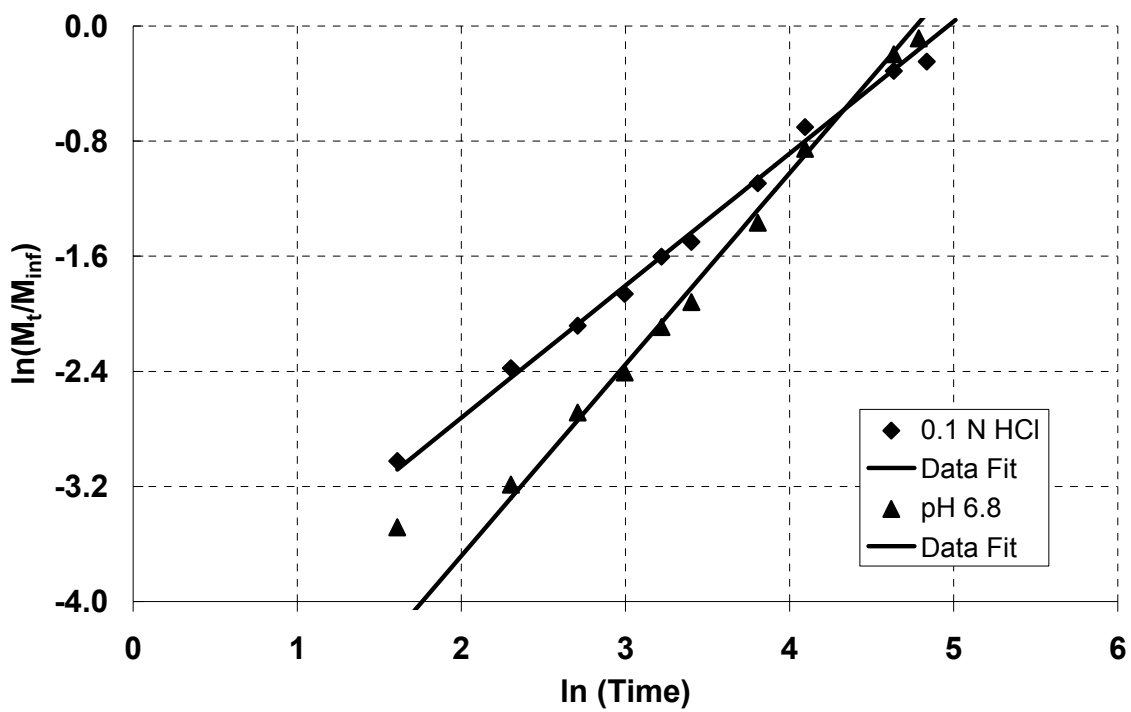


Figure 6.14 Diffusional analysis of the release of the model drug theophylline from minitabiet matrices containing crosslinked PAA (0.75 mol % APE) microparticles in 0.1 N HCl and pH 6.8 buffer.

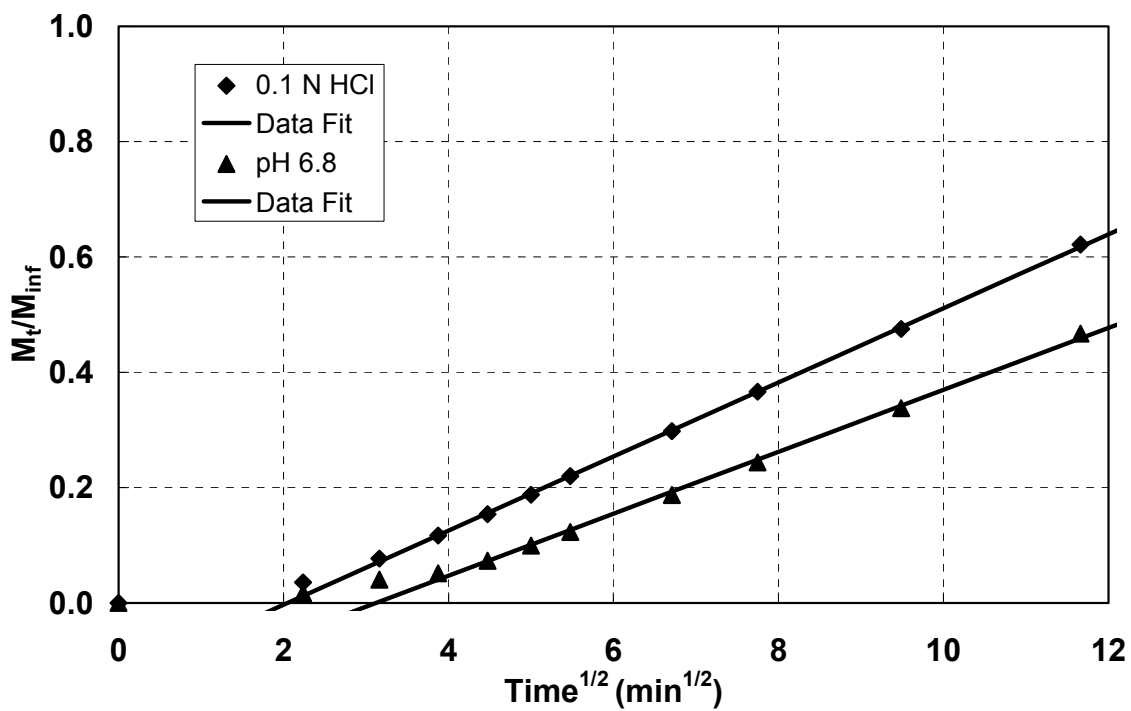


Figure 6.15 Diffusional analysis of the release of the model drug theophylline from minitabiet matrices containing Carbopol 971P-NF microparticles in 0.1 N HCl and pH 6.8 buffer.

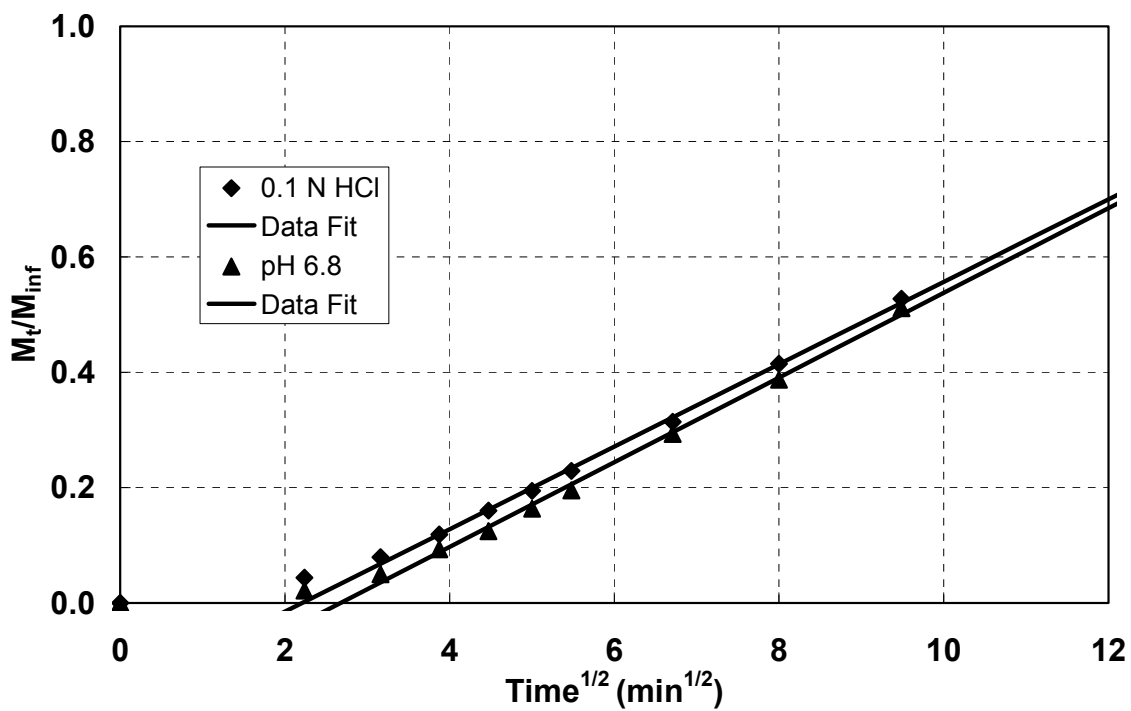


Figure 6.16 Diffusional analysis of the release of the model drug theophylline from minitabiet matrices containing Carbopol 974P-NF microparticles in 0.1 N HCl and pH 6.8 buffer.

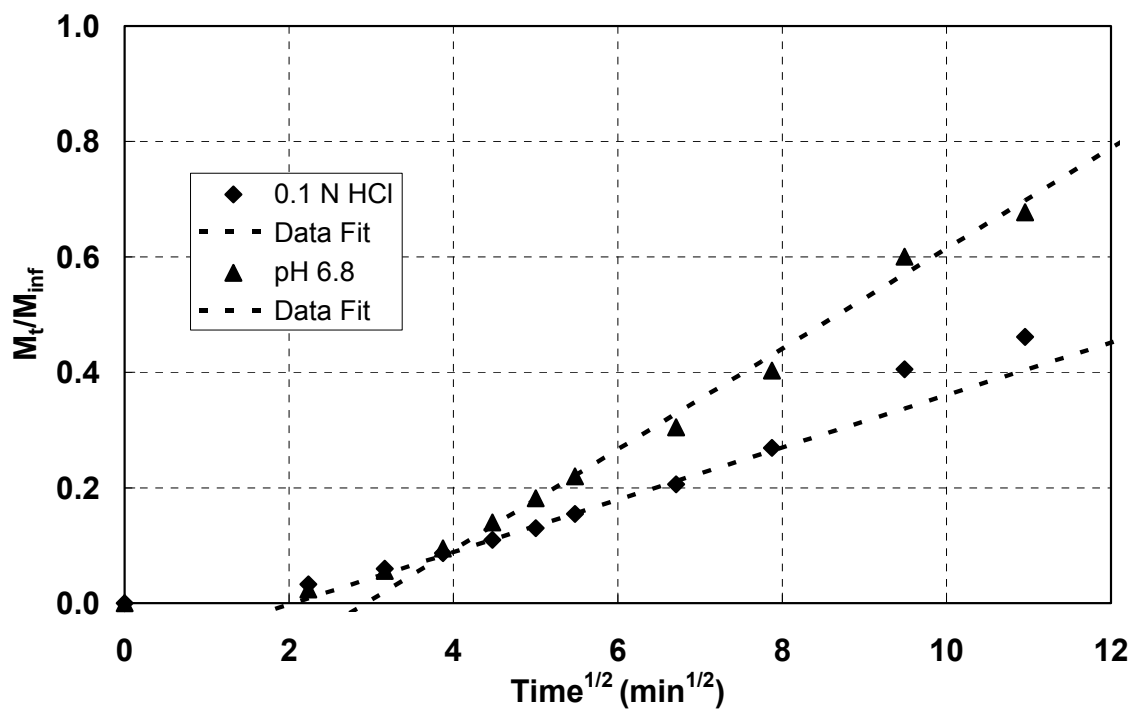


Figure 6.17 Diffusional analysis of the release of the model drug theophylline from minitabiet matrices containing PMAA microparticles in 0.1 N HCl and pH 6.8 buffer.

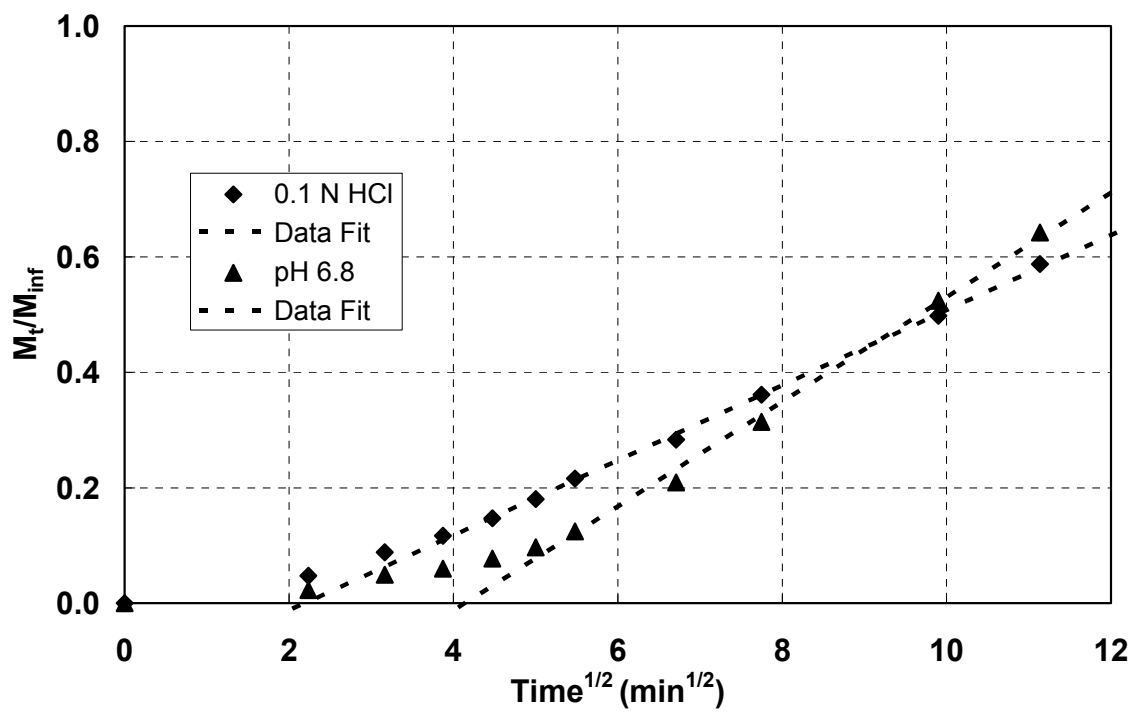


Figure 6.18 Diffusional analysis of the release of the model drug theophylline from minitabiet matrices containing crosslinked PMAA (0.43 mol % PETA) microparticles in 0.1 N HCl and pH 6.8 buffer.

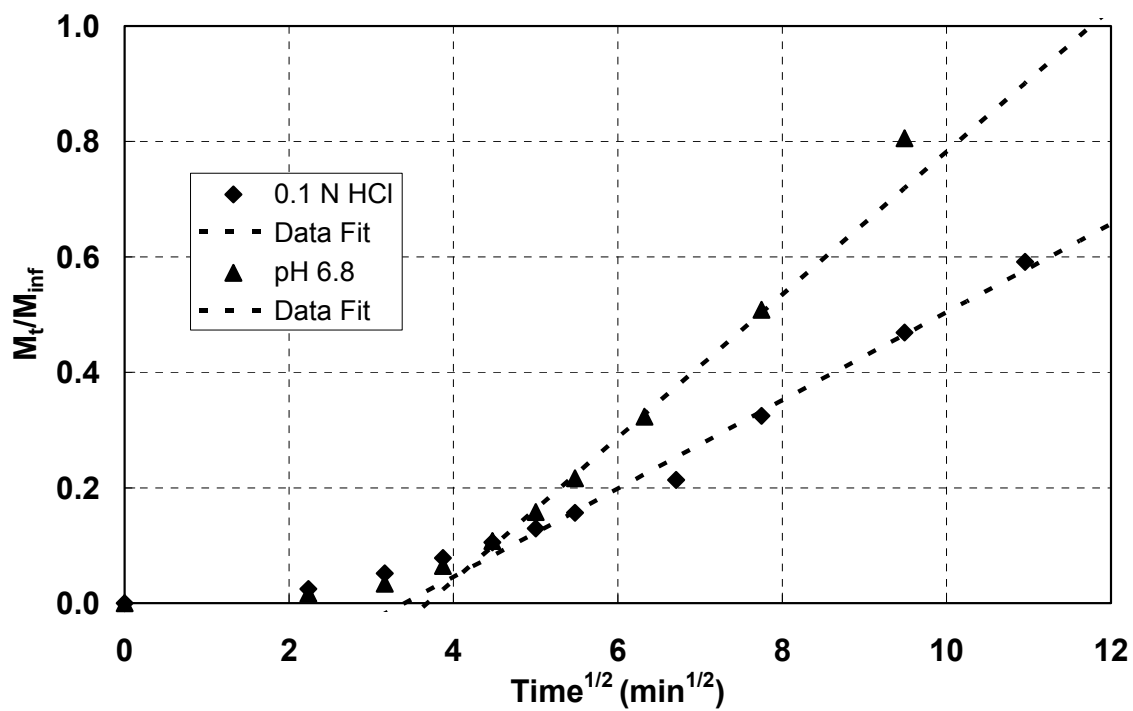


Figure 6.19 Diffusional analysis of the release of the model drug theophylline from minitabiet matrices containing crosslinked PMAA (0.75 mol % PETA) microparticles in 0.1 N HCl and pH 6.8 buffer.

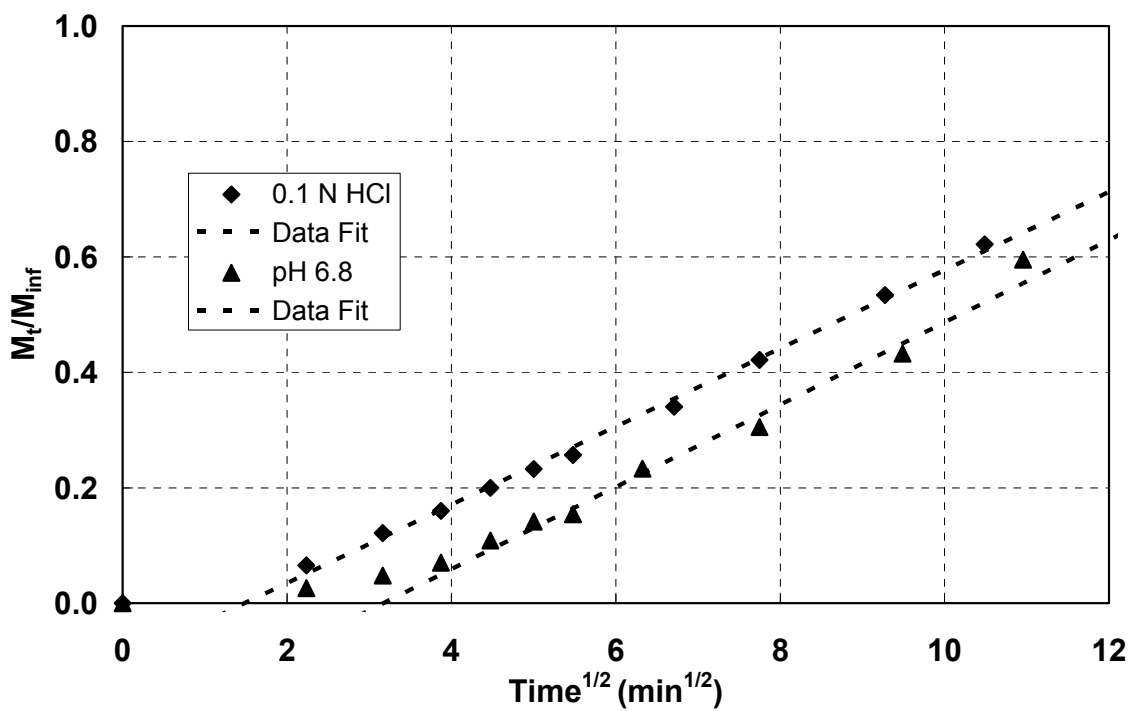


Figure 6.20 Diffusional analysis of the release of the model drug theophylline from minitabiet matrices containing P(AA-g-PEG), PEG-300, 90:10, microparticles in 0.1 N HCl and pH 6.8 buffer.

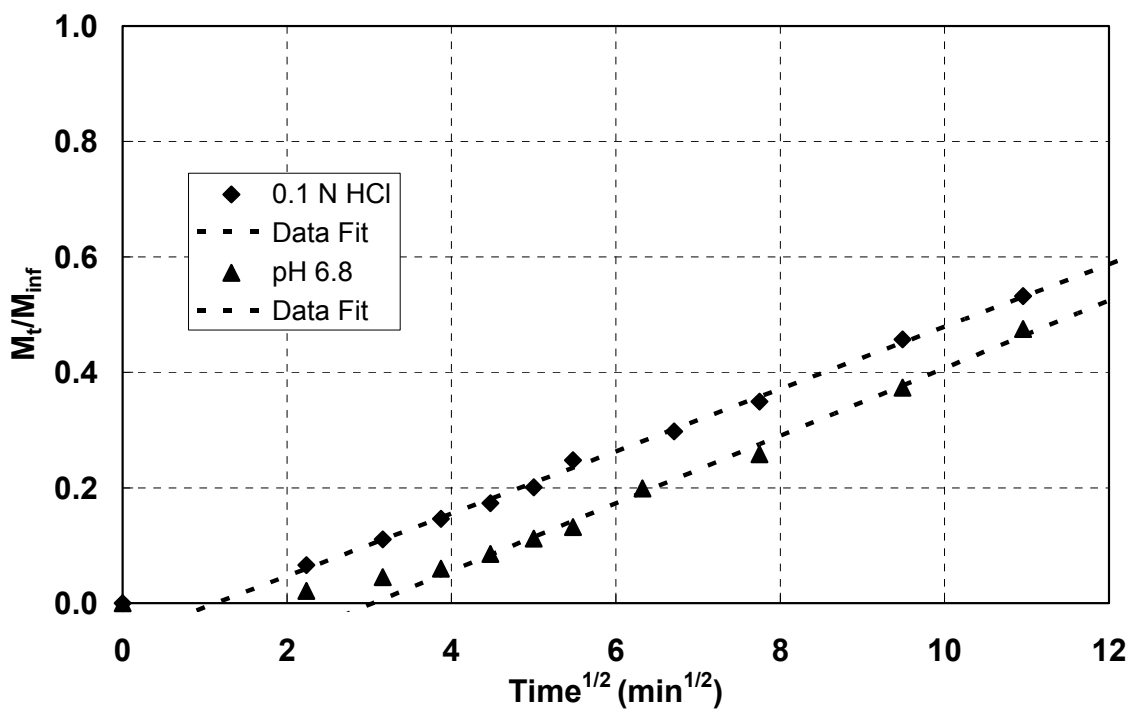


Figure 6.21 Diffusional analysis of the release of the model drug theophylline from minitabiet matrices containing P(AA-g-PEG), PEG-300, 70:30, microparticles in 0.1 N HCl and pH 6.8 buffer.

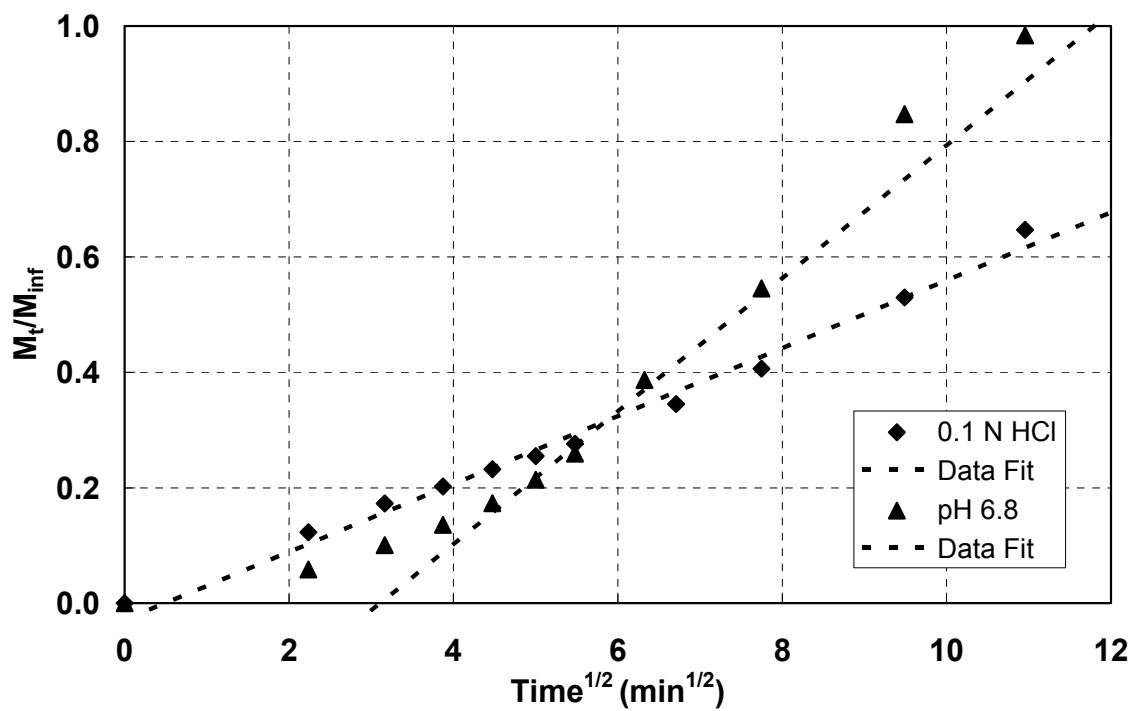


Figure 6.22 Diffusional analysis of the release of the model drug theophylline from minitabiet matrices containing P(AA-g-PEG), PEG-300, 50:50, microparticles in 0.1 N HCl and pH 6.8 buffer.

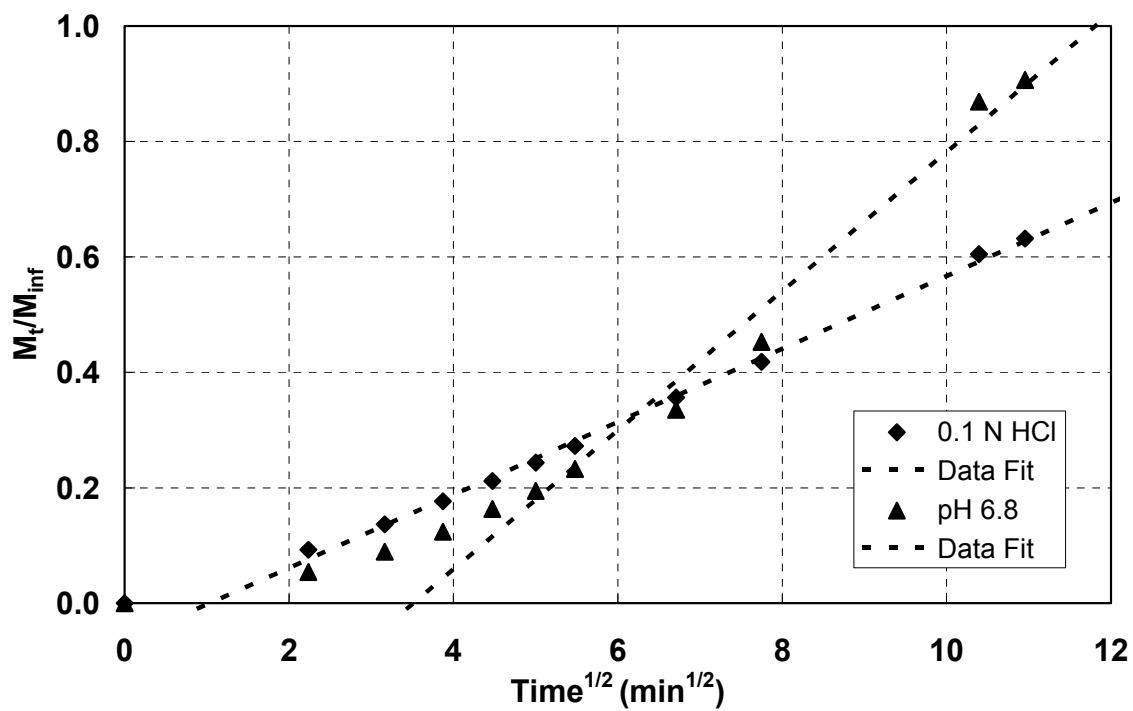


Figure 6.23 Diffusional analysis of the release of the model drug theophylline from minitabiet matrices containing P(AA-g-PEG), PEG-2000, 70:30, microparticles in 0.1 N HCl and pH 6.8 buffer.

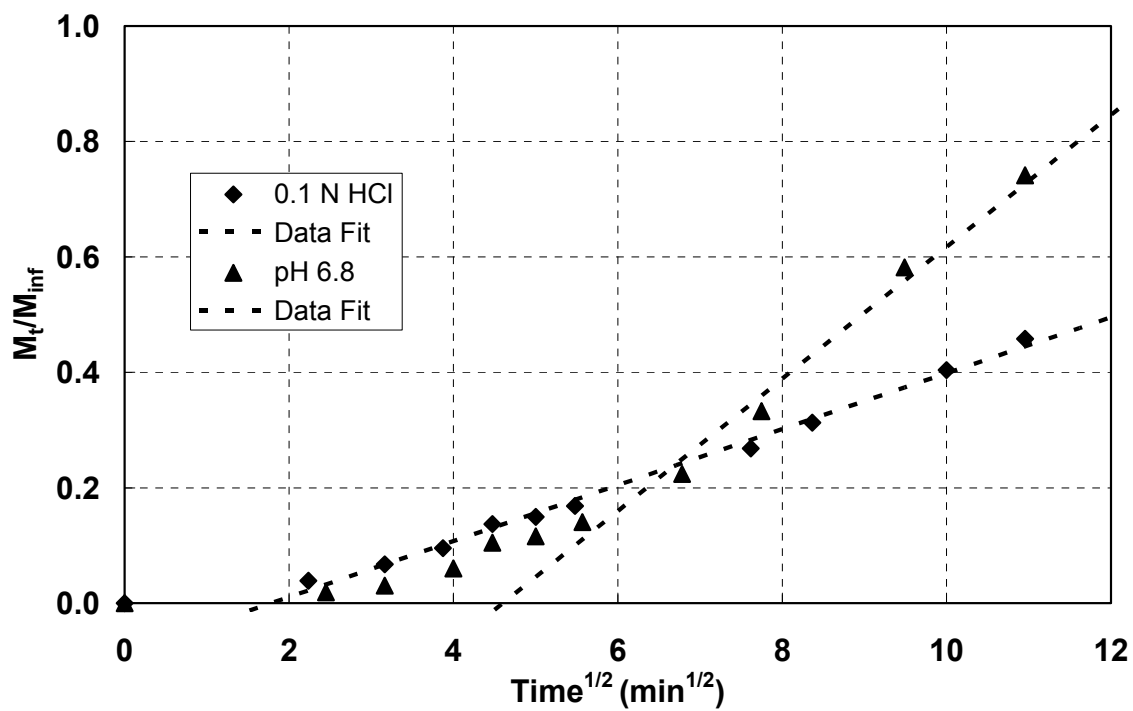


Figure 6.24 Diffusional analysis of the release of the model drug theophylline from minitabiet matrices containing P(MAA-g-PEG), PEG-1000, 80:20, microparticles in 0.1 N HCl and pH 6.8 buffer.

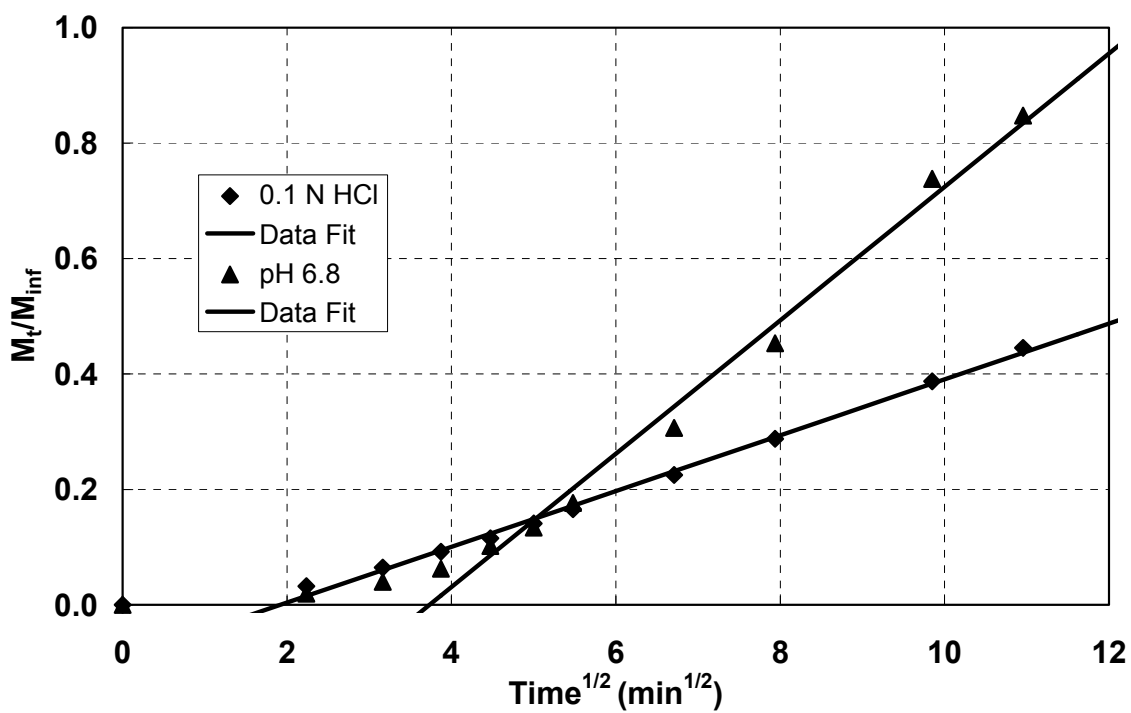


Figure 6.24 Diffusional analysis of the release of the model drug theophylline from minitabiet matrices containing P(MAA-g-PEG), PEG-1000, 70:30, microparticles in 0.1 N HCl and pH 6.8 buffer.

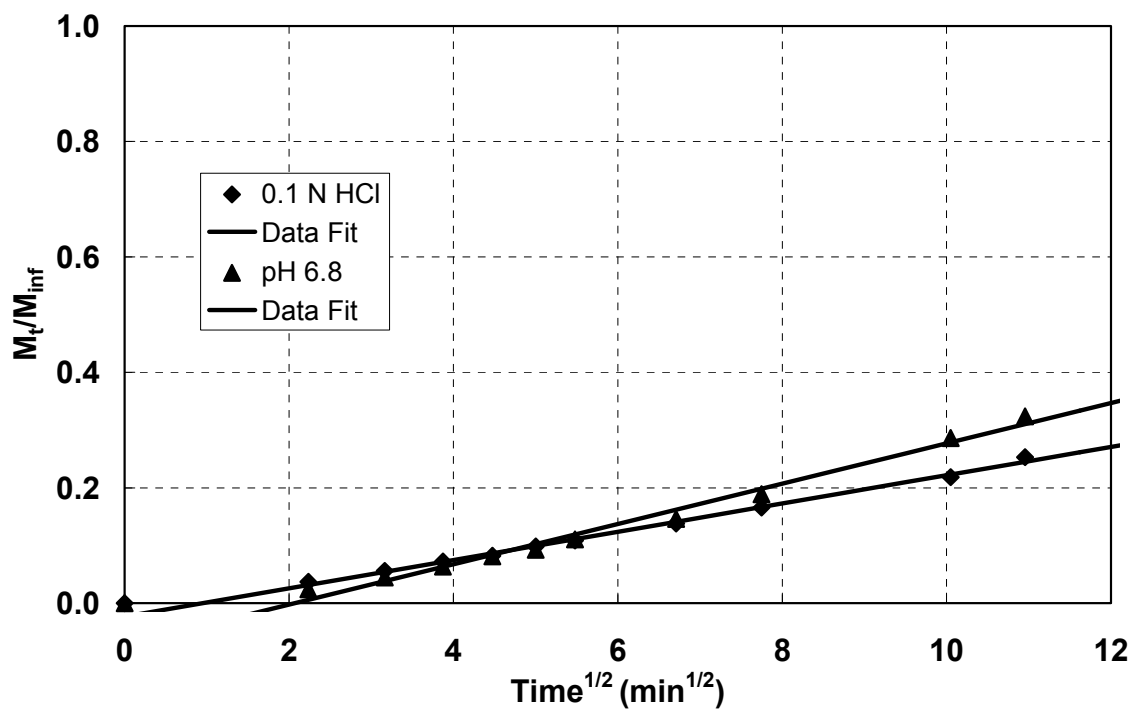


Figure 6.24 Diffusional analysis of the release of the model drug theophylline from minitabiet matrices containing P(MAA-g-PEG), PEG-1000, 50:50, microparticles in 0.1 N HCl and pH 6.8 buffer.

Chapter 7: Conclusions

The field of bioadhesion is one that is rapidly evolving to aid in the development of materials that are capable of more effective drug delivery, enhanced disease treatment, and the prevention and understanding of disease transmission. Biomimetic materials are quickly replacing those first-generation materials that relied heavily on the non-specific interactions they had with the natural tissue. Drug delivery systems are employing nature's method of covalent bond formation (thiomers) and specific interactions (lectins) through carefully designed surfaces (tethered surfaces). Tissue engineering matrices are incorporating macromolecules that the body is capable of recognizing and utilizing in the rehabilitation of organ dysfunction and failure. Some disease transmissions can be attributed to the ability of a microorganism or pathogen to adhere to an epithelial surface, and the fundamental understanding of this binding event could lead to more effective ways of prevention and treatment.

Successfully engineered materials for bioadhesive applications, or the prevention of bioadhesion in some instances, will continue to incorporate biologically relevant moieties to aid in their effective use by the biological host. Carbohydrates and their role in cell-cell and cell-matrix interactions are becoming increasingly important, and both the incorporation of carbohydrate structures and their binding molecules will be crucial for the success of biomedical devices.

The synthesis and characterization of pH responsive hydrogels were evaluated in this work to understand their application in bioadhesive controlled release drug delivery systems. The effect of the addition of a PEG tether on the dynamics of these materials was investigated. Novel drug delivery systems were designed that incorporated these pH responsive mucoadhesive biomaterials.

In the first part of this thesis, the synthesis of pH responsive microparticles composed of either poly(acrylic acid) or poly(methacrylic acid) were investigated. The structure-property relationships of these biomaterials were evaluated. The amount of crosslinking agent was varied to examine its effect on the dynamics of the materials.

Microparticles composed of (meth)acrylic acid were successfully prepared using a thermally-initiated free-radical precipitation polymerization in ethyl acetate. Particle size was shown to be dependent on crosslinking and monomer. Slight morphological differences were observed due to differing polymer growth at the surface of the primary particle. Structural differences were observed and interpreted using FT-IR with only slight differences being observed due to the presence of the methyl group. The glass transition behavior of the materials was significantly different with MAA-based materials exhibiting a much higher T_g . The T_g was also heavily dependent on the amount of crosslinking present in the network. Crosslinked PAA possesses a higher swelling ratio than crosslinked PMAA with both polymers exhibiting pH dependent swelling.

In the second part of this thesis, the synthesis and characterization of materials containing a PEG tether were evaluated. The precipitation synthesis technique and microparticle formation was elucidated. The fundamental understanding of the behavior of tethered gel networks has implications in tissue engineering, adhesion, and drug delivery. In this research, ionizable hydrogel networks containing a PEG tether were successfully synthesized using a thermally initiated free radical precipitation polymerization. The effects of the PEG tether on the structure of the microparticles were evaluated. The addition of the PEG was shown to cause disruption of the dimer formation of PAA. Differential scanning calorimetry exhibited a concentration dependent decrease in the T_g of xerogels. At low concentrations, the network exhibits a

heterogeneous behavior which is evident through a lowered ΔC_p and the presence of two distinct T_g 's.

The gel adhesion of a neutralized gel was shown to be dependent on the amount of PEG incorporated into the network, which in turn affected the viscosity of the gel. These materials possess interesting swelling properties which can be beneficial in the development of pH responsive drug delivery systems.

In the final part of this thesis, novel minitabket drug delivery systems containing the pH responsive microparticles and a model drug were formulated. The release of a model drug was shown to be dependent on the amount of crosslinking agent incorporated during microparticle synthesis with lower degrees of crosslinking being preferred for effective release characteristics. The amount of PEG was shown to significantly alter the release behavior due to interpolymer complexation between the ether oxygens and the carboxylic acid groups. The release behavior was modeled according to a simplified model for monolithic matrices taking into account a lag time. The effective diffusion coefficient was calculated and shown to be affected by the monomer type, degree of crosslinking, and presence of PEG tether.

To summarize, this work contributed to the understanding of the potential of developing multifunctional polymers and drug delivery systems capable of controlling diffusion and modulating adhesion. The PEG tether was shown to be effective in enhancing the pH responsive nature of the systems. Also, the adhesive effects of the incorporation of PEG were elucidated.

Appendix A: Nanotechnology and Biomaterials

Authors: J. Brock Thomas¹, Nicholas A. Peppas^{1,2,3}, Michiko Sato⁴, and Thomas J. Webster^{4,5}

¹Department of Chemical Engineering, CPE 3.466, 1 University Station, C-0400, The University of Texas at Austin, Austin, TX 78712-0231, USA

²Department of Biomedical Engineering, CPE 3.466, 1 University Station, C-0400, The University of Texas at Austin, Austin, TX 78712-0231, USA

³Division of Pharmaceutics, CPE 3.466, 1 University Station, C-0400, The University of Texas at Austin, Austin, TX 78712-0231, USA

⁴School of Materials Engineering, Purdue University, 501 Northwestern Avenue, West Lafayette, IN 47907

⁵Department of Biomedical Engineering, Purdue University, 1296 Potter Building, West Lafayette, IN 47907

INTRODUCTION

Biomaterials have received a considerable amount of attention over the last 30 years as a means of treating diseases and easing suffering. The focus of treatment is no longer a conventional pharmaceutical formulation but rather a combination of device-integrated biomaterial and the necessary therapeutic treatment. Biomaterials have found applications in approximately 8,000 various kinds of medical devices (1) which have been used in repairing skeletal systems, returning cardiovascular functionality, replacing organs, and repairing or returning senses (2). Even though biomaterials have had a pronounced impact in medical treatment, a need still exists to be able to design and develop better polymer, ceramic, and metal systems (3).

Polymeric biomaterials originated as off-the-shelf materials that clinicians were able to use in solving a problem—for example, dialysis tubing was originally made of cellulose acetate, vascular grafts were fabricated from Dacron, and artificial hearts were molded from polyurethanes (2). However, these materials did not possess the chemical, physical, and biological properties necessary to prevent further complications. Recent advances in synthetic techniques have allowed these properties to be imparted on polymeric biomaterials which help to alleviate accompanying biocompatibility issues. Nanotechnology, as this chapter will describe, further adds to the ability of chemically tailoring polymeric materials to provide more opportunities for revolutionary breakthroughs in the science and technology associated with developing novel devices. Undoubtedly, nanoscale science and engineering has the potential to have a profound impact on medical science and technology which will lead to improved diagnostics and enhanced therapeutic methods (4).

For ceramics and metals, similar advancements through the use of nanotechnology can be envisioned. For example, over the past nine decades of administering bioimplants to humans, most synthetic prostheses consist of ceramic or metal particles and/or grain sizes with conventional dimensions (on the order of 1 to 104 μm). But the lack of sufficient bonding of these synthetic implants to surrounding body tissues have, in recent years, led to the investigations of novel material formulations. One such classification of materials, nanophase ceramics and metals (or materials with constituent components less than 100 nm in at least one direction), can be used to synthesize implants with similar surface roughness to that of natural tissues. Natural tissues have numerous nanometer features available for cellular interactions since they are composed of many nanostructures (specifically, proteins). Several nanophase ceramic and metals biomedical implants are currently being investigated, and are likely to gain approvals for clinical use in the near future.

One area in which nanophase polymers, ceramics, and metals are being heavily investigated involves orthopedic/dental applications and this is for good reason. Since 1990, the total number of hip replacements, which is the replacement of the femoral and hip bones, has been steadily increasing (5-11). In fact, the 152,000 total hip replacements in 2000 is a 33% increase from the number performed in 1990 and a little over half of the projected number of total hip replacements (272,000) by the year 2030 in the United States alone (5-8). However, in 1997, 12.8% of the total hip arthroplasties were simply due to revision surgeries of previously implanted failed hip replacements (5-8).

The fact that such a high percentage of hip replacements performed every year are revision surgeries is not surprising when you consider the life expectancy of the implant versus that of the patient receiving the implant. Consistently, over 30% of those requiring total hip replacements have been below the age of 65 and even those at the age of 65 have

a life expectancy of 17.9 years (9-11). Females, which comprise a majority of those receiving total hip replacements, have a life expectancy of 19.2 years at the age of 65. Since the longevity of implants ranges only from about 12-15 years, even the majority of those that receive bone implants at the age of 65 will require at least one revision surgery before the end of their lives (9-11).

For the dental community the story is not any better. Since dental implants may be necessary for the young and old alike, it is imperative that they are able to last for the duration of the patient's life. Recent studies have found that dental implants which have been used in over 300,000 cases in the United States, have up to a 96% success rate (meaning that the implant was not mobile and was non-inflamed) after five years, 80% after ten, and less than 75% after 15 years (5-11).

The above strongly suggests that the longevity of the current prostheses is a reoccurring problem for the orthopedic/dental community that has to be dealt with since current approaches clearly fail. Orthopedic implant failure can be due to numerous reasons including: poor initial bonding of the implant to juxtaposed bone, generation of wear debris that lodges between the implant and surrounding bone to cause bone cell death, and/or stress and strain imbalances between the implant and surrounding bone causing implant loosening and eventual failure (12). Although there are many reasons why implants fail, a central one is the lack of sufficient bone regeneration around the implant immediately after insertion (12). Shockingly, about a quarter of dental implant failures are attributed to incomplete healing of the implant to juxtaposed bone (for those that failed between three and six months) (5-11). Importantly, this leads to eventual implant loosening and regions for possible wear debris to situate between the implant and surrounding bone further complicating bone loss (12-15).

Nanotechnology is playing an important role in decreasing this failure. This is because, in order to improve biomaterial performance and hence extend the lifetime of bone implants, it is essential to design surface characteristics that interface optimally with select proteins and subsequently with pertinent bone cell types. That is, immediately after implantation, proteins will adsorb from plasma to biomaterial surfaces to control cell attachment and eventual tissue regeneration (Figure 1) (16,17). Initial protein interactions that mediate cell function depend on many biomaterial properties including chemistry, charge, wettability, and topography (16,17). Of significant influence for protein interactions is surface roughness and energy (18-22), and this represents the promise of nanophase materials in bone implant applications.

The critical factor for the merging of nanotechnology with medicine is the increasingly documented special, biologically-improved material properties of nanophase implants compared to conventional formulations of the same material chemistry. In this manner, this review paper will highlight a novel property of nanophase materials that makes them attractive for use as implants: increased tissue regeneration. Active works are focused in the domains of orthopedic, dental, bladder, neurological, vascular, cartilage, and cardiovascular applications. However, only orthopedic applications, which are the closest to clinical applications, will be emphasized here. This entry will briefly articulate the seeming revolutionary changes and the potential gains nanostructured materials can make for bone implant technology.

NANOTECHNOLOGY IN BIOMATERIALS SCIENCE

The emergence of micro- and nanoscale science and engineering has provided new avenues for engineering materials with macromolecular and even down to molecular scale precision, leading to diagnostic and therapeutic technologies that will revolutionize the way health care is administered. Biomaterials have evolved from off-the-shelf

products (e.g. Dacron for vascular grafts) to materials that have been designed with molecular precision to exhibit the desired properties for a specific application, often mimicking biological systems (2,3) .

Controlling interactions at the level of natural building blocks, from proteins to cells, facilitates the novel exploration, manipulation, and application of living systems and biological phenomena. Nanostructured tissue scaffolds and biomaterials are being applied for improved tissue design, reconstruction, and reparative medicine (23-26). Nano- and microarrays have been established as the preferred method for carrying out genetic and other biological (e.g. drug discovery) analysis on a massive scale (27). Natural nanopores (28,29), and synthetic nanopores of tailored dimensions (30,31) are probing, characterizing, and sequencing biological macromolecules and have demonstrated the possibility to analyze the structure of individual macromolecules faster and cheaper (32). Self-assembly is being applied to create new biomaterials with well-ordered structures at the nanoscale such as nanofiber peptide and protein scaffolds (33). In addition, polymer networks with precisely engineered binding sites have been created via molecular imprinting, where functional monomers are pre-assembled with a target molecule and then the structure is locked with network formation (34).

In medical diagnostics, the speed and precision with which a condition is detected directly impacts the prognosis of a patient. Point-of-care (POC) diagnostic devices, which enable diagnostic testing (in-vivo or ex-vivo) at the site of care, can enhance patient outcomes by substantially abbreviate analysis times as a result of the intrinsic advantages of the miniature device and by eliminating the need for sample transport to an onsite or off-site laboratory for testing. The development of micro or miniaturized total analysis systems (μ -TAS), also referred to as lab-on-a-chip devices, has profoundly impacted the corresponding development of POC diagnostic devices. These μ -TAS

devices integrate microvalves, micropumps, micro-separations, microsensors, and other components to create miniature systems capable of analysis that typically requires an entire laboratory of instruments. Since introduced as a novel concept for chemical sensing devices (35), μ -TAS devices have been applied as innovative biological devices (36) and point-of-care diagnostic devices (37,38). With the further development of micro- and nanosensors, POC diagnostic devices will provide for improved medical management, leading eventually to self-regulated point-of-care diagnostic devices that intermittently or continuously monitor the biological molecule of interest and deliver therapeutic agents as required.

Additionally, nanoscale science and engineering has accelerated the development of novel drug delivery systems and led to enhanced control over how a given pharmaceutical is administered, helping biological potential to be transformed into medical reality (39). Micro- and nanoscale devices have been fabricated using integrated circuit processing techniques and have been demonstrated to allow for strict control over the temporal control of drug release. Silicon microchips that can provide controlled release of single or multiple chemical substances on demand via electrochemical dissolution of the thin anode membranes covering microreservoirs have been created (40). The advantages of this microdevice include that it has a simple release mechanism, very accurate dosing, ability to have complex release patterns, potential for local delivery, and possible biological drug stability enhancement by storing in a microvolume that can be precisely controlled. More recently, multi-pulse drug delivery from a resorbable polymeric microchip device was demonstrated (41).

In particular, the development of polymer systems that are able to interact with their environment in an “intelligent” manner has led to novel materials and applications. These intelligent materials are attractive options as functional components in micro- and

nanodevices, due to the ease with which their recognition and actuation properties can be precisely tailored. In this section of the book, neutral and intelligent polymers and networks based on environmentally responsive hydrogels and biomimetic polymer networks will be discussed for application as sensing/recognition elements in novel diagnostic devices, such as microsensors and microarrays, and therapeutic devices, for tailoring loading and release properties.

In addition to advances in polymer nanotechnology for sensing and recognizing changes in microenvironments, advances have been made concerning tissue regeneration on ceramic and metallic nanomaterials. Broadly speaking, nanotechnology embraces a system whose core of materials is in the range of nanometers (10^{-9} m) (42-52). The application of nanomaterials for medical diagnosis, treatment of failing organ systems or prevention and cure of human diseases can generally be referred to as nanomedicine (51,52). The branch of nanomedicine devoted to the development of biodegradable or non-biodegradable prostheses fall within the purview of nano biomedical science and engineering (51,52). Although various definitions are attached to the word “nanomaterial” by different experts, the commonly accepted concept refers nanomaterials as that material with the basic structural unit in the range 1-100 nm (nanostructured), crystalline solids with grain sizes 1-100 nm (nanocrystals), individual layer or multilayer surface coatings in the range 1-100 nm (nanocoatings), extremely fine powders with an average particle size in the range 1-100 nm (nanopowders) and, fibers with a diameter in the range 1-100 nm (nanofibers) (42,43).

Since nature itself exists in the nanometer regime, especially tissues in the human body (53), it is clear that nanotechnology can play an integral role in tissue regeneration. Specifically, bone is composed of numerous nanostructures – like collagen and hydroxyapatite that, most importantly, provide a unique nanostructure for protein and

bone cell interactions in the body (Figure 2) (50). Although mimicking constituent components of bone is novel in itself, there are additional reasons to consider nanomaterials for tissue regeneration such as in orthopedic applications: their special surface properties compared to conventional (or micron constituent component structured) materials (47-50). For example, a nanomaterial has increased numbers of atoms at the surface, grain boundaries or material defects at the surface, surface area, and altered electron distributions compared to conventional materials (Figure 3) (50) in summary, nanophase material surfaces are more reactive than their conventional counterparts. In this light, it is clear that proteins which influence cell interactions that lead to tissue regeneration will be quite different on nanophase compared to conventional implant surfaces (Figure 1).

Despite this, the evolution of tissue engineering has centered on the use of materials with non-biologically inspired micron surface features (55,56), mostly changing in chemistry or micron roughness but not degree of nanometer roughness (Figure 4). In this manner, it should not be surprising why the optimal tissue engineering material (in particular, to regenerate bone) has not been found.

CURRENT RESEARCH EFFORTS TO IMPROVE BIOMEDICAL PERFORMANCE AT THE NANOSCALE

Nanoscale materials currently being investigated for bone tissue engineering applications can be placed in the following categories: ceramics, metals, polymers, and composites thereof. Each type of material has distinct properties that can be advantageous for specific bone regrowth applications. For example, hydroxyapatite, a ceramic mineral present in bone (Figure 2), can also be made synthetically. Ceramics, however, are not mechanically tough enough to be used in bulk for large scale bone fractures, however,

they have found applications for a long time as bioactive coatings due to their ionic bonding mechanisms favorable for osteoblast (or bone-forming cells) function (57).

Unlike ceramic materials, metals are not found in the body. However, due to their mechanical strength and relative inactivity with biological substances, metals (specifically, Ti, Ti6Al4V, and CoCrMo) have been the materials of choice for large bone fractures (55,56). Polymers exhibit unique properties (such as viscosity, malleability, moldability) and possess mechanical strength that is comparable to many soft (not hard) tissues in the body (54). To date, because of their excellent friction properties, polymers (like ultra high molecular weight polyethylene) have been primarily used as articulating components of orthopedic joint replacements (58). Additionally, some polymers (particularly the polyester family) can be resorbed or degraded in the body, which opens the window for controllable repair of damaged bone that is actively being investigated in tissue engineering circles. Lastly, composites of any or all of the above, can be synthesized to provide a wide range of material properties to increase bone implant performance (71); such ability to tailor composite properties to specific orthopedic applications makes them attractive.

Due to the numerous materials currently being used and investigated in orthopedics, this review will cover select efforts to create nanoscale surfaces in all of these categories: ceramics, metals, polymers, and composites. Several current and potential materials that have shown promise in nanotechnology for bone biomedical applications, as well as needed future directions, will be emphasized.

SOFT BIOMATERIALS

Polymers are only one of the four major classes of biomaterials; however, polymeric biomaterials have a significant advantage over metals, ceramics and natural materials in the fact that they can be chemically synthesized or modified according to the

desired application. Hydrogels, hydrophilic and cross-linked polymeric structures, have received considerable attention for use in biomedical applications due to the biocompatible nature of their physical properties (72-74). Poly(hydroxyethyl methacrylate) (PHEMA, 75) is the most widely used hydrogel, and the crosslinked variant has been frequently used in soft contact lenses (76,77). Hydrogels are also widely used in pharmaceutical applications especially for the oral delivery of therapeutic proteins (78). This class of materials is also capable of responding to changes in the external pH (Figure 20), temperature, ionic strength, nature and composition of the swelling agent, enzymatic or chemical reaction, and electrical or magnetic stimuli (79).

Much consideration must be given when designing a material for a specific application. Certain properties of the material must be controlled so as to perform the necessary function and elicit the appropriate response. These properties can be tailored to the specific need by carefully controlling structural characteristics, modifying the surface properties, and employing biomimesis in the material design. Hydrogels are a desirable type of material for biomedical devices because these properties can be controlled during or after the chemical synthesis, providing a significant amount of flexibility to aid in need-specific design applications.

Structural Characteristics

The hydrogel networks are prepared via chemical cross-linking, photopolymerization, or irradiative cross-linking (80) with the behavior of the materials dependent on their equilibrium and dynamic swelling behavior in water. Flory (81) was the first to develop the theory of the swelling behavior of cross-linked polymers based upon a Gaussian distribution of the polymer chains. Various parameters have been employed to define the equilibrium-swelling behavior. Q , the volume degree of swelling, is the ratio of the actual volume of a sample in the swollen state divided by its volume in

the dry state; whereas, q , the weight degree of swelling, is the ratio of the weight of the swollen sample to that of the dry sample (74). The basic structure of the hydrogel is described by the molecular weight between cross-links, M_c , and the crosslinking density, ρ_x , and can be calculated from Eq. 1 and 2 respectively. The structural characteristics influence the diffusion coefficient of solutes through the network, optical properties, mechanical properties and surface mobility.

$$\frac{1}{M_c} = \frac{2}{M_n} \frac{\frac{\bar{v}}{V_1} [\ln(1 - \nu_{2,s}) + \nu_{2,s} + \chi \nu_{2,s}^2]}{\left(\nu_{2,s}^{\frac{1}{3}} - \frac{\nu_{2,s}}{2} \right)} \quad (1)$$

$$\rho_x = \frac{1}{\nu M_c} \quad (2)$$

These key properties of the hydrogel are typically determined during initial synthesis of the biomaterial and are representative of the bulk structure of the material. Advances in nanotechnology have afforded the ability to further refine the structure by molecularly engineering the hydrogel to impart a recognitive capacity. Domains within the molecularly designed hydrogel are able to recognize specific molecules through highly select non-covalent interactions between the building blocks of both the hydrogel network and the recognizable molecule (82).

Surface Properties

In addition to the bulk structural characteristics of the biomaterial, the surface plays a key role in the ability of the material to function as designed. A surface provides a low energy barrier to mobility, a high accessibility for reaction, enhanced reaction turnover rates, and ultimately allows for molecular recognition (83). As the first biomaterials were developed (intraocular lenses, hip joint replacements, and blood-contacting devices), the importance of the surface properties, protein-surface interaction,

and surface modification was evident to researchers (84,85). Baier (86) introduced methods having the ability to determine the driving mechanisms behind bioreactions. Hoffman (87) demonstrated that materials could be engineered so as to provide the desired biological responses necessary for effective biomaterial functionality.

In this light, poly(ethylene glycol) (PEG) has received considerable attention for its use at the biomaterial/host interface to prevent protein fouling (88-90). Castner and Ratner (83) list other strategies in addition to PEG that have been employed in biomaterials to prevent protein adsorption. However, possessing the ability to design surface properties has not been able to fully solve the issues associated with the biocompatibility of the material. True biocompatibility will be achieved when absorbing proteins are able to maintain their conformation, eliminating the detrimental foreign body reaction to this newly formed unnatural layer of denatured proteins (83). The surface of the material must be designed so as to provide components inherent to the natural wound healing process. This is an important contribution nanotechnology can make to improve biomaterial performance.

Biomimetics

The design and development of biomaterials has primarily been focused on the biocompatibility of the device with its surroundings, overlooking the biomolecular interactions that occur. The paradigm for biomaterial characterization has shifted from one focusing on broad design parameters to one that focuses on eliciting specific molecular responses from the physiological environment. Biomimetic materials emulate nature and mimic biological architecture to elicit a desired cellular response (91,126). Because of their hydrophilic structure, hydrogels inherently possess the characteristics of natural tissue; however, these materials in device form are much larger than the

individual cells. The major thrust of biomimesis is to design structures that have the ability to interact on a sub cellular basis.

In designing biomaterials one must understand the mechanisms by which cells interact in order for efficient biological mimicking. Three specific interactions that are crucial in material development include cell adhesion, morphogenic stimuli signaling and endocytosis (91); since all of these are events controlled at the nanoscale, biomimetics is a field critical in nanotechnology.

Nanoscale Biopolymer Carriers

Polymer nanoparticle and nanosphere carriers (Figure 17,18) are very attractive for biomedical and pharmaceutical applications, due to their unique and tailorable properties. In the case of polymer networks, the release profile can be precisely controlled through the design of its molecular structure, such as degree of crosslinking and ionic characteristics of the pendent functional groups (59,60).

Polymer nanospheres have been molecularly designed to be responsive to the pH of their environment, enabling for the protection of fragile therapeutic peptides (Figure 19) and proteins in the harsh, acidic stomach environment and then release in the more amiable environment of the upper small intestine (61-63). In addition, nanoparticle carriers have been designed to have stealth properties, allowing extended residence time without being recognized by the immune system (64,65). In other efforts, synthetic delivery systems, including polymeric nanoparticles, have been developed for application in gene delivery (66,67). By creating polymer drug delivery systems that are biodegradable, the need for removal of the system post-delivery is eliminated, since the polymer can be naturally resorbed by the body (68). Also, a number of companies are reformulating insoluble drugs as nanoparticles and nanocrystals to control uptake through cellular membranes.

Microchips (Figure 21) have been created for the storage and then delivery of multiple drugs in a controlled manner. For instance, a solid-state silicon microchip that can provide controlled release of single or multiple chemical substances on demand was fabricated and demonstrated (40,69). The release is achieved via electrochemical dissolution of the thin anode membranes covering the microreservoirs filled with chemicals in solid, liquid, or gel form. The advantages of this microdevice include that it has a simple release mechanism, very accurate dosing, ability to have complex release patterns, potential for local delivery, and possible biological drug stability enhancement by storing in a microvolume that can be precisely controlled. Recently, multi-pulse drug delivery from a resorbable polymeric microchip device was demonstrated (70).

The aforementioned microdevices demonstrate only a few examples of the wide variety of novel applications that exist for integration of micro- and nanofabrication technologies with drug delivery, revealing the immaturity of the field. These novel drug delivery devices can enable efficient delivery that was unattainable with conventional drug delivery techniques, resulting in the enhancement of the therapeutic activity of a drug.

CERAMIC NANOMATERIALS

Perhaps slightly more mature, is the application of nanophase ceramics in bone tissue engineering applications. The next series of sections will highlight the improvement in bone regeneration that can be obtained through the use of ceramic nanotechnology.

Increased Osteoblast Functions

The first report correlating increased bone cell function with decreased material grain or particulate size into the nanometer regime dates back to 1998 and involves ceramics (92). Such reports described that in vitro osteoblast (bone-forming cell)

adhesion, proliferation, differentiation (as measured by intracellular and extracellular matrix protein synthesis such as alkaline phosphatase), and calcium deposition was enhanced on ceramics with particulate or grain sizes less than 100 nm (92-101). Specifically, this was first demonstrated for a wide range of ceramic chemistries including titania (Figure 5), alumina, and hydroxyapatite (94). For example, four, three, and two times the amount of calcium-mineral deposition was observed when osteoblasts were cultured for up to 28 days on nanophase compared to conventional alumina, titania, and hydroxyapatite, respectively (96). It is important to note that for each respective nanophase and conventional ceramic mentioned in these first reports, similar chemistry and material phase were studied (92-101). That is to say, only the degree of nanometer surface features were altered between respective nanophase and conventional alumina, titania, and hydroxyapatite. This is important since as previously discussed it is well known that alterations in surface chemistry will influence bone cell function (12,55-71), but this was the first time changes in the degree of nanometer roughness alone were reported to enhance bone cell responses (92).

Although these studies provided preliminary evidence that osteoblast functions can be promoted on nanostructured compared to conventional materials regardless of ceramic chemistry, Elias et al. further described a study where the topography of compacted carbon nanometer fibers were transferred to poly-lactic-glycolic acid (PLGA) using well established silastic mold techniques (102). The same was done for compacts composed of conventional carbon fibers. The successful transfer of nanometer compared to micron surface features from the carbon nanometer compared to conventional fiber compacts, respectively, is illustrated in Figure 6 (102). Importantly, osteoblast adhesion increased on PLGA molds made from nanometer compared to conventional carbon fibers (102). Increased osteoblast functions were also observed on the starting materials of

nanometer compared to conventional carbon fiber compacts (102). In this manner, this study provided further evidence of the importance of nanometer surface features (and not chemistry) in promoting functions of bone-forming cells.

Equally as interesting, a step-function increase in osteoblast performance has been reported at distinct ceramic grain sizes: specifically, at alumina and titania spherical grain sizes below 60 nm (94). This is intriguing since when creating alumina or titania ceramics with average grain sizes below 60 nm, a drastic increase in osteoblast function was observed compared to respective ceramics with grain sizes just 10 nm higher (i.e, those with average grain sizes of 70 nm) (94). This critical grain size for improving osteoblast function is also of paramount importance since numerous other special properties (such as mechanical, electrical, catalytic, etc.) of materials have been reported when grain size is specifically reduced to below 100 nm (42-50). With this information, evidence has been provided to show for the first time that the ability of nanophase ceramics to promote bone cell function is indeed limited to grain sizes (or subsequent surface features) below 100 nm, specifically those below 60 nm (94). Thus, another novel size-dependent property of nanostructured ceramics has been elucidated by these studies.

Although an exact explanation as to why greater bone regeneration is observed on smaller grain size ceramics into the nanometer regime is not known to date, it is believed that the importance of this specific grain size in improving osteoblast function is connected with interactions of vitronectin (a protein known to mediate osteoblast adhesion with linear dimensions remarkably similar to the critical grain size of 60 nm mentioned above) (95,100). Moreover, as previously mentioned, several studies have indicated that vitronectin and other proteins important for osteoblast adhesion are more well-spread and, thus, expose amino acid sequences to a greater extent when interacting with nanometer compared to conventional ceramics (95,100). It is also intriguing to note

that numerous investigators have confirmed that the minimum distance between protein ligands (such as Arginine-Glycine-Aspartic Acid or RGD) necessary for cell attachment and spreading is in the nanometer regime (specifically, from 10 to 440 nm depending on whether the study was completed with full proteins, protein fragments, or single RGD units) (103-108). Therefore, an underlying substrate surface that mediates protein spreading (as opposed to protein folding) to expose such ligands coupled with a nanometer surface roughness to further project such ligands to the cell, may promote cell adhesion due to this optimal ligand spacing.

Increased Osteoclast Function

In addition to studies highlighting enhanced osteoblast function on nanophase ceramics, increased functions of osteoclasts (bone-resorbing cells) have been reported on nanospherical compared to larger grain size alumina, titania, and hydroxyapatite (HA) (101). Specifically, osteoclast synthesis of tartrate-resistant acid phosphatase (TRAP) and subsequent formation of resorption pits was up to two times greater on nanophase compared conventional ceramics such as hydroxyapatite. Coordinated functions of osteoblasts and osteoclasts are imperative for the formation and maintenance of healthy new bone juxtaposed to an orthopedic implant (12). Frequently, newly formed bone juxtaposed to implants is not remodeled by osteoclasts and thus becomes unhealthy or necrotic (57). At this time, the exact mechanism of greater functions of osteoclasts on nanophase ceramics is not known, but it may be tied to the well-documented increased solubility properties of nanophase compared to conventional materials (48). In other words, due to larger numbers of grain boundaries at the surface of smaller grain size materials, increased diffusion of chemicals (such as TRAP) may be occurring to subsequently result in the formation of more resorption pits.

Collectively, results of promoted functions of osteoblasts coupled with greater functions of osteoclasts imply increased formation and maintenance of healthy bone juxtaposed to an implant surface composed of nanophase ceramics. In fact, although not compared to conventional grain size apatite coated metals, some studies have indeed demonstrated increased new bone formation on metals coated with nanophase apatite (109). As shown in Figure 7, bone formation can be clearly seen on the surface of metals coated with nano apatite, whereas there is no indication of new bone formation on the underlying metal without the coating (109). Incidentally, coating metals with nanophase HA has been problematic (110). For example, due to their small grain size, techniques which use high temperatures (like plasma spray deposition) are not an option since they will result in HA grain growth into the micron regime (110). To circumvent such difficulties, some investigators have allowed nanophase HA to precipitate on metal surfaces; this can be time consuming and not very controllable (109). In contrast, others have developed novel techniques which use high pressure based processes that do not significantly create elevated temperatures to coat nanophase ceramics on metals so as to retain their bioactive properties (Figure 8) (111).

Decreased Competitive Cell Functions

Importantly, it has also been shown that competitive cells do not respond in the same manner to nanophase materials as osteoblasts and osteoclasts do (95,102,112). In fact, decreased functions of fibroblasts (cells that contribute to fibrous encapsulation and callus formation events that may lead to implant loosening and failure (12) and of endothelial cells (cells that line the vasculature of the body) have been observed on nanophase compared to conventional ceramics (95). In fact, the ratio of osteoblast to fibroblast adhesion increased from 1:1 on conventional alumina to 3:1 on nanophase alumina (95).

Previously, such selectively in bone cell function on materials has only been observed through delicate surface chemistry (such as through the immobilization of peptide sequences such as Lys-Arg-Ser-Arg or KRSR) (113). It has been argued that immobilized delicate surface chemistries may be comprised once implanted due to macromolecular interactions that render such epitopes non-functional in vivo. For these reasons, it is important to note that studies demonstrating select enhanced osteoblast and osteoclast functions with decreased functions of competitive cells on nanophase materials have been conducted on surfaces that have not been chemically modified by the immobilization of proteins, amino acids, peptides, or other entities (95,102,112). Rather it is the unmodified, raw material surface that is specifically promoting bone cell functions.

Fibroblast function was also investigated in the same study that was previously mentioned in which Elias et al. transferred the topography of compacted carbon nanometer compared to conventional fibers to PLGA using well-established silastic mold techniques (again please refer Figure 6) (95). Similar to the observed greater osteoblast adhesion already noted, decreased fibroblast adhesion was measured on PLGA molds synthesized from carbon nanometer compared to conventional fibers (95). Again, this was the same trend observed on the starting material of carbon nanometer compared to conventional fiber compacts (95). Thus, this study demonstrated the importance of a nanometer surface roughness (and not chemical composition of the material) in decreasing functions of fibroblasts that may lead to undesirable fibrous encapsulation and callus formation events inhibiting osseointegration of orthopedic implants with surrounding bone.

Increased Osteoblast Functions on Nanofibrous Materials

Recently, researchers have further modified nanophase ceramics to simulate not only the nanometer dimension but also the aspect ratio of proteins and hydroxyapatite

crystals found in the extracellular matrix of bone (112). For example, consolidated substrates formulated from nano-fibrous alumina (diameter: 2 nm, length > 50 nm; Figure 9) increased osteoblast functions in comparison with similar alumina substrates formulated from the aforementioned nanospherical particles (112). Specifically, Price et al. determined a two-fold increase in osteoblast cell adhesion density on nanofiber versus conventional nanospherical alumina substrates, following only a two-hour culture (112). Greater subsequent functions leading to new bone synthesis has also been reported on nanofibrous compared to nano and conventional spherical alumina (112). Thus, perhaps not only is the nanometer grain size of components of bone important to mimic in materials, but the aspect ratio may also be key to simulate in synthetic materials to optimize bone cell response.

Another classification of novel biologically-inspired nanofiber materials that have been investigated for orthopedic applications are self-assembled helical rosette nanotubes (114). These organic compounds are composed of guanine and cytosine DNA pairs that self assembled when added to water to form unique nanostructures (Figure 10). These nanotubes have been reported to be 1.1 nm wide and up to several millimeters wide (114). Compared to currently used titanium, recent studies have indicated that osteoblast function is increased on titanium coated with helical rosette nanotubes (Figure 10) (114). Although in these studies it has not been possible to separate the influence of nanometer dimensions from the effects of nanotube chemistry on cell functions, it is clear that these nanotubes are another category of novel nanostructured materials that can be used to promote bone formation. It is also intriguing to consider what role self-assembled nanofibers may play in orthopedics since bone itself is a self-assembled collection of nanofibers.

In this context it is important to mention that only nanophase materials can mimic the unique aspect ratio of hydroxyapatite and proteins found in the extracellular matrix of bone; it is not possible for micron sized materials to simulate the unique nanometer constituent components of bone. As previously mentioned, results concerning the importance of nanofibrous materials in promoting functions of osteoblasts have been reported for carbon and polymer molds of carbon nanofibers (Figure 6) (102). These findings consistently testify to the unprecedented ability to create nanomaterials to mimic the dimensions of components of physiological bone to promote new bone formation.

METAL NANOMATERIALS

Although much more work has been conducted on nanophase ceramics for orthopedic applications to date, several recent studies have focused on the analysis of bone regeneration on nanophase metals. Metals investigated to date include titanium, Ti6Al4V, and CoCrMo (115). While many have attempted to create nanostructured surface features using chemical etchants (such as HNO₃) on titanium, results concerning increased bone synthesis have been mixed (58). Moreover, through the use of chemical etchants it is unclear to what the cells may be responding – changes in chemistry or changes in topography. For this reason, as was done for the ceramics in this review, it is important to focus on studies that have attempted to minimize large differences in material chemistry and focus only on creating surfaces that alter in their degree of nanometer roughness.

One such study by Ejiofor et al. utilized traditional powder metallurgy techniques without the use of heat to avoid changes in chemistry to fabricate different particle size groups of Ti, Ti6Al4V, and CoCrMo (Figure 11) (115). Increased osteoblast adhesion, proliferation, synthesis of extracellular matrix proteins (like alkaline phosphatase and collagen), and deposition of calcium containing mineral was observed on respective

nanophase compared conventional metals (115). This was the first study to demonstrate that the novel enhancements in bone regeneration previously seen in ceramics by decreasing grain size can be achieved in metals.

Interestingly, when Ejiofor et al. examined spatial attachment of osteoblasts on the surfaces of nanophase metals, they observed directed osteoblast attachment at metal grain boundaries (Figure 12) (115). Because of this, the authors speculated that the increased osteoblast adhesion may be due to more grain boundaries at the surface of nanophase compared to conventional metals. As was the case with nanophase ceramics (95,100), it is plausible that protein adsorption and conformation at nanophase metal grain boundaries may be greatly altered compared to non-grain boundary areas and/or conventional grain boundaries; in this manner, protein interactions at grain boundaries may be key for osteoblast adhesion.

POLYMERIC NANOMATERIALS

For ceramics and metals, most studies conducted to date have created desirable nanometer surface features by decreasing the size of constituent components of the material: for example, a grain, particle, or fiber. However, due to the versatility of polymers, many additional techniques exist to create nanometer surface roughness values. In addition, polymers contribute even further to rehabilitating damaged tissue by possibly providing a degradable scaffold that dissolves within a controllable time while the native tissue reforms. Techniques utilized to fabricate nanometer features on polymers include e-beam lithography, polymer demixing, chemical etching, cast-mold techniques, and the use of spin-casting (115-123). For those that have been applied to bone regeneration, chemical etching followed by mold casting and polymer demixing techniques have received the most attention (116,117).

For chemical etching techniques, polymers investigated to date include poly-lactic-co-glycolic acid (PLGA; Figure 13), polyurethane, and polycaprolactone (117,119-121). The idea proposed by Kay et al. has been to treat acidic polymers with basic solutions (i.e., NaOH) and basic polymers with acidic solutions (i.e., HNO₃) to create nanosurface features (117). While only on two-dimensional films, Kay et al. observed greater osteoblast adhesion on PLGA treated with increasing concentrations and exposure times of NaOH. As expected, data was also provided indicating larger degrees of nanometer surface roughness with increased concentrations and exposure times of NaOH on PLGA. Park et al. took this one step further and fabricated three-dimensional tissue engineering scaffolds by NaOH treatment of PLGA (119). When comparing osteoblast functions on such scaffolds, even though similar porosity properties existed between non-treated and NaOH treated PLGA (since similar amounts and sizes of NaCl crystals were used to create the pores through salt-leaching techniques), greater numbers of osteoblasts were counted on and in NaOH treated PLGA (119). Unfortunately, due to these fabrication techniques, it is unclear whether the altered PLGA chemistry or nano-etched surface promoted osteoblast adhesion; however, in light of the previous studies mentioned in this review, the authors of that study suggested the nanometer surface roughness of the NaOH-treated PLGA played an important role (119).

Studies have also been conducted on cell responses to polymers with changes in nanometer surface roughness without changes in chemistry. Specifically, Li et al. utilized polymer demixing techniques to create well-controlled nanometer islands of polystyrene and polybromo-styrene (122). Although osteoblast functions have not been tested on these constructs to date, fibroblast morphology was significantly influenced by incremental nanometer changes in polymer island dimensions (Figure 14). Again, this

study points to the unprecedented control that can be gained over cell functions by synthesizing materials to have nanometer surface features.

Although not related to orthopedic applications, vascular and bladder cell responses have also been promoted by altering the topography of polymeric materials in the nanometer regime (117,119,121,123). In these studies, chondrocytes (117), bladder (121), and vascular smooth muscle cell (120) adhesion and proliferation were greater on two-dimensional nanometer surfaces of biodegradable polymers such as PLGA, polyurethane, and polycaprolactone; similar trends have recently been reported on three-dimensional PLGA scaffolds (123).

COMPOSITE NANOMATERIALS

Due to the previous information of increased osteoblast function on ceramics and polymers, investigators have also determined bone cell function on nanophase ceramic polymer composites. Specifically, studies conducted to date show promoted osteoblast responses on composites of PLGA combined separately with nanophase alumina, titania, and hydroxyapatite (30:70 wt.% PLGA:ceramic) (117,124). For example, up to three times more osteoblasts adhered to PLGA when it contained nanophase compared to conventional titania particles (117). Since similar porosity (both % and diameters) existed between PLGA with conventional compared to nanophase titania, another novel property of nanophase ceramic composites was elucidated in this study: increased osteoblast functions. This is in addition to numerous reports in the literature highlighting greater toughness of nanophase compared to conventional ceramic:polymer composites (44-46).

Moreover, promoted responses of osteoblasts have also been reported when carbon nanofibers were incorporated into polymer composites; specifically, three times the number of osteoblasts adhered on polyurethane (PU) with increasing weight percentages of nanometer not conventional dimension carbon fibers (125). As mentioned,

reports in the literature have demonstrated higher osteoblast adhesion on carbon nanofibers in comparison with conventional carbon fibers (or titanium (ASTM F-67, Grade 2) (125), but this study demonstrated greater osteoblast adhesion with only a 2 wt. % increase of carbon nanofibers (CN) in the PU matrix. Up to three and four times the number of osteoblasts that adhered on the 100:0 PU:CN wt. %, adhered on the 90:10 and the 75:25 PU:CN wt.% composites, respectively (125). This exemplifies the unprecedented ability of nanophase materials to increase functions of bone cells whether used alone or in polymer composite form.

AREAS OF APPLICATION

While there has already been some effort spent on incorporating nanotechnology into orthopedic applications, it is clear that this is only the beginning for the incorporation of nanotechnology into biology; below some additional avenues are highlighted.

Drug Delivery

Polymers have found a significant role in the development of novel drug delivery systems. Biomaterials for mucoadhesive drug delivery applications have been improved through the addition of poly(ethylene glycol) as an adhesion promoter (127-130). Additionally, smart hydrogel drug carriers have been molecularly designed to safely carry proteins and peptides to the duodenum region, avoiding the harsh, acidic conditions of the stomach and the proteolytic enzymes present along the gastrointestinal tract (131-133). Drug delivery systems composed degradable polymers such as polyanhydrides (134-137), polyorthoesters (138,139), and poly(lactic-co-glycolic acid) (PLGA,140,141) have been implemented in chemically-controlled drug delivery.

Lu and Chen (142) have highlighted recent developments in the nano-fabrication of biodegradable drug delivery systems, and Leoni and Desai (143) have offered a review

of the abilities to create nanoporous structures containing an optimal pore size and distribution. Nanoporous structures (144) have the ability to allow mass transport of desirable compounds but limit those that are undesirable. An example given in the aforementioned review is the nanoporous encapsulation of pancreatic islet cells. The controlled pore size could allow certain molecules' transport such as glucose but significantly hinder the diffusion of molecules responsible for causing immune response mediate device failure such as immunoglobulin G and M molecules (IgG, IgM).

Nano drug delivery systems are quickly evolving in their ability to integrate biologically complex components into a functional nanodevice. Lee et. al. (145) offers the bacmid process as an object-oriented approach for designing novel nanosystems and outlines the possibility of using this type of design process for effective delivery of vaccines. Santini et. al. (40) have demonstrated the ability to deliver nanoliter quantities of therapeutics on demand from an array of sealed reservoirs. Drug discovery and delivery are becoming sciences that encompass skills developed in nanotechnology, microtechnology, and biology to effectively design systems more capable of achieving efficient and effective therapeutic treatments (147).

Much effort has been dedicated to engineering naoparticulate drug delivery systems (148,149). Surface modification allows the specific targeting of the particles and enhances their ability to interact with certain types of cells (150). Size plays a key role in the ability of particles to participate in intracellular uptake, and biodegradable nanoparticles can be used as sustained release delivery systems once inside the cytoplasm (151).

Tissue Engineering

Tissue engineering strives to create living tissue and organs through the use of synthetic, hybrid, or natural materials that have been designed or fabricated in a way to

elicit a desirable cellular response from the scaffold (152). The major thrust of developing materials for tissue engineering is providing the cells an environment in which they can continue their normal functionality. Biodegradable and resorbable materials are favorable due to the lack of necessity of a material structure to be present once the matrix has been formed. Poly(lactic acid), poly(glycolic acid), and their copolymers (PLGA) were first utilized in the development of biodegradable materials for tissue engineering applications, followed by other types of materials that include polyurethanes (153), polyanhydrides (154,155), and, more recently, poly(ether-anhydrides) (156).

This chapter already provided some nanotechnology-based examples of tissue engineering advances in orthopedics. In addition, Tsang and Bhatia (157) offer an extensive review into the fabrication techniques developed to aid in the development of novel tissue scaffolds. Significant advances in fabrication using heat, light, adhesives, and molding are elaborated upon. The use of cells to self-assemble native cellular matrices and cell/scaffold hybrids are also highlighted. Biomimetic materials are actively being pursued as integral components of novel tissue engineering biomaterials (158,159). Various techniques are being employed to take advantage of the ability to modify the surface of tissue engineering materials, with RGD modification receiving the most attention (160).

Synthetic hydrogels have traditionally been employed in the development of tissue engineering scaffolds due to their high biocompatibility, hydrophilicity, and tissue-like properties. The molecular design of these materials affords the engineer to impart certain physical properties into the device to obtain the necessary physiological response. Poly(lactic acid)-g-poly(vinyl alcohol) (PLA-g-PVA) have been developed into heart valves (161), and PVA/poly(vinyl pyrrolidone) (PVA/PVP) blends have been proposed

for nucleus pulposus replacement (162). Natural materials that have been developed for tissue engineering applications include collagen, hyaluronic acid, alginate, and chitosan (163).

Hybrid materials are being utilized to take advantage of the ability to synthesize polymeric materials with specific properties combined with a bioactive entity that helps elicit a particular biological response. PVA, a synthetic polymer, and chondroitin sulfate, a biological polymer, have been used to synthesize hydrogels that promote chondrogenesis (164). Mixtures of peptides and synthetic polymers are combined in order to mimic extracellular matrix (ECM) proteins to enable natural wound healing and reduce the formation of fibrous encapsulation. RGD has been used frequently to impart these properties into a biomaterial (160).

Biological Micro-Electro-Mechanical Systems (BioMEMS)

Most research focusing on BioMEMS is for their use in diagnostic devices and for the detection of DNA, viruses, proteins, and other biologically derived molecules (165). Nanoscale BioMEMS could allow for the real time detection and analysis of signaling pathways, which would further our knowledge and understanding of the basic mechanisms and functions of the cell. While nanoscale BioMEMS is at its infancy, it is clear that nanotechnology will play an important role in its development.

CONSIDERATIONS AND FUTURE DIRECTIONS

Although preliminary attempts to incorporate nanotechnology into biomedical applications seem promising, numerous urgent questions still remain about this new field. First and foremost, the safety of nanoparticles once in the human body remains largely unanswered both from a manufacturing point of view and when used in full or as a components of an implantable device. Since such particles are smaller than many pores of

biological tissues, it is clear that this information will have to be obtained before further consideration of implantable nanomaterials is undertaken. Such nanoparticles can easily become dislodged from implants during surgical implantation or from fragmentation of articulating components of a joint prosthetic composed of nanophase materials. Although preliminary in vitro studies highlight a less adverse influence of nanometer compared to micron particulate wear debris on bone cell viability (166,167), many more experiments are needed especially in vivo to evaluate their efficacy.

Specifically for orthopedic applications, additional questions remain. For example, once exact optimal nanometer surface features are elucidated for increasing bone regeneration, inexpensive tools that can be used in industry will be required. In this context, if the only nanofabrication devices that can be used to synthesize desirable nanometer surface features for bone regeneration are e-beam lithography or other equally expensive techniques, industry may not participate in this boom of nanotechnology at the intersection of tissue engineering. Inexpensive, but effective, nanometer synthesis techniques must continually be a focus of many investigators.

Still, the direction of the nanotechnology should be and is geared toward dealing with these issues. For example, according to the U.S. government's research agenda, the current and future broad interests in nano biomedical activity can be categorized in three broad related fronts (51,52):

- (i) development of pharmaceuticals for inside-the-body applications – such as drugs for anticancer and gene therapy;
- (ii) development of diagnostic sensors and lab-on-a-chip techniques for outside-the-body applications – such as biosensors to identify bacteriological infections in biowarfare; and
- (iii) development of prostheses and implants for inside-the-body uses.

Whereas the European governments emphasize commercial applications in all three fronts above according to Marsch (52), the U.S. government tends to gear towards fundamental research on biomedical implants and biodefense, leaving commercial applications to industry. Both classifications identify nanophase biomedical implants as potential interests. The biological and biomimetic nanostructures to be used as an orthopedic implant involve some sort of an assembly in which smaller materials later on assume the shape of a body part, such as hipbone. These final biomimetic, bulk nanostructures can start with a predefined nanochemical (like an array of large reactive molecules attached to a surface) or nanophysical (like a small crystal) structure. It is believed that by using these fundamental nanostructured building blocks as seed molecules or crystals, a larger bulk material will self-assemble or keep growing by itself.

In summary, it is now believed that significant evidence exists that highlights the promise nanotechnology has for biological applications, particularly in the bone arena. Clearly, nanomaterials as mentioned here are at their infancy and require much more testing before their full potential can be realized. However, even if nanophase materials never make it to the marketplace due to safety concerns, we have already learned much about how cells interact with surfaces through their application in the orthopedic environment.

ACKNOWLEDGEMENTS

JBT is supported through a Department of Homeland Security graduate research fellowship. JBT and NAP wish to thank NIH and NSF for support of the research summarized here. MS and TJW would like to thank the NSF and NIH for funding part of the research summarized here through the Bio-nanotechnology National Initiative.

REFERENCES

1. Ratner, B.D. et al. Biomaterials Science: A Multidisciplinary Endeavor, in Biomaterials Science: An Introduction to Materials in Medicine, 2nd Edition, B.D. Ratner et al. eds., Academic Press, San Diego, 2004, pp. 1-9.
2. Langer, R. and Peppas, N.A. Advances in biomaterials, drug delivery, and nanotechnology, *AIChE J.*, 49, 2990, 2003.
3. Peppas, N.A. and Langer, R. New challenges in biomaterials, *Science*, 263, 1715, 1994.
4. Hilt, J.Z. Nanotechnology and biomimetic methods in therapeutics: molecular scale control with some help from nature, *Adv. Drug Delivery Rev.*, 56, 1533, 2004.
5. <http://www.aaos.org/wordhtml/press/arthropl.htm> (accessed 2004)
6. <http://www.azcentral.com/health/0617newhips17/html> (accessed 2004)
7. <http://www.aaos.org/wordhtml/press/joinrepl.htm> (accessed 2004)
8. http://www.aaos.org/wordhtml/press/hip_knee.htm (accessed 2004)
9. Minino, A.M. and Smith, B.L. Vital Statistics, *National Vital Statistics Reports*, 49, 12, 2001.
10. <http://www.cdc.gov/nchs/fastats/lifexpec.htm> (accessed 2004)
11. Dowson, D. New joints for the millennium: Wear control in total hip replacement hip joints, *Proceedings of the Institution of Mechanical Engineers. Part H- Journal of Engineering in Medicine*, 215(4), 335, 2001.
12. Kaplan, F.S. et al. *Bone in Orthopedic Basic Science*, Simon, S.P., Ed., American Academy of Orthopedic Surgeons, Columbus, OH, 1994, pp. 127.
13. Oparaugo, P.C. et al. Correlation of wear debris-induced osteolysis and revision with volumetric wear-rate of polyethylene: A survey of 8 reports in literature, *Acta Orthopaed. Scandavica*, 72, 22, 2001.
14. Urban, R.M. et al. Dissemination of wear particles to the liver, spleen, and abdominal lymph nodes of patients with hip or knee replacement, *Amer. J. Bone Joint Surg.*, 82, 457, 2000.

15. Lerouge, S. et al. Characterization of in vitro wear debris from ceramic-ceramic total hip arthroplasties, *J. Biomed. Mat. Res.*, 32, 627, 1996.
16. Horbett, T.A. Proteins: structure, properties and adsorption to surfaces in *Biomaterials Science: An Introduction to Materials in Medicine*, Ratner, B.D., Hoffman, A.S., Schoen, F.S., and Lemmons, J.E., Eds., Academic Press, New York, NY, 1996, pp. 133.
17. Schakenraad, J.M. Cell: Their surfaces and interactions with materials in *Biomaterials Science: An Introduction to Materials in Medicine*, Ratner, B.D., Hoffman, A.S., Schoen, F.S., and Lemmons, J.E., Eds., Academic Press, New York, NY, 1996, pp. 133.
18. Brunette, D.M. The effects of implant surface topography on the behavior of cells, *Int. J. Oral Max. Implants*, 3, 231, 1988.
19. Martin, J.Y. et al. Effect of titanium surface roughness on proliferation, differentiation, and protein synthesis of human osteoblast-like cells (MG63), *J. Biomed. Mat. Res.*, 29, 389, 1995.
20. Wen, H.B., Cui, F.Z., and Zhu, X.D., Microstructural features of non-union of human humeral shaft fracture, *J. Structural Bio.*, 119, 239, 1997.
21. Larsson, C. et al. Bone response to surface modified titanium implants: studies on electropolished implants with different oxide thicknesses and morphology, *Biomaterials*, 15(13), 1062, 1994.
22. Bordji, K. et al. Cytocompatibility of Ti-6Al-4V and Ti-5Al-2.5Fe alloys according to three surface treatments, using human fibroblasts and osteoblasts, *Biomaterials*, 17(9), 929, 1996.
23. Lalan, S., Pomerantseva, I., and Vacanti, J.P. Tissue engineering and its potential impact on surgery, *World J. Surg.*, 25, 1458, 2001.
24. H. Andersson, A. van den Berg. Microfabrication and microfluidics for tissue engineering: state of the art and future opportunities, *Lab on a chip*, 4, 98, 2004.
25. Saltzman, W.M. and Olbricht, W.L. Building drug delivery into tissue engineering, *Nat. Rev. Drug Discov.*, 1, 177, 2002.
26. Tirrell, M., Kokkoli, E., and Biesalski, M. The role of surface science in bioengineered materials, *Surface Science*, 500, 61, 2002.
27. Gershon, D. Microarray technology an array of opportunities, *Nature*, 416, 885, 2002.

28. Meller, A. et al. Rapid nanopore discrimination between single polynucleotide molecules, *Proc. Natl. Acad. Sci. USA*, 97, 1079, 2000.
29. Bayley, H. and Cremer, P. Stochastic sensors inspired by biology, *Nature*, 413, 226, 2001.
30. Li, J. et al. DNA molecules and configurations in a solid-state nanopore microscope, *Nature Materials*, 2, 611, 2003.
31. Storm, A. et al. Fabrication of solid-state nanopores with single-nanometre precision, *Nature Materials*, 2, 537, 2003.
32. Wang, H. and Branton, D. Nanopores with a spark for single-molecule detection. *Nat. Biotechnol.*, 19, 622, 2001.
33. Zhang, S. Fabrication of novel biomaterials through molecular self-assembly, *Nature Biotechnol.*, 21, 1171, 2003.
34. Byrne, M.E., Park, K., and Peppas, N.A. Molecular imprinting within hydrogels, *Adv. Drug Deliv. Rev.*, 54, 149, 2002.
35. Manz, A., Graber, N., and Widmer, H. Miniaturized total chemical analysis systems: a novel concept for chemical sensing, *Sensor. Actuat. B – Chem.*, 1, 244, 1990.
36. Jakeway, S., de Mello, A., and Russell, E. Miniaturized total analysis systems for biological analysis, *Fresen. J. Anal. Chem.*, 366, 525, 2000.
37. Tudos, A., Besselink, G., and Schasfoort, R. Trends in miniaturized total analysis systems for point-of-care testing in clinical chemistry, *Lab on a chip*, 1, 83, 2001.
38. Liu, Y., Garcia, C., and Henry, C. Recent progress in the development of μ TAS for clinical analysis, *Analyst*, 128, 1002, 2003.
39. LaVan, D., Lynn, D., and Langer, R. Moving smaller in drug discovery and delivery, *Nat. Rev. Drug Disc.*, 1, 77, 2002
40. Santini, Jr., S., Cima, M., and Langer, R. A controlled-release microchip, *Nature*, 397, 335, 1999.
41. Grayson, A.C. et al. Multi-pulse drug delivery from a resorbable polymeric microchip device. *Nat. Mater.*, 2, 767, 2003.
42. Siegel, R.W. and Fougere, G.E. Mechanical properties of nanophase materials, in *Nanophase Materials: Synthesis-Properties Applications*, Hadjipanayis, G.C. and Siegel, R.W., Eds., Kulwer, Dordrecht, 1994, pp. 233.

43. Roco, M.S., Williams, R.S, and Alivisatos, P., Nano-Technology Research Directions, in IWGN Workshop Report, 1999.
44. Siegel, R.W. and Fougere, G.E. Mechanical properties of nanophase metals, *Nanostructured Materials*, 6, 205, 1995.
45. Siegel, R.W. Creating nanophase materials, *Sci. Amer.*, 275, 42, 1996.
46. Siegel, R.W., Hu, E., and Roco, M.C., *Nano-Structure Science and Technology*, Kluwer Academic Press, Boston, MA, 1999.
47. Baraton, M.I., Chen, X., and Gonsalves, K.E. FTIR study of nanostructured alumina nitride powder surface: determination of the acidic/basic sites by CO, CO₂, and acetic acid adsorptions, *Nanostructured Materials*, 8, 435, 1999.
48. Klabunde, K.J. et al. Nanocrystals as stoichiometric reagents with unique surface chemistry, *J. Phys. Chem.*, 100, 12141, 1996.
49. Wu, S.J., DeJong, L.C., and Rahaman, M.N. Sintering of nanophase γ -Al₂O₃ powder, *Journal of American Ceramic Society*, 79, 2207, 1996.
50. Martyanov, I.N. and Klabunde, K.J., Photocatalytic oxidation of gaseous 2-chloroethyl ethyl sulfide over TiO₂, *Environmental Science & Technology*, 37(15), 3448, 2003.
51. Malsch, I. Biomedical applications of nanotechnology, *The Industrial Physicist*, June/July, 15, 2002.
52. Malsch, I. The nano-body: sense and non-sense on biomedical applications of nanotechnology, Lecture for COST and NanoSTAG Conference, Leuven, Oct. 29, 2001.
53. Ayad, S. et al., *The Extracellular Matrix Factsbook*, Academic Press Inc., San Diego, CA, 1994, pp. 29.
54. Cowin, R., *Handbook of Bioengineering*, McGraw Hill, New York, NY, 1987.
55. Brunette, D. The effect of surface topography of cell migration and adhesion, in *Titanium in Medicine*, Brunette, D.M., Tengvall, P., Textor, M., and Thomsen, P., Springer-Verlag, New York, NY, 2001, pp. 486-512.
56. Buser, D. et al. Interface shear strength of titanium implants with a sandblasted and acid-etched surface: a biomechanical study in the maxilla of miniature pigs, *J. Biomed. Mat. Res*, 45(2), 75, 1999.

57. Hench, L.L. and Paschall, H.A., Histochemical responses at a biomaterial's interface, *J. Biomed. Mat. Res*, 8(3), 49, 1974.
58. Litsy, A.S. and Spector, M. Biomaterials, in *Orthopedic Basic Science*, Simon, S.P., Ed., American Academy of Orthopedic Surgeons, Columbus, OH, 1994, pp. 482.
59. Peppas, N. and Khare, A. Preparation, structure and diffusional behavior of hydrogels in controlled release. *Adv. Drug Deliver. Rev.* 1993, 11, 1-35.
60. Peppas, N.A. et al. Hydrogels in pharmaceutical formulations. *Eur. J. Pharm. Biopharm.* 50, 27, 2000.
61. Torres-Lugo, M. and Peppas, N.A. Preparation and characterization of p(MAA-g-EG) nanospheres for protein delivery applications. *J. Nanoparticle Research.* 4, 73, 2002.
62. Donini, C et al. Preparation of poly(methacrylic acid-g-poly(ethylene glycol)) nanospheres from methacrylic monomers for pharmaceutical applications. *Int. J. Pharm.*, 245, 83, 2002.
63. Robinson, D. and Peppas, N.A. Preparation and characterization of pH-responsive poly(methacrylic acid-g-ethylene glycol) nanospheres. *Macromolecules*, 35, 3668, 2002.
64. Gref, R et al. Biodegradable long-circulating polymeric nanospheres. *Science*, 263, 1600, 1994.
65. Peracchia, M.T. Stealth nanoparticles for intravenous administration. *S.T.P. Pharma Sci.*, 13 (3), 155, 2003.
66. Cohen, H. et al. Sustained delivery and expression of DNA encapsulated in polymeric nanoparticles. *Gene Ther.*, 7, 1896, 2000.
67. Luo, D. and Saltzman, W. Synthetic DNA delivery systems. *Nat. Biotechnol.*, 18, 33, 2000.
68. Brannon-Peppas, L. Recent advances on the use of biodegradable microparticles and nanoparticles in controlled drug delivery. *Int. J. Pharm.*, 116, 1, 1995.
69. Santini, Jr., J. et al. Microchips as controlled drug-delivery devices. *Angew. Chem. Int. Ed.*, 39, 2396-2407, 2000.
70. Grayson, A.C. et al., Multi-pulse drug delivery from a resorbable polymeric microchip device. *Nat. Mater.*, 2 , 767, 2003.

71. Nikolovski, J. and Mooney, D.J. Smooth muscle cell adhesion to tissue engineering scaffolds, *Biomaterials*, 21, 2025 2000.
72. Peppas, N.A. *Hydrogels in Medicine and Pharmacy*, CRC Press, Boca Raton, 1987.
73. Peppas, N.A. Gels for drug delivery, in *Encyclopedia of Materials: Science and Technology*, Elsevier, Amsterdam, 2001, pp. 3492.
74. Peppas, N.A. Hydrogels, in *Biomaterials Science: An Introduction to Materials in Medicine*, 2nd Edition, B.D. Ratner et al. eds., Academic Press, San Diego, CA, 2004, pp. 100.
75. Wichterle, O. and Lim, D. Hydrophilic gels for biological use, *Nature*, 185, 117, 1960.
76. Tighe, B.J. The design of polymers for contact lens applications, *Brit. Polym. J.*, 8, 71, 1976.
77. Peppas, N.A. and Yang, W.H.M., Properties-based optimization of the structure of polymers for contact lens applications, *Contact Intraocular Lens Med. J.*, 7, 300, 1981.
78. Peppas, N.A, Wood, K.M., and Blanchette, J.O. Hydrogels for oral delivery of therapeutic proteins, *Expert Opinion on Bio. Therapy*, 4, 881, 2004.
79. Peppas, N.A. Fundamentals of pH- and temperature-sensitive delivery systems, in *Pulsatile Drug Delivery*, Gurny, R., Junginger, H.E., and Peppas, N.A. eds., Wissenschaftliche Verlagsgesellschaft, Stuttgart, 1993, pp. 41-56.
80. Peppas, N.A. et al. Physicochemical foundations and structural design of hydrogels in medicine and biology, *Ann. Rev. Biomed. Eng.*, 2, 9, 2000.
81. Flory, P.J. *Principles of Polymer Chemistry*, Cornell Univ. Press, Ithaca, NY, 1953.
82. Hilt, J.Z. and Byrne, M.E. Configurational biomimesis in drug delivery: molecular imprinting of biologically significant molecules, *Adv. Drug Delivery Rev.*, 56, 1599, 2004.
83. Castner, D.G. and Ratner, B.D. Biomedical surface science: Foundations to frontiers, *Surface Science*, 500, 28, 2002.
84. Vroman, L. Effects of hydrophobic surfaces upon blood coagulation, *Thrombos. Diathes. Haemorrh.*, 10, 455, 1964.

85. Vroman, L. and Adams, A.L. Findings with the recording ellipsometer suggesting rapid exchange of specific plasma proteins at liquid/solid interfaces, *Surf. Sci.*, 16, 438, 1969.
86. Baier, R.E et al. Surface properties determine bioadhesive outcomes: methods and results, *J. Biomed. Mater. Res.*, 18, 337-355, 1984.
87. Hoffman, A.S. Principles governing biomolecule interactions in foreign interfaces, *J. Biomed. Mater. Res. Symp.*, 5, 77, 1974.
88. Lopez, G.P. et al. Plasma deposition of ultrathin films of poly(2-hydroxy-ethyl methacrylate): Surface analysis and protein adsorption measurements, *Macromolecules*, 26, 3247, 1993.
89. Merrill, E.W., Pol(ethylene oxide) blood contact, in Harris, J.M. ed., *Poly(ethylene glycol) chemistry: Biotechnical and biomedical applications*, Plenum Press, New York, 1992, pp. 199-220.
90. Mar, M.N., Ratner, B.D., and Yee, S.S. An intrinsically protein-resistant surface plasmon resonance biosensor based upon a RF-plasma-deposited thin film, *Sensors and Actuators B*, 54, 125, 1999.
91. Drotleff, S. et al. Biomimetic polymers in pharmaceutical and biomedical sciences, *Eur. J. Pharm. Biopharm.*, 58, 385-407, 2004.
92. Webster, T.J., Siegel, R.W., and Bizios, R. An in vitro evaluation of nanophase alumina for orthopaedic/dental applications, in *Bioceramics 11: Proceedings of the 11th International Symposium on Ceramics in Medicine*, LeGeros, R.Z. and LeGeros, J.P., Eds., World Scientific, New York, NY, 1998, pp. 273.
93. Webster, T.J., Siegel, R.W., and Bizios, R. Design and evaluation of nanophase alumina for orthopaedic/dental applications, *Nanostructured Materials*, 12, 983, 1999.
94. Webster, T.J., Siegel, R.W., and Bizios, R. Osteoblast adhesion on nanophase ceramics, *Biomaterials*, 20, 1221, 1999.
95. Webster, T.J. et al. Specific proteins mediate enhanced osteoblast adhesion on nanophase ceramics, *J. Biomed. Mat. Res.*, 51(3), 475, 2000.
96. Webster, T.J., Siegel, R.W., and Bizios, R. Enhanced functions of osteoblasts on nanophase ceramics, *Biomaterials*, 21, 1803, 2000.
97. Webster, T.J., Siegel, R.W., and Bizios, R. Enhanced surface and mechanical properties of nanophase ceramics for increased orthopaedic/dental implant efficacy, in *Bioceramics 13: Proceedings of the 13th International Symposium on*

- Ceramics in Medicine, Giannini S. and Moroni, A., Eds., World Scientific, New York, NY, 2000, pp. 321.
98. Webster, T.J. The future of orthopedic and dental implant materials, in *Advances in Chemical Engineering* Vol. 27, Ying J.Y., Ed., Academic Press, New York, NY, 2001, pp. 125.
 99. Webster, T.J et al. Mechanisms of enhanced osteoblast adhesion on nanophase alumina involve vitronectin, *Tissue Engineering*, 7(3), 291, 2001.
 100. Webster, T.J et al. Enhanced functions of osteoclast-like cells on nanophase ceramics, *Biomaterials*, 22(11), 1327, 2001.
 101. Webster, T.J., Siegel, R.W., and Bizios, R. Nanoceramic surface roughness enhances osteoblast and osteoclast functions for improved orthopaedic/dental implant efficacy, *Scripta Materialia*, 44, 1639, 2001.
 102. Elias, K.L., Price, R.L., and Webster, T.J. Enhanced functions of osteoblasts on nanometer diameter carbon fibers, *Biomaterials*, 23, 3279, 2002.
 103. Danilov, Y.N. and Juliana, R.L. (Arg-Gly-Asp)_n-albumin conjugates as a model substratum for integrin-mediated cell adhesion, *Exp. Cell Res.*, 182, 186, 1989.
 104. Hughes, R.C. et al. Molecular requirements for adhesion and spreading of hamster fibroblasts, *Exp. Cell Res.*, 121, 307,, 1979.
 105. Humphries, M.J. et al. Identification of an alternatively spliced site in human plasma fibronectin that mediates cell type-specific adhesion, *J. Cell Biol.*, 103, 2637, 1986.
 106. Singer, I.I. et al. Cell surface distribution of fibronectin and vitronectin receptors depends on substrate composition and extracellular matrix accumulation, *J. Cell Biol.*, 104, 573, 1987.
 107. Underwood, P.A. and Bennett, F.A. A comparison of the biological activities of the cell-adhesive proteins vitronectin and fibronectin, *J. Cell Sci.*, 93, 641, 1989.
 108. Massia, S.P. and Hubbell, J.A. Human endothelial cell interactions with surface-coupled adhesion peptides on a nonadhesive glass substrate and two polymeric biomaterials, *J. Cell Bio.*, 14(5), 1089, 1991.
 109. Li, P. Biomimetic nano-apatite coating capable of promoting bone ingrowth, *J. Biomed. Mat. Res.*, 66, 79, 2003.

110. Thull, R. and Grant, D. Titanium surface modification, in *Titanium in Medicine*, Brunette, D.M., Tengvall, P., Textor, M., and Thomsen P., Eds., Springer – Verlag, New York, NY, 2001, pp. 284.
111. Sato, M. et al. Novel nanophase hydroxyapatite coatings on titanium, 29th International Conference on Advanced Ceramics and Composites, Cocoa Beach, FL, 2005.
112. Price, R.L. et al. Osteoblast function on nanophase alumina materials: Influence of chemistry, phase, and topography, *J. Biomed. Mat. Res*, 67 (4), 1284-1293, 2003.
113. Dee, K.C. et al. Conditions which promote mineralization at the bone-implant interface: a model in vitro study, *Biomaterials*, 17, 209, 1996.
114. Chun, A. et al. Helical rosette nanotubes: a more effective orthopaedic implant material, *Nanotechnology*, 15, S234, 2004.
115. Ejiogor, J.U. and Webster, T.J. Increased osteoblast functions on nanostructured metals, ASM Conference, Las Vegas, NV, 2004.
116. Dalby, M.J. et al. In vitro reaction of endothelial cells to polymer demixed nanotopography, *Biomaterials*, 23, 2945, 2002.
117. Kay, S. et al. Nanostructured polymer:nanophase ceramic composites enhance osteoblast and chondrocyte adhesion, *Tissue Engineering*, 8, 753, 2002.
118. Zhang, R. and Ma, P.X. Porous poly(L-lactic acid)/apatite composites created by biomimetic process, *J. Biomed. Mat. Res*, 45(4), 285, 1999.
119. Park, G.E et al. Accelerated chondrocyte functions on NaOH-treated PLGA scaffolds, *Biomaterials*, 26(16), 3075, 2005.
120. Miller, D.C. et al. Endothelial and vascular smooth muscle cell function on poly(lactic-co-glycolic acid) with nano-structured surface features, *Biomaterials*, 25, 53, 2004.
121. Thapa, A., et al. Nano-structured polymers enhance bladder smooth muscle cell function, *J. Biomed. Mat. Res*, 67, 1374, 2003.
122. Li, W.-J. et al. Electrospun nanofibrous structure: A novel scaffold for tissue engineering, *J. Biomed. Mat. Res*, 60, 613-621, 2002.
123. Pattison, M., et al. Three-dimensional, nano-structured PLGA scaffolds for bladder tissue replacement applications, *Biomaterials*, in press, 2004 (available online).

124. Smith, T.A. and Webster, T.J. Improved osteoblast functions on polymer:nanophase ceramic composites, *J. Biomed. Mat. Res*, in press, 2004.
125. Price, R.L. et al. Select bone cell adhesion on formulations containing carbon nanofibers, *Biomaterials*, 24(11), 1877, 2003.
126. Tu, R. and Tirrell, M. Bottom-up design of biomimetic assemblies, *Adv. Drug Delivery Rev.*, 56, 1537, 2004.
127. Huang, Y. et al. Molecular aspects of muco- and bioadhesion: Tethered structures and site-specific surfaces, *J. Contr. Rel.*, 65, 63, 2000.
128. Huang, Y., Szleifer, I., and Peppas, N.A. Gel-gel adhesion by tethered polymers, *J. Chem. Phys.*, 114, 3809, 2001.
129. Efremova, N.V et al. Direct measurement of interactions between tethered poly(ethylene glycol) and adsorbed mucin layers, *Langmuir*, 18, 836, 2002.
130. Peppas, N.A. and Huang, Y. Nanoscale technology of mucoadhesive interactions, *Adv. Drug Delivery Rev.*, 56, 1675, 2004.
131. Oral, E. and Peppas, N.A. Responsive and recognitive hydrogels using star polymers, *J. Biomed. Mater. Res.*, 68A, 439, 2004.
132. Nakamura, K. et al. Oral insulin delivery using P(MAA-g-EG) hydrogels: Effect of network morphology on insulin delivery characteristics, *J. Controlled Release*, 95, 589, 2004.
133. Doninin, C. et al. Preparation of P(MAA-g-EG) nanospheres for pharmaceutical applications, *Int. J. Pharm.*, 245, 83, 2002.
134. Quick, D.J., Macdonald, K.K., and Anseth, K.S. Delivering DNA from photocrosslinked, surface eroding polyanhydrides, *J. Controlled Release*, 97, 333, 2004.
135. Gopferich, A. and Tessmar, J. Polyanhydride degradation and erosion, *Adv. Drug Delivery Reviews*, 54, 911, 2002.
136. Burkoth, A.K., Burdick, J., and Anseth, K.S. Surface and bulk modifications to photocrosslinked polyanhydrides to control degradation behavior, *J. Biomed. Mater. Res.*, 51, 352, 2000.
137. Dang, W.B. and Saltzman, W.M. Controlled-release of macromolecules from a degradable polyanhydride matrix, *J. Biomat. Sci.—Polymer Edn.*, 6, 297, 1994.

138. Shi, M. et al. Double-walled POE/PLGA microspheres: encapsulation of water-soluble and water-insoluble proteins and their release properties, *J. Controlled Release*, 89, 167, 2003.
139. Merkil, A. et al. Synthesis and characterization of a new biodegradable semisolid poly(ortho ester) for drug-delivery systems, *J. Biomat. Sci.—Polymer Edn.*, 4, 505, 1993.
140. Cegnar, M., Kos, J., and Kristi, J. Cystatin incorporated in poly(lactide-co-glycolide) nanoparticles: development and fundamental studies on preservation of its activity, *Eur. J. Pharm. Sci.*, 22, 357, 2004.
141. Kempen, D.H.R. et al. Development of biodegradable poly(propylene fumarate)/poly(lactic-co-glycolic acid) blend microspheres: I. Preparation and characterization, *J. Biomed. Mater. Res. Part A*, 70A, 283, 2004.
142. Lu, Y. and Chen, S.C. Micro and nano-fabrication of biodegradable polymers for drug delivery, *Adv. Drug Delivery Reviews*, 56, 1621, 2004.
143. Leoni, L. and Desai, T.A. Micromachined biocapsules for cell-based sensing and delivery, *Adv. Drug Delivery Reviews*, 56, 211-229, 2004.
144. Desai, T.A. et al. Nanoporous Microsystems for islet cell replacement, *Adv. Drug Delivery Reviews*, 56, 1661, 2004.
145. Lee, S.C., Bhalerao, K., and Ferrari, M. Object-oriented design tools for supramolecular devices and biomedical nanotechnology, *Ann. N.Y. Acad. Sci.*, 1013, 110, 2004.
146. Santini, J.T. Jr., Cima, M.J., and Langer, R. A controlled-release microchip, *Nature*, 397, 335, 1999.
147. LaVan, D.A., Lynn, D.M., and Langer, R. "Moving smaller in drug discovery and delivery," *Nature Reviews Drug Discovery*, 1, 77, 2002.
148. Crommelin, D.J.A. et al. Nanotechnological approaches for the delivery of macromolecules, *J. Controlled Release*, 87, 81, 2003.
149. Brannon-Peppas, L. and Blanchette, J.O. Nanoparticle and targeted systems for cancer therapy, *Adv. Drug Delivery Reviews*, 56, 1649, 2004.
150. Gupta, A.K and Curtis, A.S.G. Surface modified superparamagnetic nanoparticles for drug delivery: Interaction studies with human fibroblasts in culture, *J. Mater. Sci.: Mat. Med.*, 18, 493, 2004.

151. Panyam, J. and Labhasetwarm, V. Biodegradable nanoparticles for drug and gene delivery to cells and tissue, *Adv. Drug Delivery Reviews*, 55, 329, 2003.
152. Griffith, L.G., Emerging design principles in biomaterials and scaffolds for tissue engineering, *Ann. N.Y. Acad. Sci.*, 961, 83, 2002.
153. Buma, P. et al. Tissue engineering of the meniscus, *Biomaterials*, 25, 1523, 2004.
154. Burkoth, A.K. and Anseth, K.S. A review of photocrosslinked polyanhydrides: in situ forming degradable networks, *Biomaterials*, 21, 2395, 2000.
155. Muggli, D.S., Burkoth, A.K., and Anseth, K.S. Crosslinked polyanhydrides for use in orthopedic applications: Degradation behavior and mechanics, *J. Biomed. Mater. Res.*, 46, 271, 1999.
156. Kim, B.S., Hrkach, J.S., and Langer, R. Synthesis and characterization of novel degradable photocrosslinked poly(ether-anhydride) networks, *J. Polym. Sci. Part A—Polym. Chem.*, 38, 1277, 2000.
157. Tsang, V.L. and Bhatia, S.N. Three-dimensional tissue fabrication, *Adv. Drug Delivery Rev.*, 56, 1635, 2004.
158. Shin, H., Jo, S., and Mikos, A.G. Biomimetic materials for tissue engineering, *Biomaterials*, 24, 4353, 2003.
159. Hacker, M. et al. , “Towards biomimetic scaffolds: Anhydrous scaffold fabrication from biodegradable amine-reactive diblock copolymers,” *Biomaterials*, 24, 4459, 2003.
160. Hersel, U., Dahmen, C., and Kessler, H. RGD modified polymers: biomaterials for stimulated cell adhesion and beyond, *Biomaterials*, 24, 4385, 2003.
161. Nuttelman, C.R., Henry, S.M., and Anseth K.S. Synthesis and characterization of photocrosslinkable, degradable poly(vinyl alcohol)-based tissue engineering scaffolds, *Biomaterials*, 23, 3617, 2002.
162. Thomas, J., Lowman, A., and Marcolongo, M. Novel associated hydrogels for nucleus pulposus replacement, *J. Biomed. Mater. Res. Part A*, 67A, 1329, 2003.
163. Drury, J.L. and Mooney, D.J. Hydrogels for tissue engineering: scaffold design variables and applications, *Biomaterials*, 24, 4337, 2003.
164. Bryant, S.J. et al. Synthesis and characterization of photopolymerized multifunctional hydrogels: Water-soluble poly(vinyl alcohol) and chondroitin sulfate macromers for chondrocyte encapsulation, *Macromolecules*, 37, 6726, 2004.

165. Bashir, R., BioMEMS: state-of-the-art in detection, opportunities and prospects, *Adv. Drug Delivery Rev.*, 56, 1565, 2004.
166. Gutwein, L.G. and Webster, T.J. Osteoblast and chondrocyte proliferation in the presence of alumina and titania nanoparticles, *Journal of Nanoparticle Research*, 4, 231, 2002.
167. Price, R.L. and Webster, T.J. Increased osteoblast viability in the presence of smaller nano-dimensioned carbon fibers, *Nanotechnology*, 15(8), 892, 2004.

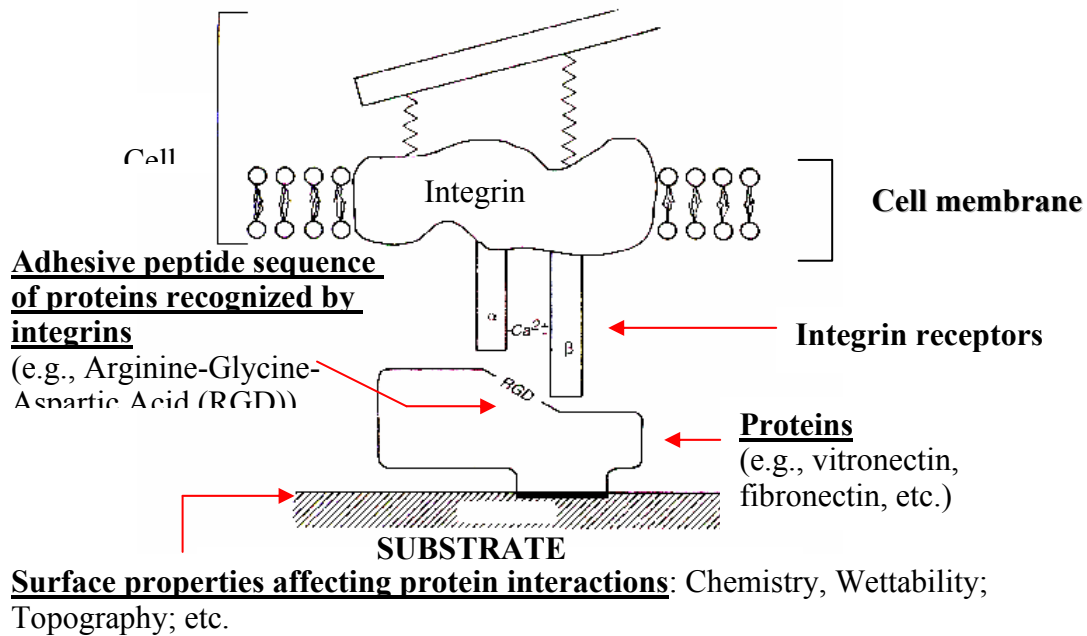


Figure A.1: Cell recognition of biomaterial surfaces controlled by initial protein interactions. Initial protein interactions can influence cell adhesion and, thus, degree of bone tissue formation on biomaterials. Changing material properties will alter protein interactions and influence subsequent cell function. (Adapted and redrawn from Schakenraad, J.M., in *Biomaterials Science: An Introduction to Materials in Medicine*, Ratner, B.D., Hoffman, A.S., Schoen, F.S., and Lemmons, J.E., Eds., Academic Press, New York, NY, 1996, pp. 133-140. With permission.)

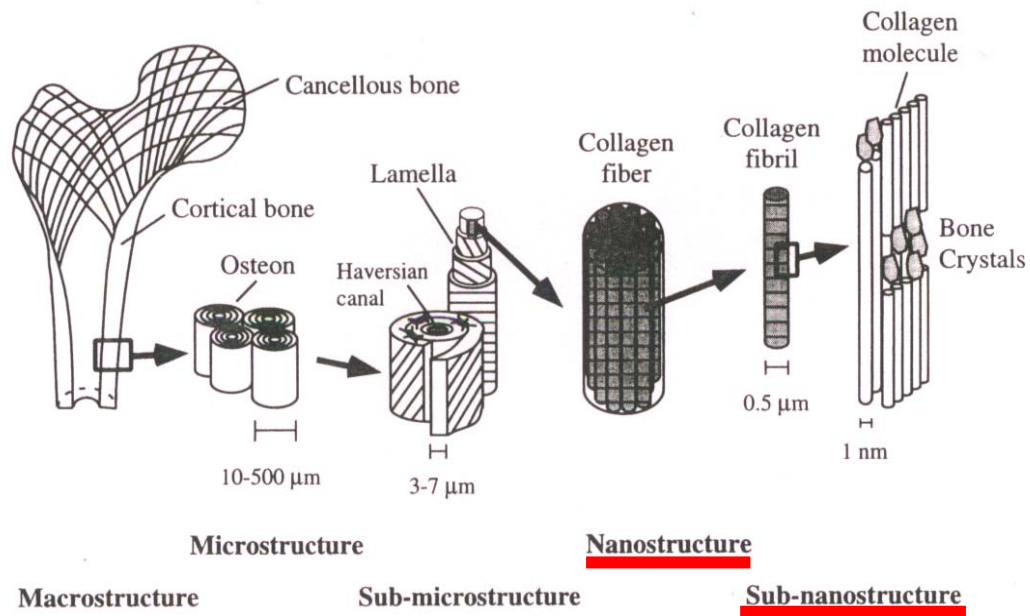
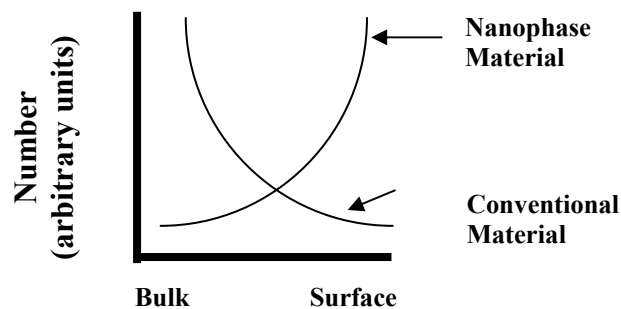
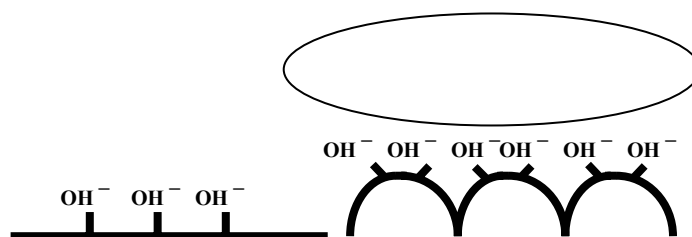


Figure A.2: Nanocomponents of bone provide a high degree of nanostructured surface roughness for bone cells. (Adapted and redrawn from Cowin, R., Handbook of Bioengineering, McGraw Hill, New York, NY, 1987. With permission.)



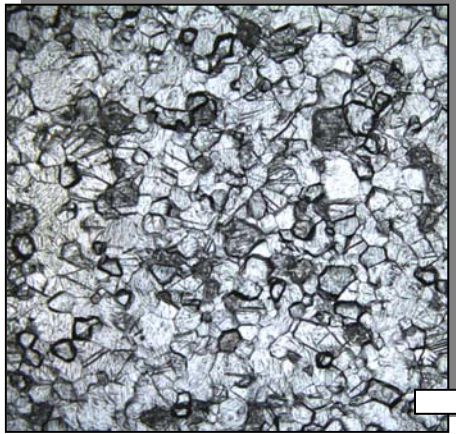
(a)



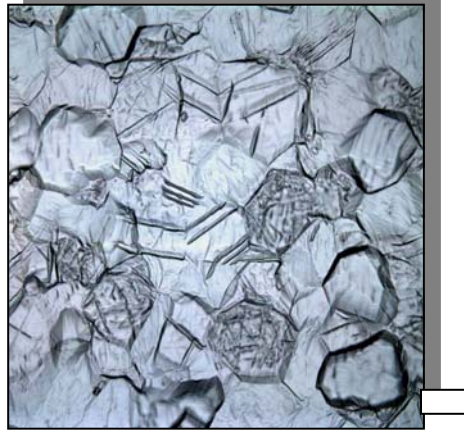
(a) Conventional
(grain size: > 100 nm)

(b)

Figure A.3: Special surface properties of nanophase materials. (a) Higher number of atoms at the surface for nanophase compared to conventional materials. (b) Nanophase materials have higher surface areas, possess greater numbers of material defects at the surface, and altered electron delocalization. Such special properties will influence protein interactions for controlling cell functions. (Adapted and redrawn from Klabunde, K.J. et al., *J. Phys. Chem.*, 100, 12141, 1996. With permission.)



Ti (Medical Grade 2) at a magnification of 100X



Ti (Medical Grade 2) at a magnification of 400X

Figure A.4: Conventional grain size of currently used orthopedic implants. Bar = 10 and 1 micron for the left and right micrograph, respectively.

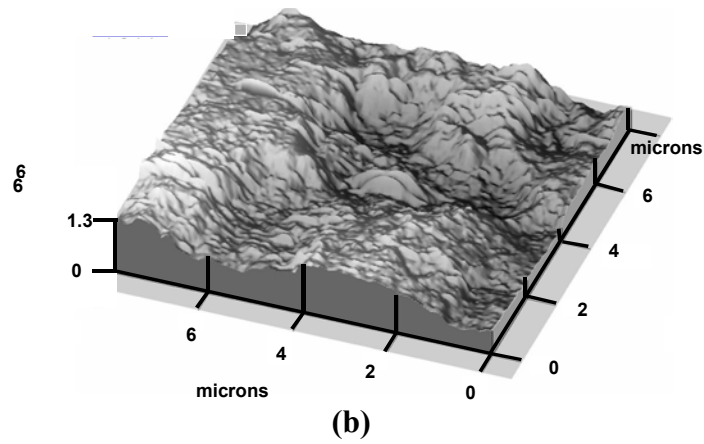
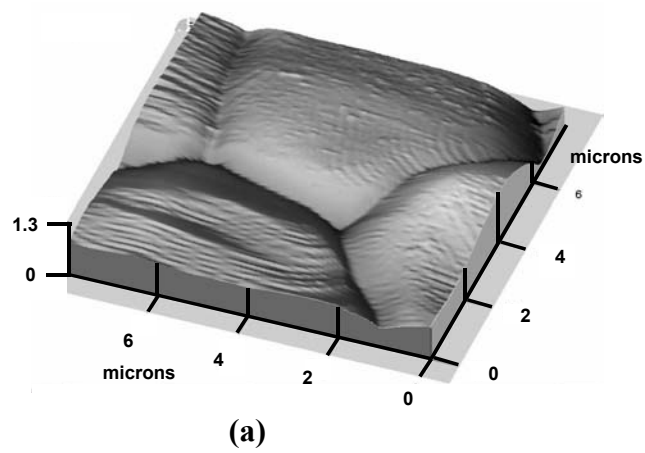


Figure A.5: (a) Conventional and (b) nanophase titania. One of the first studies correlating increased osteoblast function with decreasing ceramic grain size was done on titania as pictured here. (From Webster, T.J., Siegel, R.W., and Bizios, R., *Biomaterials*, 20, 1221, 1999. With permission.)

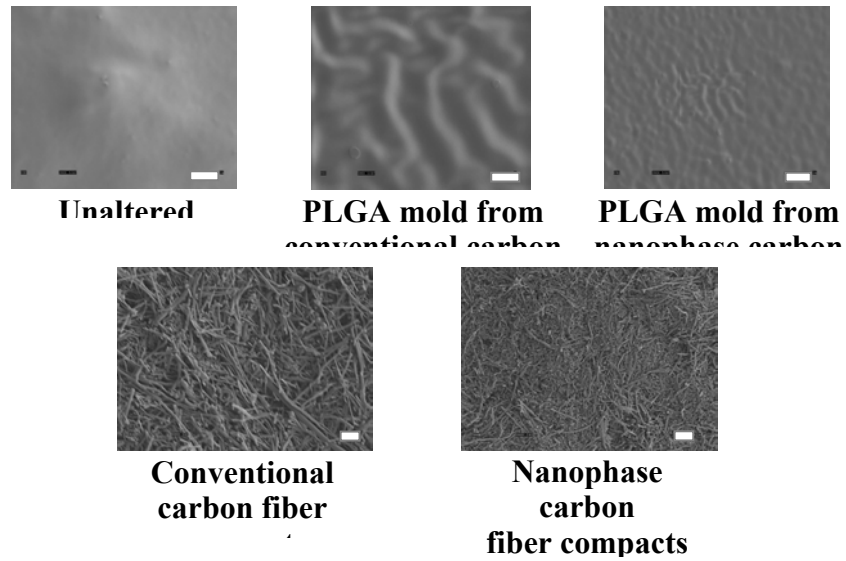


Figure A.6: Poly-lactic-glycolic acid (PLGA) molds of conventional and nanophase carbon fiber compacts. To highlight the importance of nanometer surface roughness regardless of substrate chemistry, studies have shown increased functions of osteoblasts on PLGA molds of nanophase compared to conventional carbon compacts. Studies have also shown increased functions of osteoblasts on compacts composed of nanometer compared to conventional carbon fibers. Bar = 1 micron. (From Elias, K.L., Price, R.L., and Webster, T.J., *Biomaterials*, 23, 3279-3287, 2002. With permission.)

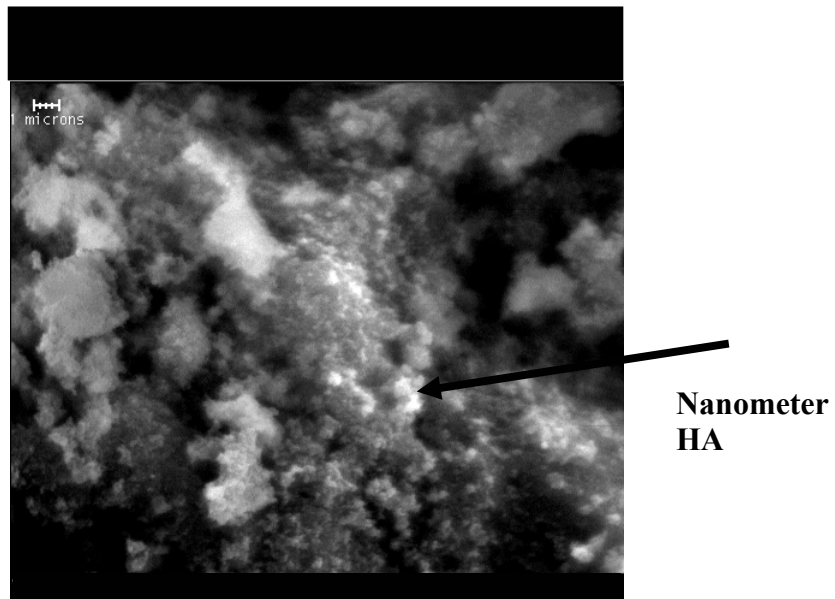
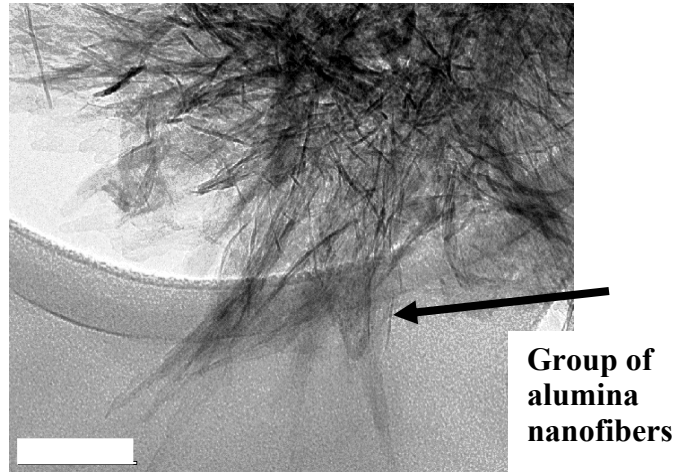


Figure A.8: Nanophase hydroxyapatite coated on titanium. Due to elevated temperatures, traditional coating techniques, like plasma spray deposition, cannot be used to coat metals with nanophase ceramics. This process developed by Spire Biomedical (Bedford, MA) uses high pressure at low temperatures so as to not allow for grain growth. Bar = 1 micron (upper left).



**Group of
alumina
nanofibers**

Figure A.9: Transmission electron microscope image of alumina nanofibers. Compared to spherical conventional alumina, increased functions of osteoblasts have been reported on nanophase fibrous alumina. Scale bar = 10 nm. (From Price, R.L. et al., *J. Biomed. Mat. Res*, 67 (4), 1284, 2003. With permission.)

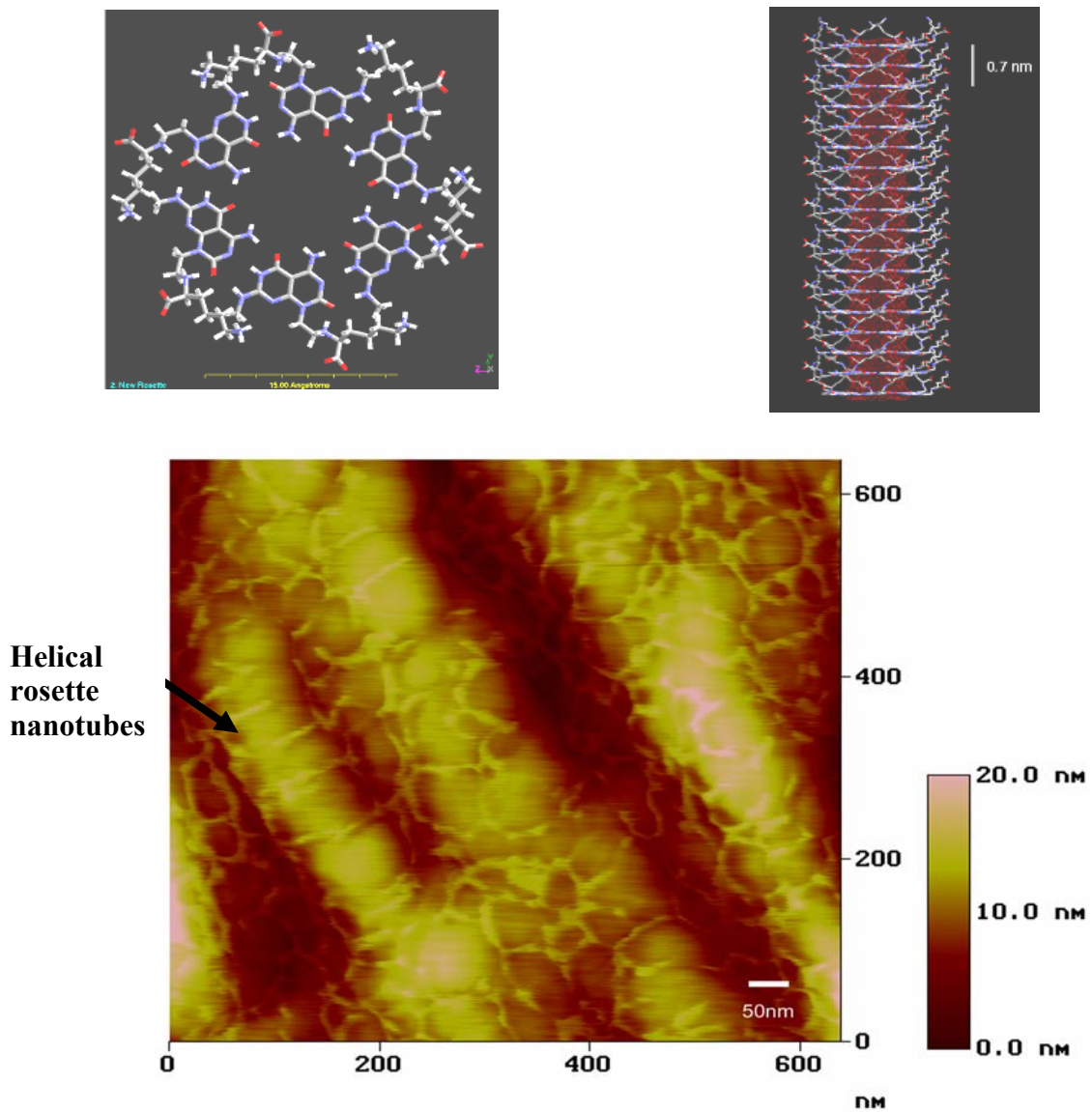


Figure A.10: Helical rosette nanotubes. Drawing of the cross-sectional (left) and longitudinal (right) view of self-assembled helical rosette nanotubes is depicted in (a) while helical rosette nanotubes coated on titanium is depicted in (b). Note the nanophase dimension of these organic tubes. Increased osteoblast function has been observed on helical rosette nanotubes coated on Ti. (From Chun, A. et al., *Nanotechnology*, 15, S234, 2004. With permission.)

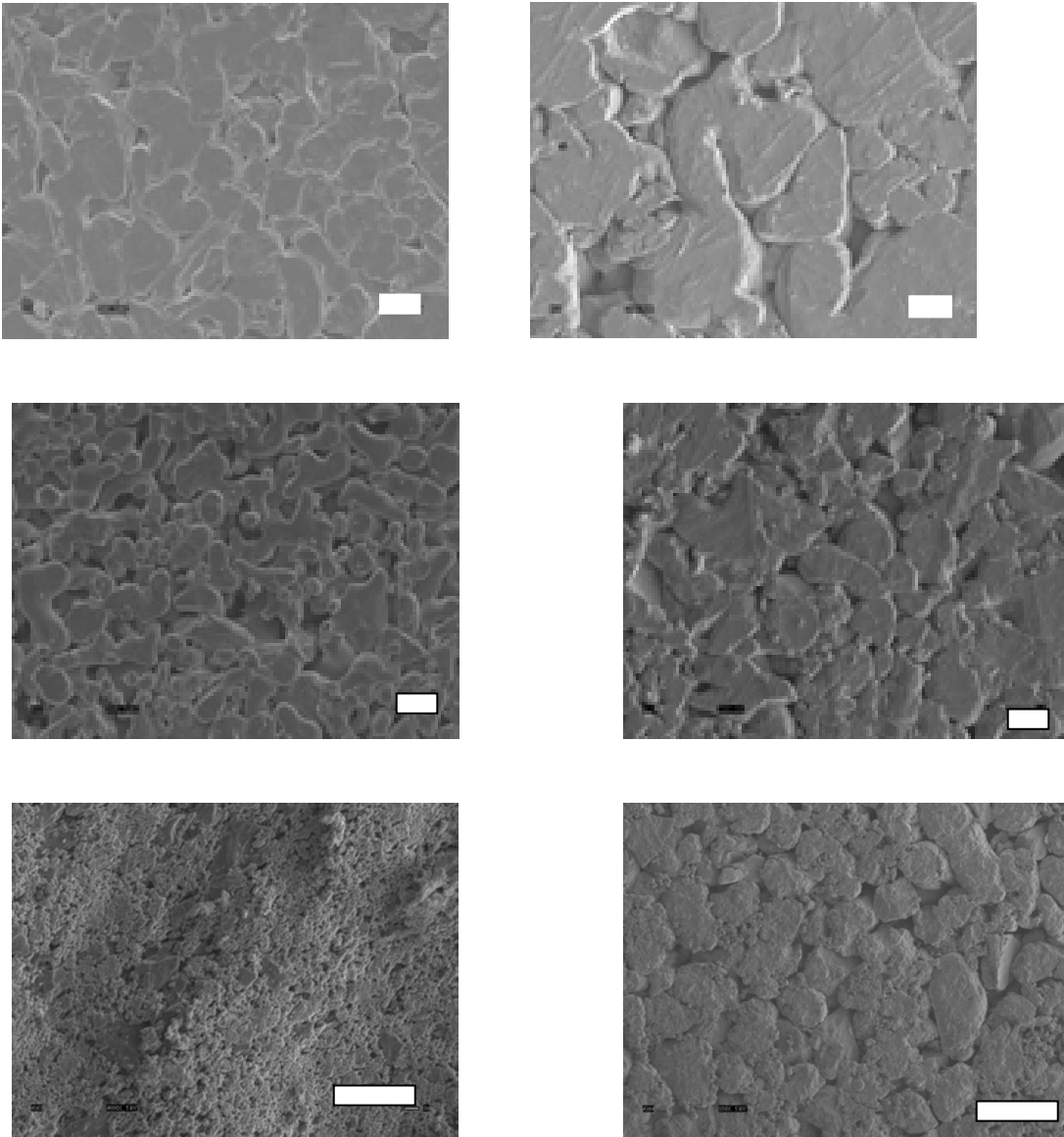


Figure A.11: Scanning electron micrographs of nanophase metals. Increased functions of osteoblasts have been observed on nanophase compared to conventional c.p. Ti, Ti6Al4V, and CoCrMo. Scale bar = 1 micron for nanophase Ti/Ti6Al4V and 10 microns for conventional Ti/Ti6Al4V. Scale bar = 10 microns for nanophase and conventional CoCrMo. (From Ejiofor, J.U. and Webster, T.J., ASM Conference, Las Vegas, NV, in press, 2004. With permission.)

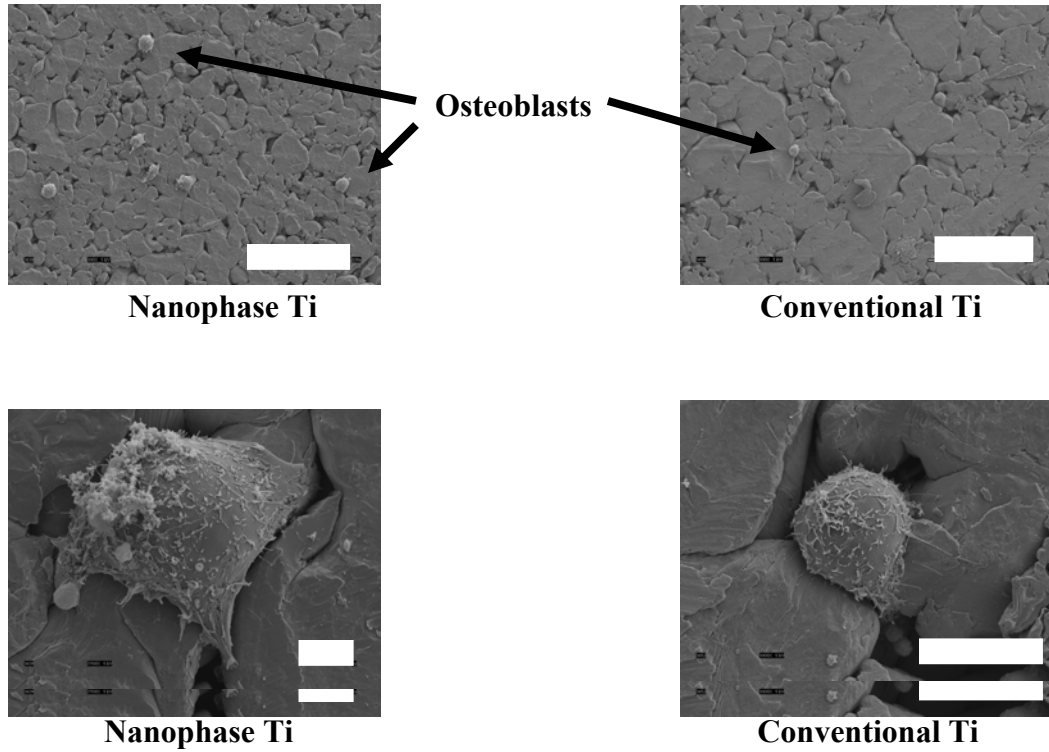
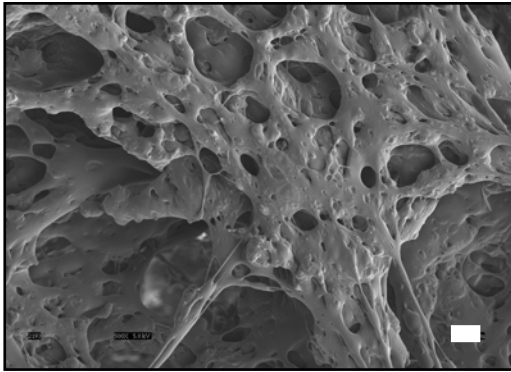
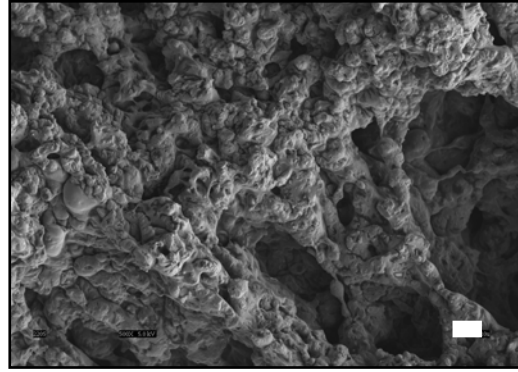


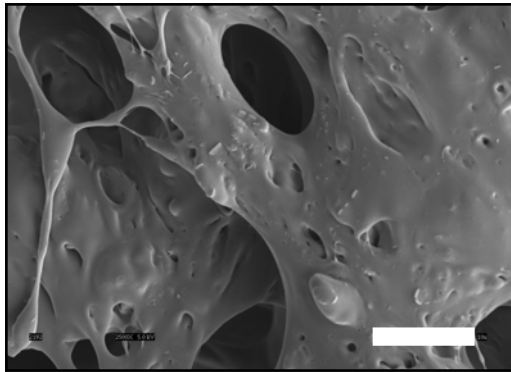
Figure A.12: Scanning electron micrographs of adherent osteoblasts on nanophase c.p. Ti. Directed osteoblast adhesion on nanophase metal grain boundaries has been reported. Scale bar = 100 microns for top and 10 microns for bottom. Adhesion time = 30 minutes. (From Ejiofor, J.U. and Webster, T.J., ASM Conference, Las Vegas, NV, in press, 2004. With permission.)



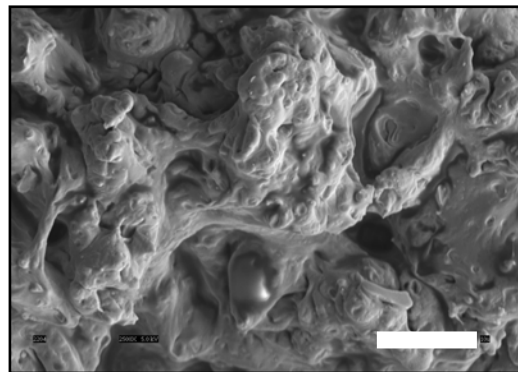
a) Conventional PLGA



b) Nano-structured PLGA



c) Conventional PLGA



d) Nano-structured PLGA

Figure A.13: Scanning electron micrographs of conventional and nanophase PLGA scaffolds. Increased osteoblast functions have been demonstrated on nanophase PLGA scaffolds. Scale bar = 10 microns. (From Park, G.E., Park, K., Webster, T.J., *Biomaterials*, in press, 2004. With permission.)

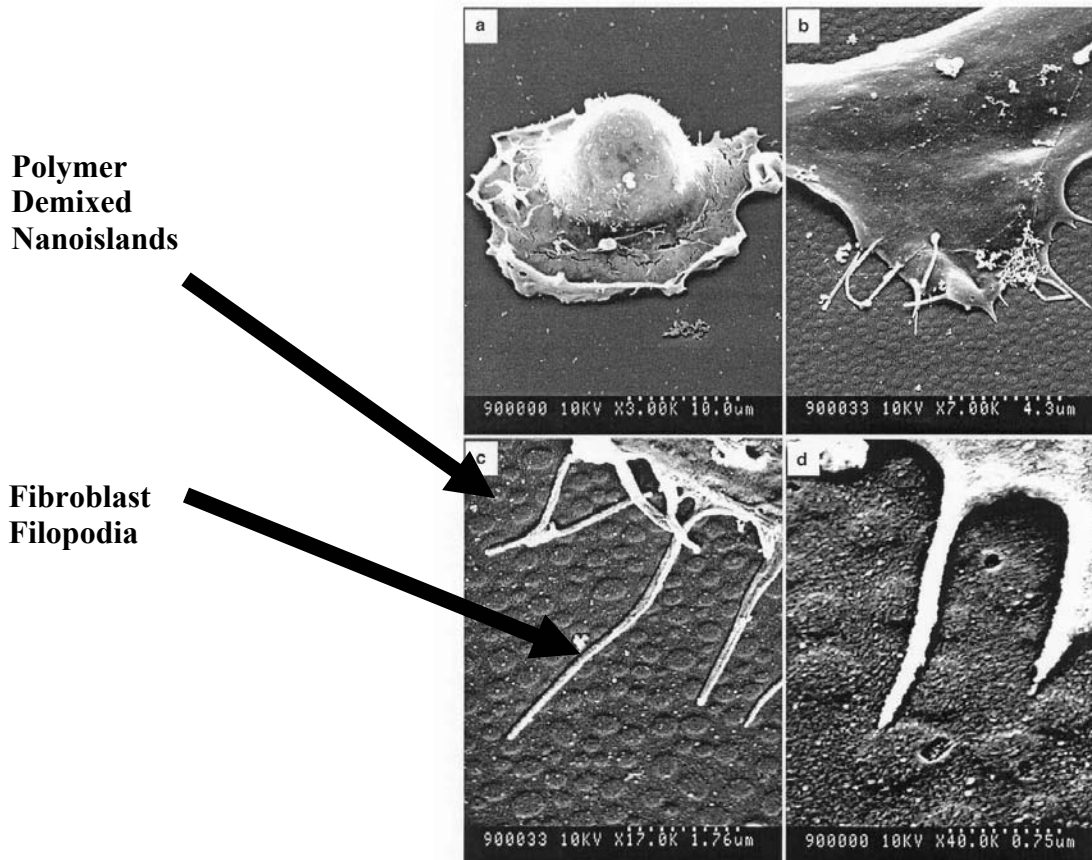
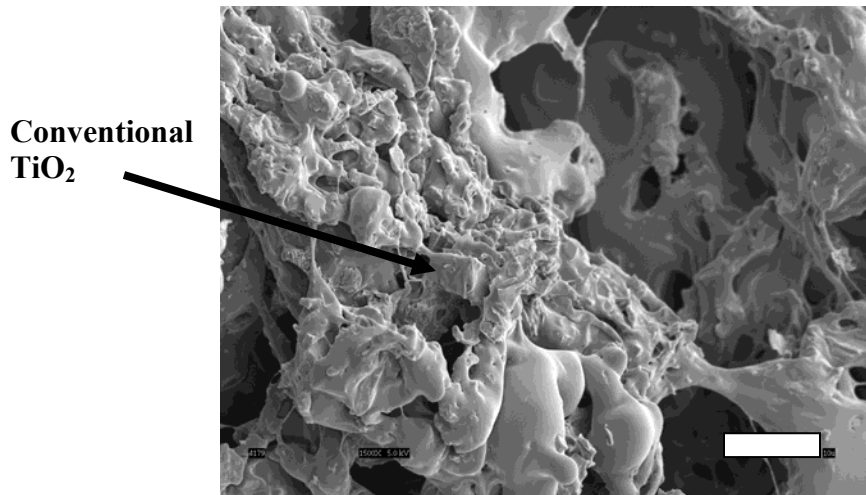
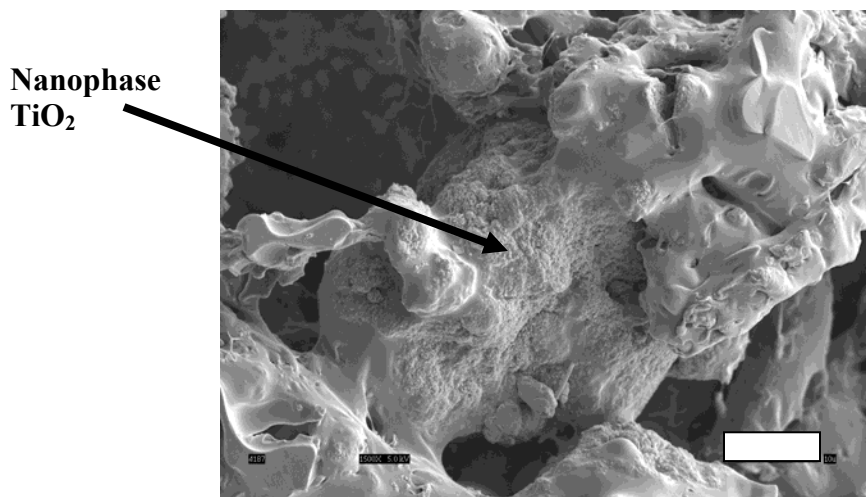


Figure A.14: Polymer nanoislands created by demixing polystyrene and polybromostyrene. Altered cell functions have been observed on polymer nanoislands compared to conventional polymer topographies. (a) through (d) represents increased magnification. (From Li, W.-J. et al., *J. Biomed. Mat. Res.*, 60, 613-621, 2002. With permission.)

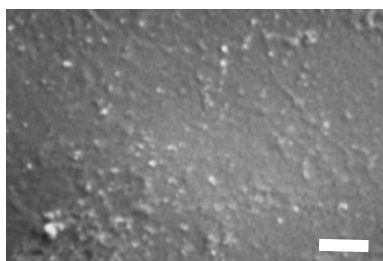


**PLGA: Conventional TiO₂
(70:30 wt.%)**

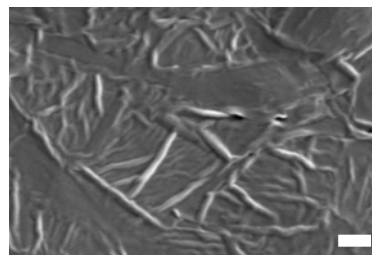


**PLGA: Nanophase TiO₂
(70:30 wt.%)**

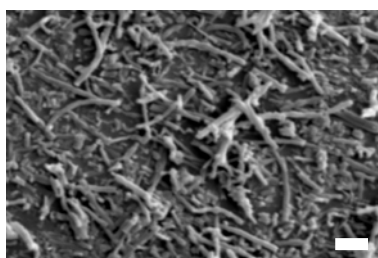
Figure A.15: Scanning electron micrographs of poly-lactic-glycolic acid (PLGA): titania composites. Increased osteoblast function has been observed on polymer composites containing nanophase compared to conventional ceramics. Scale bar = 10 microns. (From Smith, T.A. and Webster, T.J., J. Biomed. Mat. Res, in press, 2004. With permission.)



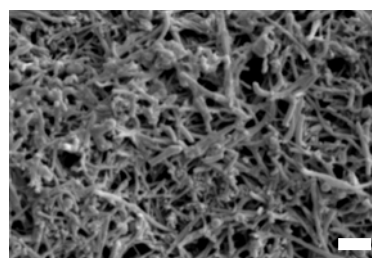
(a) 100:0 (PU:CN wt. %)



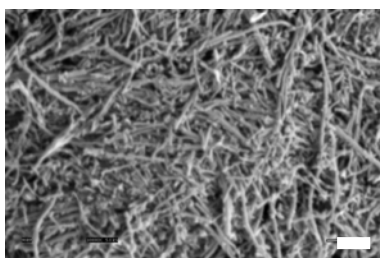
(b) 98:2 (PU:CN wt. %)



(c) 90:10 (PU:CN wt. %)



(d) 75:25 (PU:CN wt. %)



(e) 0:100 (PU:CN wt. %)

Figure A.16: Scanning electron micrographs of poly-ether-urethane (PU): carbon nanofibers (wt.%) composites. Increased functions of osteoblasts have been observed on polymer composites containing carbon nanofibers. Scale bar = 1 micron. (From Price, R.L. et al., *Biomaterials*, 24(11), 1877, 2003. With permission.)

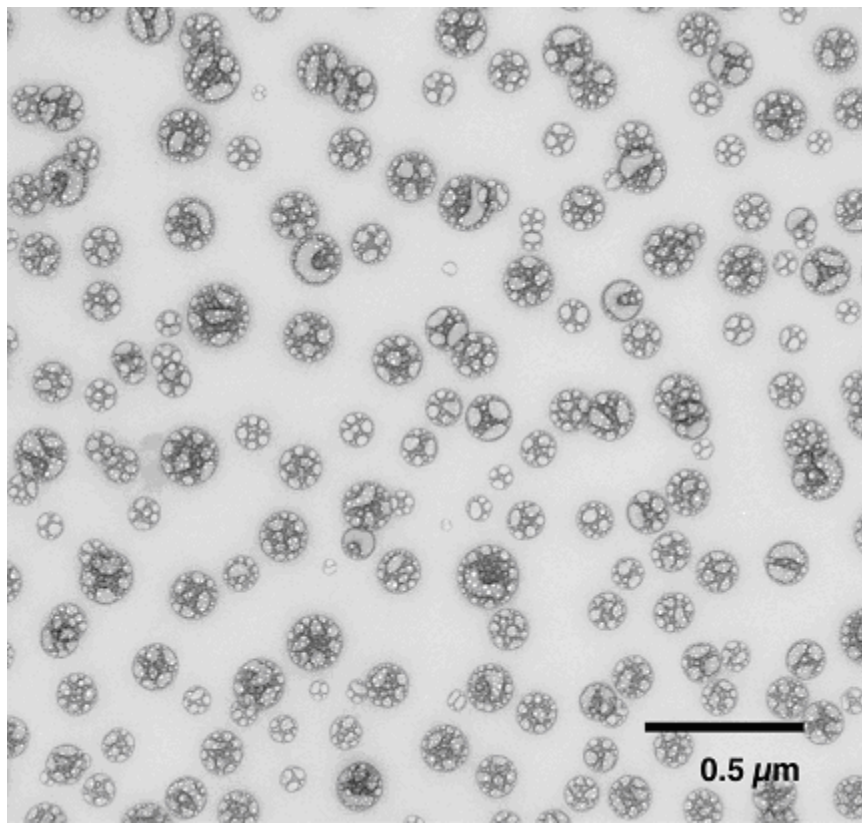


Figure A.17: TEM image of P(MAA-g-EG) nanospheres prepared from a MAA/EG molar feed ratio of 1:1. The P(MAA-g-EG) nanospheres were stained with uranyl acetate with a pH value of 4.0.

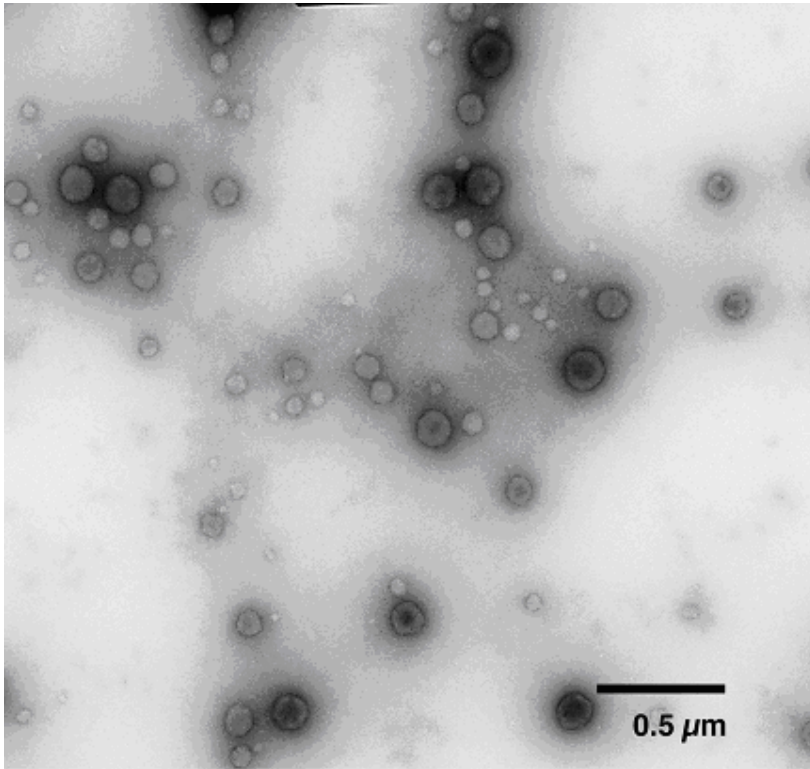


Figure A.18: TEM image of P(MAA-g-EG) nanospheres prepared from a MAA/EG molar feed ratio of 1:1. The P(MAA-g-EG) nanospheres were stained with phosphotugstic acid with a pH value of 7.2.

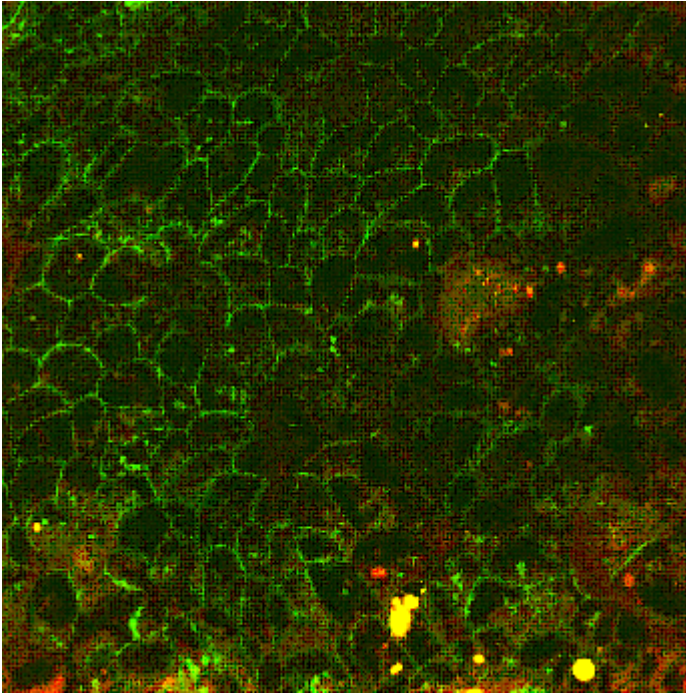


Figure A.19: Optical section of a Caco-2 cell monolayer grown on microporous Transwell® plates obtained with a confocal microscope. FITC-labeled insulin (green) was added to the apical chamber of the cell monolayer in the presence of poly(methacrylic acid-grafted-ethylene glycol) microparticles for 120 min and images were taken after fixing the cells with 3.7% formaldehyde.

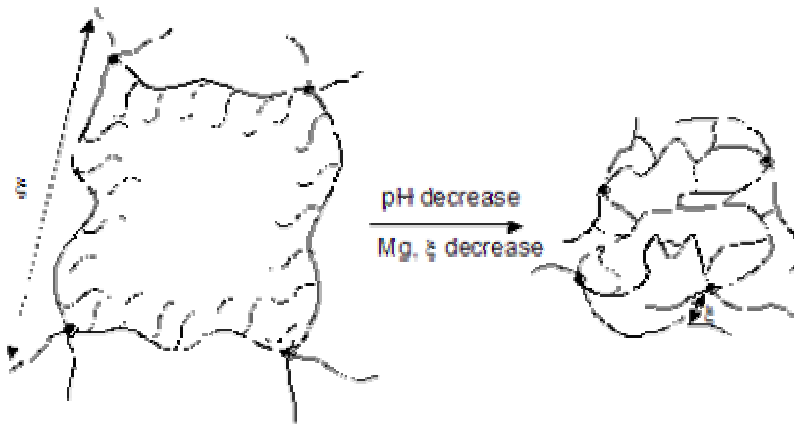


Figure A.20: Network structural changes due to variations on environmental pH. Higher pHs disrupt the interpolymer complexes and ionic moieties deprotonize leading to extensive swelling (left). As pH is decreased, interactions between the tethered grafts with the protonized ionic moieties increase leading to the formation of interpolymer complexes.

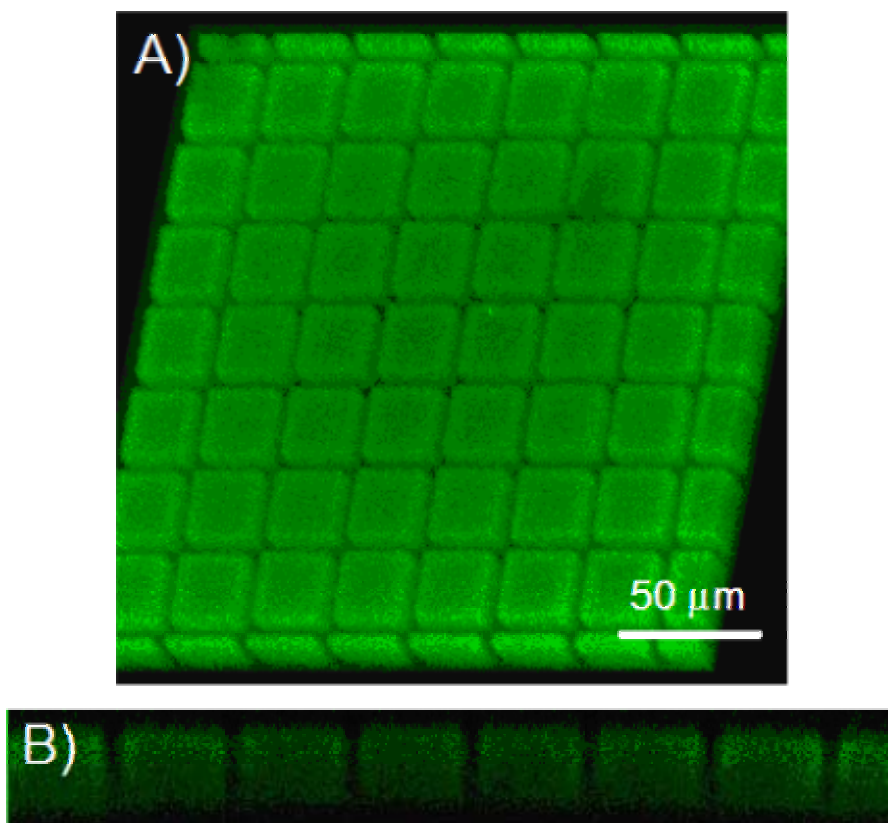


Figure A.21: In (A) 3D projection a micropatterned square array of a biomimetic polymer network based on a crosslinked polyacrylamide obtained utilizing a confocal microscope. In (B) a slice of the square array is demonstrated.

References

- Achar L and Peppas NA, Preparation, Characterization And Mucoadhesive Interactions Of Poly(Methacrylic Acid) Copolymers With Rat Mucosa, *J. Control. Release*, 31:271-276, 1994.
- Allen A, Hutton DA, Pearson JP, and Sellers LA, Mucus Glycoprotein Structure, Gel Formation And Gastrointestinal Mucus Function, *Ciba Foundation Symp.*, 109:137-156, 1984.
- Argade AB and Peppas NA, Poly(acrylic acid) poly(vinyl alcohol) copolymers with superabsorbent properties, *J. Appl. Polym. Sci.*, 70:817-829, 1998.
- Askari F, Nafisi S, Omidian H, and Hashemi SA, Synthesis And Characterization Of Acrylic-Based Superabsorbents, *J. Appl. Polym. Sci.*, 50:1851-1855, 1993.
- Atuma C, Strugala V, Allen A, and Holm L, The adherent gastrointestinal mucus gel layer: thickness and physical state in vivo, *Am. J. Physiol.-Gastroint. Liver Physiol.*, 280:G922-G929, 2001.
- Baldus SE, Engelmann K, and Hanisch FG, MUC1 and the MUCs: A family of human mucins with impact in cancer biology, *Crit. Rev. Clin. Lab. Sci.*, 41:189-231, 2004.
- Barrett KEJ and Thomas HR, Kinetics of Dispersions Polymerization of Soluble Monomers. I. Methyl Methacrylate, *J. Polym. Sci.*, 7:2621-2650, 1969.
- Barrett KEJ and Thomas HR, *Kinetics and Mechanism of Dispersion Polymerization*, in *Dispersion Polymerization in Organic Media*, Barrett KEJ, Editor. 1975, John Wiley & Sons: New York, NY. p. 115-200.
- Baughman RA, Kapoor SC, Agarwal RK, Kisicki J, Catella-Lawson F, and FitzGerald GA, Oral delivery of anticoagulant doses of heparin - A randomized, double-blind, controlled study in humans, *Circulation*, 98:1610-1615, 1998.
- Bell CL and Peppas NA, Modulation of drug permeation through interpolymer complexed hydrogels for drug delivery applications, *J. Control. Release*, 39:201-207, 1996.
- Bernkop-Schnurch A, Thiomers: A new generation of mucoadhesive polymers, *Adv. Drug Deliv. Rev.*, 57:1569-1582, 2005.
- Bies C, Lehr CM, and Woodley JF, Lectin-mediated drug targeting: history and applications, *Adv. Drug Deliv. Rev.*, 56:425-435, 2004.

- Boekhorst J, Helmer Q, Kleerebezem M, and Siezen RJ, Comparative analysis of proteins with a mucus-binding domain found exclusively in lactic acid bacteria, *Microbiology-(UK)*, 152:273-280, 2006.
- Brochardwyart F, Degennes PG, Leger L, Marciano Y, and Raphael E, Adhesion Promoters, *J. Phys. Chem.*, 98:9405-9410, 1994.
- Bromberg L, Temchenko M, Alakhov V, and Hatton TA, Bioadhesive properties and rheology of polyether-modified poly(acrylic acid) hydrogels, *Int. J. Pharm.*, 282:45-60, 2004.
- Bures P and Peppas NA, Structural and Morphological Characteristics of Carriers Based on Poly(acrylic acid), *Polym. Prepr.*, 40:345-346, 1999.
- Camesano TA and Logan BE, Probing bacterial electrosteric interactions using atomic force microscopy, *Environ. Sci. Technol.*, 34:3354-3362, 2000.
- Caston A, Davis S, and Williams P, The potential of fimbrial proteins for delaying intestinal transit of oral drug delivery system, *Proceed. Intern. Symp. Controlled Release Bio. Mat.*, 17:313-314, 1990.
- Chickering DE and Mathiowitz E, *Definitions, Mechanisms, and Theories of Bioadhesion*, in *Bioadhesive Drug Delivery Systems: Fundamentals, Novel Approaches, and Development*, Mathiowitz E, Chickering DE, and Lehr CM, Editors. 1999, Marcel Dekker, Inc.: New York, NY. p. 1-10.
- Christensen J, *Motility of the intestine*, in *Gastrointestinal Disease: Pathophysiology/Diagnosis/Management*, Sleisenger MH and Fordtran JS, Editors. 1993, W.B. Saunders Co.: Philadelphia, PA. p. 822-837.
- Cleary J, Bromberg L, and Magner E, Adhesion of polyether-modified poly(acrylic acid) to mucin, *Langmuir*, 20:9755-9762, 2004.
- Davis SS, Formulation strategies for absorption windows, *Drug Discov. Today*, 10:249-257, 2005.
- De Ascentiis A, Degrazia JL, Bowman CN, Colombo P, and Peppas NA, Mucoadhesion Of Poly(2-Hydroxyethyl Methacrylate) Is Improved When Linear Poly(Ethylene Oxide) Chains Are Added To The Polymer Network, *J. Control. Release*, 33:197-201, 1995.
- Decuzzi P, Lee S, Decuzzi M, and Ferrari M, Adhesion of microfabricated particles on vascular endothelium: A parametric analysis, *Ann. Biomed. Eng.*, 32:793-802, 2004.

- Degennes PG, Conformations Of Polymers Attached To An Interface, *Macromolecules*, 13:1069-1075, 1980.
- Dekker J, Rossen JWA, Buller HA, and Einerhand AWC, The MUC family: an obituary, *Trends Biochem.Sci.*, 27:126-131, 2002.
- Derjaguin BV, Aleinikova IN, and Toporov YP, On The Role Of Electrostatic Forces In The Adhesion Of Polymer Particles To Solid-Surfaces, *Prog. Surf. Sci.*, 45:119-123, 1994.
- Ditsch A, Laibinis PE, Wang DIC, and Hatton TA, Controlled clustering and enhanced stability of polymer-coated magnetic nanoparticles, *Langmuir*, 21:6006-6018, 2005.
- Dodou D, Breedveld P, and Wieringa PA, Mucoadhesives in the gastrointestinal tract: revisiting the literature for novel applications, *Eur. J. Pharm. Biopharm.*, 60:1-16, 2005.
- Dong J, Ozaki Y, and Nakashima K, Infrared, Raman, and near-infrared spectroscopic evidence for the coexistence of various hydrogen-bond forms in poly(acrylic acid), *Macromolecules*, 30:1111-1117, 1997.
- Drotleff S, Lungwitz U, Breunig M, Dennis A, Blunk T, Tessmar J, and Gopferich A, Biomimetic polymers in pharmaceutical and biomedical sciences, *Eur. J. Pharm. Biopharm.*, 58:385-407, 2004.
- Eckburg PB, Bik EM, Bernstein CN, Purdom E, Dethlefsen L, Sargent M, Gill SR, Nelson KE, and Relman DA, Diversity of the human intestinal microbial flora, *Science*, 308:1635-1638, 2005.
- Efremova NV, Huang Y, Peppas NA, and Leckband DE, Direct measurement of interactions between tethered poly(ethylene glycol) chains and adsorbed mucin layers, *Langmuir*, 18:836-845, 2002.
- Ende MTA and Peppas NA, Transport of ionizable drugs and proteins in crosslinked poly(acrylic acid) and poly(acrylic acid-co-2-hydroxyethyl methacrylate) hydrogels.2. Diffusion and release studies, *J. Control. Release*, 48:47-56, 1997.
- Felt O, Buri P, and Gurny R, Chitosan: A unique polysaccharide for drug delivery, *Drug Dev. Ind. Pharm.*, 24:979-993, 1998.
- Ficek B and Peppas N. *Biomaterials for Drug and Cell Delivery*. in *Materials Research Society*. 1994. Pittsburgh, PA.
- Goldberg M and Gomez-Orellana I, Challenges for the oral delivery of macromolecules, *Nat. Rev. Drug Discov.*, 2:289-295, 2003.

- Gu JM, Robinson JR, and Leung SHS, Binding Of Acrylic Polymers To Mucin Epithelial Surfaces - Structure-Property Relationships, *Crit. Rev. Ther. Drug Carr. Syst.*, 5:21-67, 1988.
- Gum JR, Human mucin glycoproteins: Varied structures predict diverse properties and specific functions, *Biochem. Soc. Trans.*, 23:795-799, 1995.
- Gum JR, Hicks JW, Toribara NW, Rothe EM, Lagace RE, and Kim YS, The Human Muc2 Intestinal Mucin Has Cysteine-Rich Subdomains Located Both Upstream And Downstream Of Its Central Repetitive Region, *J. Biol. Chem.*, 267:21375-21383, 1992.
- Harding SE, *Analysis of polysaccharides by ultracentrifugation. Size, conformation and interactions in solution*, in *Polysaccharides 1: Structure, Characterization And Use*. 2005. p. 211-254.
- Hejazi R and Amiji M, Chitosan-based gastrointestinal delivery systems, *J. Control. Release*, 89:151-165, 2003.
- Hilt JZ, Gupta AK, Bashir R, and Peppas NA, Ultrasensitive biomems sensors based on microcantilevers patterned with environmentally responsive hydrogels, *Biomed. Microdevices*, 5:177-184, 2003.
- Hooper LV and Gordon JI, Commensal host-bacterial relationships in the gut, *Science*, 292:1115-1118, 2001.
- Hou SYE, Cowles VE, and Berner B, Gastric retentive dosage forms: A review, *Crit. Rev. Ther. Drug Carr. Syst.*, 20:461-497, 2003.
- Huang YB, Leobandung W, Foss A, and Peppas NA, Molecular aspects of muco- and bioadhesion: Tethered structures and site-specific surfaces, *J. Control. Release*, 65:63-71, 2000.
- Huang YB, Szleifer I, and Peppas NA, Gel-gel adhesion by tethered polymers, *J. Chem. Phys.*, 114:3809-3816, 2001.
- Huang YB, Szleifer I, and Peppas NA, A molecular theory of polymer gels, *Macromolecules*, 35:1373-1380, 2002.
- Hubbell JA, Biomaterials In Tissue Engineering, *Bio-Technology*, 13:565-576, 1995.
- Ishida M, Machida Y, Nambu N, and Nagai T, Pharmaceutical Interactions In Dosage Forms And Processing.21. New Mucosal Dosage Form Of Insulin, *Chem. Pharm. Bull.*, 29:810-816, 1981.

- Jabbari E, Wisniewski N, and Peppas NA, Evidence Of Mucoadhesion By Chain Interpenetration At A Poly(Acrylic Acid) Mucin Interface Using Atr-Ftir Spectroscopy, *J. Control. Release*, 26:99-108, 1993.
- Jeon SI, Lee JH, Andrade JD, and Degennes PG, Protein Surface Interactions In The Presence Of Polyethylene Oxide.1. Simplified Theory, *J. Colloid Interface Sci.*, 142:149-158, 1991.
- Junginger HE, Thanou M, and Verhoef JC, *Mucoadhesive Hydrogels in Drug Delivery*, in *Encyclopedia of Pharmaceutical Technology*, Swarbrick J and Boylan JC, Editors. 2002, Marcel Dekker, Inc.: New York, NY. p. 1848-1863.
- Kaelble DH and Moacanin J, Surface-Energy Analysis Of Bioadhesion, *Polymer*, 18:475-482, 1977.
- Kast CE, Frick W, Losert U, and Bernkop-Schnurch A, Chitosan-thioglycolic acid conjugate: a new scaffold material for tissue engineering? *Int. J. Pharm.*, 256:183-189, 2003.
- Kelm S and Schauer R, *Sialic acids in molecular and cellular interactions*, in *International Review Of Cytology - A Survey Of Cell Biology, Vol 175*. 1997, Academic Press Inc: San Diego. p. 137-240.
- Kim B, La Flamme K, and Peppas NA, Dynamic swelling Behavior of pH-sensitive anionic hydrogels used for protein delivery, *J. Appl. Polym. Sci.*, 89:1606-1613, 2003.
- Lazzari M, Kitayama T, Hatada K, and Chiantore O, Effect of stereoregularity on the thermal behavior of poly(methacrylic acid)s. 2. Decomposition at low temperatures, *Macromolecules*, 31:8075-8082, 1998.
- Lee JW, Park JH, and Robinson JR, Bioadhesive-based dosage forms: The next generation, *J. Pharm. Sci.*, 89:850-866, 2000.
- Leger L, Raphael E, and Hervet H, *Surface-anchored polymer chains: Their role in adhesion and friction*, in *Polymers In Confined Environments*. 1999, Springer-Verlag Berlin: Berlin. p. 185-225.
- Lehr CM, Bioadhesion Technologies For The Delivery Of Peptide And Protein Drugs To The Gastrointestinal-Tract, *Crit. Rev. Ther. Drug Carr. Syst.*, 11:119-160, 1994.
- Lehr CM, Lectin-mediated drug delivery: The second generation of bioadhesives, *J. Control. Release*, 65:19-29, 2000.

- Lehr CM, Bodde HE, Bouwstra JA, and Junginger HE, A Surface-Energy Analysis Of Mucoadhesion.2. Prediction Of Mucoadhesive Performance By Spreading Coefficients, *Eur. J. Pharm. Sci.*, 1:19-30, 1993.
- Lehr CM, Bouwstra JA, Bodde HE, and Junginger HE, A Surface-Energy Analysis Of Mucoadhesion - Contact-Angle Measurements On Polycarbophil And Pig Intestinal-Mucosa In Physiologically Relevant Fluids, *Pharm. Res.*, 9:70-75, 1992.
- Lehr CM, Bouwstra JA, Kok W, Noach ABJ, Deboer AG, and Junginger HE, Bioadhesion By Means Of Specific Binding Of Tomato Lectin, *Pharm. Res.*, 9:547-553, 1992.
- Lehr CM, Poelma FGJ, Junginger HE, and Tukker JJ, An Estimate Of Turnover Time Of Intestinal Mucus Gel Layer In The Rat Insitu Loop, *Int. J. Pharm.*, 70:235-240, 1991.
- Li A and Wang AQ, Synthesis and properties of clay-based superabsorbent composite, *Eur. Polym. J.*, 41:1630-1637, 2005.
- Lopez JE and Peppas NA, Effect of poly (ethylene glycol) molecular weight and microparticle size on oral insulin delivery from P(MAA-g-EG) microparticles, *Drug Dev. Ind. Pharm.*, 30:497-504, 2004.
- Lowman AM, Cowans BA, and Peppas NA, Investigation of interpolymer complexation in swollen polyelectrolyte networks using solid-state NMR spectroscopy, *J. Polym. Sci. Pt. B-Polym. Phys.*, 38:2823-2831, 2000.
- Lowman AM, Morishita M, Kajita M, Nagai T, and Peppas NA, Oral delivery of insulin using pH-responsive complexation gels, *J. Pharm. Sci.*, 88:933-937, 1999.
- Lowman AM and Peppas NA, Analysis of the complexation/decomplexation phenomena in graft copolymer networks, *Macromolecules*, 30:4959-4965, 1997.
- Lowman AM and Peppas NA, Solute transport analysis in pH-responsive, complexing hydrogels of poly(methacrylic acid-g-ethylene glycol), *J. Biomater. Sci.-Polym. Ed.*, 10:999-1009, 1999.
- Lowman AM and Peppas NA, Molecular analysis of interpolymer complexation in graft copolymer networks, *Polymer*, 41:73-80, 2000.
- Mann BK, Schmedlen RH, and West JL, Tethered-TGF-beta increases extracellular matrix production of vascular smooth muscle cells, *Biomaterials*, 22:439-444, 2001.

- Mann BK, Tsai AT, Scott-Burden T, and West JL, Modification of surfaces with cell adhesion peptides alters extracellular matrix deposition, *Biomaterials*, 20:2281-2286, 1999.
- Mathiowitz E, Chickering DE, and Lehr CM, *Bioadhesive Drug Delivery Systems: Fundamentals, Novel Approaches, and Development*. 1999, New York, NY: Marcel Dekker, Inc.
- Mikos AG, Mathiowitz E, Langer R, and Peppas NA, Interaction Of Polymer Microspheres With Mucin Gels As A Means Of Characterizing Polymer Retention On Mucus, *J. Colloid Interface Sci.*, 143:366-373, 1991.
- Mikos AG and Peppas NA, Measurement Of The Surface-Tension Of Mucin Solutions, *Int. J. Pharm.*, 53:1-5, 1989.
- Moncada DM, Kammanadiminti SJ, and Chadee K, Mucin and Toll-like receptors in host defense against intestinal parasites, *Trends Parasitol.*, 19:305-311, 2003.
- Morishita M, Goto T, Nakamura K, Lowman AM, Takayama K, and Peppas NA, Novel oral insulin delivery systems based on complexation polymer hydrogels: Single and multiple administration studies in type 1 and 2 diabetic rats, *J. Control. Release*, 110:587-594, 2006.
- Morishita M, Goto T, Peppas NA, Joseph JI, Torjman MC, Munsick C, Nakamura K, Yamagata T, Takayama K, and Lowman AM, Mucosal insulin delivery systems based on complexation polymer hydrogels: effect of particle size on insulin enteral absorption, *J. Control. Release*, 97:115-124, 2004.
- Nagai T and Machida Y, Advances In Drug Delivery - Mucosal Adhesive Dosage Forms, *Pharm. Int.*, 6:196-200, 1985.
- Peppas NA, Molecular calculations of poly(ethyleneglycol) transport across a swollen poly(acrylic acid) mucin interface, *J. Biomater. Sci.-Polym. Ed.*, 9:535-542, 1998.
- Peppas NA, Devices based on intelligent biopolymers for oral protein delivery, *Int. J. Pharm.*, 277:11-17, 2004.
- Peppas NA and Buri PA, Surface, Interfacial and Molecular Aspects of Polymer Bioadhesion on Soft Tissues, *J. Control. Release*, 2:257-275, 1985.
- Peppas NA and Huang YB, Nanoscale technology of mucoadhesive interactions, *Adv. Drug Deliv. Rev.*, 56:1675-1687, 2004.
- Peppas NA, Little MD, and Huang Y, *Bioadhesive Controlled Release Systems*, in *Handbook of Pharmaceutical Controlled Release Technology*, Wise DL, Editor. 2000, Marcel Dekker, Inc.: New York, NY. p. 255-269.

- Peppas NA and Mongia NK, Ultrapure poly(vinyl alcohol) hydrogels with mucoadhesive drug delivery characteristics, *Eur. J. Pharm. Biopharm.*, 43:51-58, 1997.
- Peppas NA and Sahlin JJ, Hydrogels as mucoadhesive and bioadhesive materials: A review, *Biomaterials*, 17:1553-1561, 1996.
- Peppas NA and Tennenhouse D, Semicrystalline poly(vinyl alcohol) films and their blends with poly(acrylic acid) and poly(ethylene glycol) for drug delivery applications, *J. Drug Deliv. Sci. Technol.*, 14:291-297, 2004.
- Podual K, Doyle FJ, and Peppas NA, Dynamic behavior of glucose oxidase-containing microparticles of poly(ethylene glycol)-grafted cationic hydrogels in an environment of changing pH, *Biomaterials*, 21:1439-1450, 2000.
- Ponchel G, Touchard F, Wouessidjewe D, Duchene D, and Peppas NA, Bioadhesive Analysis Of Controlled-Release Systems.3. Bioadhesive And Release Behavior Of Metronidazole-Containing Poly(Acrylic Acid)-Hydroxypropyl Methylcellulose Systems, *Int. J. Pharm.*, 38:65-70, 1987.
- Read N and Houghton L, *Physiology of Gastric Emptying and Pathophysiology of Gastroparesis*, in *Gastroenterology Clinics of North America: Motility Disorders*, Ouyang A, Editor. 1989, W.B. Saunders Co.: Philadelphia, PA. p. 359-373.
- Reyes CD and Garcia AJ, Engineering integrin-specific surfaces with a triple-helical collagen-mimetic peptide, *J. Biomed. Mater. Res. Part A*, 65A:511-523, 2003.
- Robinson DN and Peppas NA, Preparation and characterization of pH-responsive poly(methacrylic acid-g-ethylene glycol) nanospheres, *Macromolecules*, 35:3668-3674, 2002.
- Ruoslahti E and Pierschbacher MD, New Perspectives In Cell-Adhesion - Rgd And Integrins, *Science*, 238:491-497, 1987.
- Sahlin JJ and Peppas NA, Enhanced hydrogel adhesion by polymer interdiffusion: Use of linear poly(ethylene glycol) as an adhesion promoter, *J. Biomater. Sci.-Polym. Ed.*, 8:421-436, 1997.
- Schultz J and Nardin M, *Theories and Mechanisms of Adhesion*, in *Handbook of Adhesive Technology*, Pizzi A and Mittal K, Editors. 1994, Marcel Dekker, Inc.: New York, NY.
- Sellers LA, Allen A, Morris ER, and Rossmurphy SB, Mucus Glycoprotein Gels - Role Of Glycoprotein Polymeric Structure And Carbohydrate Side-Chains In Gel-Formation, *Carbohydr. Res.*, 178:93-110, 1988.

- Serra L, Domenech J, and Peppas NA, Design of poly(ethylene glycol)-tethered copolymers as novel mucoadhesive drug delivery systems, *Eur. J. Pharm. Biopharm.*, 63:11-18, 2006.
- Shinya K, Ebina M, Yamada S, Ono M, Kasai N, and Kawaoka Y, Influenza virus receptors in the human airway, *Nature*, 440:435-436, 2006.
- Singh BN and Kim KH, Floating drug delivery systems: an approach to oral controlled drug delivery via gastric retention, *J. Control. Release*, 63:235-259, 2000.
- Smart JD, Recent developments in the use of bioadhesive systems for delivery of drugs to the oral cavity, *Crit. Rev. Ther. Drug Carr. Syst.*, 21:319-344, 2004.
- Smart JD, The basics and underlying mechanisms of mucoadhesion, *Adv. Drug Deliv. Rev.*, 57:1556-1568, 2005.
- Smith DC, *Adhesives and Sealants*, in *Biomaterials Science: An Introduction to Materials in Medicine*, Ratner BD, Hoffman AS, Schoen FJ, and Lemons JE, Editors. 2004, Academic Press: San Diego, CA. p. 572-583.
- Soeno K, Suzuki S, Taira Y, Sawase T, and Atsuta M, Influence of mechanical properties of two resin cements on durability of bond strength to dentin after cyclic loading, *Dent. Mater. J.*, 24:351-355, 2005.
- Sosson F, Chateauminois A, and Creton C, Investigation of shear failure mechanisms of pressure-sensitive adhesives, *J. Polym. Sci. Pt. B-Polym. Phys.*, 43:3316-3330, 2005.
- Stevens MM, Allen S, Davies MC, Roberts CJ, Schacht E, Tandler SJB, VanSteenkiste S, and Williams PM, The development, characterization, and demonstration of a versatile immobilization strategy for biomolecular force measurements, *Langmuir*, 18:6659-6665, 2002.
- Takishima J, Onishi H, and Machida Y, Prolonged intestinal absorption of cephadrine with chitosan-coated ethylcellulose microparticles in rats, *Biol. Pharmacol. Bull.*, 25:1498-1502, 2002.
- Talukder R and Fassihi R, Gastroretentive delivery systems: A mini review, *Drug Dev. Ind. Pharm.*, 30:1019-1028, 2004.
- Thomas JB, Creecy CM, McGinity JW, and Peppas NA, Synthesis and properties of lightly crosslinked poly((meth)acrylic acid) microparticles prepared by free radical precipitation polymerization, *Polym. Bull.*, 57:11-20, 2006.

- Thomas JB, Tingsanchali J, Creecy CM, Rosales AM, McGinity JW, and Peppas NA, Dynamics of Poly(ethylene glycol) Tethered pH Responsive Biomaterials, (*in preparation*), 2006.
- Torres-Lugo M and Peppas NA, Molecular design and in vitro studies of novel pH-sensitive hydrogels for the oral delivery of calcitonin, *Macromolecules*, 32:6646-6651, 1999.
- Torres-Lugo M and Peppas NA, Transmucosal delivery systems for calcitonin: a review, *Biomaterials*, 21:1191-1196, 2000.
- vanKlinken BJW, Dekker J, Buller HA, DeBolos C, and Einerhand AWC, Biosynthesis of mucins (MUC2-6) along the longitudinal axis of the human gastrointestinal tract, *Am. J. Physiol.-Gastroint. Liver Physiol.*, 36:G296-G302, 1997.
- Vanklinken BJW, Dekker J, Buller HA, and Einerhand AWC, Mucin Gene Structure And Expression - Protection Vs Adhesion, *Am. J. Physiol.-Gastroint. Liver Physiol.*, 32:G613-G627, 1995.
- Wang C, Tam KC, and Jenkins RD, Dissolution behavior of HASE polymers in the presence of salt: Potentiometric titration, isothermal titration calorimetry, and light scattering studies, *J. Phys. Chem. B*, 106:1195-1204, 2002.
- Williams SJ, Wreschner DH, Tran M, Eyre HJ, Sutherland GR, and McGuckin MA, MUC13, a novel human cell surface mucin expressed by epithelial and hemopoietic cells, *J. Biol. Chem.*, 276:18327-18336, 2001.
- Xu LC, Vadillo-Rodriguez V, and Logan BE, Residence time, loading force, pH, and ionic strength affect adhesion forces between colloids and biopolymer-coated surfaces, *Langmuir*, 21:7491-7500, 2005.
- Yan XL and Gemeinhart RA, Cisplatin delivery from poly(acrylic acid-co-methyl methacrylate) microparticles, *J. Control. Release*, 106:198-208, 2005.
- Zhang J and Peppas NA, Structure and Solute Size Exclusion of Poly(N-isopropylamide)/Poly(methacrylic acid) Interpenetrating Polymeric Networks, *Polym. Prepr.*, 39:228-229, 1998.
- Zhang J and Peppas NA, Molecular interactions in poly(methacrylic acid)/Poly(N-isopropyl acrylamide) interpenetrating polymer networks, *J. Appl. Polym. Sci.*, 82:1077-1082, 2001.
- Zhang J and Peppas NA, Morphology of poly(methacrylic acid)/poly(N-isopropyl acrylamide) interpenetrating polymeric networks, *J. Biomater. Sci.-Polym. Ed.*, 13:511-525, 2002.

Zisman WA, *Influence of Constitution on Adhesion*, in *Handbook of Adhesives*, Skeist I, Editor. 1977, Van Nostrand Reinhold Company: New York, NY. p. 33-66.

Vita

J. Brock Thomas was born on June 12, 1980, to Jackie L. Thomas and Carolyn W. Thomas. He grew up in Henderson, TN, where he graduated high school from Chester County High School in 1998. Brock went on to major in chemical engineering at the University of Tennessee at Knoxville, and he earned his Bachelor's Degree in Chemical Engineering (Honors) in May 2003, graduating Summa Cum Laude as a University Honors Scholar. While at UT-K, he interned with Sonoco Flexible Packaging in Morristown, TN; Kobe Alcoa Aluminum (KAAL) in Sydney, Australia; Eastman Chemical Company in Kingsport, TN; and Merck in Albany, GA. He married Christian M. Thomas on July 26, 2004.

After graduation, Brock joined the University of Texas at Austin as a Department of Homeland Security Graduate Research Fellow working with Professors Nicholas A. Peppas and James W. McGinity. While at UT-A, he performed a summer research internship at Brookhaven National Laboratory working under the supervision of John J. Dunn.

Permanent address: 15637 Imperial Jade Dr., Austin, TX 78728

This dissertation was typed by the author.